Mechanisms of cardiovascular hypoxia detection by ^{64}Cu-ATSM

Shaughnessy, Fiona Sarah

Awarding institution:
King's College London

Mechanisms of cardiovascular hypoxia detection by ^{64}Cu-ATSM

A thesis submitted by

Fiona Shaughnessy

In fulfilment of the requirements for the degree of

Doctor of Philosophy

University of London

2014

Division of Imaging Sciences and Medical Engineering, King's College, London

Abstract

^{64}Cu-Diacetyl-bis(N^4-methylthiosemicarbazone) (^{64}Cu-ATSM) is a hypoxia-selective positron emission tomography (PET) tracer and has potential imaging applications in cardiology. To fully exploit and develop ^{64}Cu-ATSM, it is essential to understand its mode of action. It has been suggested that intracellular reductants, such as thiols, reduce the uncharged Cu(II)-ATSM complex to Cu(I)-ATSM$^-$ which dissociates to deposit its radiocopper in hypoxic tissue. It is also possible that this process may be accelerated by intracellular acidosis, which is a hallmark of ischaemic tissue. The sensitivity of Cu-ATSM to intracellular thiol status or pH would impact upon its hypoxia specificity and potentially restrict its diagnostic utility.

An isolated perfused rat heart model and cultured bovine aortic endothelial cells (BAEC) were therefore utilised to investigate the importance of intracellular thiol status and intracellular acidosis on the hypoxia selectivity and pharmacokinetics of ^{64}Cu-ATSM.

During these studies the hypoxia selective retention of ^{64}Cu from ^{64}Cu-ATSM was confirmed in isolated perfused rat hearts. It was also demonstrated that intracellular thiol concentration has no effect on ^{64}Cu retention from ^{64}Cu-ATSM in normoxic or hypoxic hearts. Conversely, hypoxic BAEC incubated with high concentrations of thiols displayed significantly higher ^{64}Cu retention from ^{64}Cu-ATSM, while thiol depletion had no effect. It was therefore concluded that while thiols may be necessary for the initial reduction of Cu-ATSM, physiological changes in thiol concentration do not affect Cu-ATSM pharmacokinetics, or underlie its hypoxia selectivity.

It was also demonstrated that the hypoxic myocardium is not acidotic, and that acidosis cannot be a prime determinant of Cu-ATSM retention during hypoxia. Subsequent experiments suggest that acidosis may suppress ^{64}Cu retention from ^{64}Cu-ATSM during normoxia and hypoxia; but that this may be secondary to the oxygen-sparing effect that acidosis has on the hypoxic heart, by impairing cardiac contractility. These findings provide further insight into the mechanisms of Cu-ATSM hypoxia selectivity, and support its use as a hypoxia-specific imaging agent.

Declaration

I Fiona Shaughnessy confirm that no part of this thesis has been submitted in support of any other application for a degree or qualification of King's College, or any other university or institute of learning. I confirm that this work is my own. Where information has been derived from other sources it has been indicated in this thesis.

Acknowledgments

I begin by thanking my supervisor, Dr Rick Southworth, for all his support and guidance throughout my Ph.D. In particular I thank him for his help and comments during writing this thesis: by leaving no stone unturned I got there in the end! I also appreciate that he trusted me to work with very expensive, delicate pieces of equipment and remained calm and in good spirits when they (accidently) got broken.

From the cardiovascular group I would like to thank my 2nd supervisor, Dr Richard Siow, for supervising the *in vitro* project in this thesis and for allowing me to work in his lab and freeing up important equipment when necessary. I would also like to thank Prof. Giovanni Mann for his help and support in this. I thank Dr Tabasum Mughal, Dr Sarah Chapple, Bijal Patel and Salil Srivastava for being so accommodating and making my life as easy as possible when I had experiments on. In particular I owe a special thanks to Shane McSweeny for providing me with cells for that project and working weekends to do so. I owe a special mention to undergraduate, Martin Davies, for his hard work in helping me with the extensive *in vitro* studies at the beginning of that project.

I would like to thank Prof. Philip Blower for his support, advice and for sharing his extensive knowledge of the Cu-BTSC complexes whenever I asked for it.

I owe a big thank-you to Dr Thomas Eykyn for teaching me the ropes of NMR spectroscopy and enthusing over the results, and again, for remaining as calm as possible when certain pieces of equipment broke.

I would like to thank my partner in crime Dr Maxwell Handley, and also Dr Jennifer Williams and Julia Blower for keeping my morale up throughout particularly testing periods of my Ph.D. Also a big thank-you to Dr Erika

Mariotti, not only for her friendship but also for sharing her kinetic modelling wisdom with me. Thanks also to the lovely Zaitul Saffee for kindly helping me out in the lab in times of need.

I would also like to thank David Thakor and Barry Crook for helping me acquire equipment, often at short notice, without which these experiments would not have been possible.

I owe a big thank-you to Dr Karen Shaw for helping me with pretty much everything: providing ^{64}Cu-ATSM, letting me down gently when ^{64}Cu production failed, helping me with NMR spectroscopy and talking to me in the lab when everybody else had gone home.

Finally, I would like to thank my family and friends: my father Gordon Shaughnessy for putting up with me being a student for so many years, my lovely sister Aleanna Shaughnessy for taking my fair share of family responsibilities and my dearest friends Charlene Constantine and Lucy Esmond for understanding my lack of sociability, particularly over the last few years. I owe an extra-special thanks to my superhero nephew, Christopher, for his love and for trying to “help” me work by watching Adventure Time on my laptop and drawing dinosaurs in my note books: if anything it helped me smile when I needed it the most.

Most importantly I would like to thank my wonderful boyfriend, Jason Smith, and my mother, Philomena Shaughnessy for their fantastic support emotionally and financially over the years. In particular I thank my mother for pushing me in the right direction and making sure I had everything I needed to be where I am today. I also thank her in advance for not crying when she reads this. It is to her I would like to dedicate this thesis.

Table of contents

List of figures

Chapter 1

Chapter 2

Chapter 3

Chapter 4

Chapter 5

List of tables

Chapter 2

Chapter 3

Chapter 4

Chapter 5

List of equations

Chapter 1

Chapter 2

List of Abbreviations

3-KAT: 3-keotacyl CoA thiolase

3-OH-ACAD: 3-OH acyl coenzyme A dehydrogenase

ACAD: Acyl coenzyme A dehydrogenase

ADP: Adenosine diphosphate

ATP: Adenosine triphosphate

ATSM: Diacetyl-bis(N^4-methyl-3-thiosemicarbazone)

BAEC: Bovine aortic endothelial cells

BPM: Beats per minute

Bq: Becquerel

BSO: Buthionine sulphoximine

BTSC: Bis (thiosemicarbazone)

CAD: Coronary artery disease

CAS: Coronary artery spasm

CAT: Carnitine: acylcarnitine translocase

CHO: Chinese hamster ovary

CK: Creatine kinase

MVD: Microvascular disease

Co A: Coenzyme A

CPT: Carnitine palmitoyltransferase

CT: Computed tomography

DEM: Diethyl maleate

DMEM: Dulbecco's modified Eagle's medium

ECAH: Enoyl coenzyme A hydratase

EDTA: Ethylenediaminetetraacetic acid

EMT6: Murine mammary tumour cell line

eNOS: Endothelial NOS

EPR: Electron paramagnetic resonance

ETC: Electron transport chain

$FABP_{pm}$: Plasma membrane fatty acid binding protein

FACS: Fatty acyl Co A synthase

$FADH_2$: Flavin adenine dinucleotide

FAT: Fatty acid translocase

FATP: Fatty acid transport protein

GAPDH: Glyceraldehyde phosphate dehydrogenase

GDP: Guanosine diphosphate

GLUT: Glucose transporter

GS: Glycogen synthase

GSH: Reduced glutathione (γ-gluatamyl-cysteinyl-glycine)

GSH-Px: Glutathione peroxidase

GSNO: S-nitrosoglutathione

GSSG: Oxidised glutathione

GTP: Guanosine triphosphate

HIF: Hypoxia-inducible factor

HK: Hexokinase

H_2O_2: Hydrogen peroxide

$^{\cdot}HO_2^{\cdot}$ Hydroperoxyl radical

LAD: Left anterior descending artery

LDL: Low density lipoprotein

LPC: Lactate/proton co-transporter

LVDP: Left ventricular developed pressure

LVEDP: Left ventricular end diastolic pressure

MCT: Monocarboxylase transporter

MPT: Mitochondrial permeability transition

MRI: Magnetic resonance imaging

MTT: Dimethylthiazol diphenyltetrazolium

NAC: N-acetylcysteine

NADH: Nicotinamide adenine dinucleotide

NADPH: Nicotinamide adenine dinucleotide phosphate

NCX: Na^+/Ca^{2+} exchanger

NHE: Na^+/H^+ exchanger

NH_2Cl: Chloramine

NMR: Nuclear magnetic resonance

NO: Nitric oxide

$^{\cdot}NO_2$: Nitrite radical

NOS: Nitric oxide synthase

$^{\cdot}O_2^-$: Superoxide anion

$^{\cdot}OH$: Hydroxyl anion

$ONOO^-$: Peroxynitrite anion

PAEC: Pulmonary artery endothelial cells

PBS: Phosphate buffered saline

PCr: Phosphocreatine

PDH: Pyruvate dehydrogenase kinase

PET: Positron emission tomography

PFK: Phosphofructokinase

PGI: Phosphoglucose isomerase

PGK: Phosphoglycerate kinase

PGM: Phosphoglycerate mutase

Ph: Glycogen phosphorylase

pH_i: Intracellular pH

P_i: Inorganic phosphate

PK: Pyruvate kinase

pO_2: Oxygen partial pressure

ppm: Parts per million

PTSM: Pyruvaldehyde-bis-(N^4-methyl-3-thiosemicarbazone)

ROS: Reactive oxygen species

SH: Thiol

SPECT: Single photon emission computed tomography

SOD: Superoxide dismutase

TCA *(in chapter 1)*: Tricarboxylic acid

TCA *(in chapters 2-4)*: Trichloroacetate

TNF-α: Tumour necrosis factor α

TPI: Triosephosphate isomerase

TTFA: Thenoyltrifluoroacetone

XO: Xanthine oxidase

Chapter 1

Introduction

1.1 Ischaemic heart disease

Ischaemic heart disease is currently the leading cause of global mortality with an increase in incidence expected over the next 20 years[1,2]. Ischaemia is characterised as a condition in which there is inadequate blood supply to satisfy the metabolic demands of a tissue[3], resulting in limited delivery of nutrients, energy substrates, oxygen and the accumulation of waste products within affected tissues. Without surgical or pharmacological intervention, the heart is increasingly prone to myocardial infarction in the acute setting, while in the less severe chronic setting, it progresses along a path of hypertrophy, adverse remodelling, and ultimately, heart failure[4].

Many current imaging techniques aimed at diagnosing and characterising ischaemically compromised myocardium rely on changes in physical properties such as contractility and perfusion[5]. Although these techniques can be used to assess the degree of ischaemia and provide an index of the appropriateness of intervention, they detect abnormalities in physical parameters which occur further down the ischaemic cascade and may be associated with cell injury and remodelling. There is therefore a need for more sensitive techniques to detect earlier signs of the progression of ischaemia before these physical changes manifest. As a key early feature of impending cardiac injury, the ability to detect myocardial hypoxia or changes in redox status would provide new insights into ischaemia related pathologies, and help guide therapies in patients with ischaemic heart disease earlier on in its progression.

1.2 The pathogenesis of myocardial ischaemia

The ultimate fate of an ischaemic cell without intervention is death. In the heart this may lead to myocardial infarction or heart failure and is frequently fatal. Cell death occurs as a consequence of a cascade of events which progress with increasing ischaemic severity or time. Discussed here are some of the pathologies associated with ischaemic heart disease and the relevance of hypoxia and redox status.

1.2.1 Atherosclerosis

Atherosclerosis is a chronic inflammatory disease of the arteries. The formation of atherosclerotic plaque in the arterial intima results in wall thickening and narrowing of the lumen[6]. Changes in arterial redox status and oxygen tension have been implicated in atherogenesis. Common risk factors for atherosclerosis include hypercholesterolaemia, diabetes, hypertension, smoking and age; each of which increase the likelihood of reactive oxygen species (ROS) generation in the endothelial, smooth muscle and adventitial cells of arteries[7]. ROS initiate endothelial activation which can lead to endothelial dysfunction, oxidation of low density lipoprotein (LDL), plaque formation and plaque rupture[8]. Atherosclerosis is initiated upon ROS induced endothelial activation which increases uptake of LDL into the vessel wall, migration of monocytes and their differentiation into macrophages. Macrophages then accumulate the oxidised-LDL to form foam cells. These lesions progress into plaques as a result of foam cell accumulation, smooth muscle cell migration from the arterial media to the site of the lesion and collagen deposition. As plaque formation progresses, the arterial lumen becomes narrowed limiting blood flow downstream and potentially resulting in

ischaemia. Plaques may also rupture and occlude the coronary vessels leading to acute coronary syndromes such as myocardial infarction[9]. Atherosclerosis is a complex pathophysiological process which may also give rise to coronary vasospasm, further inflammation, microvascular disease and endothelial dysfunction, all of which may result in myocardial ischaemia[10]. Although ROS play a key role in atherogenesis and plaque formation, plaques may also be hypoxic due to increased plaque size and/or elevated oxygen demand induced by inflammation[11].

1.2.2 Coronary artery disease

Coronary artery disease (CAD) is the progressive narrowing of coronary blood vessels due to atherosclerotic plaque formation. It is a chronic disease, which is generally asymptomatic for many years before any clinical manifestation. As CAD results from vessel narrowing rather than complete occlusion, blood flow is frequently restricted but may still be sufficient to prevent ischaemia at rest. Increased myocardial demand for blood, such as during exercise, can induce demand ischaemia resulting in chest pain (angina pectoris). In the long term, these frequent bouts of ischaemia may cause myocardial damage, tissue fibrosis and depressed cardiac function[12]. While the effects of CAD on the myocardium are commonly slow and progressive in combination with coronary artery spasm (CAS), they can be fatal. CAS is the sudden vasoconstriction of an epicardial coronary artery. CAS combined with CAD can result in complete vessel occlusion and severe myocardial ischaemia. While the pathogenesis of CAS is not fully understood, endothelial dysfunction and ROS generation have been implicated[13].

1.2.3 Coronary microvascular disease

Coronary microvascular disease (MVD) is a cardiovascular pathology affecting the microvessels which branch from myocardial coronary arteries. The microcirculation is responsible for matching blood flow with oxygen demand by regulating vascular resistance. Microvascular dysfunction can therefore cause a disparity between blood delivery and oxygen supply leading to hypoxia in the affected tissue. MVD can result from a wide variety of microvascular dysfunctions including vessel obstruction, vascular remodelling and endothelial and smooth muscle cell dysfunction. MVD can manifest in the presence or absence of CAD and the main symptom is chronic angina[14]. MVD has been suggested as the primary cause of angina in patients without any other cardiac or systemic diseases; however, currently there are no techniques available for the direct visualisation of coronary microvessels or the diagnosis of patients with MVD[13,15]. Coronary arteries can be imaged via angioplasty; however, this only detects gross cardiac perfusion and cannot detect areas affected by MVD where local perfusion is poor even when gross perfusion is normal. As MVD compromises myocardial blood flow and results in local myocardial ischaemia and hypoxia, a hypoxia tracer may be useful in identifying regions of the myocardium affected by MVD.

1.2.4 Myocardial hibernation

Myocardial hibernation is a term used to describe the downregulation of cardiac myocardial contractility in response to an impaired perfusion reserve[16]. It is currently unclear whether this low perfusion is constant, or periodic, and as

such causes low level chronic ischaemia or intermittent acute ischaemia, either of which could explain the chronic depression of cardiac contractility [17,18].

Myocardial hibernation can manifest for years after onset. As hibernating tissue is viable, it is potentially reversible by revascularisation surgery, but left untreated may lead to heart failure[19]. As the hibernating myocardium may be hypoxic, hypoxia specific imaging agents could provide new insights into this pathology and help guide revascularisation therapy in the future[5].

1.2.5 Myocardial hypertrophy

Various cardiac pathologies such as myocardial hibernation, ischaemia-reperfusion and myocardial infarction result in impaired contractile function. Myocardial hypertrophy is the enlargement of cardiac myocytes, a protective mechanism designed to overcome losses in contractile force[20]. Without compensatory angiogenesis, however, hypertrophic cells may become hypoxic due to an increase in the diffusion distance from blood vessels across the enlarged cells[21]. Although this adaptive mechanism serves to maintain cardiac contractile function and cardiac output, hypertrophy increases synthesis of extracellular matrix components such as collagen which induces myocardial fibrosis[22]. Fibrosis increases myocardial stiffness, therefore impairing cardiac function and can lead to heart failure[23]. Ischemia increases circulating levels of angiotensin II and tumour necrosis factor α (TNF-α), which increase hydrogen peroxide and superoxide generation by NADPH oxidases in cardiac myocytes and vascular smooth muscle cells[24]. ROS signalling has therefore been implicated as the origin of myocardial hypertrophy and may stimulate myocyte apoptosis by direct genotoxicity or by activating apoptotic pathways[8]. Hypoxia

and/or redox sensitive imaging modalities may therefore be beneficial in identifying hypertrophic myocardium.

1.3 Myocardial aerobic metabolism

The contracting myocardium needs a constant supply of adenosine triphosphate (ATP) to meet its high energy demands. Over 95% of ATP utilised by the heart is generated through mitochondrial respiration, and the remainder through glycolysis or guanosine triphosphate (GTP) synthesis from the tricarboxylic acid (TCA) cycle[25]. The mitochondria utilises substrates from the metabolism of a range of substrates including fatty acids, glucose, lactate, ketones and amino acids in order to generate ATP[26]. The main pathways involved in myocardial ATP production are described below.

1.3.1 Fatty acid β-oxidation

Fatty acid metabolism accounts for the majority (up to 70%) of ATP generation in the healthy adult heart [25]. The complete β-oxidation of an oleic acid molecule, for example, yields 146 ATP molecules. Fatty acids enter the myocardium via transport proteins in the sarcolemmal membrane and are converted into long-chain acyl coenzyme A (CoA) esters by fatty acyl CoA synthase (FACS) in the cytosol (figure 1.1 A). Carnitine palmitoyltransferase 1 (CPT1), situated on the outer mitochondrial membrane, converts these long-chain CoA esters to acylcarnitine, which enters the mitochondrial matrix via carnitine: acylcarnitine translocase (CAT) in exchange for carnitine. In the matrix, acylcarnitine is converted back to a long-chain acyl CoA via CPT2 and enters the β-oxidation

spiral (figure 1.1 B). At each cycle of the β-oxidation spiral, the long chain acyl CoA is shortened by two carbon atoms, producing flavin adenine dinucleotide ($FADH_2$), nicotinamide adenine dinucleotide (NADH), and acetyl CoA. The mitochondrial electron transport chain (ETC) utilises this $FADH_2$ and NADH to pump protons across the inner mitochondrial membrane to generate the proton gradient which drives ATP synthesis, (see section 1.3.3)[27,28].

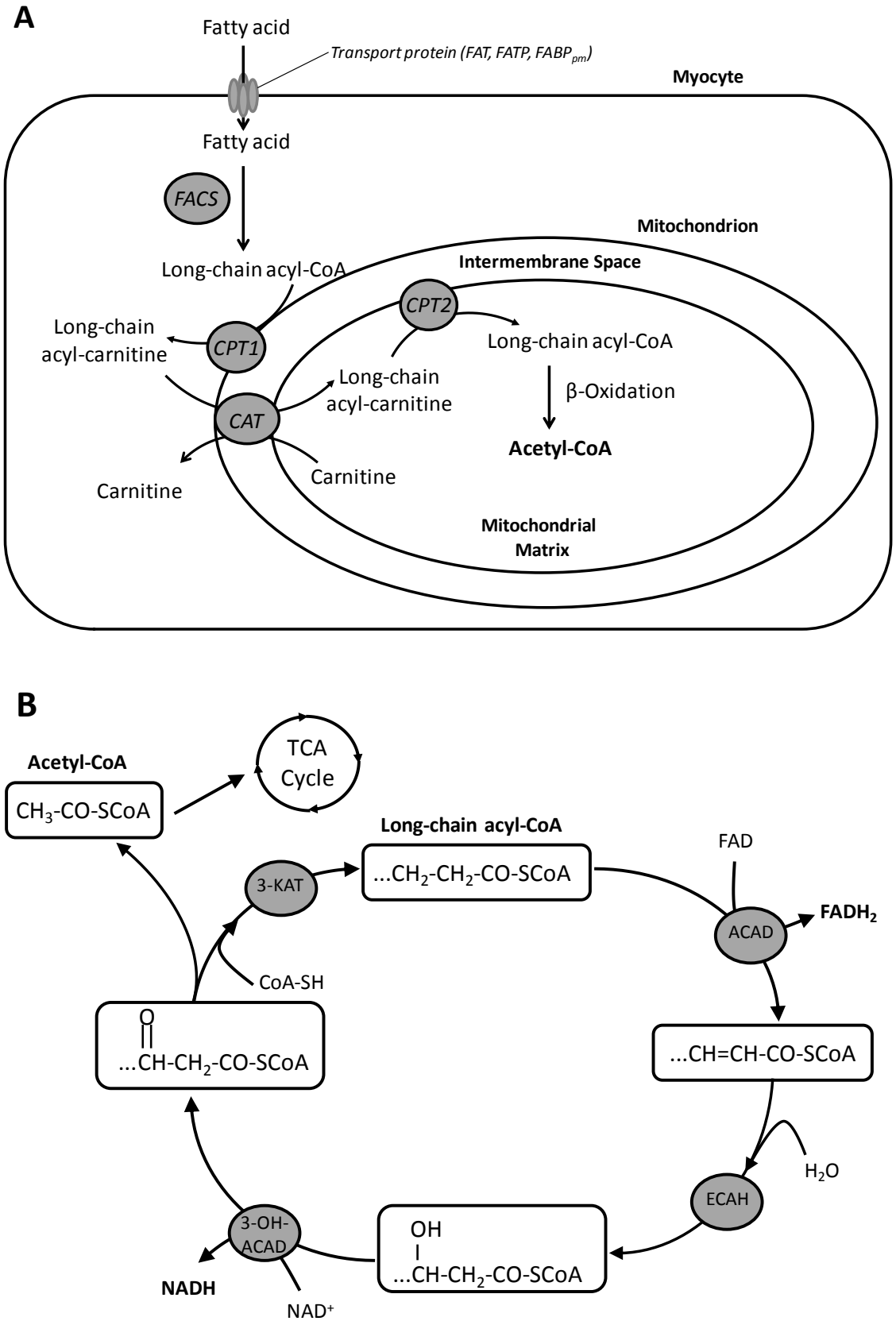

Figure 1.1. Fatty acid translocation (A) and subsequent β-oxidation (B). Adapted from Lopaschuk et al., 2010[25].

1.3.2 Glycolysis

In addition to fatty acid β-oxidation, glycolysis generates ATP directly, as well as providing further energy substrates for oxidation in the mitochondrion. One glucose molecule is converted to two molecules of pyruvate, generating two ATP and two NADH molecules (figure 1.2.)[29]. During aerobic glucose metabolism, pyruvate enters the mitochondria via monocarboxylase transporter (MCT), and is oxidised by pyruvate dehydrogenase (PDH) to acetyl CoA which then enters the TCA cycle[30]. A net of 31 ATP molecules are produced from the oxidative metabolism of one glucose molecule[31].

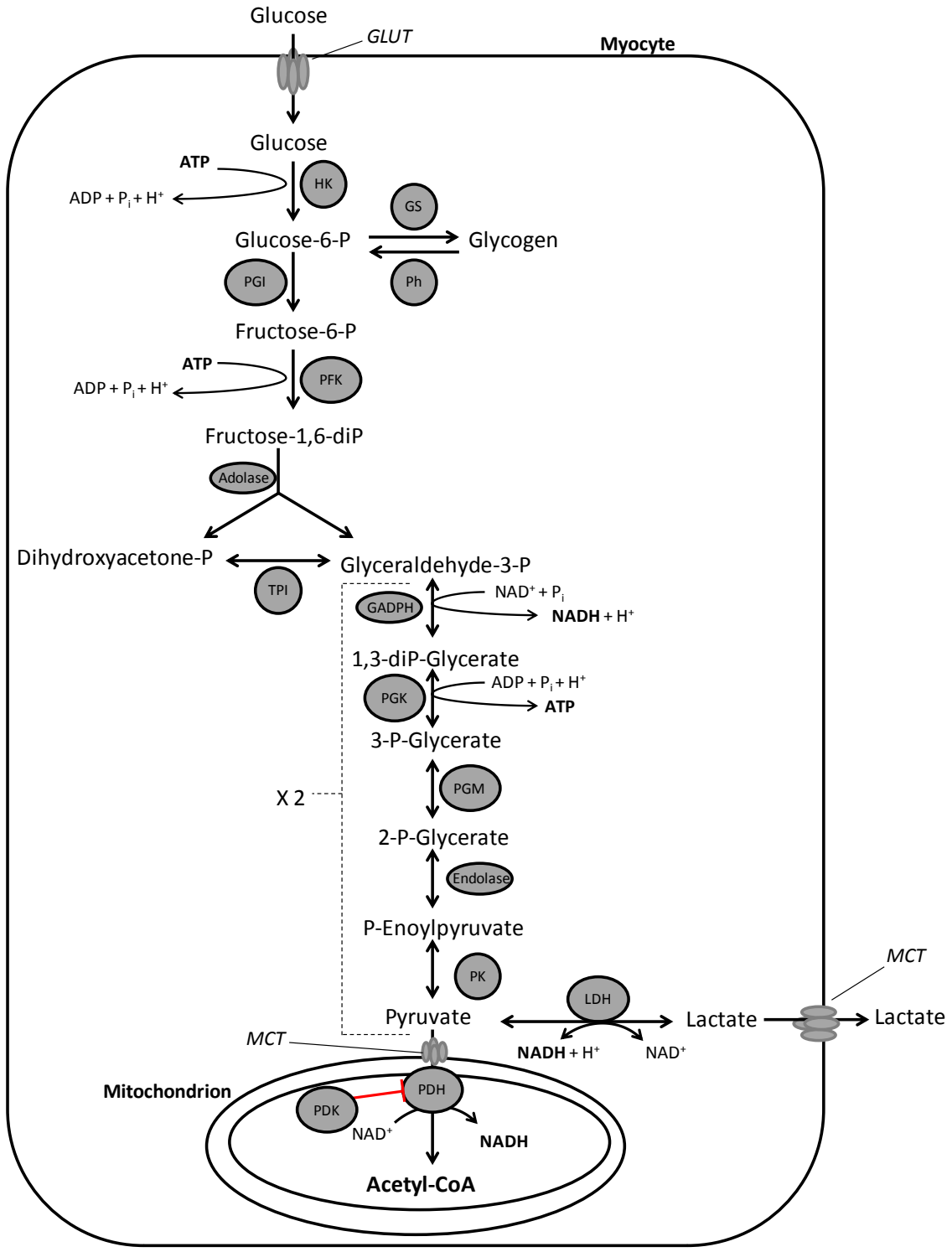

Figure 1.2. Glucose metabolism. Red bar represents inhibition of PDH. Adapted from Katz 1977, Jafri et al., 2001 and Depre et al., 1999[27,29,30].

1.3.3 The tricarboxylic acid cycle

Acetyl CoA produced from fatty acid β-oxidation and glycolysis is oxidised by the mitochondrial enzymes of the TCA cycle (figure 1.3). This process takes place in the mitochondrial matrix and generates further NADH and $FADH_2$ molecules for ATP production via the electron transport chain[29]. In addition, the hydrolysis of succinyl CoA results in the transfer of a high energy phosphate bond to guanosine diphosphate (GDP), generating a GTP molecule, which in turn transfers this bond to ADP to form an ATP molecule[27].

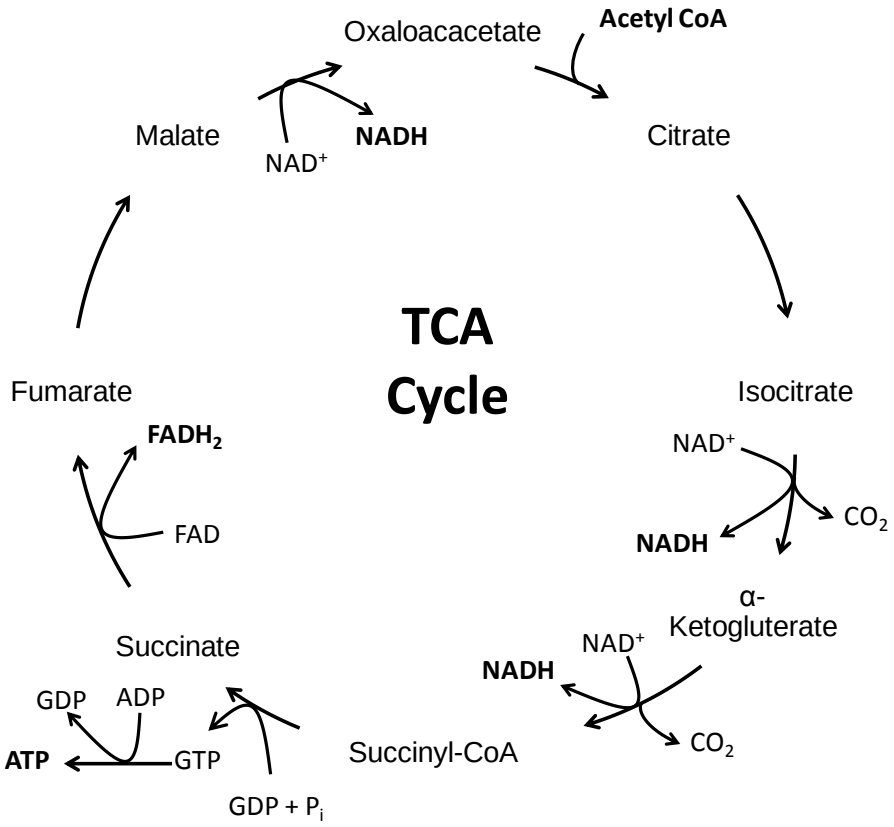

Figure 1.3. The tricarboxylic acid cycle. Adapted from Katz, 1977[27].

1.3.4 Mitochondrial respiration (oxidative phosphorylation)

The respiratory substrates NADH and $FADH_2$ are utilised by the mitochondria to generate ATP by a series of enzymatic complexes which form the ETC (figure 1.4). Complexes I-IV, ubiquinone (located in the inner mitochondrial membrane) and cytochrome c (in the intermembrane space) transfer electrons down a redox-potential gradient to oxygen at the end of the chain[29,32,33]. The oxidation of NADH at complex I and $FADH_2$ at complex II releases electrons which reduce ubiquinone to the mobile intramembrane electron carrier ubiquinol. Ubiquinol transfers these electrons to complex III, which reduces the haem group of the small mobile protein cytochrome c, which in turn reduces complex IV. Complex IV finally reduces molecular oxygen form water[34]. The passage of electrons through each of these proteins leads to the pumping of protons across the inner mitochondrial membrane from the matrix to the intermembrane space to generate a proton gradient. These protons re-enter the matrix down this gradient, by driving the rotation of the F_1 unit of ATP synthase, which catalyses the phosphorylation of ADP to generate ATP. As the terminal electron acceptor in this entire process, the reduction of oxygen is the fundamental rate limiting step for oxidative phosphorylation, and the reason that we are obligate aerobes.

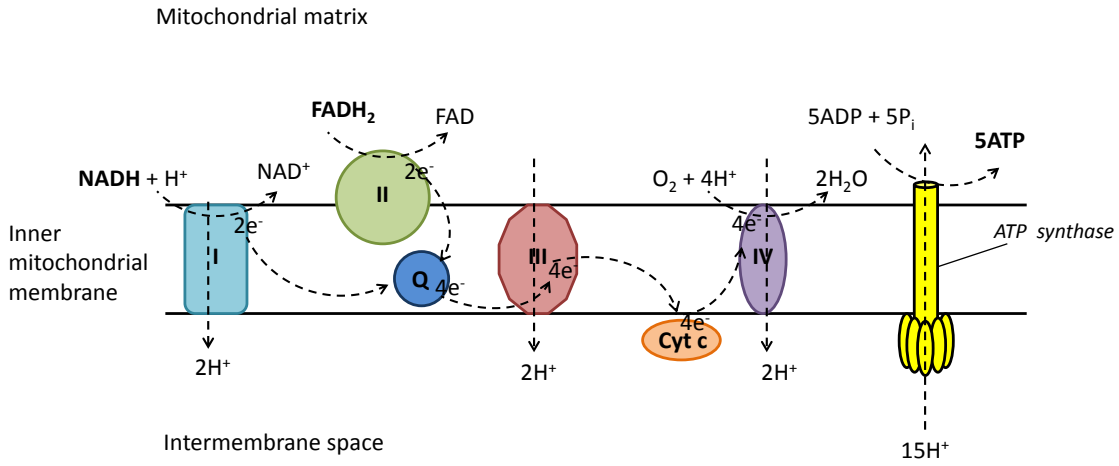

Figure 1.4. The mitochondrial ETC. Adapted from Fillmore and Lopaschuk, 2013 and Papa et al., 2012[31,32].

1.3.5 Myocardial anaerobic metabolism

Ischaemic heart disease is associated with a range of pathologies, including MVD, CVD, myocardial hibernation and hypertrophy, which are characterised as hypoxic due to disparities between blood flow and oxygen demand of the affected tissue[27].

As oxygen demand supersedes oxygen supply, less oxygen is available to accept electrons from complex IV of the mitochondrial ETC. This prevents the reduction of each complex and thus electrons are no longer transferred down the chain. As a result proton flux into the intermembrane space by complex I, III and IV ceases, the proton gradient becomes insufficient to drive ATP synthase, and ATP production stops[4,35]. As NADH and $FADH_2$ can no longer be recycled to their oxidised forms, the TCA cycle also becomes inhibited, and the heart becomes dependent upon anaerobic glycolysis to produce ATP.

Hypoxia-inducible factor 1 (HIF-1) is a transcription factor which exists in all cell types. HIF-1 binds to the hypoxia responsive element (HRE), located in the

promoter region of over 100 genes, to activate the transcription of genes which help cellular adaption to hypoxic conditions. Under normoxic conditions, HIF-1 is expressed as two separate subunits; HIF-1α and HIF-1β. HIF-1β is constitutively stable whereas HIF-1α proline residues become hydroxylated by prolyl hydroxylate enzymes which uses oxygen as a co-substrate. The von Hippel-Lindau protein targets hydroxylated HIF-1α subunits and labels them for rapid degradation by the proteasome. Factor inhibiting HIF (FIH) can also hydroxylate HIF-1α at the asparagine residue which prevents the binding of HIF-1α to transcriptional co-activators p300 and CREB-binding protein, therefore preventing activation of the HRE[36,37]. In conditions where oxygen is insufficient, however, hydroxylation of the HIF-1α subunit is prevented and HIF-1α translocates to the nucleus where it binds to HIF-1β bind to form a heterodimer. The HIF-1 heterodimer binds to the HRE and interacts with the transcriptional co-activators to induce gene transcription.

HIF-1 activation during hypoxia promotes glucose transporter 4 (GLUT-4) and hexokinase (HK) expression, and increases maximal myocardial glucose uptake and metabolism capacity[36]. HIF-1 also increases the expression of pyruvate dehydrogenase kinase (PDK) and lactate dehydrogenase (LDH). PDK inhibits the conversion of pyruvate to acetyl-CoA by PDH and therefore prevents pyruvate from entering the mitochondria. Pyruvate is then converted to lactate by LDH which recycles NADH to NAD^+ in the process. NAD^+ is required for further glycolysis, therefore increased expression of PDK and LDH increases ATP generation under low oxygen conditions[38]. Thus hypoxic tissue gains the capacity to both increase glucose uptake, and glycolytic flux.

As described earlier, the β-oxidation of oleic acid produces enough energy substrates to generate 146 ATP molecules via TCA cycle and oxidative phosphorylation. The complete aerobic metabolism of one molecule of glucose produces a net of 31 ATP molecules. During hypoxia, however, the complete anaerobic glycolysis only produces 2 ATP molecules per glucose molecule[39]. As anaerobic glycolysis is less efficient at generating ATP than aerobic energy metabolism, ATP is utilised faster than it is recycled. If the release of protons from ATP hydrolysis is not matched with the consumption of protons in ADP phosphorylation, protons accumulate and intracellular pH decreases. In ischaemic tissue the lack of residual flow causes protons to accumulate, resulting in tissue acidosis. Acidosis decreases the sensitivity of contractile proteins to Ca^{2+} which depresses cardiac contractile function[27,40,41].

The increase in proton concentration also stimulates Na^+ influx via Na^+/H^+ exchanger (NHE). Na^+ is extruded via the Na^+/Ca^{2+} exchanger (NCX) in exchange for Ca^{2+}, therefore acidosis increases intracellular Ca^{2+} concentrations. Elevated intracellular Ca^{2+} levels activate proteases and phospholipases which compromise the integrity of the cell through digestion of cytoskeleton proteins and membrane phospholipids[4]. Increases in Ca^{2+} also increases ROS generation via mitochondrial swelling and electron leakage, impairs myocardial relaxation and increases the susceptibility of the myocardium to arrhythmia[42].

The lack of ATP generated through anaerobic glycolysis also decreases Na^+/K^+ ATPase activity, leading to additional Na^+ influx and K^+ efflux. The imbalance in electrolytes increases membrane permeability, and therefore cell uptake of small ions and water, which causes the cell to swell[4,36]. Irreversible cell injury

from membrane phospholipid damage and/or loss and destruction to the cellular cytoskeleton results in myocardial infarction[43].

Whether hypoxia induces or suppresses mitochondrial ROS generation is currently controversial; it is likely a question of degree. In extreme hypoxia, the lack of oxygen as a substrate would inhibit ROS production. Several studies, however, have demonstrated that mitochondrial ROS generation increases in cardiac myocytes as a result of hypoxia[44,45]. Under normoxic conditions a small amount of electrons leak from complex I-III of the ETC and generate ROS in the mitochondrial matrix and intermembrane space[46]. As oxygen is the terminal electron acceptor, a lack of oxygen prevents the transfer of electrons down the ETC. This causes electrons to accumulate and increases electron leakage generating ROS under hypoxic conditions. In the normoxic cell cytochrome c is capable of scavenging superoxide. During hypoxia, the backlog of electrons means that cytochrome c remains in its reduced form; its ability to scavenge superoxide is suppressed and mitochondrial superoxide leakage increases[47]. ROS also prevents the hydroxylation of HIF-1α by proline dehydroxylase enzymes, therefore preventing HIF-1degradation and promoting transcription of HRE genes[48]. It is therefore possible that increased mitochondrial ROS generation in response to hypoxia is an oxygen sensing process which protects cardiac myocytes from hypoxia induced damage. Increased ROS generation causes lipid peroxidation and oxidative damage to cell proteins and DNA, , compromising cell membrane integrity, function, and ultimately cell viability[4].

1.3.6 Energy metabolism in the vascular endothelium

The energy demands and oxygen consumption of the endothelium are much lower than that of cardiac myocytes[49,50]. Under aerobic conditions the endothelium is capable of oxidising both fatty acids and glucose; however, the majority of endothelial cell ATP is generated via glycolysis[49,51]. LDH, glyceraldehyde phosphate dehydrogenase (GAPDH) and phosphofructokinase (PFK) activities are higher in endothelial cells, increasing lactate production under normoxic conditions. Lactate is extruded from the microvascular endothelium and diffuses across the endothelial membrane into the blood or surrounding cells, therefore endothelial derived lactate may be utilised by myocytes to produce additional ATP[52,53]. As endothelial oxygen consumption is relatively low compared to cardiac myocytes, endothelial energy metabolism is sustained at low oxygen tensions provided there is a sufficient glucose supply. A decrease in endothelial ATP production occurs only when oxygen tension falls to that comparable to zero flow ischaemia and endothelial cells are generally more resistant to hypoxia than cardiac myocytes[50].

1.4. Changes to cardiovascular redox status

The myocardium and vascular endothelium generate free radicals as a result of hypoxia and cardiac ischaemia-reperfusion. When radical generation exceeds antioxidant capacity to defend against it, the cell experiences oxidative stress (section 1.4.2). This triggers a cascade of events which depresses cardiac function in the acute term, increases the likelihood of arrhythmias, and

chronically can lead to heart failure[54,55]. It has been suggested that heart failure severity is proportional to the degree of free radical generation[56].

1.4.1 Reactive oxygen species

Free radicals are highly reactive chemical species which possess one or more unpaired electrons. The main free radicals implicated in the pathogenesis of heart failure are superoxide ($^{\cdot}O_2^-$), the hydroxyl radial ($^{\cdot}OH$) and hydrogen peroxide (H_2O_2)[57]. As these species are derived from oxygen they are termed reactive oxygen species (ROS). While H_2O_2 does not contain an unpaired electron and is not a free radical, it is a potent oxidising agent, and is therefore also considered a ROS[57]. $^{\cdot}O_2^-$ is generated by the direct reduction of molecular oxygen by an electron (equation 1a). Further reduction of $^{\cdot}O_2^-$, which may be carried by the antioxidant enzyme superoxide dismutase, generates H_2O_2 (1b) which in turn is reduced to $^{\cdot}OH$ by the iron catalysed Fenton reaction (1c). Finally, $^{\cdot}OH$ may be reduced to water (1d).

$$O_2 + e^- \longrightarrow {}^{\cdot}O_2^- \qquad (a)$$

$$2\,{}^{\cdot}O_2^- + 2H^+ + 2e^- \longrightarrow H_2O_2 \qquad (b)$$

$$H_2O_2 + H^+ + e^- \longrightarrow OH^{\cdot} \qquad (c)$$

$$OH^{\cdot} + H^+ + e^- \longrightarrow H_2O \qquad (d)$$

Equation 1.1. Generation of $^{\cdot}O_2^-$, $^{\cdot}OH$ and H_2O_2.

$^{\cdot}O_2^-$ is capable of either reduction or oxidation of other molecules and production of further $^{\cdot}OH$. $^{\cdot}OH$ is an even more reactive than $^{\cdot}O_2^-$, reacting with the first

molecule it comes into contact with. $^{\cdot}OH$ may also be produced by the spontaneous combination of $^{\cdot}O_2^-$ and H_2O_2 via the Haber-Weiss reaction (2a) or through the reaction $^{\cdot}O_2^-$ or H_2O_2 catalysed by transition metals (the Fenton reaction) which also generates further $^{\cdot}O_2^-$ (2b-d).

$$^{\cdot}O_2^- + H_2O_2 \longrightarrow O_2 + OH^{\cdot} \quad (a)$$

$$Fe^{2+} + H_2O_2 \longrightarrow Fe^{3+} + {}^{\cdot}O_2^- + OH^{\cdot} + OH^- \quad (b)$$

$$Fe^{3+} + H_2O_2 \longrightarrow Fe^{2+} + {}^{\cdot}O_2^- + H^+ \quad (c)$$

$$^{\cdot}O_2^- + Fe^{3+} \longrightarrow O_2 + Fe^{2+} \quad (d)$$

Equation 1.2. Further generation of $^{\cdot}O_2^-$ and $^{\cdot}OH$ through (a) the Haber-Weiss reaction (a) and (b-d) Fenton reactions.

Both $^{\cdot}O_2^-$ and $^{\cdot}OH$ are hydrophilic and do not passively diffuse across plasma membranes. $^{\cdot}O_2^-$ is transported across membranes via anion channels and can therefore affect adjacent cells. The life span of $^{\cdot}OH$ is much shorter due to its reactivity and therefore localises close to its site of production[58]. H_2O_2 is more stable and oxidises molecules more slowly, however, its lipophilicity allows membrane diffusion and therefore access to other cells or organelles where it can generate further $^{\cdot}O_2^-$ and $^{\cdot}OH$. Singlet oxygen ($^1O_2$) is another non-radical classified as a ROS and can arise from H_2O_2 reactions with hypochlorite ions (OCl^-; equation 3)[59]. It contains the same number of electrons as molecular oxygen, however, one of these electrons is in a higher energy orbital[57]. The excess energy of $^1O_2$ is released through light emission or reaction with other molecules.

$$Cl_2 + OH^- \longrightarrow Cl^- + OCl^- + H^+ \quad (a)$$

$$OCl^- + H_2O_2 \longrightarrow Cl^- + H_2O + {}^1O_2 \quad (b)$$

Equation 1.3. Generation of singlet oxygen. OCl^- generation (a) and reaction with H_2O_2 to produce $^1O_2$ (b).

1.4.2 Myocardial ROS generation

Several ROS generation pathways have been implicated in cardiac hypoxia and ischaemia-reperfusion injury. During ischaemia the myocardium releases chemotactic factors, such as TNF-α and interleukins, which stimulate neutrophil migration to ischaemic areas during reperfusion[60]. Neutrophil activation is a common feature in patients with heart failure and has been positively linked with increased infarct size[61]. Activated neutrophils generate $^{\cdot}O_2^-$ by NADPH-dependent oxidase resulting in further H_2O_2, $^{\cdot}OH$ and $^1O_2$ generation. These ROS stimulate further inflammation by activating further chemotactic factors resulting in additional neutrophil activation, migration to the endothelium and further cytotoxic $^{\cdot}O_2^-$ generation[57]. Neutrophils also produce chloramine (NH_2Cl), a lipophilic radical capable of reacting with peptide bonds resulting in protein damage. Neutrophil depletion decreases myocardial infarct size caused by ischaemia-reperfusion in dogs, further supporting the role of neutrophil derived ROS in ischaemia-reperfusion injury[62].

As mentioned in section 1.3.4, oxygen is utilised in the mitochondria as the terminal electron acceptor at complex IV of the ETC. Under normal physiological conditions, up to 5% of this oxygen leaks from this pathway and is converted to $^{\cdot}O_2^-$ via univalent reduction[57]. During hypoxia or ischaemia,

however, acidosis increases $^{\cdot}O_2^-$ protonation, forming the highly reactive hydroperoxyl radical ($^{\cdot}HO_2$)[63].

The mitochondrial permeability transition (MPT) describes the opening of the mitochondrial permeability transition pore (MPTP) in the inner mitochondrial membrane, stimulated by increases in Ca^{2+} and inorganic phosphate (P_i) levels[64], which increases its permeability to solutes of molecular masses up to 1500 Da[65]. Not only does it depolarise and uncouple the mitochondria, but it also causes mitochondrial damage by osmotic swelling. With elevated intracellular Ca^{2+} and P_i levels, hypoxia increases the propensity for MPTP opening and ETC uncoupling. As the ETC uncouples, its capacity to leak electrons increases, causing increased ROS formation. As the MPTP are open at this point, this may also increase the likelihood of ROS to leaking into the cytosol[57,66].

The continued breakdown of ATP during hypoxia leads to an increase in intracellular ADP and AMP, and their further breakdown to the nucleosides adenosine and inosine and the purines, hypoxanthine and xanthine[67]. While xanthine and hypoxanthine are usually oxidised to urea by xanthine dehydrogenase using NAD^+ as an electron acceptor, Ca^{2+} dependent proteases convert xanthine dehydrogenase to xanthine oxidase during ischaemia[68] which uses oxygen as an electron acceptor, to generate $^{\cdot}O_2^-$. Increased $^{\cdot}O_2^-$ generation has been documented in various models of ischaemia-reperfusion *in vivo*, which is suppressed by the xanthine oxidase inhibitor allopurinol, implicating xanthine oxidase as a ROS source[57]. Allopurinol also decreased myocardial infarct size in canine hearts post ischaemia, further

demonstrating the role of xanthine oxidase derived $^{\cdot}O_2^-$ in myocardial ischaemia-reperfusion injury[69].

1.4.3 Endothelial nitric oxide generation

Nitric oxide (NO) contains one unpaired electron and reacts rapidly with other molecules including $^{\cdot}O_2^-$. The reaction between NO and $^{\cdot}O_2^-$ generates peroxynitrite ($ONOO^-$) which can generate further $^{\cdot}OH$ (equation 4).

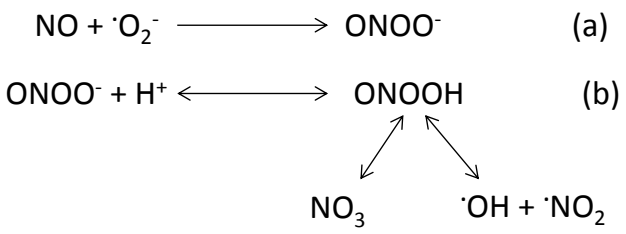

Equation 1.4. Reaction of NO with $^{\cdot}O_2^-$ (a) generates nitrogen radicals and $^{\cdot}OH$ (b).

Although NO is capable of forming potentially damaging $ONOO^-$ and $^{\cdot}OH$, it is also an important cell signalling molecule, and is generated by several nitric oxide synthase (NOS) isoforms. Endothelial NOS (eNOS) produces NO to induce vascular relaxation and maintain coronary perfusion pressure[57]. During reperfusion following ischaemia, NO generation increases and induces vasorelaxation to facilitate blood flow to ischaemic tissue. NO also inhibits many atherogenic processes including platelet aggregation and adhesion, oxidation of LDL by macrophages and smooth muscle cells proliferation[57].

1.4.4 Lipid, protein and DNA damage

Lipid peroxidation is a well characterized effect of ROS production and can result in significant damage to the phospholipid membranes of cells and

organelles, with serious implications for cell integrity and function[8]. ROS react with lipid molecules to create lipid radicals (equation 5), which in turn react with molecular oxygen to create lipid peroxy radicals (lipid-OO$^{\cdot}$). Lipid-OO$^{\cdot}$ initiate a chain reaction by reacting with other lipids to generate further lipid radicals.

$$^{\cdot}OH + \text{Lipid-H} \longrightarrow H_2O + \text{Lipid}^{\cdot}$$

$$\text{Lipid}^{\cdot} + O_2 \longrightarrow \text{Lipid-OO}^{\cdot}$$

$$\text{Lipid-OO}^{\cdot} + \text{Lipid-H} \longrightarrow \text{Lipid-OOH} + \text{Lipid}^{\cdot}$$

Equation 1.5. Lipid peroxidation cascade.

In the presence of transition metal ions, lipid peroxides (lipid-OOH) are converted to either lipid-OO$^{\cdot}$ or alkoxy radicals (lipid-O$^{\cdot}$) which can also cause structural changes to the cell membrane[57]. In addition to playing a role in lipid peroxidation, lipid-OOH interfere with proteins by initiating polymerisation, breaking peptide chains and oxidising amino acids to form carbonyl and sulphydryl derivatives[70]. Damage to membrane proteins, such as transmembrane ion channels, also compromises membrane integrity. ROS mediated lipid and protein damage may therefore induce increased membrane permeability, cellular swelling and cellular necrosis.

Non-membrane bound proteins are also vulnerable to ROS damage. $^{\cdot}OH$ may promote protein polymerisation, resulting in cross linkages between two or more proteins. This may denature contractile proteins or decrease Ca^{2+} sensitivity, which would account for depressed contractile function following ischaemia-reperfusion[8,57]. $^{\cdot}OH$ may also react with purine and pyrimidine bases and deoxyribose, resulting in DNA damage[59]. $^{1}O_2$ is also capable of attacking carbon : carbon double bonds and may induce DNA, protein and lipid damage[59].

1.4.5 The effect of ROS upon Ca^{2+} and Na^{+} homeostasis

The sarcoplasmic reticulum of muscle is responsible for intracellular Ca^{2+} homeostasis and sequesters intracellular Ca^{2+} via Ca^{2+}ATPase, which is essential for initiating muscle relaxation following contraction. ROS have been demonstrated to decrease Ca^{2+}ATPase activity, which decreases sarcoplasmic reticulum Ca^{2+} reuptake and interferes with contractile function during reperfusion following ischaemia[8,57]. As a result, intracellular Ca^{2+} overload leads to activation of contractile proteins and excessive force generation causing hypercontraction and decreased diastolic relaxation[71]. Hypercontraction causes severe injury to myocyte cytoskeletal structures and, if irreversible, initiates cellular necrosis.

The sarcolemmal membrane Na^{+}/K^{+} ATPase maintains intracellular Na^{+} and K^{+} concentrations and therefore is important for membrane potential regulation. Damage of the Na^{+}/K^{+} ATPase by ROS contributes to ischaemia-reperfusion injury by elevating intracellular Na^{+} levels, adding to the Na^{+} caused by acidosis[57,66]. As mentioned earlier, Na^{+} enhances Ca^{2+} pool levels by the NCX, therefore an increased intracellular Na^{+} exacerbates Ca^{2+} overload and hypertrophy.

1.4.6 The effect of ROS upon endothelial dysfunction

Endothelial NO production is an important signalling molecule initiating vasorelaxation and preventing atherosclerosis. An increase in ROS, however, decreases NO availability through direct interaction (generating $^{\cdot}OH$) or the downregulation of eNOS[57]. NO depletion decreases the responsiveness of the

endothelium to stimuli, decreases NO dependent vasorelaxation and results in loss of endothelial cells, termed as endothelial dysfunction. Endothelial dysfunction contributes to hypertension, atherosclerosis and other acute coronary syndromes with often lead to heart failure [55,72]. Most of the ROS responsible for endothelial dysfunction derives from inflammatory cytokines, which initiate a vicious cycle of further ROS generation, inflammation and endothelial dysfunction[72].

1.4.7 Antioxidants

Redox status is a term which describes the balance between free radical generation and antioxidant capacity. Antioxidants are molecules which detoxify oxidants, such as free radicals, and prevent the oxidation of other molecules[73]. They are therefore essential in protecting the heart from ROS induced injury. Superoxide dismutase (SOD), catalyses the dismutation of $^{\cdot}O_2^-$ to H_2O_2, which in turn is decomposed to water and oxygen by catalase. α-tocopherol (Vitamin E) reacts with peroxyl radicals to yield a stable tocopheroxyl radical which is recycled back to α-tocopherol by ascorbate. Ascorbate also scavenges $^{\cdot}O_2^-$, $^{\cdot}HO_2$ and $^{\cdot}OH$[59]. Glutathione peroxidise (GSH-Px) uses reduced glutathione (GSH) as a substrate to decompose peroxides (including lipid peroxides and H_2O_2) to form water and oxidised glutathione (GSSG). GSH itself is an antioxidant which has a strong tendency to donate electrons and is capable of reducing other molecules directly, therefore is capable of recycling other oxidised antioxidants, for example, ascorbate.

Numerous studies have demonstrated the importance of the antioxidant system in protecting the heart from ROS induced injury. For example, mice over expressing SOD subjected to ischaemia for 35 minutes displayed decreases in myocardial infarction size post ischaemia compared to wild type mice[74]. SOD knockout mice display more myocardial hypertrophy in response to ischaemia induced myocardial infarction compared to wild type mice[75]. Upon reperfusion, SOD administration improved myocardial contractile function in ischaemic-reperfused rabbit hearts compared to control hearts[76]. GSH administration also improved myocardial contractile dysfunction on the reperfusion of ischaemic isolated rat hearts[77]. Ascorbate and α-tocopherol have also been implicated in the protection against ischaemia induced myocardial injury[78,79]. These studies emphasise the importance of ROS generation and altered redox status in myocardial dysfunction.

To summarise, hypoxia and ROS generation, and changes in cellular redox status as a result of myocardial ischaemia can eventually cause irreversible cell injury, leading to necrosis and myocardial infarction. Identification of hypoxic myocardium and/or altered myocardial redox status may therefore provide an opportunity to diagnose vulnerable tissue and intervene before ischaemic injury becomes irreversible.

1.5 Current techniques for the detection of cardiac redox status

Currently, most redox sensing techniques involve the detection of free radicals rather than antioxidants. The short half-life of free radicals limits the direct detection of their formation in real time in biological systems. Although

technically challenging, some techniques have been developed to measure free radical generation and redox status. There is, however, a need to for better redox sensitive probes that are practical for the measurement of cardiac redox biology.

1.5.1 Electron paramagnetic spin resonance spectroscopy

EPR spectroscopy has been utilised for decades for the detection of free radicals in the heart. A variety of spin traps have been developed which, upon reaction with free radicals, form stable spin adducts which are detectable by EPR spectroscopy. The burst of free radicals associated with reperfusion following ischaemia, for example, has been measured in real time using EPR spectroscopy with spin traps N-tert-butyl-a-phenylnitrone (PBN) and 5,5-di-methyl- 1-pyroline-n-oxide (DMPO) in isolated perfused rat and rabbit hearts[80-82]. Although EPR spectroscopy is a common technique utilised for *ex vivo* free radical detection and has a number of probes specific for individual free radicals, it has several limitations. EPR spectroscopy lacks sensitivity and therefore requires potentially toxic concentrations of spin traps in order to gain a measurable signal[57]. It is not ideal for detection of free radicals *in vivo* as spin traps and adducts may be metabolised. The instability of spin adducts *in vivo* also limits its use. As EPR spectroscopy quantifies the products of ROS and spin trap reactions it does not measure ROS directly. Furthermore, ROS-spin trap interactions may be affected by changes in exogenous or endogenous cellular components[83].

1.5.2 Fluorescent ROS probes

A vast number of fluorescent probes have been developed for ROS detection. Like EPR, fluorescent redox probes form products upon reaction with targeted ROS. Dihydroethidium (DHE), for example, is oxidised by $^{\cdot}O_2^-$, forming the fluorescent ethidium which is measurable by excitation fluorescence 355nm/ emission at 480 nm[84]. N-acetyl-3,7-dihydroxyphenoxazine (amplex red) reacts with H_2O_2 to produce the highly fluorescent resorufin and sodium terephthalate reacts with $^{\cdot}OH$ to produce fluorescent bi-product 2-hydroxyterephthalate (excitation 530nm/emission 590nm)[85]. Used appropriately, fluorescent probes can be a good method of measuring ROS due to high spatial resolution and sensitivity. Although DHE is specific for $^{\cdot}O_2^-$ it can also catalyse the dismutation of $^{\cdot}O_2^-$ therefore the fluorescence signal may decrease with increasing $^{\cdot}O_2^-$ concentrations[86]. Furthermore, it has been suggested that $^{\cdot}OH$ decreases ethidium fluorescence[87]. At concentrations above 50 µM/ L amplex red can auto-oxidise to produce $^{\cdot}O_2^-$ and H_2O_2 which would interfere with the fluorescence signal[84]. Use of these probes is therefore limited in the detection of ROS generation associated with ischaemia and/or hypoxia.

1.5.3 Luminescence

Luminescent techniques can be used to measure the emission of light as a result of ROS generation. For example, $^1O_2$ has one electron at a higher energy state and emits the surplus energy as light when relaxes to its ground state[57]. Although luminescence can be used to measure $^1O_2$ on a cellular level, its

application for quantifying $^1O_2$ in intact tissues *in vivo* is hampered by light absorption, scatter, and the very low levels of light emitted[88].

The chemiluminescence probe lucigenin is specific for detecting $^{\cdot}O_2^-$. Lucigenin is reduced by $^{\cdot}O_2^-$ to form a lucigenin radical. The lucigenin radical reacts with a second $^{\cdot}O_2^-$ to generate an energy rich dioxetane molecule which then emits light[84]. Although lucigenin is specific for $^{\cdot}O_2^-$, the lucigenin radical produced upon its reduction is capable of reacting with molecular oxygen to create further $^{\cdot}O_2^-$. Lucigenin could therefore overestimate ROS generation.

1.5.4 Ascorbyl radicals

Most redox sensitive probes target free radicals directly. An alternative approach is to measure the change in antioxidant status as an indirect index of ROS production. Virtually every ROS is capable of oxidising ascorbate to an ascorbate radical, which can be detected directly by EPR spectroscopy[57]. More recently this approach has been enhanced by quantifying the uptake and metabolism of hyperpolarised ascorbate and/or dehydroascorbate by ^{13}C-NMR spectroscopy [89-91]. The ratios of ^{13}[C]-dehydroascorbate and ^{13}[C]-ascorbate detected by NMR spectroscopy can therefore give real time measurements of intracellular ROS and antioxidant activity and therefore redox status. To date ^{13}[C]-dehydroascorbate and ^{13}[C]-ascorbate have been detected in whole mice and rats *in vivo*. Hyperpolarised ^{13}[C] labelled complexes, however, undergo rapid thermal decomposition and the signal can decay in minutes, limiting the time course of the experiment to minutes rather than hours. It also requires the injection of supraphysiological concentrations of substrates which may

significantly alter the kinetics of the systems under investigation, requiring great care in the interpretation of the data that it achieves. Nevertheless, while still in its infancy, this approach shows promise as a potential means of probing intracellular redox status.

1.6 Current techniques for the detection of myocardial hypoxia

1.6.1 Invasive probes

Oxygen sensing needles, such as the Eppendorf polygraphic electrode and Oxylab/Oxylite™ systems, are the current gold standard method in measuring tissue oxygenation[92]. The Eppendorf polygraphic electrode consists of a gold cathode and silver-chloride anode which electrochemically reduce oxygen at the probe tip. The current produced is proportional to the partial pressure of oxygen. The oxygen consumption of these probes, however, leads to a decrease in signal over time, potentially leading to an underestimation of tissue pO_2[93]. In contrast, the Oxylite system contains a fibre optic tip which is quenched in the presence of oxygen, therefore the signal increases with decreasing oxygen[94]. These electrodes are capable of reading lower pO_2 than polygraphic electrodes and can be kept in the same location over time. However, both of these techniques are invasive, and often need guidance via ultrasound or computed tomography (CT) to place a needle containing the electrode in the correct tissue. They are more commonly used in assessing tumour pO_2 and have not yet been used for the detection of myocardial hypoxia. Even if this was possible, oxygen sensing probes can only be placed in accessible blood vessels or interstitial spaces and cannot measure intracellular pO_2 directly. They also offer

little or no spatial information and are of limited use in providing diagnostic or prognostic information in cardiology.

1.6.2 Non-invasive imaging

Various imaging techniques have been employed for the assessment myocardial ischaemia. Most of these techniques measure contractile function, tissue perfusion, cellular metabolism, and do not directly identify myocardial hypoxia. This section discusses some of the imaging modalities currently used to identify ischaemic myocardium.

1.6.2.1 Magnetic resonance imaging

Magnetic resonance imaging (MRI) is a technique that uses the natural magnetic properties of the body to provide anatomical and functional information. Protons possess a spin which makes them act like a magnetic dipole. An MRI scanner applies a large external magnetic field to the patient, which causes an alignment of the proton axes, either in line with this field (low energy state), or antiparallel to this field (high energy state). An oscillating radiofrequency is applied which perturbs the magnetisation, followed by a recovery period in which initial equilibrium is restored (hence Nuclear Magnetic Resonance). This is characterised by two relaxation times; T_1 which is a time constant for the recovery of magnetisation and T_2 which is a time constant for the decay of magnetisation. Water T_1 and T_2 vary between different tissues and environments; therefore the contrast of an MRI image is dependent on factors which effect T_1 and T_2[95].

Blood oxygen level dependent (BOLD) MRI is an example of how MRI can be used to measure oxygen status. BOLD-MRI detects the difference between levels of oxyhaemoglobin and deoxyhaemoglobin as a measure of blood oxygenation[96]. As haemoglobin becomes deoxygenated its magnetisation increases which causes a more rapid decay of magnetisation (T_2) of the water molecules that surround it, resulting in an oxygen-dependent loss of signal. As BOLD-MRI measures the oxygen status of haemoglobin in the bloodstream, it does not detect tissue hypoxia directly. The oxygenation of the myocardium itself would be better quantified by detection of myoglobin oxygenation, which is possible but it is difficult to quantify and produces a particularly weak signal; methods to detect this are only in the early stages of development[97].

1.6.2.2 Cardiac Nuclear Medicine

The term emission tomography encompasses the two major imaging modalities used in nuclear medicine: single photon emission computed tomography (SPECT) and positron emission tomography (PET). Both SPECT and PET are used to detect radioisotopes which have been injected into a subject. SPECT is used to detect radioisotopes which emit a single gamma ray photon upon decay. A collimator filters gamma rays travelling in a specific direction which are then detected by a gamma camera. The paths of the emitted gamma rays can then be used to determine the site of radioisotope decay for image reconstruction. PET detects radioisotopes which upon decay emit positrons. The emitted positrons collide with surrounding electrons and annihilation occurs, resulting in the emission of two photons which travel in opposite directions. PET utilises an array of gamma cameras surrounding the subject to

detect the gamma rays as they are emitted. Because the system detects two positrons at 180 degrees to each other (using coincidence circuitry to select those that arose from the same annihilation), the paths of the gamma rays can be used to determine the site of radioisotope decay without the use of collimators[98].

Numerous radiotracers have been developed for the detection of ischaemic or hypoxic tissue using SPECT or PET. Perfusion radiotracers are commonly used to image myocardial blood flow and characterise tissue at risk of ischaemia. The PET tracer $^{13}NH_3$ is extracted from the blood by well perfused tissue and is converted to glutamine to become trapped within cardiac myocytes[99,100]. The SPECT tracer ^{99m}Tc-sestamibi is also extracted by well perfused myocardium and accumulates in the mitochondria of viable myocytes. The depolarisation of the mitochondrial membrane, which occurs with ischaemia induced injury, results in the decreased uptake of ^{99m}Tc-sestamibi[100]. Although imaging myocardial perfusion provides an indication of tissue at risk of ischaemia and hypoxia, these tracers rely on energy dependent processes to become trapped. These tracers therefore do not image perfusion alone and may underestimate perfusion in hypoxic regions of the myocardium where flow is normal, but energy is depleted[5].

The PET tracer ^{18}F-Fluorodeoxyglucose (^{18}FDG) is a glucose analogue used to assess tissue glucose metabolism. ^{18}FDG is transported into cells by glucose transporters where it is phosphorylated to ^{18}FDG-phosphate by hexokinase to become trapped in the myocardium[101]. While a small proportion of ^{18}FDG-phosphate undergoes further metabolism, the majority of these metabolites also remain trapped within the myocardium, which mean that it is a generally

accepted, although possibly a flawed means of assessing glucose utilisation[102]. As hypoxic tissue switches from fatty acid to glucose metabolism, an increase in cardiac ^{18}FDG uptake delineates hypoxic regions in the myocardium. Metabolic tracers, however, are not specific to changes in metabolism due to hypoxia alone. Cardiac uptake of ^{18}FDG is affected by blood glucose concentrations, dietary status, and diabetes, all of which are potentially confounding factors in interpreting cardiac ^{18}FDG PET scans, as is the fact that increased ^{18}FDG uptake is also characteristic of inflammatory processes[5].

1.7 Nitroimidazoles for imaging tissue hypoxia

Nitroimidazoles were originally developed as radiosensitisers to improve the effectiveness of radiotherapy in hypoxic tumours[103]. Their ability to target hypoxic tissue has since lead to their development as hypoxia targeting probes. A variety of radiolabelled nitroimidazoles have been investigated as hypoxia imaging agents for PET (^{18}F) and SPECT (^{99m}Tc). The mechanism of nitroimidazole hypoxia selectivity is shown in figure 1.5. Nitroimidazole compounds are lipophilic, and passively diffuse across cells membranes regardless of oxygen status. Intracellularly, the nitroimidazole becomes reduced to a radical form, $R\text{-}NO_2^{\cdot -}$. Under normoxic conditions, $R\text{-}NO_2^{\cdot -}$ is reoxidised by molecular oxygen to an uncharged $R\text{-}NO_2$, which passively diffuses out of the cell ($^{\cdot}O_2^-$ is released as a by-product in this process). In hypoxic environments, however, the lack of oxygen favours the retention of the charged, less permeable $R\text{-}NO_2^{\cdot -}$ species. This species can also reduce further to nitroso, hydroxylamine and finally amine compounds, the latter of which may bind to macromolecules to become trapped.

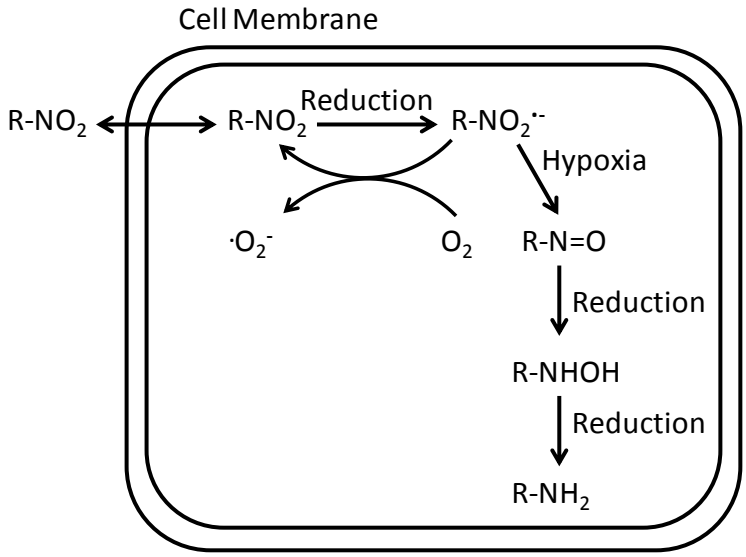

Figure 1.5. Hypoxia selective trapping mechanism of nitroimidazole compounds. Adapted from Martin et al., 1990[103].

Of the various nitroimidazole derivatives, ^{18}F labelled misonidazole (^{18}FMISO) is the most extensively researched, mostly for applications in oncology, although its potential application in cardiology has also been explored. Increased ^{18}FMISO retention has been demonstrated in hypoxic cardiomyocytes[104] and ischaemic myocardium in canine hearts post coronary artery occlucion[104-106]. Furthermore, ^{18}FMISO retention was greater in viable regions of the heart compared to necrotic regions, and was found to be inversely related to blood flow, demonstrating its potential for selective non-invasive hypoxia imaging[106,107]. Imaging of the heart, however, was only possible 60 minutes post ^{18}FMISO injection, because it clears very slowly from the blood, and has a very low first pass tissue uptake. It also exhibits very high hepatic uptake, which may be problematic for imaging the heart. It has therefore been suggested that for optimum signal detection, imaging with ^{18}FMISO should be performed at least 2 hours post injection [108]. Due to the short half-life of ^{18}F (110 minutes), a higher

dose of injected radioactivity would be required for a sufficient signal after an hour or more, increasing the radiation dose of the subject, which is not ideal.

Other radiolabelled nitroimidazoles investigated for their hypoxia targeting properties include SPECT agent ^{99m}Tc-BMS181321 and PET agent ^{18}F-fluoroazomycin arabinoside (^{18}F-FAZA). ^{99m}Tc-BMS181321 displays similar properties to ^{18}FMISO as it accumulates in hypoxic, viable myocardium and retention is independent of flow[103]. Like ^{18}FMISO, however, ^{99m}Tc-BMS181321 is limited as a hypoxia imaging agent due to its slow clearance from normoxic tissue and high first pass liver uptake. ^{18}F-FAZA displays better clearance from both blood and normoxic tissue than ^{18}FMISO, but has a poorer hypoxic to normoxic retention than other nitroimidazoles[92]. These limitations have prevented the transition of radiolabelled nitroimidazoles for use as cardiac hypoxia imaging agents in the clinic.

1.8 Copper bis (thiosemicarbazone) (Cu-BTSC) complexes

There is a growing body of experimental evidence demonstrating the hypoxia selectivity of Cu-ATSM. ^{64}Cu-ATSM has displayed higher hypoxia sensitivity than other Cu-BTSC complexes, including ^{64}Cu-pyruvaldehyde-bis-(N^4-methylthiosemicarbazone) (^{64}Cu-PTSM), in hypoxic Chinese hamster ovary cells[109] and EMT6 tumour cells[110-112]. ^{64}Cu-ATSM also displayed significantly higher hypoxia selectivity than ^{18}FMISO in EMT6 cells[112]. $^{61/64/67}$Cu-ATSM retention in hypoxic regions of tumours *in vivo* has been demonstrated, whereas ^{64}Cu-PTSM displayed non-specific tissue distribution[*112,113*]. ^{64}Cu retention from ^{64}Cu-ATSM has also been demonstrated in cardiac myocytes[114] and in an *ex vivo* isolated perfused rat heart model during hypoxia but not normoxia[114,115].

Lewis *et al*. used three models of hypoxia in dogs to demonstrate the hypoxia selectivity of $^{60/61/64}$Cu-ATSM in the heart: global hypoxia induced by inhalation of hypoxic gas, acute ischaemia by occlusion of the LAD and demand ischaemia by LAD stenosis with dobutamine administration to increase heart rate[116]. Significant accumulation of Cu from Cu-ATSM was seen in hypoxic regions of all three heart models.

While ^{60}Cu-ATSM has been approved for the clinical diagnosis of lung tumours at Washington University Medical School (St. Louis, US)[112] there have been few trials investigating the potential of Cu-ATSM for the diagnosis of hypoxic myocardium. A preliminary clinical trial in 2001 compared the accumulation of ^{18}FDG to that of ^{62}Cu from ^{62}Cu-ATSM in seven patients with CAD[117]. While accumulation of ^{18}FDG was detected in five of these patients, ^{62}Cu accumulation was only detected in one. It is possible that ^{62}Cu-ATSM is only capable of detecting very severe hypoxia, which is inducible (and survivable) in acute experimental models, but does not commonly occur in cardiac patients. Other analogues of Cu-ATSM are currently being screened, which selectively accumulate in myocardium at less severe degrees of hypoxia.

Although it has been established that Cu-ATSM targets hypoxic tissue, there may be other important factors which contribute to Cu-ATSM hypoxia selectivity. The importance of such factors on Cu-ATSM hypoxia selectivity is still relatively under researched, yet understanding them is crucial for the appropriate application of any tracer[5].

1.8.1 The proposed trapping mechanism of Cu-BTSC complexes

Figure 1.6 displays a proposed mechanism of the trapping of a hypoxia selective Cu-BTSC[5]. Cu-BTSC are small, lipophilic complexes and enter the cell through passive diffusion across the cell membrane. Intracellularly, the Cu-BTSC encounters bioreductive molecules (as yet unidentified) which reduce the chelated Cu^{2+} to Cu^{+}, converting the neutral Cu(II)-BTSC species to a charged $[Cu(I)\text{-}BTSC]^{-}$ species, which is less lipophilic, and therefore less capable of diffusion out of the cell[118]. If the cell is normoxic and has sufficient oxygen, the $[Cu(I)\text{-}BTSC]^{-}$ species is readily re-oxidised back to Cu(II)-BTSC, which may diffuse out of the cell and wash out into the blood stream. If the $[Cu(I)\text{-}BTSC]^{-}$ encounters a more hypoxic environment, however, the lack of oxygen prevents reoxidation to Cu(II)-BTSC. The $[Cu(I)\text{-}BTSC]^{-}$ is less stable than Cu(II)-BTSC and may dissociate to the BTSC ligand and the copper ion, which becomes trapped. It has been suggested that the [Cu(I)-BTSC] complex is prone to protonation, forming the Cu(I)-BTSCH complex, before dissociation of copper from the ligand[119,120]. An acidotic environment where protons are more abundant may therefore accelerate the dissociation of copper from the ligand[118]. The free copper released by the complex is then chelated by intracellular macromolecules (currently unidentified) and trapped[121].

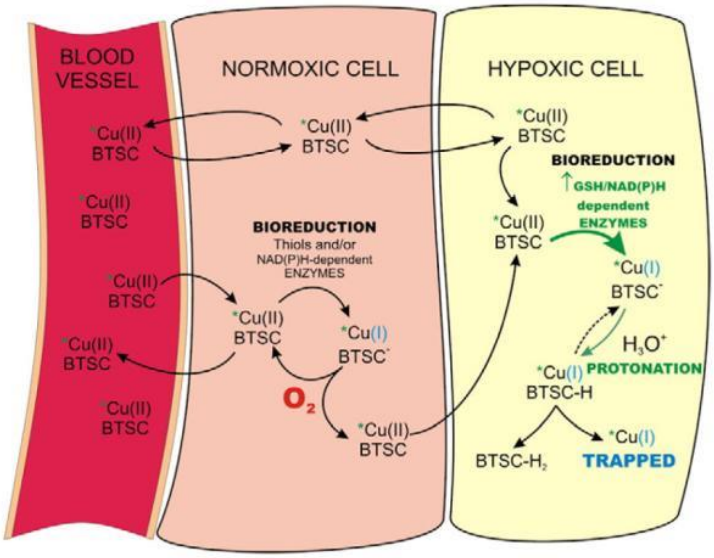

Figure 1.6. Proposed uptake and trapping mechanism of copper from hypoxia selective Cu-BTSC, replicated from Handley et al., 2011[5].

1.8.2 Cu-BTSC redox potential and hypoxia selectivity

Previous studies have demonstrated a relationship between Cu-BTSC redox potential and hypoxia selectivity. Using cyclic voltammetry the Cu(II/I) reduction/oxidation (redox) potential for a range of Cu-BTSC with different alkyl substitutions were compared to their corresponding hypoxia selectivites[110,122]. A general inverse relationship was established between hypoxia selectivity and redox potential, i.e. the ratio of intracellular hypoxic : normoxic radiocopper retention increases as the redox potential decreases[110]. As the redox potential becomes more negative, the complex becomes harder to reduce and is therefore more stable. For example Cu-ATSM has a Cu(II/I) redox potential of -0.59V, whereas Cu-PTSM has a redox potential of -0.51V. Although Cu-PTSM and Cu-ATSM are both taken up into normoxic tissue, Cu-PTSM is more easily reduced than Cu-ATSM and therefore less stable, such that it dissociates and deposits its copper core into tissues even when they are normoxic. In contrast,

Cu-ATSM is stable in normoxic tissue, and only dissociates where there is insufficient oxygen to reoxidise it, thereby providing it with hypoxia selectivity.

1.8.3 Tuning Cu-BTSC redox potential

The redox potential of Cu-BTSC complexes may be altered through chemical modification of the ligand[109,110,122]. The Cu-BTSC family of complexes therefore possess a range of hypoxia sensitivities. Alkylation at the R_1-R_4 positions changes the ligand backbone to create a different BTSC species. This renders each BTSC more or less hypoxia selective. For example, Cu-ATSM is alkylated at the R_1-R_4 positions and is more hypoxia selective than Cu-PTSM, which is alkylated at R_1, R_3 and R_4 positions (figure 1.6).

The redox potential of each complex is manipulable by the alkylation at the R_1 and R_2 positions, which increases the electron donating strength of the ligand[110,119]. Doing so makes the complex harder to reduce and increases its stability, and thus its hypoxia selectivity. This offers an explanation to the increased hypoxia selectivity of Cu-ATSM compared with Cu-(PTSM)[123].

Maurer et al., used density functional theory to model Cu-BTSC electron density to better understand the chemical reduction of these complexes[119]. It was suggested that double alkylation at the R_1 and R_2 positions of Cu-ATSM protects the complex from electron reduction, such that only the copper ion is reduced, generating a $[Cu(I)ATSM]^-$ species. The single R_1-R_2 alkylation of Cu-PTSM allows the electron reduction of the PTSM complex itself, to generate a $[Cu(II)\text{-}PTSM]^-$ species. $Cu(II)\text{-}PTSM]^-$ is less readily oxidised compared with $Cu(I)\text{-}[ATSM]^-$, even under normoxic conditions, meaning that it remains as an anion. It is also more prone to protonation, accelerating dissociation and the

release of its radiocopper core, even under normoxic conditions. For this reason Cu-PTSM may be utilised as a perfusion tracer as it is trapped in tissue with adequate perfusion[124]. The $[Cu(I)\text{-}ATSM]^-$ species is much more stable than $[Cu(II)\text{- }PTSM]^-$ and therefore resides in the cell for longer, increasing the likelihood that it may interact with molecular oxygen to become reoxidised. When oxygen is eliminated from the environment (i.e. hypoxia) the transiently trapped $[Cu(I)\text{-}ATSM]^-$ becomes more likely to dissociate. Cu-ATSM is therefore more hypoxia selective than Cu-PTSM.

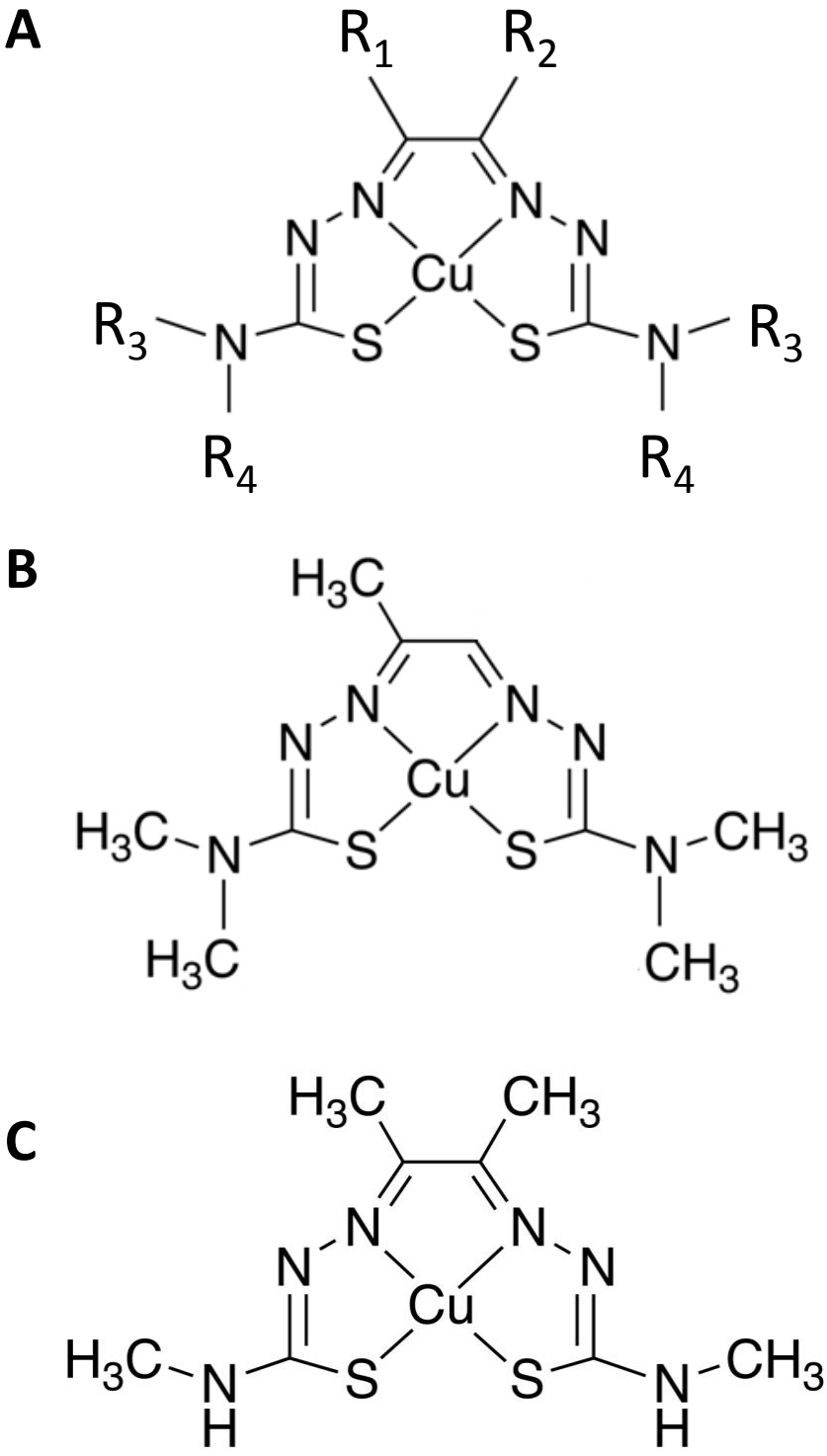

*Figure 1.7. Structure of A) general Cu-BTSC, B) Cu-PTSM and C) Cu-ATSM. * N_3 and N_4 nitrogen positions (from left to right).*

1.8.4 Potential Cu-BTSC reductants: NADH dependent enzymes

Under hypoxic conditions the intracellular NADH/NAD^+ ratio is elevated[125], particularly within the mitochondria, potentially providing a reducing environment capable of contributing to the overall reduction of hypoxia selective Cu-BTSC[118]. Early studies demonstrated that NADH alone was not capable of reducing Cu-KTS, even when in vast excess[126]. Similarly NADH had no effect on Cu-PTSM reduction alone, however, when incubated with sub mitochondrial brain particles, Cu-PTSM reduction became NADH dependent. This suggests that while NADH is not capable of Cu-BTSC reduction alone, it may be an essential cofactor[127]. Further to this, the NADH concentration required for mitochondrial Cu-ATSM reduction is higher than that for Cu-PTSM, supporting the theoretical NADH sensitivity of Cu-ATSM in hypoxic conditions where NADH is elevated. In an attempt to identify whether the BTSC complexes are reduced by the ETC, mitochondrial fractions were incubated with ^{62}Cu-PTSM and treated with three inhibitors of the ETC: Rotenone which inhibits electron transfer from NADH to ETC complex I, TTFA which inhibits transfer from $FADH_2$ to complex II, and Antimycin A which blocks electron transfer from ubiquinol to complex III. Antimycin A and Rotenone caused increased ^{62}Cu accumulation, whereas TTFA had no effect, suggesting that Complex I of the ETC may be a key reductant in Cu-BTSC dissociation. Results from similar experiments involving rotenone also implicate Complex I as a Cu-ATSM reductant[115]. These data support the suggestion that although NADH alone is incapable of reducing Cu-ATSM, mitochondrial NADH dependent mechanisms may be responsible for Cu-ATSM hypoxia selectivity. It is worth noting, however, that these experiments were carried out in isolated brain mitochondria. While this may

have implications in utilising Cu-ATSM or Cu-PTSM in brain imaging, these results are not necessarily transferable to other hypoxic organs. Subcellular fractionation was used to demonstrate that while Cu-ATSM and Cu-PTSM reduction in brain tissue is mediated by the mitochondria, reduction occurs predominantly in the cytosol in Ehrlich ascites tumour cells and cardiac myocytes[114,115,127,128]. Furthermore, hypoxia increased overall Cu-ATSM reduction yet did not alter the ratio of where it was reduced[114]. Although these studies indicate that copper released from Cu-BTSC complexes accumulates in different subcellular locations in different cell types, the mechanism of Cu-BTSC reduction cannot be confirmed from these data.

1.8.5 Potential Cu-BTSC reductants: thiols

Thiol containing molecules have also been implicated as potential Cu-ATSM reductants. The most abundant intracellular thiol is the cysteine containing tri-peptide GSH, which exists in a mM range of concentrations. Reduced GSH acts as an antioxidant through its strong electron donating tendency. In 1972, Petering measured a spectrophotometric colour change when Cu-KTS, which has a higher hypoxia selectivity than Cu-PTSM, was incubated with GSH (monothiol) and dithiolthreitol (dithiol) under anaerobic conditions[126]. He also demonstrated that the reaction rate increased with increasing thiol concentration. Furthermore, thiol depletion in Ehrlich ascites tumour cells with thiol conjugating agent N-ethylmaleimide and through heat treatment caused a decrease in Cu-KTS reduction intracellularly[129], suggesting that thiols may be a key BTSC reductant. More recently, systemic administration of GSH depletion agents buthionine sulphoximine (BSO) and diethyl maleate (DEM) was

demonstrated to decrease heart, lung, liver and kidney ^{67}Cu retention in rats injected with ^{67}Cu-PTSM, which supported this assertion; however, actual tissue thiol concentrations were not reported in this study, which makes it difficult to confirm whether this was indeed the case[130].

Results from a study performed by Xiao et al., implied that Cu-ATSM does not react with thiols to become reduced[131]. Copper chelating proteins Atx1 and Ctrl c were incubated with GSH and Cu-ATSM in an anaerobic glovebox. Spectrophotometry was used to read the absorbance of each solution to determine Cu-ATSM dissociation, which decreases the absorbance at 562 nm. As no change in absorbance was observed, results indicated that thiols were not capable of reducing Cu-ATSM. However, the amount of Cu-ATSM used in these studies was much higher (µM range) than of that in physiological models (<fM) to allow a measureable change in UV absorbance, therefore a large portion of Cu-ATSM may not have been reduced. It is difficult to extrapolate these findings to the clinical conditions where these tracers may be applied, where tracer concentrations of Cu-ATSM are greatly exceeded by the presence thiols, such as GSH, in mM concentrations. While thiols, and in particular GSH, may be responsible for the initial reduction of Cu-BTSC to a charged, unstable Cu-BTSC^{-} species, it is unclear whether changes in thiol status have any impact on the hypoxia selectivity of the BTSC complexes.

1.8.6 The effect of ROS on Cu-BTSC dissociation

As the hypoxia selectivity of each Cu-BTSC is determined by its redox potential, changes in cellular redox state could affect the reduction of these complexes. Few studies have measured the direct effects of a compromised redox state on

the reduction of Cu-BTSC complexes. One study demonstrated the increase of Cu retention from Cu-ATSM in neuroblastoma cells pre-treated with the GSH depletion agent, BSO[132]. Although there was evidence of oxidative protein damage implicating an increase in ROS generation, GSH levels were not measured; therefore the effect of GSH concentration on Cu-ATSM reduction cannot be confirmed. These cells were also incubated with a very high concentration of BSO (5mM) which may have affected cell viability and Cu accumulation. ^{62}Cu retention from ^{62}Cu-ATSM has recently been demonstrated in the brains of patients with mitochondrial myopathy, encephalopathy, lactic acidosis and stroke-like episodes[133]. This syndrome is associated with increased ROS generation through mitochondrial dysfunction, however, it is unlikely that ^{62}Cu-ATSM was targeting areas of oxidative stress alone (acidosis has also been implicated in Cu-ATSM dissociation), and these regions may have also been subject to focal hypoxia or ischaemia.

1.8.7 The effect of intracellular pH on Cu-BTSC dissociation

In addition to reduction, it has been suggested that Cu-BTSC dissociation is dependent on protonation[119,120]. As previously discussed, ischaemic tissue is frequently acidotic due to anaerobic glycolysis, loss of ionic homeostasis and lack of washout. It is therefore feasible that hypoxic selective uptake of Cu-BTSC may be modified by intracellular pH status. UV-vis spectroscopy studies demonstrated that the stability of Cu-KTS decreased substantially as pH decreased, rendering Cu-KTS more susceptible to dissociation[126]. Consequent studies, however, also demonstrated that as pH decreased, the reaction rate between Cu-BTSC and GSH also decreased[134]. It was concluded, however,

that a decrease in pH affected Cu-KTS dissociation more strongly than it did it reaction with thiols, meaning that a decrease in pH would favour Cu-KTS dissociation despite slowing the reduction process. Further to this, the effect of acidosis on the dissociation of Cu-ATSM and Cu-PTSM was explored[119] using cyclic voltammetry, where it was apparent that Cu-PTSM was less stable in more acidic environments than Cu-ATSM. Cu-PTSM became less prone to re-oxidation, while Cu-ATSM was still readily oxidised with acid present. Interestingly, Cu-PTSM required a higher concentration of acid for reduction to become irreversible compared to Cu-GTS, which contains no alkyl groups at the R_1-R_2 backbone positions. Computational energy calculations also predicted that protonation of the Cu-BTSC complexes would preferentially occur on at least one of the N_3 or N_4 positions of the ligand (figure (b)), which would then become less stable and prone to dissociation. Studies have also estimated that the pK_a of each Cu-BTSC complex has a similar relationship to alkylation at the R_1 and R_2 position as redox potential does i.e. Cu-ATSM has a lower pKa than Cu-PTSM, and is therefore more stable under control conditions [135]. This implies that Cu-BTSC complexes are less stable and vulnerable to dissociation in acidotic environments.

1.9 Aims of this project

The tissue deposition of copper from hypoxia selective Cu-BTSC such as Cu-ATSM may therefore rely on these key factors: reductants, ROS, oxygen and pH. The relative importance of each factor, however, remains unclear. This thesis therefore investigates the effects of thiol concentration and acidosis on the hypoxia selectivity of Cu-ATSM. As thiols are strong electron donors they

therefore increase intracellular antioxidant capacity. In addition to altering the reduction rate of Cu-ATSM, thiol concentration may impact ROS generation which has also been suggested in Cu-ATSM reduction and hypoxia selectivity. To address these questions, an isolated perfused rat heart model and cultured bovine aortic endothelial cells (BAEC) were utilised to investigate the effect of thiol concentration modification (and therefore altered redox state) and intracellular acidosis on the pharmacokinetics and hypoxia selectivity of ^{64}Cu-ATSM.

Chapter 2

Materials and methods

2.1 Introduction

Experiments investigating the possible mechanisms which promote Cu-ATSM hypoxia selectivity are detailed in chapters 3-5. Two main biological models were employed; an isolated perfused rat heart model and an isolated bovine aortic endothelial cell (BAEC) model. This chapter describes the methods employed for each experiment.

2.2 The isolated perfused heart model

2.2.1 Coronary perfusion *in vivo*

Adequate perfusion of the heart itself is crucial in providing essential components such as oxygen and energy substrates, but also in removing any waste products which accumulate (e.g. CO_2, lactic acid). The heart is constantly working and needs sufficient blood flow to meet its metabolic needs. An extensive coronary vasculature system therefore exists that supplies and removes blood to and from the myocardium itself.

in vivo, the heart pumps blood from the left ventricle through the aorta and then to the systemic vasculature. As the left ventricle fills with blood from the left atrium, the pressure increases until it exceeds that of the aorta and the ventricle contracts, ejecting blood into the aorta. The decrease in ventricular pressure compared to aortic pressure causes the aortic valve to close and prevents the blood from re-entering the left ventricle. This pressure also drives blood into the coronary ostia located behind the aortic valve, which subsequently enters the main coronary arteries, arterioles and capillaries which penetrate the entire myocardium. Venules deliver blood from the capillary bed to veins, blood drains

into the coronary sinus and then into the right atrium with blood from the systemic circulation[136].

2.2.2 Langendorff isolated heart perfusion

The isolated perfused heart is a widely utilised *ex vivo* model. The first description of this method with mammalian hearts was published by Oskar Langendorff in 1895[137]. The heart is excised from the donor animal, hung on a metal cannula via the aorta and perfused in a retrograde manner with a physiological salt solution containing excess glucose.

2.2.3 Why use the Langendorff isolated heart perfusion technique?

There are several advantages and disadvantages to using an isolated perfused organ model such as the Langendorff technique. Evidently this *ex vivo* method lacks certain factors which usually affect the heart *in vivo*, such as neurotransmitters, hormones, central and autonomic nervous stimulation. Experimental results gained from an isolated perfused heart model therefore cannot be directly translated to an *in vivo* model. However, as the heart can be studied directly without these peripheral influences it permits investigation of pharmacological, biochemical and physiological interventions which may otherwise be detrimental or even fatal to an animal *in vivo* [138,139].

When planning experiments with isolated perfused hearts it is important to appreciate that although the heart can be studied for several hours it is continuously deteriorating and may deteriorate more rapidly with certain

interventions. It is therefore important to have an appropriate timeline for all perfusion protocols.

Practically the Langendorff technique is a quick, low cost model that yields reproducible results in large numbers. Rat hearts are usually preferred over smaller species as they are relatively easy to prepare, however, it may be of interest to the investigator to use other species to suit their needs. Mouse hearts, for example, which are more difficult to prepare and perfuse, allow the investigation of genetic modification on cardiac function and biochemistry[139].

Isolated perfused heart protocols typically use crystalloid solutions such as Krebs-Henseleit buffer (KHB) to perfuse the heart. It is possible to perfuse the heart with blood from a donor animal, however, this preparation is more complicated as it requires the two subjects to be closely monitored (the heart and the donor animal). Blood perfused preparations also eliminate the possibility of introducing pharmacological interventions as the blood is circulated back to the donor animal. Perfusing the heart with a crystalloid buffer also has its limitations. First, crystalloid buffers have a much lower oxygen carrying capacity than blood[140]. It is therefore necessary to compensate for this by increasing the coronary flow rate to approximately 4-5 times that of flow rate *in vivo*. The vast increase in flow gives rise to endothelial stress which can compromise the integrity of the vessel walls[138]. The absence of proteins lowers the osmotic pressure of such buffers, which can increase the incidence of tissue oedema[141]. There is also a lack of antioxidants and glucocorticosteroids which will contribute to the deterioration of the heart as it becomes more susceptible to immune stimuli and free radical damage[138]. Despite these challenges, buffer

perfused hearts are easy and cheap to prepare and remain physiological for several hours.

2.2.4 Basic perfusion apparatus

A schematic diagram of the basic apparatus used in the isolated perfused heart studies is displayed in figure 2.1.

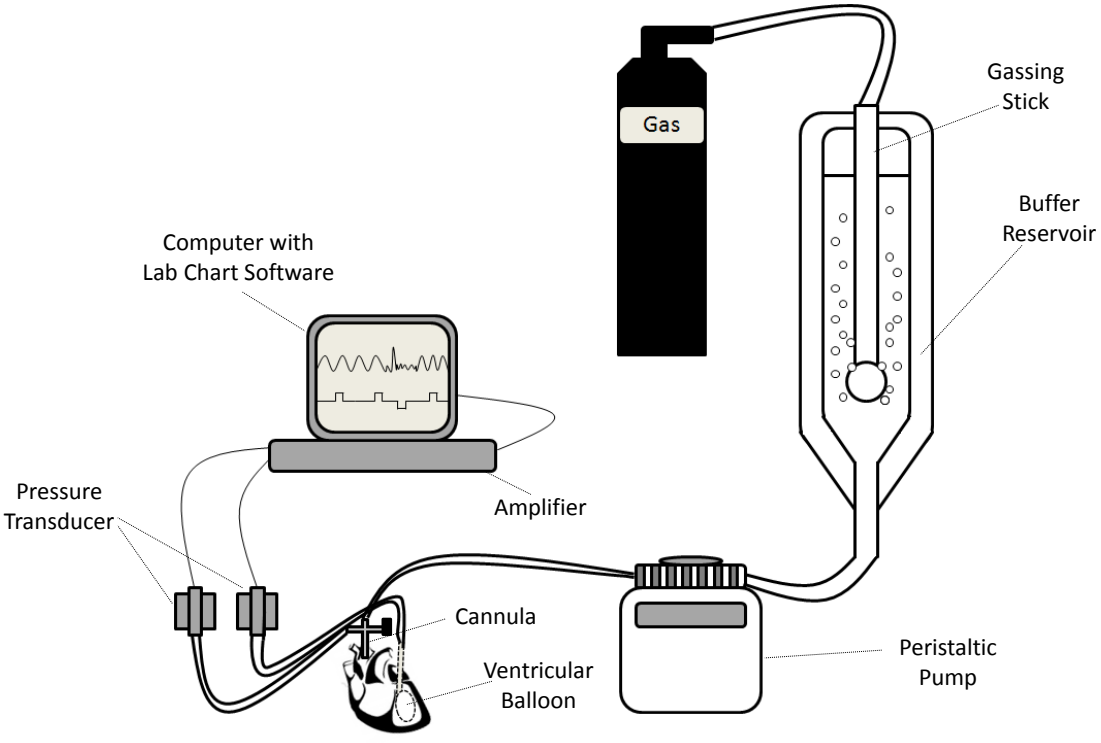

Figure 2.1. Schematic diagram of basic Langendorff preparation apparatus.

2.2.5 Krebs-Henseleit buffer

Throughout the perfusion protocols Krebs-Henseleit buffer (KHB) comprised of the following (unless otherwise stated); NaCl (118 mM), KCl (5.9 mM), $MgSO_4$

(1.16 mM), $NaHCO_3$ (25 mM), Glucose (11.1 mM), $CaCl_2$ (2.2 mM) and EDTA (0.48 mM) dissolved in distilled H_2O. This composition differs from classic KHB composition. For heart perfusion experiments, ETDA was added to chelate free heavy metal ions for purposes of ^{31}P NMR spectroscopy (described below). EDTA also chelates Ca^{2+} ions, therefore the $CaCl_2$ concentration described above is higher than that of traditional KHB compositions to account for this. The KHB composition was also phosphorus-free, again to facilitate of ^{31}P NMR spectroscopy studies, which would detect phosphorous in the perfusate and potentially obscure measurement of phosphorous metabolites in the heart. KHB was modified to pH 7.4 by adding NaOH or HCl and then filtered using a custom-made vacuum pump filtration system.

2.2.6 Gas mixtures

Normoxic KHB was gassed with 95% O_2/5% CO_2. Hypoxic KHB was gassed with 95% N_2/5% CO_2 for at least 20 minutes before it was required. In chapter 5, an additional perfusion protocol was introduced where hypoxia was induced by gassing KHB with a 20% O_2 gas mixture(20% O_2/75% N_2/5% CO_2) created by a GSM-3 gas mixer (CWE instruments, US).

During preliminary experiments, an OxyLite™ fluorescent oxygen probe connected to an Oxylab pO_2™ recorder (Oxford Optronix, Oxford, UK) was inserted into the arterial perfusion line to measure the oxygenation of the KHB before the cannula. Figure 2.2 displays the KHB pO_2 after switching to KHB gassed with 95% N_2/5% CO_2. pO_2 began to decrease 2 mins after switching to anoxic KHB and rapidly decreased from 98.0 ± 10.8 to 8.5 ± 3.1mmHg within 8

mins. By 60 mins, KHB pO_2 was 0.4 ± 0.1 mmHg. The OxyLite™ and Oxylab pO_2™ are only sensitive to pO_2 of 0-100 mmHg, therefore oxygenation of normoxic KHB or KHB gassed with 20% O_2/75% N_2/5% CO_2 could not be measured.

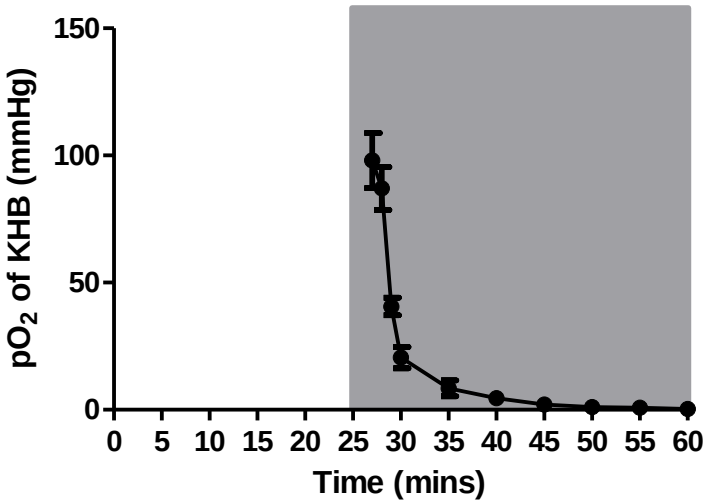

Figure 2.2 pO_2 of KHB gassed with 95% N_2/5% CO_2.Data are expressed as means ± standard deviation, n=3.

2.2.7 Temperature, flow rate and pressure measurements

Glassware was water-jacketed and supplied with water by a heater circulator to maintain KHB at 37^{o}C throughout each experiment. Once the perfusion apparatus was set up, the temperature of the KHB was measured by placing a thermometer into the lumen of the cannula. In these experiments, hearts were perfused with a constant flow of KHB which was controlled by a peristaltic pump (Gilson, USA). Flow rate was calibrated manually by adjusting the speed of the pump and measuring the volume of KHB that eluted from the cannula over 1 min.

Two DTXPlus™ pressure transducers (BD, UK) where connected to a PowerLab/4SP data acquisition system and LabChart® version 7.2 software was used to measure contractile function parameters (ADInstruments, UK). One pressure transducer was placed after the cannula to detect perfusion pressure while the other pressure transducer was connected to a fluid-filled balloon which was inserted into the left ventricle of the heart to detect heart rate, left ventricular developed pressure (LVDP) and left ventricular end diastolic pressure (LVEDP). The readings from each pressure transducer were calibrated before the experiments using a sphygmomanometer.

2.2.8 Preparation of heart for perfusion

Adult male Wistar rats (300-350g; Harlan, UK) were anaesthetised with pentobarbitone (Pentoject 0.7mL/ kg i.p) and administered heparin (200IU, i.p) simultaneously. Once the animal was anaesthetised and did not respond to reflex tests, hearts were excised and placed in ice-cold KHB. The heart was cannulated according to the Langendorff method and perfused with KHB under constant flow (14mL/ min).

2.2.9 Exclusion criteria studies

Prior to commencing experiments involving heart perfusions, cardiac contractile function was measured from 7 hearts to establish the exclusion criteria for each parameter (figure 2.3). Measurements of heart rate, perfusion pressure, LVDP and LVEDP were taken every 5 mins for 60 mins. Each parameter was within 20% of the 1st value measured at t=0 mins. Heart rate increased from 268.5 ±

33.8 to 277.5 ± 29.1 beats per minute (b.p.m.) after 60 mins perfusion. Perfusion pressure also increased from 75.6 ± 10.8 to 86.5 ± 28.8 mmHg whereas LVDP decreased from 135.8 ± 31.5 to 113.5 ± 26.8 by the end of perfusion. LVEDP was set at 5.9 ± 1.1 and increased to 7.4 ± 2.5 mm Hg by the end of perfusion. Hearts in subsequent studies underwent a 10 mins stabilisation period of 10 mins. During this period it was decided from the criteria outlined in figure 2.3 if the hearts were healthy enough for continued use in the study.

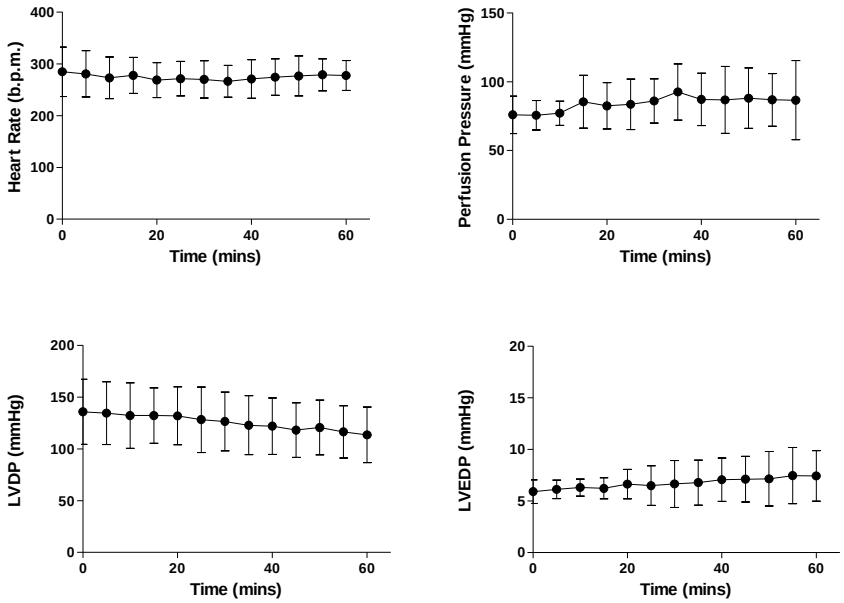

Figure 2.3. Exclusion criteria established from isolated perfused rat hearts. Data are expressed as means ± standard deviation (n=7).

2.2.10 Perfusate analysis for lactate, glucose and protein content

2.2.10.1 Lactate and glucose analysis

Perfusate samples were collected directly from the heart at appropriate time points when the perfusion protocol changed. Aliquots were kept on ice and stored at -20^{o}C. Perfusates were later defrosted and analysed for lactate and

glucose content using a 2300 STAT Plus™ glucose and lactate analyser (YSI UK Ltd, UK). The glucose and lactate analyser uses membranes containing lactate oxidase and glucose oxidase which react with lactate and glucose to produce H_2O_2. H_2O_2 is oxidised at a platinum anode to produce protons, oxygen and electrons. The electron flow is proportional to the concentration of lactate or glucose present in the sample measured[142].

2.2.10.2 Protein and creatine kinase (CK) analysis

In addition to contractile function measurements, heart viability was determined by analysing the perfusate samples for protein content. Myocardial injury increases the release of proteins such as CK into the blood/perfusate. CK measurement assays require several steps and are time consuming and prone to error. Here, the CK assay was compared to the bicinchoninic acid (BCA) protein assay and the differences in viability measurements were assessed.

Hearts were perfused according to the Langendorff method as described above and were subject to 16 minutes of zero flow ischaemia followed by a reperfusion period of 35 mins in which perfusate samples were collected from the heart. Samples were then compared to perfusates collected from normoxic control hearts for CK and protein content. Perfusate samples of 10 µL were pipetted into two 96 well microtitre plates in duplicate; one plate was analysed for CK and one for general protein content.

2.2.10.2.1 CK assay

CK catalyses the conversion of phosphocreatine (PCr) and ADP to creatine and ATP. PCr and ADP are added to the perfusate samples, hence increases in CK produces more ATP. Hexokinase is added to catalyse the reaction of ATP and glucose to form glucose-6-phosphate, which in turn is oxidised by glucose-6-phosphate dehydrogenase to thio-NADH. The conversion of glucose 6-phosphate to thio-NAD results in a measureable change in absorbance at 405 nm which can be measured using a spectrophotometer[143].

Table 2.1 lists the reagents used in the CK assay. All the reagents for the CK assay were dissolved in 0.1 mM glycylglycine (pH 6.75). Purified rabbit muscle CK was purchased from Boehringer-Mannheim, Switzerland. All other reagents were purchased from Sigma-Aldrich, UK. Fresh dithiothreitol and thiol-NAD were weighed out each day and thiol-NAD solutions were made separately and protected from light until the time of the assay. In addition to perfusate samples, a series of CK dilutions of known concentration were pipetted (10 µL) into each microtitre plate to construct a standard concentration curve. 200 µL of the reagent mixture was added to each well immediately before reading the optical absorbance at 405 nm using a spectrophotometer plate reader (SpectraMax 190, Molecular Devices). The absorbance reading was repeated every minute for 5 mins.

Table 2.1. List of reagents required for the CK assay.

Reagent	Concentration
PCr	20 mM
Glucose	20 mM
Magnesium acetate	10 mM
ADP	1 mM
AMP	10 mM
Thio-NAD	0.4 mM
Dithiothreitol	10 mM
Hexokinase	0.5 U/mL
Glucose-6-phosphate dehydrogenase	1 U/ mL

2.2.10.2.2 BCA assay

BCA assay kits were obtained from Fisher Scientific, UK. The BCA assay requires two pre-made solutions containing Cu^{2+} and BCA. In the biuret reaction, peptide bonds reduce Cu^{2+} to Cu^{+} which produces a colour change from green to blue[144]. BCA ions chelate Cu^{+} ions, producing a colour change from blue to purple which is measureable by spectrophotometry at 562 nm and is directly proportional to the amount of protein present. The Cu^{2+} and BCA solution were mixed to give a concentration ratio of 1:50 respectively. In addition to perfusate samples, a series of bovine serum albumin solutions of known concentration were pipetted (10 µL) into each microtitre plate to construct a standard concentration curve. BCA/Cu^{2+} mixture (200µL) was then pipetted into each well and plates were left to incubate at room temperature for 25 mins before reading the optical absorbance at 562 nm using a spectrophotometer plate reader (SpectraMax 190, Molecular Devices).

2.2.10.2.3 Comparison of CK and BCA assays for cardiac viability

Figure 2.4 displays standard concentration calibration curves obtained using the CK and BCA assays. In all cases, CK activity and protein concentration were directly proportional to the colourimetric changes measured at 405 nm or 652 nm respectively. Figure 2.5 displays the CK activity and protein concentrations of perfusates from ischaemic and control hearts. To display the results more clearly, only the readings from the 5 min time point are displayed from the CK assay. There was a clear increase in CK activity and protein concentration from ischaemic/reperfused hearts compared to control hearts. These results confirm that either assay can be used to measure cardiac viability, it was therefore decided to use the BCA assay to detect cardiac protein release as a measure of viability in all heart perfusion studies.

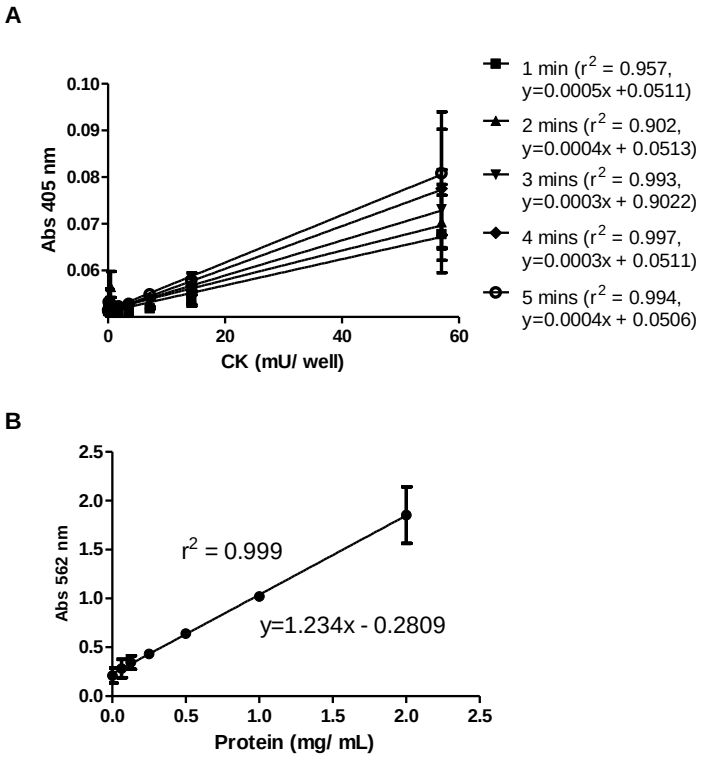

Figure 2.4. Calibration of standard solutions of (A) CK and (B) protein plotted against absorbance. Data are expressed as means ± standard deviation (n = 3).

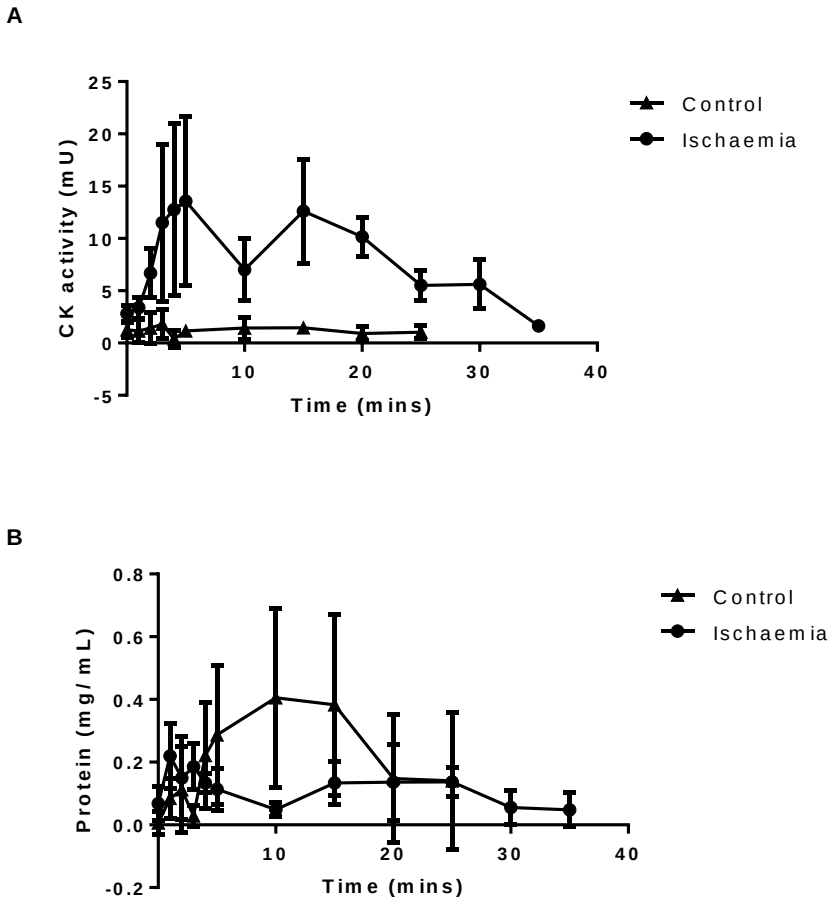

Figure 2.5. Perfusate (A) CK activity and (B) protein content from ischaemia reperfused hearts and time-matched controls. Data are expressed as means ± standard deviation (n = 3 per group).

2.3 Isolated bovine aortic endothelial cells

Vascular endothelial cells have important roles in cardiovascular homeostasis. The dysfunctional endothelium has been implicated in multiple cardiovascular pathologies including atherosclerosis, hypertension and heart failure. Endothelial dysfunction has also been associated with hypoxia. Bovine aortic endothelial cells (BAEC) was therefore used in addition to isolated perfused rat hearts to investigate the hypoxia selectivity of ^{64}Cu-ATSM in BAEC under various conditions.

2.3.1 Culture of BAEC

BAEC were isolated from bovine thoracic aortas obtained from a local abattoir. Briefly, aortas were coated in collagenase for 5 mins and gently scraped with a scalpel to isolate the endothelial monolayer from the rest of the aorta. Isolated BAEC were cultured in DMEM supplemented with 10% fetal calf serum (FCS), penicillin (100 IU/ mL), streptomycin (100 IU/ mL) and L-glutamine (2mM). Primary cultures of BAEC were grown in 25cm^2 gelatin coated flasks. Flasks were incubated at 37^{o}C and 21% O_2/5% CO_2 until confluent.

Like all endothelial cell in culture, BAEC grow in a strongly contact-inhibited monolayer and have similar morphological characteristics of the endothelium *in vivo*[145]. The BAEC phenotype is often described as having a cobblestone appearance once confluent (figure 2.6). BAEC confluence was therefore confirmed by this phenotype.

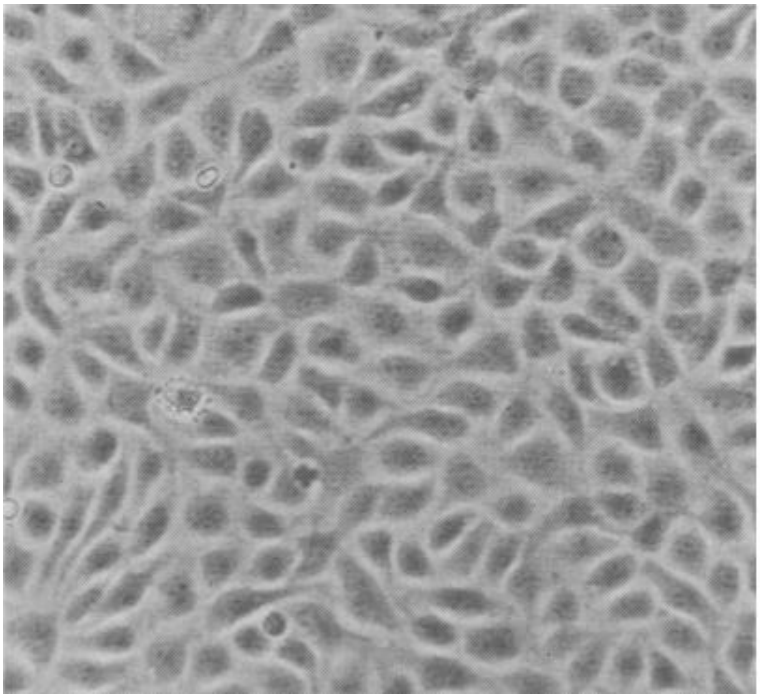

Figure 2.6. BAEC in culture. Replicated from Schwartz et al., 1978[145].

1 mL of trypsin (Sigma-Aldrich, UK) was added to 25cm^2 flasks of confluent BAEC to break down protein-protein interactions between cells and the gelatin on the flask. The trypsin was diluted in ethylenediaminetetraacetic acid (EDTA) which chelates metal ions, such as Ca^{2+} which may inhibit trypsin activity. To prevent cell damage, DMEM was added to the flask immediately at an appropriate volume as to split the culture into subsequent flasks. The BAEC culture was then split into 75cm^2 gelatin coated flasks and incubated as before.

2.3.2 MTT viability assay

To assess BAEC viability, the 3-(4,5-dimethyl-2-thiazolyl)-2,5-diphenyl-2H-tetrazolium bromide (MTT) assay was used. MTT is a water soluble salt which has a yellow colour when in solution. MTT is readily taken up into cells and reduced by NADH/ NADPH dependent enzymes in viable, metabolically active cells[146]. The reduction of MTT forms 1-(4,5-dimethylthiazol-2-yl)-3,5-diphenylformazan (MTT formazan), an insoluble purple crystalline solid which accumulates in cells which can be dissolved using organic solvents. The reduction of MTT to MTT formazan crystals produces a colour change which can be measured spectrophotometrically at 570 nm to give an index of viability.

In these studies, BAEC were seeded into 96 well plates and cultured as before. Once confluent, the medium was aspirated from each well and MTT (0.5 mg/ mL) was added (100 µL per well) for 4 hrs. The MTT was then aspirated and 50 µL DMSO was added per well. Plates were placed on a shaker for 10 mins before reading the optical absorbance at 570 nm using a spectrophotometer

plate reader (SpectraMax 190, Molecular Devices). The results were plotted as Abs 570 nm *vs.* treatment group.

2.4 Thiol measurement assays

2.4.1 Thiol concentration modification

In chapters 3 and 4, agents which pharmacologically modify thiol concentration were used: diethyl maleate (DEM), buthionine sulphoximine (BSO) and N-acetylcysteine (NAC). DEM conjugates GSH in the presence of GSH-S-transferases and therefore depletes intracellular GSH pools[147]. BSO inhibits γ-glutamylcysteine synthetase which prevents GSH synthesis, thereby also depleting GSH concentration[148]. NAC is a cysteine derivative which contributes to the intracellular thiol pool and GSH synthesis[149]. NAC also directly replenishes GSH non-enzymatically by direct thiol exchange with GSSG.

2.4.2 The DTNB assay

The results described in chapters 3 and 4 relied on accurate measurements of intracellular thiol concentration. First described by Ellman in 1959, 5,5'-dithiobis-(2-nitrobenzoic acid) (DTNB) or otherwise known as Ellman's reagent is the most widely used chemical for detection of thiol content[150]. Reduced thiols react with DTNB to cleave the disulphide bond and generate 2-nitro-5-thiobenzoate (NTB^-). In water, NTB^- becomes an NTB^{2-} ion which is yellow in colour. The change in colour associated with DTNB conversion to NTB^{2-} is therefore directly proportionally to thiol concentration.

To measure thiol content with the DTNB assay, 150 µL DTNB (Sigma-Aldrich, UK) was added to samples pipetted into clear microtitre plate. The plate was incubated for 5 mins before 50 µL of NADPH solution was added to each well and mixed with a pipette. A spectrophotometer plate reader was then used to measure the absorbance of each well at 412 nm.

2.4.3 The OPA assay

An alternative method to measuring thiol content is by reaction with *o*-phthalaldehyde (OPA). OPA is a dialdehyde which reacts with thiols and primary amines to form a fluorophore. The OPA assay is therefore considered more specific for measuring GSH, which contains both amines and thiols than the DTNB assay[151]. As OPA reacts with primary amines, protein concentration could affect measurement of thiol concentration. In these experiments, however, cellular thiol content was corrected for protein to avoid this.

OPA was purchased from Sigma-Aldrich, UK. OPA is light sensitive; therefore precautions were taken to limit exposure to light throughout protocols. OPA was dissolved in methanol (10 mg/mL) in a foil covered tube. 150 µL

phosphate/ETDA buffer (pH 8.0) was added to samples in a black opaque plate before adding 15 µL OPA solution to each well. Plates were then covered in foil and placed in a dark room for 25 mins. A microtitre plate reader was used to measure the fluorescence at 350nm excitation and 420nm emission (Chameleon V, Hidex, Finland).

2.3.4 Comparison of the DTNB and OPA assays

Prior to commencing the experiments in chapters 3 and 4, the DTNB and OPA assays were both used to measure the concentration of thiols extracted from BAEC with modified thiol concentration and the results were compared. BAEC were cultured as described above and seeded into 24 well plates. When confluent the medium was replaced with medium containing BSO (10, 25 and 100 µM) for 24 hrs or left untreated. After each treatment period, the medium was aspirated and wells were washed twice with ice-cold phosphate buffered saline (PBS; 10 mM, pH 7.4). ice-cold trichloroacetate (TCA) (6.5%; 100µL) was added to each well for 10 mins on ice, aspirated and stored at -70^{o}C. 100 µL NaOH (1M) was added to each well for 2 hrs before aspirating and storing at -20^{o}C.

10 µL of each TCA extract was pipetted into the well of a clear and a black opaque microtitre plate. In addition to TCA extracts, a series of GSH (Sigma-Aldrich, UK) solutions of known concentration were pipetted (10 µL) into each microtitre plate to construct a standard concentration curve. The DTNB and OPA assays were then carried out on the clear and black plates respectively.

Figure 2.7 displays the standard calibration curves constructed from samples of GSH of known concentration. The standard calibration graph obtained using the

DTNB assay (A) was sigmoidal. In Ellman's original paper, only the linear part of the curve was used to calculate sample thiol concentrations. It is therefore possible that some thiol concentrations outside of this range are not accurately detected by this assay. The standard calibration curve obtained from the OPA assay, however, was linear from 0-0.5 nmol GSH.

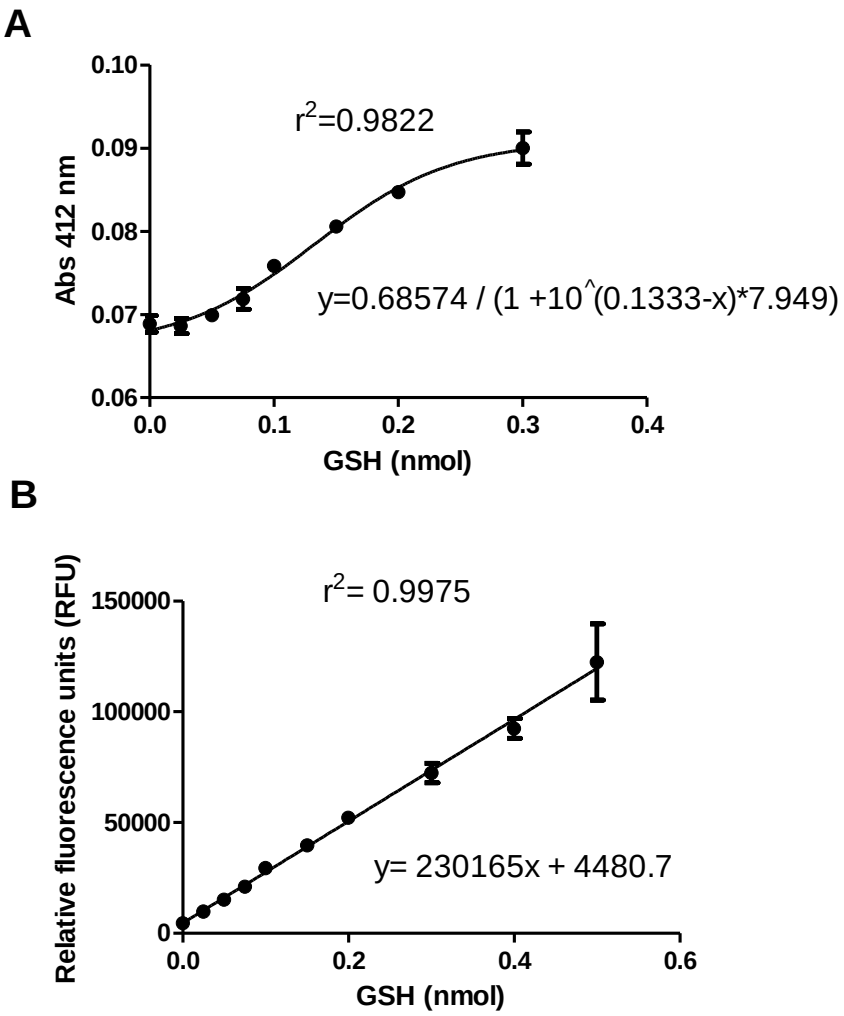

Figure 2.7. Standard GSH calibration curves from (A) DTNB and (B) OPA assays. Data is expressed as means ± standard deviation (n=3 per group).

Figure 2.8 shows thiol concentrations obtained from the same TCA extracts of BAEC incubated with BSO. As expected, BSO decreased intracellular thiol

concentrations in a dose-dependent manner. Decrease in thiol concentration appeared less marked from DTNB analysis compared with OPA analysis. This may be attributed to inaccurate extrapolation from the DTNB standard calibration curve, leading to an underestimation of the amount of thiol in a sample. It is also worth noting that the OPA assay detects thiol concentration in the presence of amines and it is therefore possible that it is more sensitive to changes in GSH content rather than general thiol concentration. As BSO treatment decreases GSH concentration rather than general thiol concentration, the OPA assay may be a more appropriate method for detecting changes in thiol concentration where GSH concentration is manipulated. The OPA assay was therefore used to measure the thiol concentration of TCA extracts from isolated perfused rat heart tissue in chapter 3 and BAEC in chapter 4.

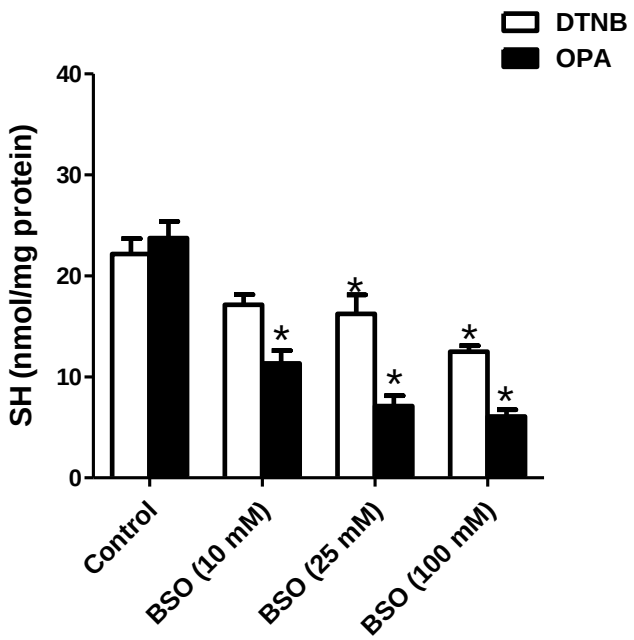

*Figure 2.8. Thiol content of TCA extracts from BSO treated BAEC. Thiol concentration was determined using the DTNB and OPA assays. Data are expressed as means ± standard deviation. *p<0.05 vs. untreated control (n = 3 per group).*

2.5 ^{31}P NMR spectroscopy

Nuclear magnetic resonance (NMR) spectroscopy is a non-invasive modality which can be used to study tissue metabolism. As described in 1.5.2.1, some atomic nuclei possess a spin which makes them act like a magnetic dipole. When a large, static magnetic field is applied, the axes of these nuclei align either in line with the magnetic field (low energy state) or antiparallel to this field (high energy state). An oscillating frequency is applied which perturbs magnetisation followed by a recovery period in which initial equilibrium is restored, hence the term nuclear magnetic resonance. The most abundant phosphorous atomic nucleus is ^{31}P which, like the ^{1}H nucleus, possesses spin which makes it act like a magnetic dipole. ^{31}P nuclei exist in different chemical environments which give rise to different resonances. The main resonances detectable by ^{31}P NMR spectroscopy are from phosphocreatine (PCr), inorganic phosphate (P_i) and adenosine triphosphate (ATP), meaning that this technique can be used to assess phosphorus metabolism and tissue energetic status in living systems[95]. Furthermore, the frequency of the P_i signal is highly sensitive to changes in pH. ^{31}P NMR spectroscopy was therefore utilised to determine intracellular pH in isolated perfused hearts undergoing protocols to induce acidosis (chapter 5).

Isolated rat hearts were perfused within the bore of a 15 mm ^{31}P/^{1}H birdcage coil which was inserted into a Bruker 9.4T Avance III NMR spectrometer. Shimming was optimised on the line shape of the water signal in each heart. The imaging gradients of the magnet were warmed to maintain the bore of the spectrometer at 37^{o}C. ^{31}P spectra were acquired with a pulse-acquire sequence with a 60^{o} flip angle, repetition time of 3.8 sec and 64 scans to give a total

experiment time of 4 mins per spectrum. ^{31}P NMR spectra were acquired sequentially in a time-resolved fashion under all interventions.

The resonance of the phosphocreatine (PCr) peak was set to 0 parts per million (ppm) and the resonance of the inorganic phosphate (P_i) was referenced to that of PCr in each spectrum. The difference in resonance between the PCr and P_i peak was used to calculate pH_i using equation 5.1, where δ_{Pi} represents the difference in PCr and P_i peak resonance[152].

$$pH_i = 6.72 + \log(\delta_{Pi} - 3.17)/ (5.72 - \delta_{Pi})$$

Equation 2.1. Measurement of pH_i using δ_{Pi} acquired from ^{31}P NMR spectra

The area under the PCr peak was set to 1 from the first spectrum from each heart and the areas under the PCr peaks from subsequent spectra and P_i, γ ATP, sugar phosphate from all spectra were compared to this to quantify their concentrations.

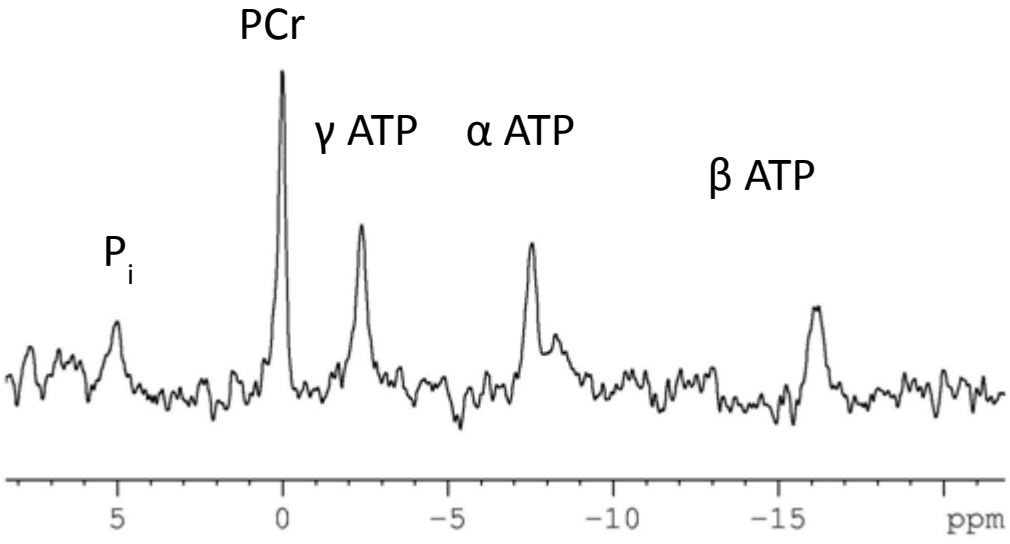

Figure 2.9. Example ^{31}P-NMR spectrum from healthy heart.

2.6 Protocols for investigating ^{64}Cu -ATSM hypoxia selectivity

2.6.1 ^{64}Cu production

^{64}Cu was provided by Dr K Shaw or Dr R Paul and was produced in the PET imaging centre, St. Thomas' Hospital, London, UK[153]. ^{64}Cu was produced by the ^{64}Ni(p,n)^{64}Cu reaction using a CTI RDS 122 cyclotron with an 11MeV proton beam with a gold target plated with ^{64}Ni. HCl (9M) was used to dissolve ^{64}Cu from the target, which was transferred to an AG1-8X anion exchange column (Bio-Rad, UK) made in 9M HCl for purification. Unreacted ^{64}Ni was eluted from the column using 9M HCl. Subsequent elutions using 6M HCl removed any co-impurities before eluting ^{64}Cu in 0.1M HCl to give a stock solution of $^{64}CuCl_2$. The amount of radioactivity was measured using a dose calibrator (CRC-25R Capintec, USA).

2.6.2 Radiolabeling ATSM with ^{64}Cu

ATSM was provided by Prof. P Blower (Imaging Sciences and Biomedical Engineering department, King's College London) and dissolved in DMSO (1 mg/ mL). 10 µL of the ATSM solution was added to 50-100 MBq $^{64}CuCl_2$ which was then diluted into 2 mL of water. The solution was agitated gently and left at room temperature for 20 min. A SEP-PAK® C18 Classic cartridge (Waters, Hertfordshire, UK) was used to filter the labelled ^{64}Cu-ATSM. 1 mL ethanol was passed through the cartridge 0.5 mL at a time; the 1st fraction was discarded and ^{64}Cu-ATSM was eluted in the 2nd fraction. ^{64}Cu-ATSM radioactivity was then measured using a radioisotope calibrator (CRC-25R Capintec, USA). 2µL ^{64}Cu-ATSM was pipetted onto a Silica Gel 60 F_{254} STRIP (Merck, Germany) and

ATSM labelling efficiency was assessed by radio-TLC (Cu-ATSM has a retention factor of 0.79), using 100% ethanol as the mobile phase. For isolated perfused heart studies, the ethanol ^{64}Cu-ATSM stock solution was diluted with KHB to 20 MBq/ mL. For isolated BAEC studies, ^{64}Cu-ATSM was diluted in Dulbecco's modified Eagle's medium (DMEM) to 1 kBq / mL. Final ethanol concentrations were 10% or less.

2.6.3 Measurement of ^{64}Cu from ^{64}Cu-ATSM in isolated perfused rat hearts

To measure cardiac ^{64}Cu retention in isolated perfused rat hearts, a custom-made triple γ-detector system (figure 2.10). Three Na/ I γ- radiation detectors (Raytest Isotopenmessgeräte GmbH, Germany) were directed at the input perfusion line (detector 1), the heart (detector 2) and the output perfusion line (detector 3). Lead collimators were placed around each detector to prevent shine-through. All three detectors were connected to a Gina Star™ data acquisition system (Raytest Isotopenmessgeräte GmbH, Germany) and data was acquired by the Gina Star™ software package (version 4.0.2.75).

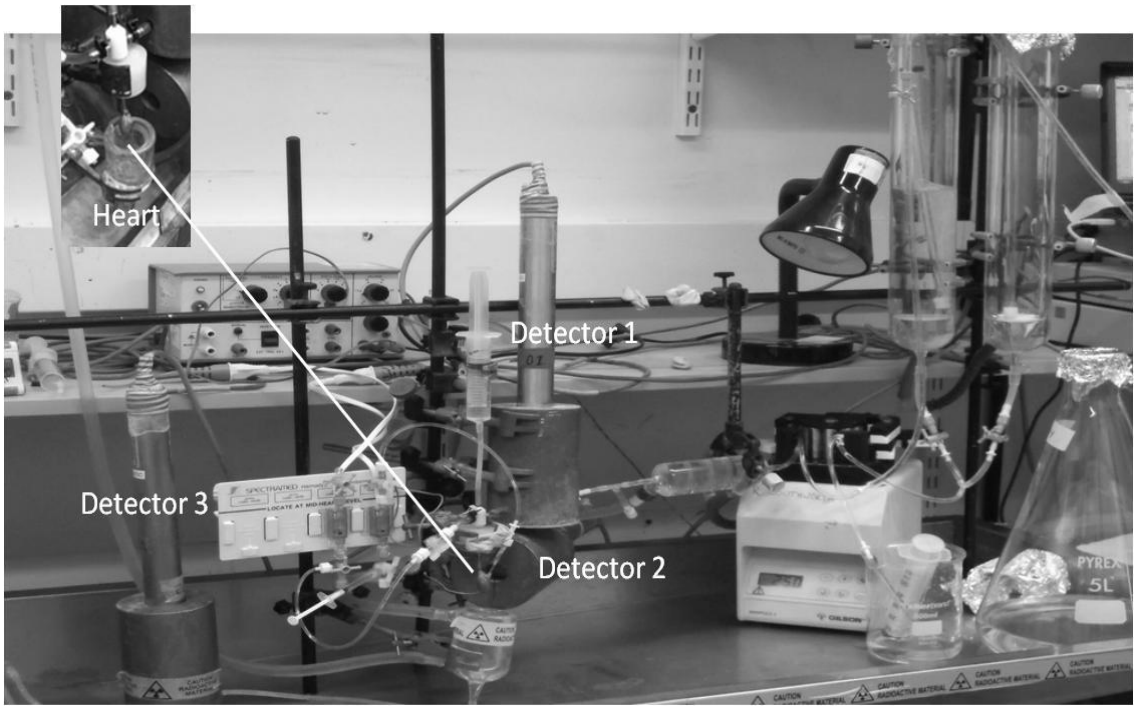

Figure 2.10. The triple γ-detector system for measurement of ^{64}Cu retention in isolated perfused rat hearts.

2.6.4 Time activity curve retention and clearance rate analysis

Figure 2.11 displays an example of the time activity curve data obtained from the Gina Star™ system. Time activity data were used to determine ^{64}Cu retention from ^{64}Cu-ATSM injections and the pharmacokinetics of each injection. ^{64}Cu retention was calculated at appropriate time points immediately before a change in perfusion protocol (i.e. switching to hypoxic buffer, infusing drugs, subsequent ^{64}Cu-ATSM injections or the end of experiment; individual perfusion protocols and ^{64}Cu-ATSM injection times are detailed in chapters 3 and 5). ^{64}Cu retention was calculated as a percentage of the maximum injected activity before the next injection and corrected for background radioactivity from previous injections.

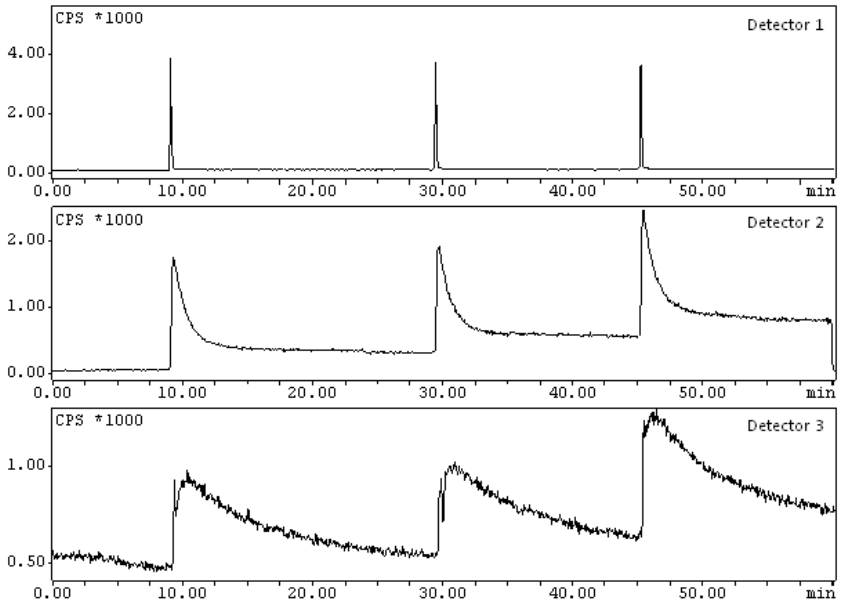

Figure 2.11. Example time activity curves of a heart administered three bolus injections of ^{64}Cu-ATSM.

Pharmacokinetic analysis of time activity curve data was performed using MATLAB® (version 7.11.0 MathWorks®, US) and fitted with a bi-exponential function (equation 2.3).

$$f(t) = ae^{-bt} + ce^{-dt}$$

Equation 2.2. Bi-exponential function fitted to all time activity curve data.

b and *d* represent the slow and fast clearance rate constants (SCR and FCR) and *a* and *c* are the amplitudes assigned to these constants respectively.

2.6.5 ^{64}Cu retention in BAEC incubated with ^{64}Cu-ATSM

The experimental protocols for BAEC incubation with ^{64}Cu-ATSM are described in more detail in chapter 4. Before executing these experiments, readings from the gamma counter were calibrated against stock solutions of $^{64}CuCl_2$ and incubation time of BAEC with ^{64}Cu-ATSM was determined.

2.6.5.1 Gamma counter calibration

Stock $^{64}CuCl_2$ was diluted to produce a series of known concentrations which were counted using a 1282 Compugamma gamma counter (LKB Wallac, Australia). The results were plotted on a graph (figure 2.12) and its equation was used to determine ^{64}Cu content in cell supernatants in subsequent experiments.

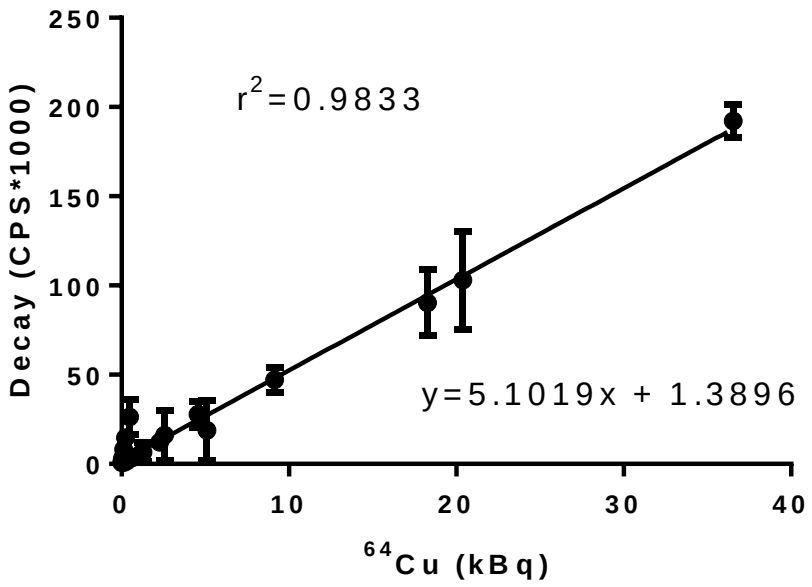

Figure 2.12 Gamma counter linearity. Decay (CPS) was plotted against the radioactivity (0-37MBq) of $^{64}CuCl_2$ aliquots. Data are expressed as means ± standard deviation, n=3.

2.6.5.2 Incubation time optimisation of ^{64}Cu-ATSM

BAEC were cultured as described in chapter 4. Confluent BAEC were incubated with 1kBq ^{64}Cu-ATSM diluted in serum free DMEM to 1 kBq/ mL. ^{64}Cu-ATSM and DMEM were removed every 15 mins for 120 mins. Cells were lysed with trypsin/ETDA immediately and aliquoted into tubes for counting. At the end of each experiment, all cell supernatants were counted for ^{64}Cu in the gamma

counter and ^{64}Cu content was determined according to figure 2.12. Supernatant protein concentration was determined using the BCA assay and ^{64}Cu BAEC retention was corrected for protein. Figure 2.13 displays the results from this incubation time optimisation study. BAEC retention of ^{64}Cu from ^{64}Cu-ATSM increased steadily over the first 60 mins and plateaued at 60 mins (3.1 ± 1.3 kBq/ mg protein). It was therefore decided that BAEC would be incubated with ^{64}Cu-ATSM for 60 mins in subsequent experiments.

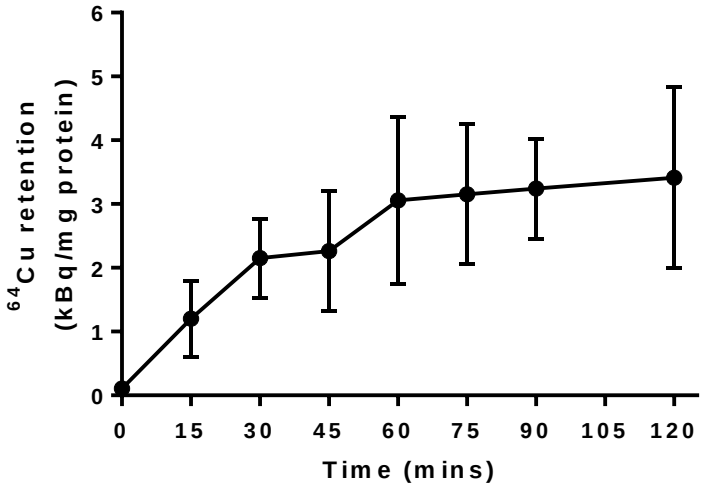

Figure 2.13 ^{64}Cu retention in BAEC incubated with ^{64}Cu-ATSM over time (0-120 minutes). Data are expressed as means ± standard deviation, n=3 plates with four replicate wells per group.

Chapter 3

Is the hypoxia selectivity of ^{64}Cu-ATSM dependent upon cardiac thiol status?

3.1 Introduction

Intracellular thiols (in particular GSH) have been suggested to be key reductants of Cu-BTSCs[118]. To date, however, there is no evidence for the direct effect of tissue thiol or GSH concentrations on the hypoxia selectivity of Cu-ATSM[5]. This is the first of two chapters describing the investigations into the effects of intracellular thiol concentration, through GSH level modification, on Cu-ATSM hypoxia selectivity in the cardiovascular system.

3.1.1 GSH changes during myocardial hypoxia and ischaemia

GSH is the most abundant intracellular thiol-containing molecule with a concentration of 0.5-10mM in mammalian cells[154]. It contains a cysteine residue which can non-enzymatically donate electrons to oxidising species such as free radicals and ROS, becoming oxidised itself and dimerising to glutathione disulphide (GSSG). Glutathione peroxidase uses GSH as an electron donor in the reduction and detoxification of intracellular peroxides. GSH is also able to directly reduce and repair oxidised thiols in cell proteins and membranes which would otherwise compromise cell function[155]. GSSG is then readily recycled to GSH by glutathione reductase, using the oxidation of NADPH. Changes in intracellular redox status are reflected in the oxidation/reduction of GSH/GSSG and are often measured as the ratio of GSH:GSSG, which is usually greater than 10:1 in healthy tissue.

A decrease in cardiac GSH:GSSG ratio by approximately 30% was observed in isolated perfused mouse hearts subject to 15 mins ischaemia and 30 mins reperfusion[156]. The decrease in GSH:GSSG reported suggests the generation

of ROS upon reperfusion. In isolated perfused rat hearts cytosolic GSH concentration decreased by 40% in the first 5 mins of reperfusion and it did not decline further during the following 25 mins of reperfusion, further suggesting that GSH depletion is mediated by the burst of ROS generation immediately upon reperfusion of ischaemic myocardium[157]. GSH synthesis is a two-step process which requires ATP-dependent enzymes γ-glutamylcysteine synthetase and GSH synthetase[155]. Thus, depletion of ATP during ischaemia further prevents GSH replenishment. Augmentation of intracellular GSH levels using the prodrug N-acetylcysteine (NAC) has been demonstrated to protect isolated perfused rabbit hearts from ischaemia-reperfusion injury[158], and decrease oxidative stress and improve post-surgical outcome in patients with CAD[159]. GSH is evidently a key protectant of the myocardium against oxidative stress. Myocardial hypoxia in the absence of ischaemia does not cause depletion of GSH[157]; similar tissue GSH concentrations have been reported in normoxic and hypoxic isolated hearts[157,160]. Hypoxia caused a decrease in GSH concentration and GSH:GSSG ratios in isolated hearts perfused with glucose free buffer, demonstrating the dependence of GSH regeneration upon glycolysis[161,162].

In summary, cardiac GSH levels are sensitive to both redox status and energy metabolism. Whilst cardiac GSH levels are maintained during hypoxia, ROS generation and downregulation of energy metabolism decrease intracellular GSH pools. Cardiac hypoxia coupled with ischaemia may also increase GSH pools. GSH status may therefore vary from heart to heart depending on the relative contributions of oxygen deficiency and impaired energy metabolism. As GSH represents the largest intracellular pool of reducing equivalents, and the first stage of Cu-ATSM trapping is reduction, it is essential (to understand the

mechanism of trapping) to determine whether intracellular thiol content (and changes in GSH concentration) play any part in the hypoxia-dependent tissue retention of Cu-ATSM.

3.1.2 Experimental approach

In this study, two well established agents which pharmacologically modify intracellular thiol concentration were used: buthionine sulphoximine (BSO) and N-acetylcysteine (NAC) to determine the effect of intracellular thiol status on ^{64}Cu-ATSM hypoxia selectivity and pharmacokinetics in isolated perfused rat hearts. BSO prevents GSH synthesis by inhibiting γ-glutamylcysteine synthetase [148], while NAC is a cysteine derivative which contributes to the intracellular thiol pool and GSH synthesis[149]. NAC also directly replenishes GSH non-enzymatically by direct thiol exchange with GSSG.

3.2 Materials and methods

3.2.1 Chemicals and reagents

BSO (DL-buthionine (S,R)-sulfoximine 99%), trichloroacetic acid (TCA) and the bicinchoninic acid (BCA) assay kit were obtained from Fisher Scientific, UK. NAC (N-acetyl-L-cysteine 99%) and O-phthalaldehyde (OPA) were both obtained from Sigma-Aldrich, UK. ^{64}Cu-ATSM was synthesised and labelled as described in chapter 2.

3.2.2 Animals

Male Wistar (275-350g) rats were used throughout. Rats were given *ad libitum* access to food and water. All experimental procedures were carried out in accordance with Home Office regulations as detailed in the Home Office Guidance on the Operation of Animals (Scientific Procedures) Act 1986.

3.2.3 Thiol concentration modification protocols

Rats were randomly assigned to treatment groups. Cardiac thiol levels were depleted by pre-treating rats bi-daily for two days with intraperitoneal (i.p) injections of BSO dissolved in 0.9% NaCl (total dose 4 mmol/ kg body weight). Hearts were excised and Langendorff-perfused 24 hrs after the final dose. Cardiac GSH levels were augmented by supplementing KHB with NAC (4 mmol/ L).

3.2.4 Perfusion protocols

Hearts were excised and perfused with KHB as described in chapter 2. All hearts were perfused with normoxic KHB for a stabilisation period of 10 min to ensure cardiac contractile function criteria were met before continuing the experiment. Hearts were perfused according to the protocols described in figure 3.1. Three boluses of ^{64}Cu-ATSM (2MBq) were injected into the perfusion line at t=10 mins, t=30 mins and t=45 mins. Samples of perfusate (approximately 1.5 mL) were collected directly from the heart at t=25, 26, 27, 28, 29, 30, 35, 40, 50 and 60 mins.

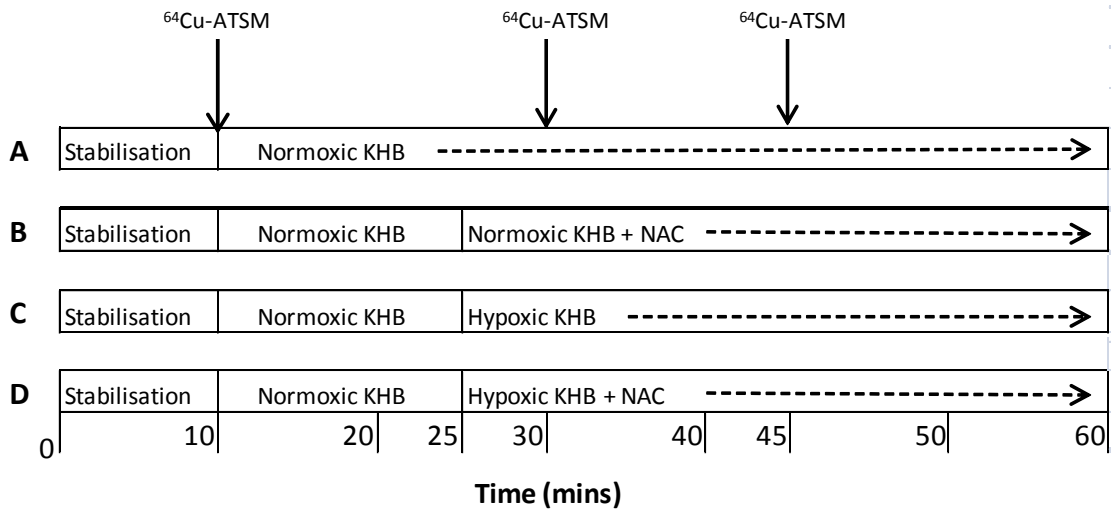

Figure 3.1. Perfusion protocols for hearts from all treatment groups. (A) normoxic control or normoxic thiol depleted (pre-treated with BSO), (B) normoxic thiol augmented, (C) hypoxic control or hypoxic thiol depleted and (D) hypoxic thiol augmented groups.

3.2.5 Thiol concentration analysis

At the end of each perfusion protocol, hearts were snap frozen in liquid nitrogen and stored at -70^{o}C. They were subsequently ground into a fine powder under liquid nitrogen using a steel pestle and mortar. 0.5g of powder was weighed into

centrifuge tubes and 2.5 mL ice-cold 6.5% TCA was added. Samples were then incubated for 20 mins on ice. Tubes were then centrifuged for 10 mins at 10,000 rpm at 4^{o}C. The TCA supernatant was aspirated and 0.25mL NaOH (1 mM) was added to the cell pellet. TCA supernatants were analysed for thiol content using the OPA fluorescence assay and NaOH samples were analysed for protein content using the BCA assay kit, both described in chapter 2.

3.2.6 ^{64}Cu-ATSM pharmacokinetic analysis

Cardiac ^{64}Cu-ATSM activity was detected utilising the custom built triple detector system. Time activity curve data were analysed with Microsoft Excel and MATLAB® to provide radiocopper retention and pharmacokinetic measurements, as described in chapter 2.

3.2.7 Statistical analysis

All data are presented as the mean ± standard deviation. Statistical significance was evaluated using ANOVA followed by Bonferroni post hoc test.

3.3 Results

3.3.1 Cardiac thiol concentration

Normoxic control hearts contained an average thiol concentration of 7.9 ± 2.0 nmol/ mg (figure 3.2). Perfusion with hypoxic buffer had no effect on thiol concentration (8.0 ± 1.7 nmol/ mg protein). Consistent with the preliminary data, pre-treatment with BSO significantly ($p<0.05$) decreased thiol concentrations (3.7 ± 1.0 nmol/ mg protein), which remained unaffected by hypoxia (3.3 ± 0.6 nmol/ mg protein). Perfusion with NAC significantly ($p<0.05$) increased cardiac thiol concentrations in normoxic (59.3 ± 8.3 nmol/ mg protein) hearts, which was not affected by perfusion with hypoxic buffer (67.1± 13.9 nmol/ mg protein).

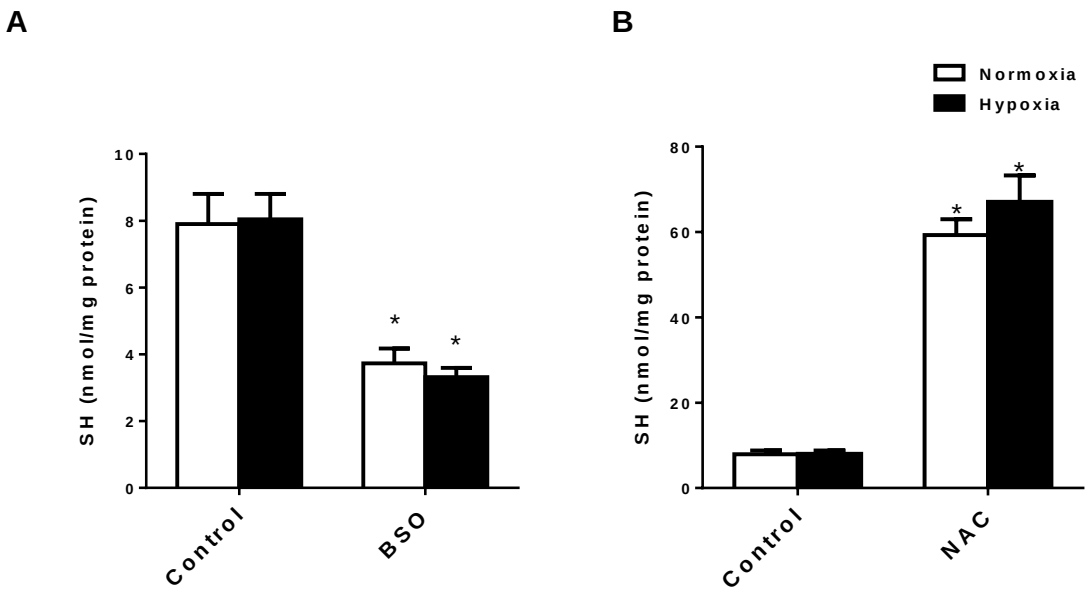

*Figure 3.2. Effect of (A) BSO pre-treatment and (B) NAC perfusion on myocardial thiol (SH) concentration. Data are expressed as means ± standard deviation (n=5 per group). *p<0.05 vs. untreated controls.*

3.3.2. Effect of cardiac thiol concentration on contractile function

Functional parameters were measured throughout each experiment to assess the effect of thiol modification and hypoxia on the heart. Heart rate, coronary perfusion pressure, left ventricular developed pressure (LVDP) and left ventricular end diastolic pressure (LVEDP) were measured in real time, while cardiac lactate and protein release into the coronary effluent was analysed after the experiment.

3.3.2.1 Heart rate

Hearts rates from all experiments are displayed in figure 3.3. Heart rates of normoxic untreated controls remained stable (altering less than 10%) until the end of perfusion (269.0 ± 17.3 to 259.3 ± 28.8 b.p.m. after 60 mins). Hypoxia caused heart rates to decrease from 264.1 ± 22.7 to 232.0 ± 24.3 b.p.m. within 5 mins of switching to hypoxic KHB and continued to decline until the end of perfusion (170±49.8 b.p.m.). Thiol depletion did not affect heart rate during normoxia (271.7 ± 33.5 to 252.0 ± 35.6 b.p.m. after 60 mins). Thiol depletion had no further effect on heart rate during hypoxia which decreased from 288.3 ± 16.0 to 201.4 ± 58.4 b.p.m. by the end of perfusion. Thiol augmentation also did not affect heart rates during normoxia (283.7 ± 12.8 to 268.3 ± 30.7 b.p.m.) or hypoxia (283.3 ± 43.3 to 188.2 ± 64.1b.p.m.).

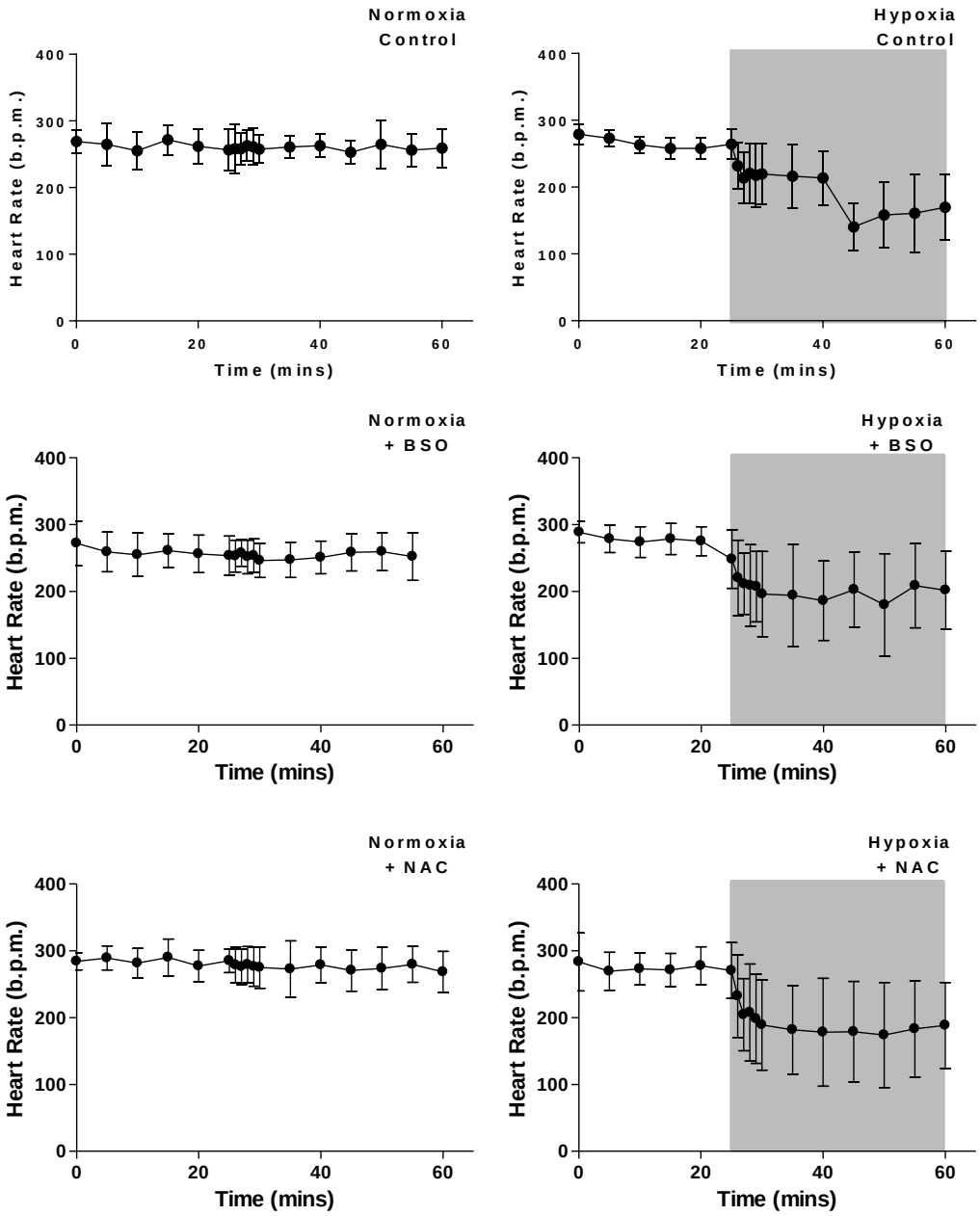

Figure. 3.3. Heart rate (mmHg) of normoxic control (top left), hypoxic control (top right), normoxic thiol depleted (centre left), hypoxic thiol depleted (centre, right) normoxic thiol augmented (bottom left) and hypoxic thiol augmented (bottom right) hearts.. Data are expressed as means ± standard deviation (n = 5).

3.3.2.2 Coronary Perfusion Pressure

Figure 3.4 displays the coronary perfusion pressures of hearts from all protocols. Perfusion pressure was maintained in normoxic control hearts throughout each experiment (69.5 ± 9.2 mmHg to 71.5 ± 5.5 mmHg). Perfusion with hypoxic buffer caused a steady increase in perfusion pressure and was 37% higher by the end of perfusion (67.7 ± 12.6 mmHg to 92.9 ± 20.9 mmHg). The average perfusion pressure of thiol depleted hearts was 16.7% higher than that of control hearts at the beginning of the perfusion protocol (79 ± 24.5 mmHg *vs.* 67.7 ± 12.6 mmHg control). Thiol depletion also caused a 38% increase in perfusion pressure after 60 mins perfusion with normoxic buffer (77.3 ± 19.8 mmHg to 107.0 ± 31.7 mmHg) and a 30% increase under hypoxic conditions (80.7 ± 29.3 mmHg to 105.1 ± 34.9 mmHg). Perfusion with buffer containing NAC also increased perfusion pressure by 17% during normoxic perfusion (70.5 ± 12.7 mmHg to 83.9 ± 21.9 mmHg) and 18% during hypoxic perfusion (76.9 ± 20.7 mmHg to 90.1 ± 33.4 mmHg).

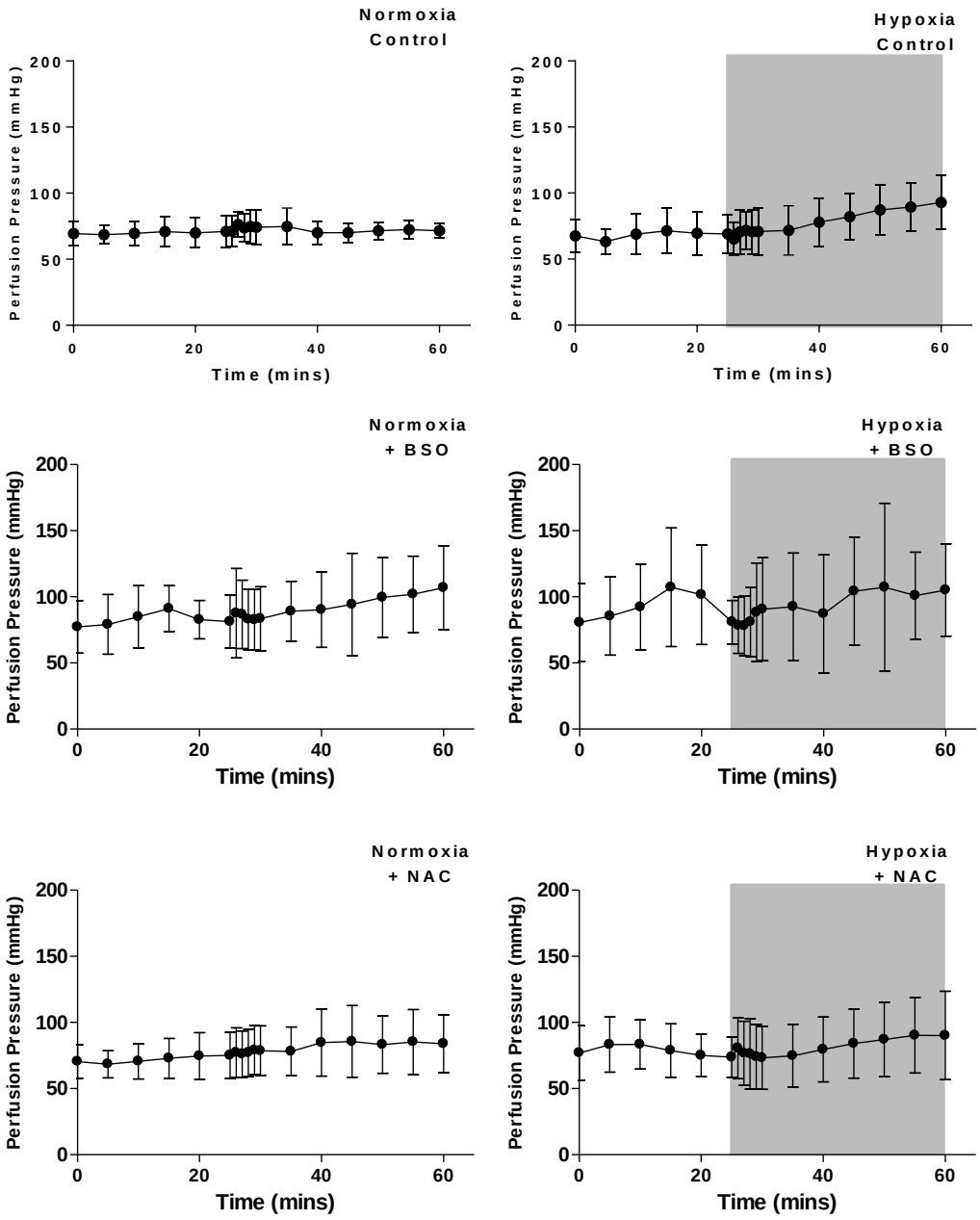

Figure 3.4. Coronary perfusion pressure (mmHg) of hearts as described in figure 3.3. Data are expressed as means ± standard deviation (n = 5).

3.3.2.3 Left ventricular developed pressure (LVDP)

During the normoxic control period, all hearts maintained a LVDP above 110mmHg with the exception of thiol depleted hearts, where LVDP was below 110mmHg for the first 25 mins of perfusion (figure 3.5). In normoxic control experiments, end LVDP was 10% less than the original starting value, consistent with the previously established exclusion criteria (122.9 ± 34.9 mmHg to 110.4 ± 14.9 mmHg). Hypoxia caused a rapid decline in LVDP, decreasing by 83.8% (122.6 ± 23.5 mmHg to 19.9 ± 10.0 mmHg). Thiol depletion did not affect LVDP in normoxic hearts (104.6 ± 28.4 mmHg to 102.5 ± 21.9mmHg), however, caused a decrease in LVDP in hypoxic hearts (110.2 ± 38.2 mmHg to 26.9 ± 18.1 mmHg) with end values 35% higher than hearts perfused with hypoxic buffer alone. Thiol augmentation also did not affect LVDP in normoxic hearts (121.6 ± 29.5 mmHg to 106.3 ± 15.6 mmHg. As with hypoxic buffer perfusion alone, thiol augmentation caused LVDP to decrease during hypoxia, however, values were 2.2 fold higher than hypoxic hearts by the end of the experimental protocol (112.0 ± 31.9 mmHg to 50.4 ± 32.3 mmHg).

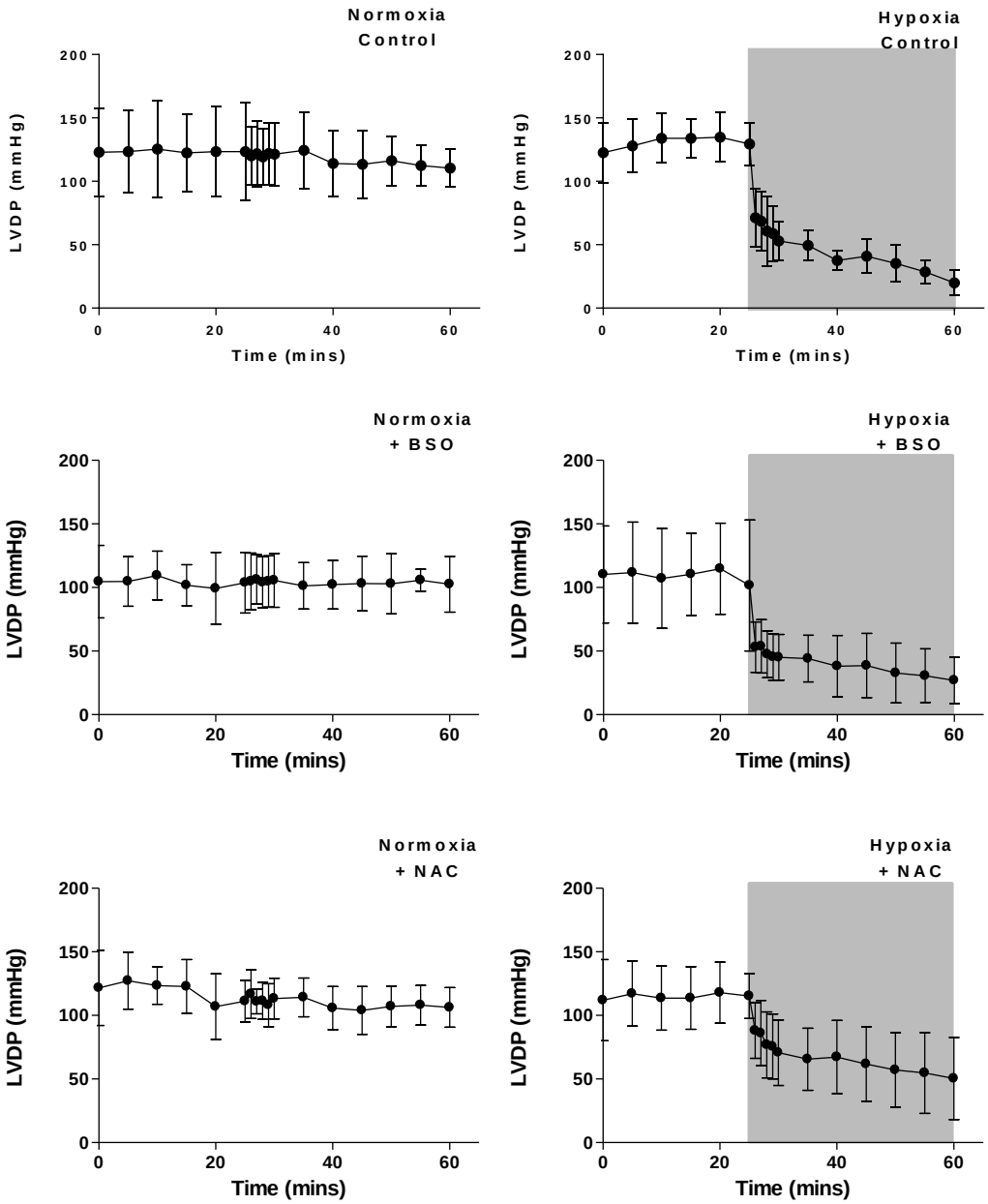

Figure. 3.5. LVDP (mmHg) of hearts as described in figure 3.3.. Data are expressed as means ± standard deviation (n = 5).

3.3.2.4 Left ventricular end diastolic pressure (LVEDP)

LVEDP was pre-set to between 4 and 10 mmHg before each experiment in all hearts (figure 3.6). During the stabilisation period, LVEDP did not alter more than 10%, consistent with exclusion criteria data, and was stable over 60 minutes perfusion with normoxic buffer, while perfusion with hypoxic buffer caused a 10 fold increase in LVEDP (5.5 ± 1.2 mmHg to 69.3 ± 19.5 mmHg). Thiol depletion caused LVEDP to almost double during normoxic perfusion (6.9 ± 1.0 mmHg to 12.2 ± 2.1 mmHg), although the increase observed due to hypoxia was not significantly ($p<0.05$) different from hypoxia alone (6.4 ± 1.1 mmHg to 65.4 ± 41.9 mmHg). Hypoxia caused LVEDP to increase in thiol augmented hearts, however, end values were 30% lower compared to hypoxia alone (6.3 ± 1.9 mmHg to 46.4 ± 25.9 mmHg).

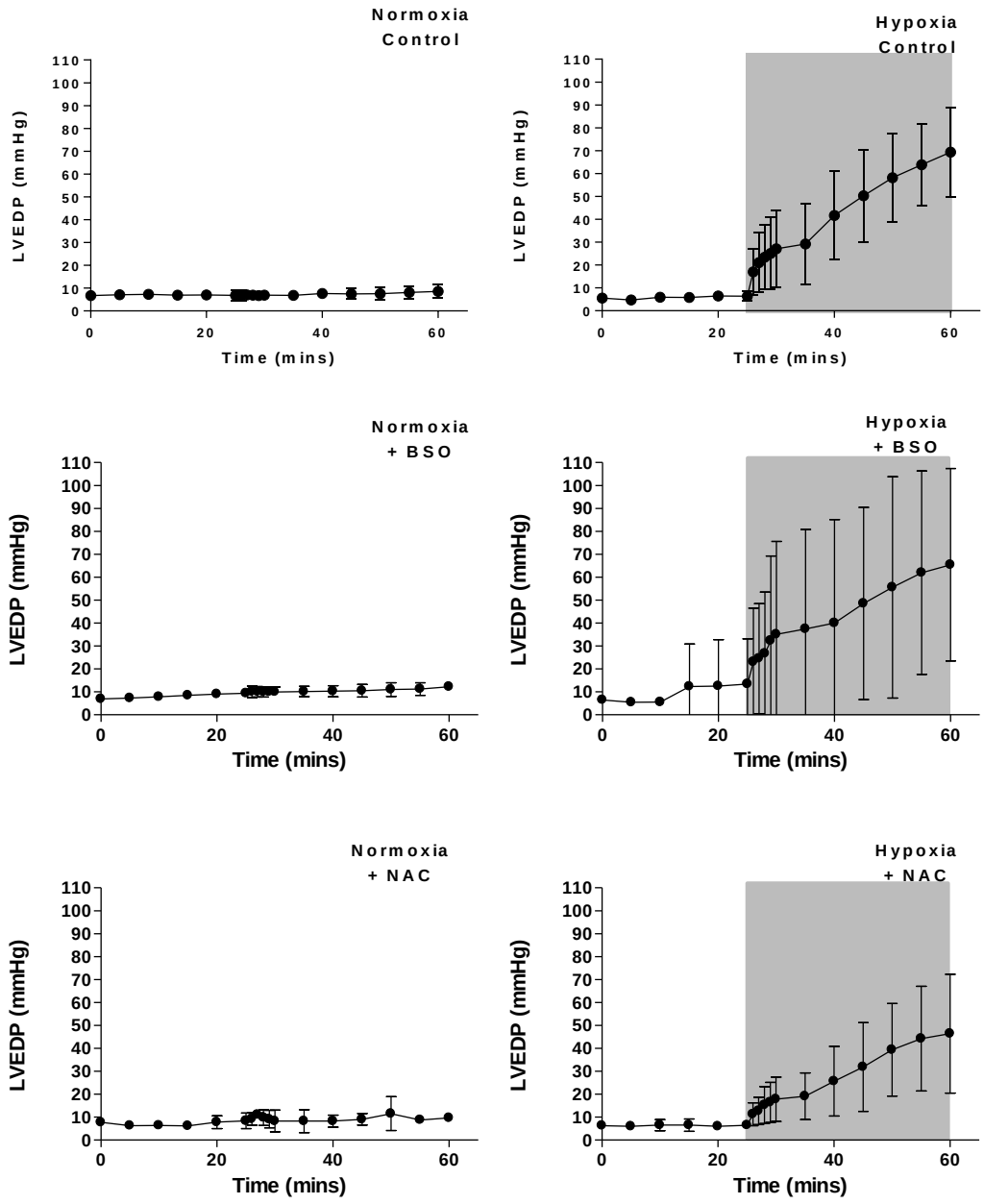

Figure. 3.6. LVEDP (mmHg) of hearts as described in figure 3.3.. Data are expressed as means ± standard deviation (n = 5).

3.3.3 Cardiac lactate release, glucose consumption and protein release

3.3.3.1 Lactate release

Figure 3.7 displays the lactate concentration of perfusate samples collected from all hearts. Lactate release from normoxic control hearts was minimal during normoxia and remained stable throughout perfusion (0.08 ± 0.01 nmol to 0.11 ± 0.07 nmol /mL /g dry wt). Lactate release increased rapidly in hypoxic control hearts within minutes of introducing hypoxic KHB buffer, peaking after 3 mins (0.40 ± 0.07 nmol /mL /g dry wt). Thiol depletion did not affect lactate release from normoxic hearts (0.08 ± 0.03 to 0.14 ± 0.06 nmol /mL /g dry wt). Lactate release was similar in hypoxic thiol depleted hearts to that of hypoxia alone, increasing from 0.07 ± 0.006 to 0.29± 0.11 nmol /mL /g dry wt within 3 mins. Thiol augmentation did not affect lactate release during normoxia (0.05 ± 0.02 to 0.09 ± 0.02 nmol /mL /g dry wt) and during hypoxia lactate release was similar to that of hypoxia alone, increasing from 0.11 ± 0.04 to 0.37 ± 0.03 nmol /mL /g dry wt after 3 mins.

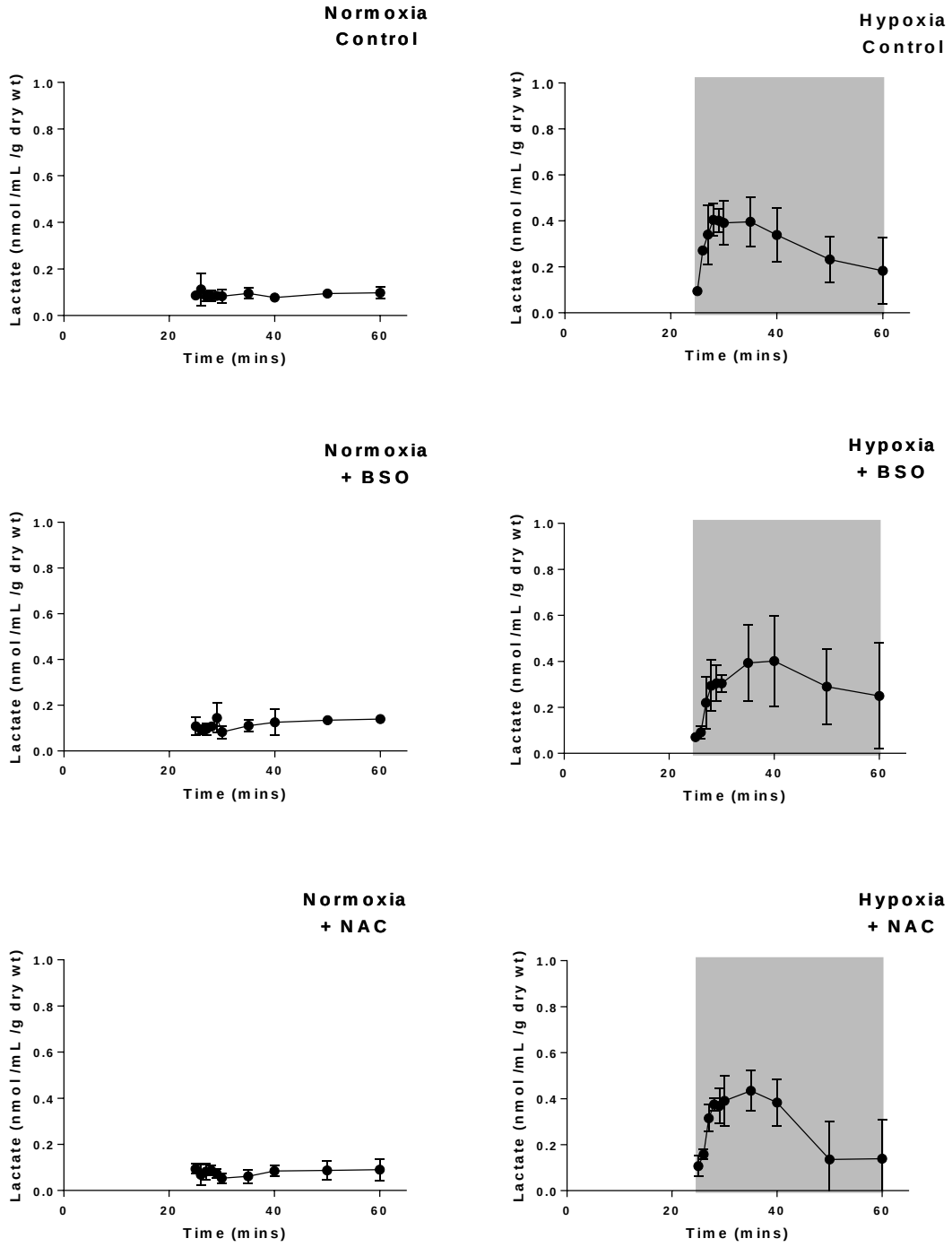

Figure 3.7. Lactate concentration of perfusate samples collected from hearts as described in figure 3.3.. Data are expressed as means ± standard deviation (n = 5).

3.3.3.2 Glucose consumption

Cardiac glucose consumption remained constant throughout all perfusion protocols (figure 3.8). There were no changes detected in myocardial glucose consumption from all protocols. During normoxic perfusions, perfusate glucose concentration ranged from 10.7± 0.03 to11.2 ± 0.54 mmol/ L in normoxic control hearts, 10.6 ± 0.23 to 11.3 ± 0.35 mmol/ L in thiol depleted hearts and 10.5 ± 0.37 to 11.2 ± 0.41 mmol/ L in thiol augmented hearts. During hypoxic perfusions, perfusate glucose concentration ranged from 10.6± 0.25 to 11.1 ± 0.19 mmol/ L in hearts perfused with hypoxic buffer alone, 10.7 ± 0.28 to 11.1 ± 0.43 mmol/ L in thiol depleted hypoxic hearts and 10.7 ± 0.61 to 11.2 ± 0.46 mmol/ L in thiol augmented hypoxic hearts.

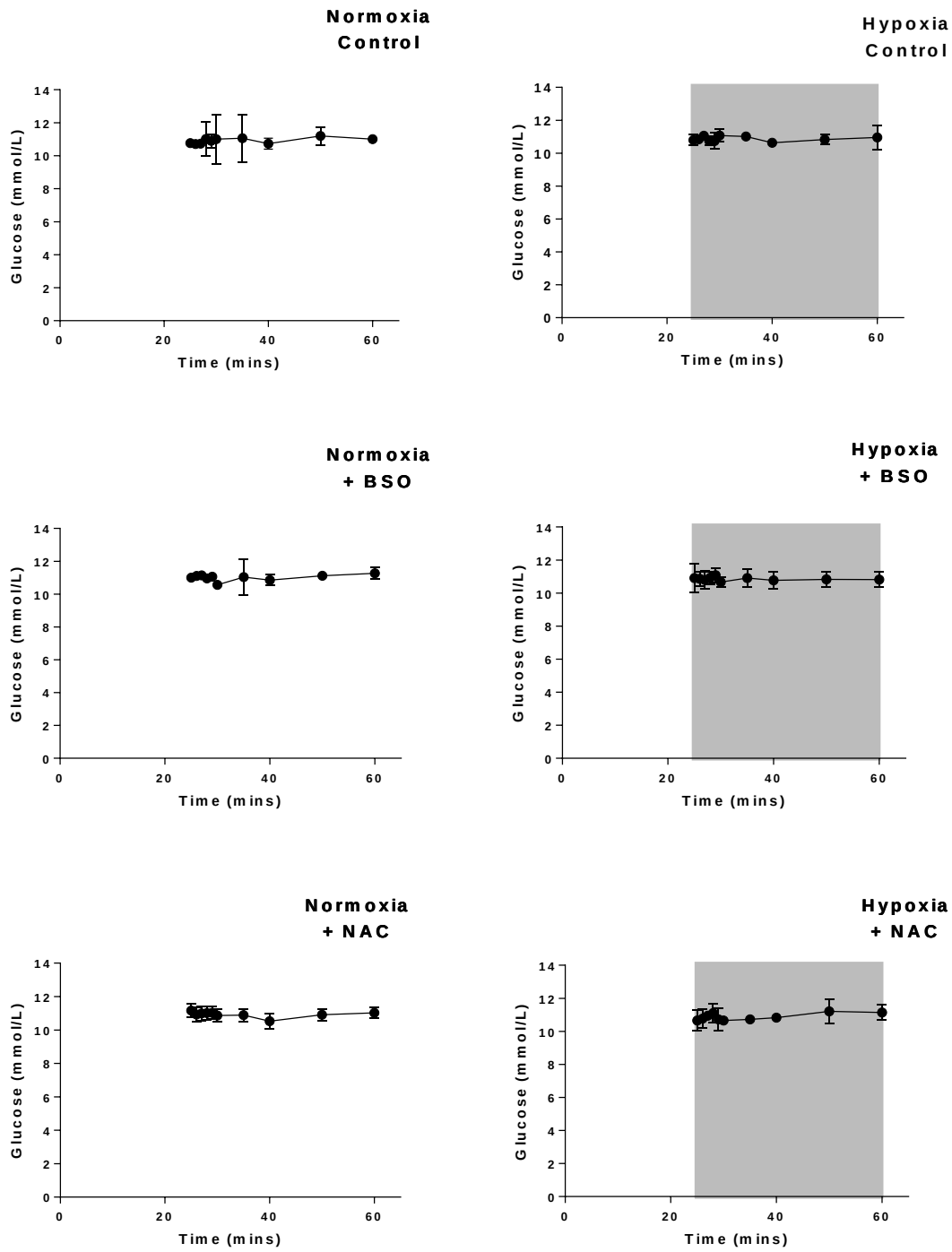

Figure 3.8. Glucose concentration of perfusate samples collected from hearts as described in figure 3.3. Data are expressed as means ± standard deviation (n = 5).

3.3.3.3 Cardiac protein release

Figure 3.9 displays protein concentrations of the perfusate collected for all hearts. Hypoxia did not cause an increase in cardiac protein release compared with normoxia (0.01 ± 0.007 to 0.02 ± 0.12 *vs.* 0.01 ± 0.006 to 0.03 ± 0.013 mg /mL /g dry wt). Thiol depletion increased protein release in hypoxic hearts (0.04 ± 0.02 to 0.05 ± 0.02 mg /mL /g dry wt *vs.* 0.01 ± 0.01 to 0.03 ± 0.008 mg /mL /g dry wt during normoxia. Thiol augmentation, however, appeared to increase cardiac protein release during both normoxia (peaking at 0.24 ± 0.15 mg /mL /g dry wt) and hypoxia (peaking at 0.54 ± 0.10 mg /mL /g dry wt), however, these results probably reflect increases in perfusate cysteine concentration rather than cardiac protein release.

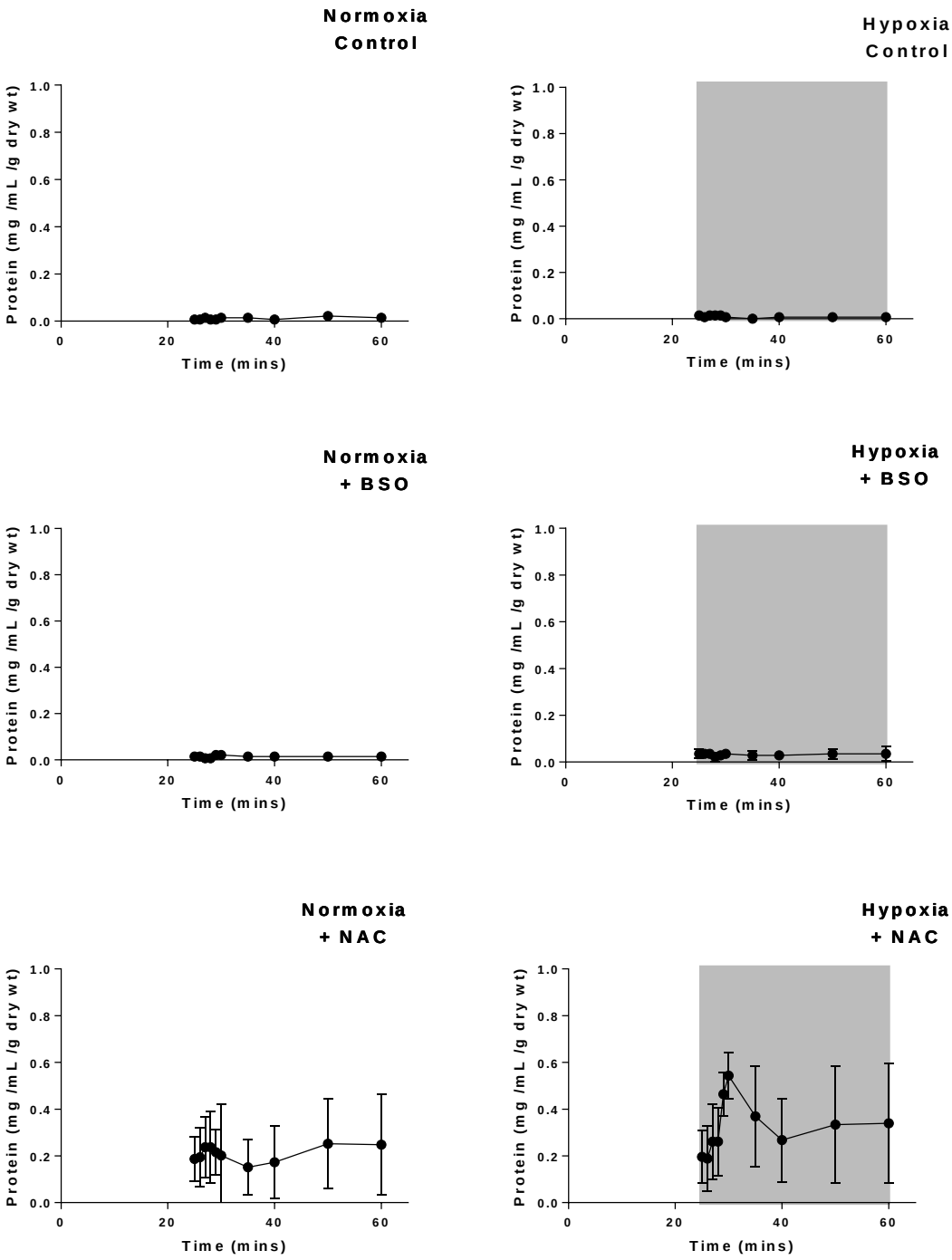

Figure 3.9. Protein concentration of perfusate samples collected from as described in figure 3.3.. Data are expressed as means ± standard deviation (n = 5).

3.3.4 Myocardial ^{64}Cu retention from ^{64}Cu-ATSM in thiol-modified hearts

Representative time-activity curves from hearts administered with three bolus injections of ^{64}Cu-ATSM are displayed in figure 3.10. These data were obtained from the 2nd γ-detector from the γ-triple detector system described in chapter 2.

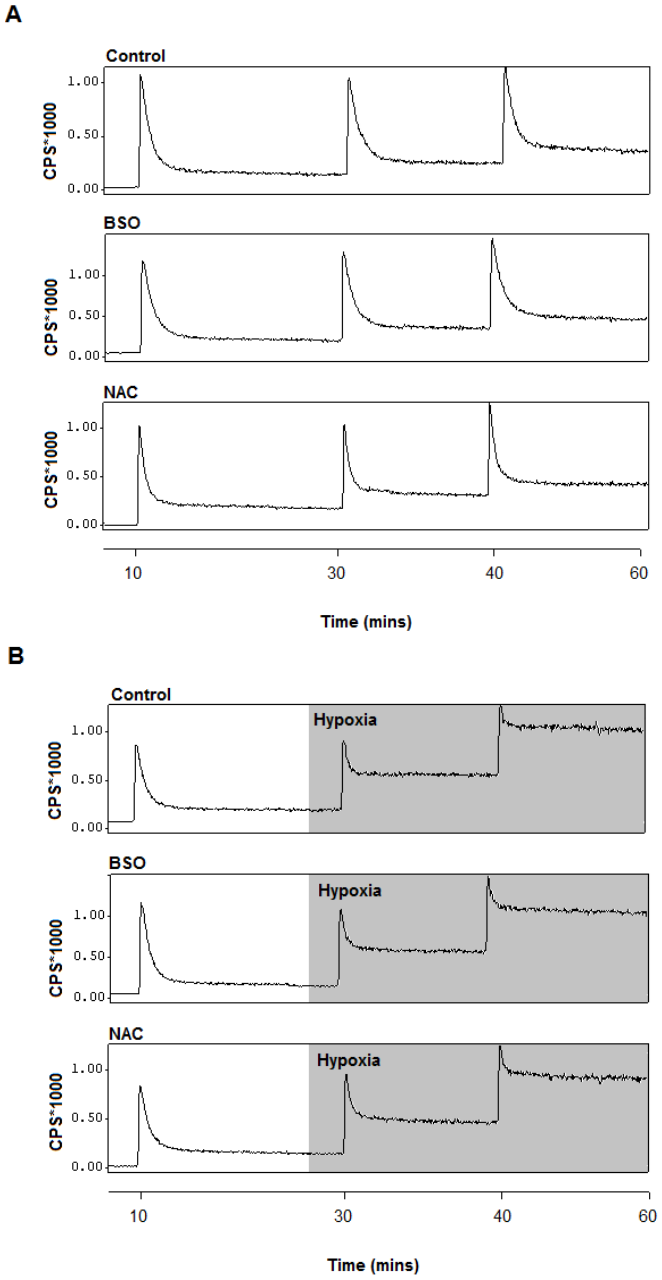

Figure 3.10. Representative time-activity curves demonstrating ^{64}Cu uptake from ^{64}Cu-ATSM in (A) normoxic hearts and (B) hypoxic hearts. Curves represent untreated hearts (control) thiol depleted hearts (BSO) and thiol augmented hearts (NAC).

The degree of cardiac tracer trapping was calculated as the amount of tracer trapped in the heart 15 minutes post injection as a percentage of the peak activity in the heart immediately after injection. Perfusion with normoxic buffer did not affect the degree of ^{64}Cu retention from ^{64}Cu-ATSM injections after 10, 30 or 45 perfusion (13.1 ± 1.7 %, 13.7 ± 3.9 % and 13.3 ± 2.1 % respectively). Perfusion with hypoxic buffer increased ^{64}Cu retention significantly ($p<0.05$) in untreated hearts after 5 mins (early hypoxia 45.6 ± 5.8 %) which increased further after 20 mins (late hypoxia 59.1 ± 6.3 %). Thiol depletion did not affect ^{64}Cu retention from any of the three ^{64}Cu-ATSM injections in normoxic protocols (13.3 ± 2.8 %, 11.1 ± 2.6 % and 13.2 ± 4.6 %), nor did it affect the retention of copper in hypoxic hearts compared to hearts perfused with hypoxic buffer alone (46.5 ± 5.5 % during early hypoxia and 51.3 ± 12.1 % during late hypoxia). Thiol augmentation also did not affect ^{64}Cu retention in normoxic hearts from any of the three ^{64}Cu injections (14.5 ± 1.9 %, 17.5 ± 4.6 % and 16.0 ± 2.6 %). Thiol augmentation did not enhance hypoxia selective ^{64}Cu retention during early hypoxia compared to that of hypoxia alone (44.9 ± 5.2 %), however, during late hypoxia thiol augmentation significantly ($p<0.05$) decreased in ^{64}Cu retention compared to hypoxia alone (41.7 ± 3.2 % *vs*. 59.1 ± 6.3 %).

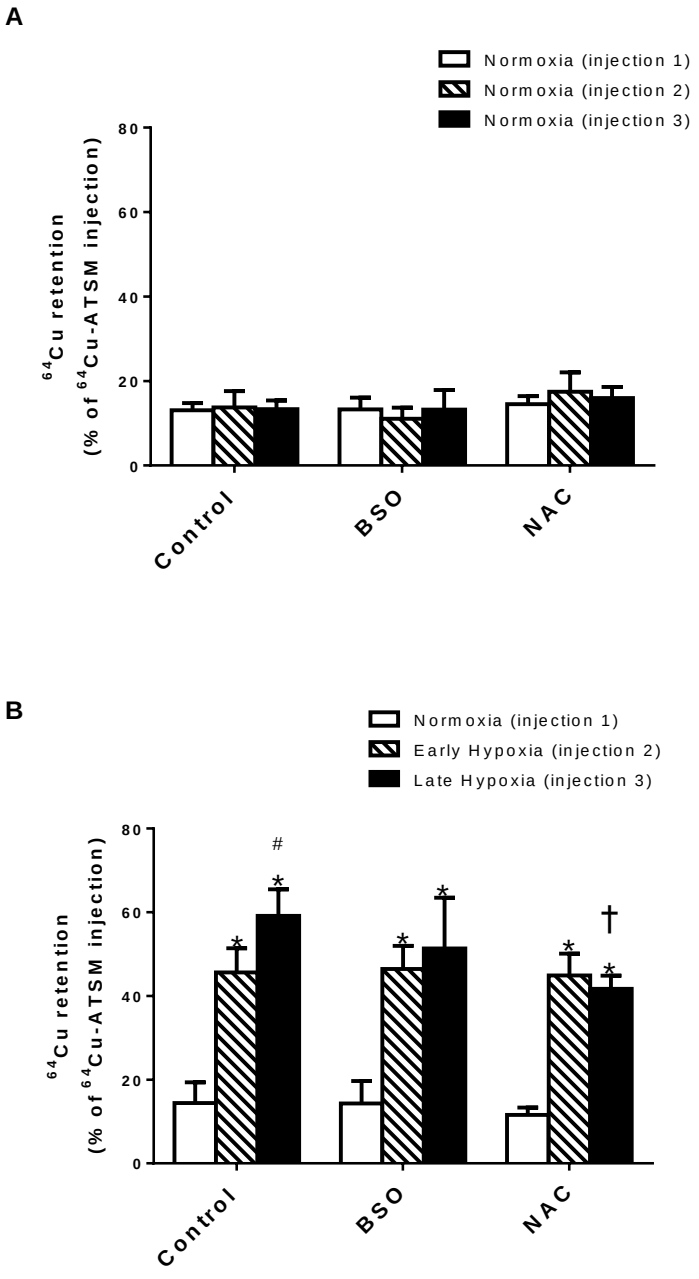

*Figure 3.11. Effect of thiol depletion (BSO) and augmentation (NAC) on ^{64}Cu retention in (A) normoxic and (B) hypoxic hearts. Data are expressed as the % of total activity injected (means ± standard deviation, n=5 per group). *p<0.05 vs. normoxia (injection 1), #p<0.05 vs. early hypoxia (injection 2) and †p<0.05 vs. late hypoxia alone (injection 3).*

3.3.5 Pharmacokinetic analysis of time-activity curve data

To determine whether thiol modification changed the pharmacokinetics of ^{64}Cu-ATSM washout, time activity curves of tracer washout were fitted with a bi-exponential function to obtain a fast clearance rate (FCR), a slow clearance rate (SCR), and indices of their respective importance in governing overall washout (their amplitudes). These data are summarised in tables 3.1 and 3.2. Neither the FCR nor the SCR or their amplitudes changed during the normoxic perfusion protocol (figures 3.12-3.13). Thiol depletion or augmentation had no effect on either FCR or SCR during normoxic perfusion, or their respective amplitudes. The amplitude of the FCR was significantly ($p<0.05$) higher than that of the SCR during normoxia, and was unaffected by thiol concentration modification (figure 3.14).

During late hypoxia, the FCR increased significantly ($p<0.05$) over control values to an equal degree in both untreated and thiol modified hearts while the SCR fell significantly ($p<0.05$) in all groups, irrespective of drug regimen (figures 3.12 and 3.11). With progressive hypoxia, the amplitude of the SCR rose significantly ($p<0.05$), and the corresponding FCR fell. This was unaffected by thiol modification (figure 3.14).

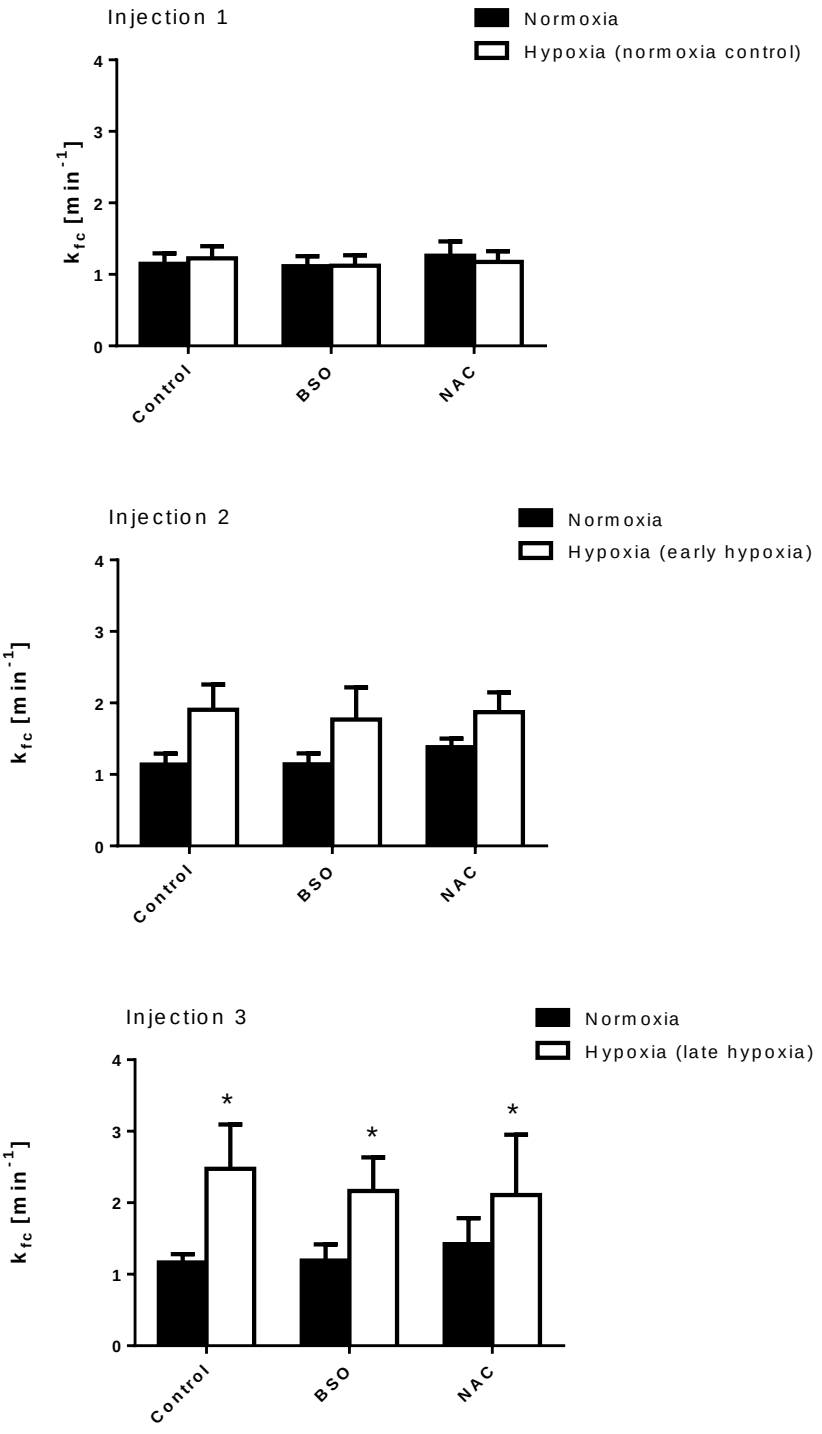

*Figure 3.12. FCR of each ^{64}Cu-ATSM injection as determined by the bi-exponential analysis of ^{64}Cu clearance from heart tissue based on time-activity curve data. Data are expressed as means ± standard deviation, n=5 per group, *p<0.05 vs. normoxic equivalent.*

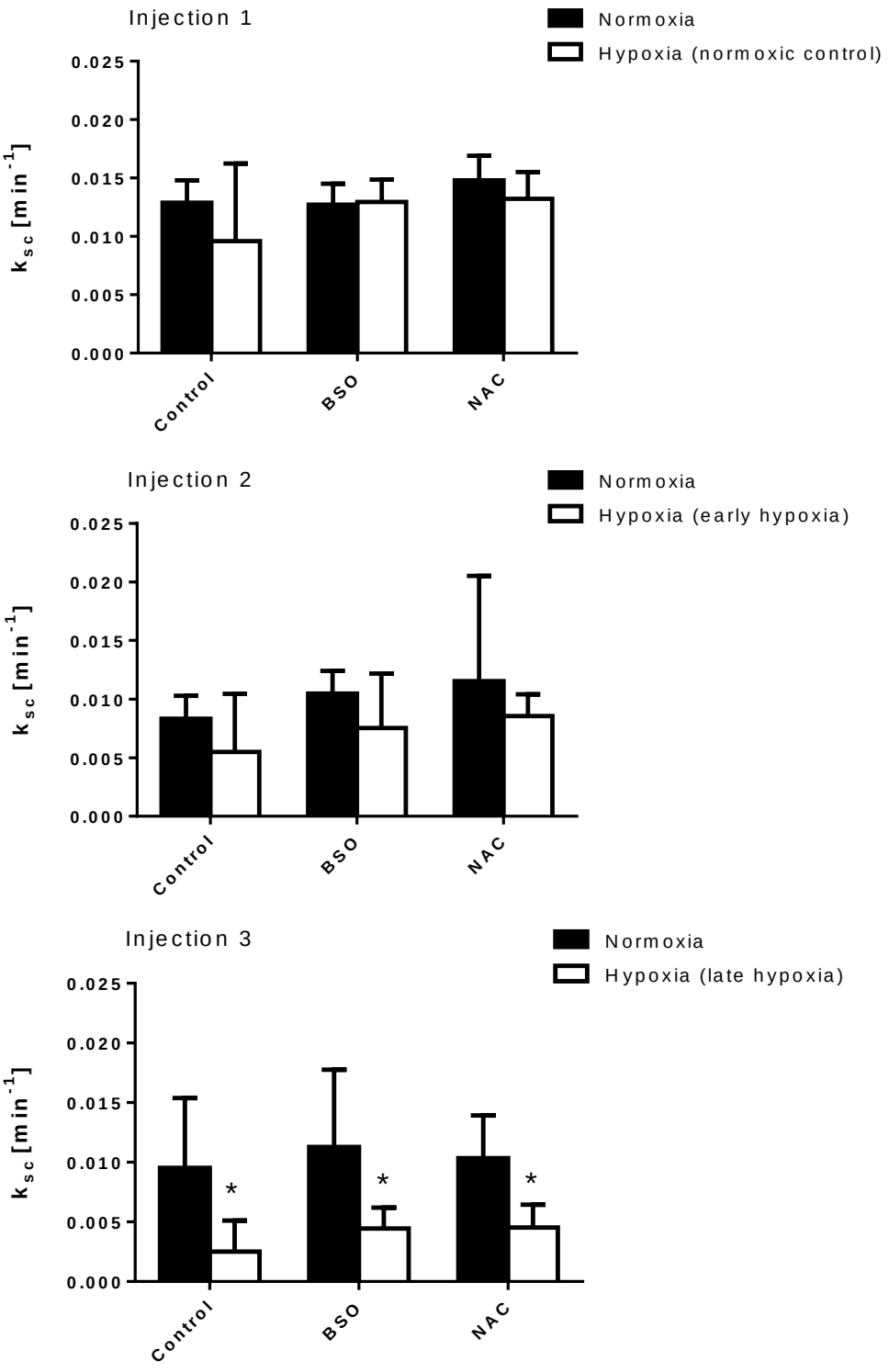

*Figure 3.13. SCR of each ^{64}Cu-ATSM injection as determined by the bi-exponential analysis of ^{64}Cu clearance from heart tissue based on time-activity curve data. Data are expressed as means ± standard deviation, n=5 per group, *p<0.05 vs. normoxic equivalent.*

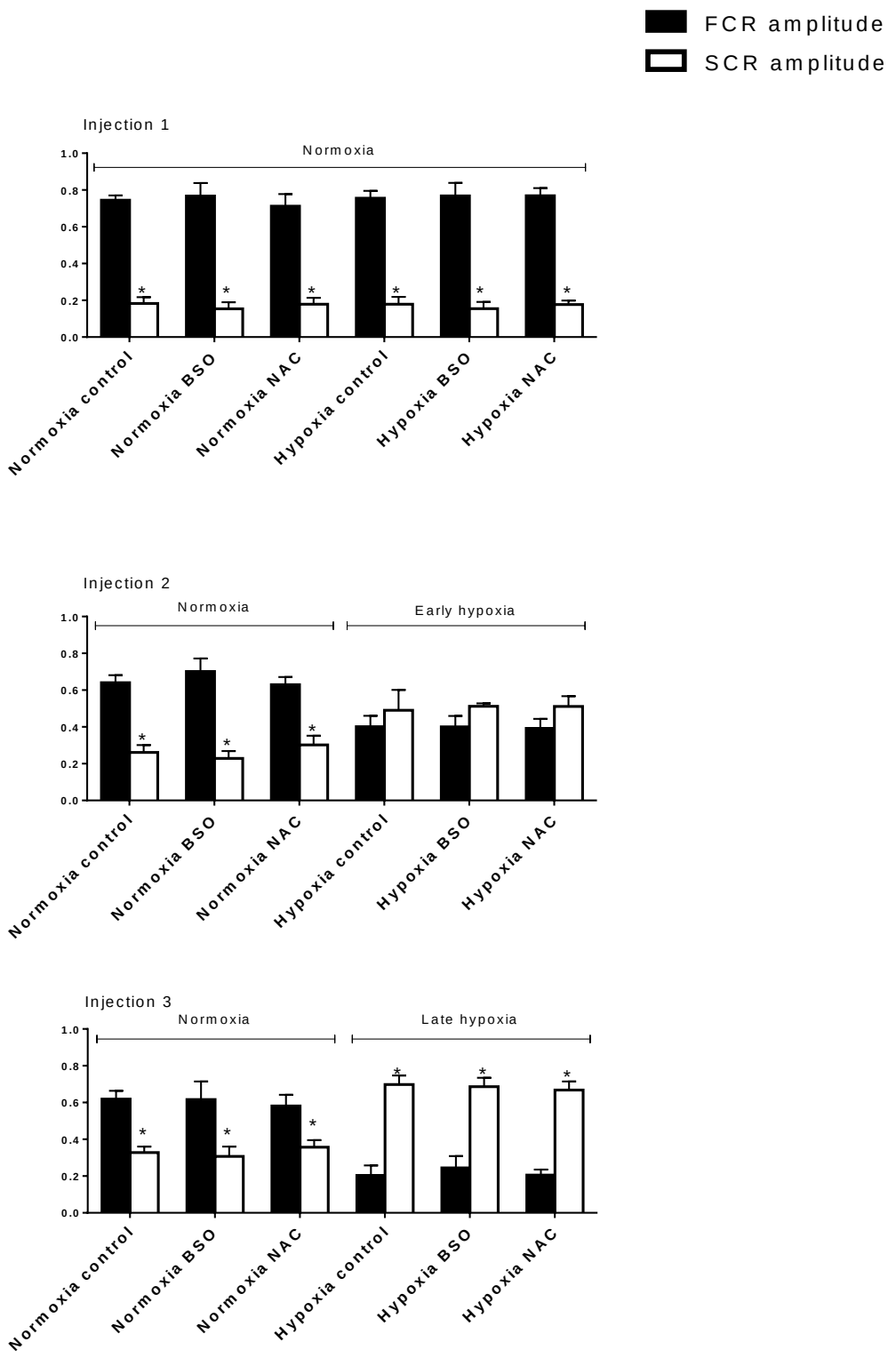

*Figure 3.14. Amplitude of the FCR and SCR for all injections of ^{64}Cu-ATSM in all hearts (means ± standard deviation, n=5 per group). *p<0.05 vs. SCR amplitude.*

Table 3.1. FCR and SCR values from figures 3.12-3.13. Data are expressed as the rates of ^{64}Cu clearance from the heart (k_{fc}[min-^{1}] or k_{sc}[min^{-1}]; means ± standard deviation, n=5 per group).

	Injection	FCR (k_{fc} [min^{-1}])		
		Control	BSO	NAC
Normoxic hearts	1: Normoxia	1.2 ± 0.2	1.1 ± 0.1	1.3 ± 0.2
	2: Normoxia	1.1 ± 0.2	1.1 ± 0.2	1.4 ± 0.1
	3: Normoxia	1.2 ± 0.1	1.2 ± 0.2	1.4 ± 0.4
Hypoxic hearts	1: Normoxia	1.2 ± 0.2	1.1 ± 0.2	1.2 ± 0.2
	2: Early hypoxia	1.9 ± 0.4	1.8 ± 0.5	1.9 ± 0.3
	3: Late hypoxia	*2.5 ± 0.6	*2.2 ± 0.5	*2.2 ± 0.8
		SCR (k_{sc} [min^{-1}])		
		Control	BSO	NAC
Normoxic hearts	1: Normoxia	0.01. ± 0.002	0.008 ± 0.002	0.01 ± 0.006
	2: Normoxia	0.01 ± 0.002	0.01 ± 0.008	0.01 ± 0.006
	3: Normoxia	0.01 ± 0.002	0.01 ± 0.004	0.01 ± 0.004
Hypoxic hearts	1: Normoxia	0.01 ± 0.007	0.01 ± 0.002	0.01 ± 0.002
	2: Early hypoxia	0.007 ± 0.005	0.008 ± 0.005	0.009 ± 0.002
	3: Late hypoxia	*0.003 ± 0.003	*0.004 ± 0.002	*0.005 ± 0.002

**p < 0.05 vs. normoxic equivalent*

Table 3.2. Amplitudes of FCR and SCR from figure 3.14. Data are expressed as weights corresponding to the ^{64}Cu FCR or SCR of each ^{64}Cu-ATSM injection (means ± standard deviation, n=5 per group).

	Injection	FCR amplitude (arbitrary units)		
		Control	BSO	NAC
Normoxic hearts	1: Normoxia	0.7 ± 0.02	0.8 ± 0.07	0.7 ± 0.07
	2: Normoxia	0.6 ± 0.04	0.7 ± 0.07	0.6 ± 0.04
	3: Normoxia	0.6 ± 0.04	0.6 ± 0.1	0.6 ± 0.06
Hypoxic hearts	1: Normoxia	0.8 ± 0.04	0.8 ± 00.07	0.8 ± 0.04
	2: Early hypoxia	0.4 ± 0.06	0.4 ± 0.06	0.4 ± 0.05
	3: Late hypoxia	0.2 ± 0.03	0.2 ± 0.06	0.2 ± 0.03
		SCR amplitude (arbitrary units)		
		Control	BSO	NAC
Normoxic hearts	1: Normoxia	* 0.2 ± 0.03	* 0.2 ± 0.04	* 0.2 ± 0.03
	2: Normoxia	* 0.3 ± 0.04	* 0.2 ± 0.04	* 0.3 ± 0.05
	3: Normoxia	* 0.3 ± 0.03	* 0.3 ± 0.05	* 0.4 ± 0.04
Hypoxic hearts	1: Normoxia	* 0.2 ± 0.04	* 0.2 ± 0.04	* 0.2 ± 0.02
	2: Early hypoxia	0.5 ± 0.1	0.5 ± 0.02	0.5 ± 0.06
	3: Late hypoxia	* 0.7 ± 0.05	* 0.7 ± 0.05	* 0.7 ± 0.05

**p < 0.05 vs. normoxic equivalent*

3.4 Discussion and conclusions

3.4.1 Effect of thiol concentration on ^{64}Cu-ATSM hypoxia selectivity

3.4.1.1 Cardiac ^{64}Cu retention from ^{64}Cu-ATSM

Our study is the first attempt to investigate the effect of modifying thiol concentration on ^{64}Cu retention from ^{64}Cu-ATSM in the heart. Donnelly *et al.* have reported that BSO incubation does not affect Cu retention from Cu-ATSM (measured using a metal-responsive element luciferase assay) in neuroblastoma SH-SY5Y cells under normoxic conditions[132]. Evidence of cellular protein oxidation in these cells indicated compromised redox status through GSH depletion; however, this group did not confirm the link by measuring intracellular thiol concentrations. In these experiments, it was demonstrated that measurable thiol depletion or augmentation does not affect ^{64}Cu retention from ^{64}Cu-ATSM. This is with the exception of the thiol augmented group where a decrease in ^{64}Cu retention was observed during late hypoxia compared to untreated hypoxic controls. It is possible that over longer periods of NAC supplementation, increases in thiol concentration prevents the reduction of Cu(II)-ATSM to Cu(I)-ATSM^{-} by free radicals. Thus, the antioxidant function of GSH may scavenge reductant which may otherwise reduce Cu-ATSM. It is not currently known whether BTSC complexes are sensitive to free radical production and the effects of free radical generation and redox status on Cu-ATSM hypoxia selectivity requires further investigation.

3.4.1.2 Cardiac ^{64}Cu-ATSM pharmacokinetics

In these studies, the hypoxia-dependent accumulation of Cu-ATSM in cardiac tissue has been confirmed, as has been shown previously[115,116, 114,163], but are the first to perform pharmacokinetic analysis in the heart. Kinetic analysis of the time-activity curve data allowed us to determine the effect of hypoxia and thiol concentration on the FCR and SCR of ^{64}Cu-ATSM in the heart. Previously the pharmacokinetics of hypoxia tracer ^{99m}Tc-nitroimidzole in isolated perfused hearts was investigated and it was suggested that the FCR represents tracer washout through the vasculature and SCR is an index of cellular tracer trapping[164]. Here, it was demonstrated that the FCR increases and the SCR decreases with increasing hypoxia severity. During normoxia, the FCR is the dominant rate governing tracer washout. It is currently unclear why the FCR may increase during late hypoxia. It is possible that as vasodilation occurs, the myocardial surface area to volume ratio of the vasculature falls, such that there is a decreased likelihood of the tracer interacting with cell membranes which would otherwise slow its passage through the heart. As the heart becomes hypoxic, the SCR becomes the dominant rate, describing the increased trapping of the tracer within the myocardium. Thiol depletion or augmentation did not affect FCR, SCR or corresponding amplitudes during normoxia or hypoxia. This reinforces the retention data demonstrating that thiol concentration does not determine ^{64}Cu-ATSM dissociation, hypoxia selectivity or pharmacokinetics.

While it has been demonstrated that cardiac thiol concentration does not influence the hypoxia selectivity or pharmacokinetics of Cu-ATSM, the

possibility that intracellular thiols are important in Cu-ATSM reduction cannot be excluded. In 1972 Petering demonstrated the reactivity of Cu-BTSC with thiols reporting that Cu-KTS, another Cu-BTSC, was reduced by incubation with GSH in a dose dependent manner[134]. Even in hearts which were significantly thiol depleted by BSO, the thiol concentrations were still in vast excess of the amount of tracer injected. Even if compromised by disease, intracellular thiol concentrations are always much greater than the small amounts of radiotracer injected. For example, ischaemia-reperfusion caused a decrease in myocardial GSH concentration from 0.56 to 0.18 μM/ gram tissue in rats, a concentration still sufficient for Cu-ATSM reduction[165]. It is therefore possible that intracellular thiols are essential in Cu-ATSM reduction leading to its dissociation in hypoxic tissue. It has been demonstrated that thiol concentration does not change during hypoxic perfusion, while ^{64}Cu retention from ^{64}Cu-ATSM significantly increases. Furthermore it was demonstrated that modification of thiol concentration does not affect ^{64}Cu retention from ^{64}Cu-ATSM under normoxic or hypoxic conditions. These results confirm that myocardial thiol concentration does not determine Cu-ATSM hypoxia selectivity or clearance from tissue; however, the presence of thiols may still be essential in Cu-ATSM reduction and copper deposition.

3.4.2 Thiol concentration modification

Our measurements of intracellular thiol concentrations of untreated normoxic control hearts were consistent with those previously reported[166]. It was demonstrated that perfusion with hypoxic KHB does not alter cardiac thiol concentration in these experiments, which has also been reported previously in

experiments where glucose-containing hypoxic buffers were used[157,160]. Others have reported that hypoxia causes a depletion of cardiac thiol content; however, this is due to the lack of energy substrate in the perfusion buffer[157,161,162]. In these studies, glucose was replaced with mannitol to maintain oncotic pressure and prevent hypoxia induced oedema[167]. GSH pools are maintained by GSH reductase which reduces GSSG to GSH using NADPH as an electron donor. Intracellular NADPH pools are replenished by the reduction of $NADP^+$ by NADH from glycolysis or fatty acid β-oxidation. GSH synthesis by γ-glutamylcysteine synthetase and GSH synthetase is also ATP dependent. Hypoxic hearts which cannot metabolise fatty acids therefore require glucose to maintain GSH levels. Since mannitol is not metabolised by the myocardium, and maintenance of GSH levels is energy substrate dependent[168,169], it is the combination of hypoxia and lack of energy substrate which depletes GSH, and not hypoxia alone.

Thiol concentrations of hearts excised from BSO pre-treated rats were approximately 60% lower than those of untreated control hearts. Our thiol depletion protocol was adopted from a previous study which reported a 70% decrease in thiol concentration, although the hearts in that study underwent an ischaemia and reperfusion protocol which would have depleted GSH further[166]. Perfusion with NAC for 35 mins increased cardiac thiol concentrations by 7 fold. A total concentration of 4mM NAC was used as this dose has been commonly used to scavenge free radicals in isolated perfused rat hearts[170-172]. To date, the myocardial thiol concentrations reported in similar studies have not been corrected to intracellular protein concentration[158,173]; meaning that the current results cannot be directly compared to previous research. These studies do

confirm, however, that NAC increases cardiac GSH in a dose-dependent manner.

3.4.3 Cardiac function

3.4.3.1 Contractile function

The contractile function of each heart was monitored during the 10 min stabilisation period at the beginning of each perfusion protocol. Only hearts with stable contractile function during this period (as determined by the exclusion criteria laid out in chapter 2) were used in this study. In normoxic untreated hearts, contractile function remained stable throughout the perfusion protocol. Switching to hypoxic KHB caused a decrease in heart rate and LVDP and an increase in perfusion pressure and LVEDP within 5 mins. This is consistent with previous reports[174,175]. Decreased oxygen availability caused the heart to switch from fatty acid to glucose metabolism for ATP generation. Glycolysis is not as efficient as fatty acid β-oxidation at generating ATP, therefore less ATP is available to sustain cardiac contractility and heart rate and LVDP fall. Increased intracellular Ca^{2+} during hypoxia prevents complete ventricular relaxation and consequently increases LVEDP and perfusion pressure[176].

To date no studies have been published investigating the combined effects of hypoxia and thiol depletion on isolated perfused rat hearts. Other studies, however, have reported that myocardial thiol depletion through BSO pre-treatment does not affect contractile function during normoxic perfusion[177,178]. In these studies, perfusion pressure was kept constant. In the model described in this thesis, where coronary flow rate is kept constant, thiol depletion caused a

38% increase in perfusion pressure after 60 mins of normoxic perfusion. There was, however, no change in other contractile parameters in these hearts. GSH depletion may result in a decreased ROS scavenging activity in the heart. Excess ROS may react with NO and prevent endothelial relaxation, resulting in vasoconstriction and increased perfusion pressure. During hypoxia, however, contractility of thiol depleted hearts was similar to untreated controls.

Although several studies have investigated the protective effects of NAC on cardiac contractile function during ischaemia-reperfusion, the effects of NAC on normoxic contractile function have not been reported. NAC increases intracellular free radical scavenging activity through thiol replenishment; it would therefore be expected that NAC perfusion would have the opposite effect to thiol depletion on perfusion pressure. In the current study, however, hearts perfused with NAC displayed a 17% increase in perfusion pressure by the end of normoxic perfusion. It is possible that NAC decreases NO generation and therefore hinders vasodilation through NO signalling. A recent report confirms that NAC decreases eNOS phosphorylation, leading to suppressed endothelial NO generation in rat aorta[179]. While the mechanism by which NAC inhibits eNOS activity remains unclear, decreases in H_2O_2 levels have been suggested. During hypoxia, NAC perfusion tended to preserve perfusion pressure, LVDP and LVEDP compared with untreated hypoxic controls. In ischaemia-reperfusion models the protective effects of NAC are attributed to antioxidant activity; however, little is known about the preservative effects of NAC in the hypoxic myocardium. It has been suggested that NAC maintains cytosolic Ca^{2+} pools by preventing or reversing ROS induced protein thiol modification of SR proteins, thereby maintaining muscle contraction during oxidative stress[180].

3.4.3.2 Lactate production, glucose consumption and viability

The hypoxic myocardium produces lactate as a byproduct of anaerobic glycolysis. Lactate exits the cell via MCT and is released into the blood (or perfusate) if there is residual flow. As expected, perfusate lactate concentration increased during hypoxia but not normoxia and was not influenced by thiol concentration. As measuring intracellular pO_2 was not possible at the time of experiment, the increase in lactate production and release confirms that hearts perfused with hypoxic buffer were oxygen deprived. Lactate release, however, was transient and began to decrease within 10 mins of switching to hypoxic buffer. This is consistent with previous studies in which perfusion with hypoxic buffer resulted in a transient increase in lactate release from the heart[181,182]. Transient increases in glycolytic intermediates fructose-6-phosphate and fructose diphosphate were also reported while inorganic phosphate and AMP levels continued to rise with increasing hypoxia[181]. As hypoxia decreased contractility in hearts in the current study, it is probable that glucose metabolism slows with decreasing energy demand and therefore less lactate is produced.

There was no detectable change in glucose consumption during hypoxia as perfusate glucose concentration stayed in close range to that of KHB (11mM). The amount of glucose extracted by the heart during hypoxia is negligible compared to the high concentration of glucose provided by KHB, which is being perfused thought the heart at 14ml/min. Changes in first pass glucose extraction were therefore unfortunately not measureable by this relatively insensitive approach.

Cardiac viability was confirmed by the lack of protein released into the perfusate from all hearts. The results display an increase in protein release, however, in

NAC perfused hearts. It was later noted that the BCA assay used to detect protein also reacts with cysteine, which explains the false positive results in these groups, however, since lactate production and cardiac function were unaffected by NAC administration, it is unlikely that cellular damage would be different in these groups either.

Chapter 4

Effect of thiol concentration on the hypoxia selectivity of ^{64}Cu-ATSM in bovine aortic endothelial cells

4.1 Introduction

4.1.1 Hypoxia induced ROS generation in the endothelium

Although the endothelium is less susceptible to hypoxia induced injury compared to cardiac myocytes, ROS generation as a result of hypoxia has been implicated in the pathophysiology of vascular disease. In the vascular endothelium ROS are generated constitutively as signalling molecules and regulate several processes including vascular tone, cell growth, inflammatory responses, proliferation and cell death[183]. An excess in endothelial ROS generation and may lead to endothelial and vascular dysfunction which contributes to other cardiovascular diseases including atherosclerosis. The mechanism by which the endothelium generates ROS anaerobically remains unclear, however, mitochondrial derived $^{\cdot}O_2^-$ has been suggested[183,184]. The balance between intracellular antioxidants, such as GSH, and ROS generation is therefore an important factor in hypoxia induced endothelial dysfunction.

4.1.2 Changes in endothelial GSH

GSH prevents ROS induced cellular injury by directly scavenging ROS, detoxifying H_2O_2 and replenishing membrane and intracellular protein thiols. In the endothelium, NO depletion through ROS-NO interactions is prevented by GSH; therefore GSH preserves NO dependent endothelial function such as vascular tone. GSH is also capable of binding NO directly to form S-nitrosoglutathione (GSNO). GSNO is more stable than NO and has been implicated in the transport of NO to other vascular cells[185,186]. GSNO reacts with GSH molecules and releases NO where GSH concentrations are sufficient[187].

The interactions between GSH and ROS/NO are therefore essential for maintaining endothelial and vascular functions. During hypoxia, however, ROS generation may exceed GSH activity and lead to endothelial dysfunction.

Several studies have demonstrated decreases in endothelial GSH concentration due to severe or prolonged hypoxia. For example, GSH levels in bovine aortic endothelial cells (BAEC) decreased to 10% of normoxic control cells after 6 hrs incubation with anoxic gas (95% N_2/5% CO_2)[186]. GSH concentration further decreased to 5% of that of normoxic cells after 24hrs. Baht *et al* observed a significant decrease in GSH in pulmonary artery endothelial cells (PAEC) after incubation with anoxic gas for 12 hrs which decreased further over time, however, was reversible upon reoxygenation for 6 hrs[188]. These findings further support the premise that hypoxia induces ROS generation in endothelial cells.

Imaging the hypoxic endothelium may therefore be beneficial in the research and diagnosis of hypoxia induced endothelial dysfunction, which may lead to in cardiovascular pathologies. To date there has been no attempt made to investigate the hypoxia selectivity of Cu-ATSM in cardiovascular endothelial cells.

4.1.3 Experimental approach

In this study, three agents which pharmacologically modify thiol concentration were utilised: diethyl maleate (DEM), BSO and NAC to determine the effect of intracellular thiol status on ^{64}Cu-ATSM hypoxia selectivity in isolated BAEC. BSO and NAC deplete and augment thiol concentration as described in chapter

3. DEM conjugates GSH in the presence of GSH-S-transferases, therefore also depletes intracellular GSH pools[147].

4.2 Materials and methods

4.2.1 Chemicals and reagents

Diethyl maleate (DEM), DL-buthionine (S,R)-sulfoximine 99% (BSO), trichloroacetic acid (TCA) and the bicinchoninic acid (BCA) assay kit were obtained from Fischer Scientific, UK. Dulbecco's modified Eagle's medium (DMEM), dimethylthiazol diphenyltetrazolium bromide (MTT), N-acetyl-L-cysteine 99% (NAC) and O-phthalaldehyde (OPA) were all obtained from Sigma-Aldrich, UK. ^{64}Cu-ATSM was synthesised as described in chapter 2.

4.2.2 Cell culture

BAEC (passage 6-10) were cultured in gelatine coated 24 well plates and cultured as described in chapter 2. For MTT assays, BAEC were cultured in 96 well plates.

4.2.3 Thiol concentration modification

4.2.3.1 MTT viability assay

DEM was dissolved in DMSO (10 mM) before diluting in DMEM. BSO and NAC were dissolved directly in DMEM. All drugs were sterile filtered before BAEC treatment. Initially, confluent BAEC were treated with DEM 100 µM, BSO (100 µM), DEM + BSO (100 µM each), NAC (10 or 100mM) for 24hrs, H_2O_2 (250 µM) for 30 mins or left untreated. After the treatment period, the MTT assay was used to determine BAEC viability (described in chapter 2).

4.2.3.2 Effect of DEM, BSO and NAC on BAEC thiol concentration: time and dose optimisation studies

24 well plates of BAEC were incubated with DEM (25, 50 or 100 µM), BSO (25, 50 or 100 µM), DEM + BSO (100 µM each) or NAC (7.5, 15 or 30 mM) for 2, 4, 6, 8 and 24 hrs. Additional plates of BAEC were incubated with NAC (0.01, 0.1, 1, 5, 10, 20 and 30 mM) for 0.5 and 1 hr.

4.2.3.3 Thiol and protein extraction and analysis

After each treatment period, the medium was aspirated and wells were washed twice with ice-cold phosphate buffered saline (PBS). 100 µL of ice-cold TCA (6.5%) was added to each well for 10 mins on ice, aspirated and stored at -70^{o}C. 100 µL NaOH (1M) was added to each well for 2 hrs before aspirating and storing at -20^{o}C. TCA extracts were analysed for thiol content using the OPA fluorescence assay and NaOH extracts were analysed for protein content using the BCA assay, both described in chapter 2.

4.2.4 Determination of hypoxia protocol

BAEC were transferred to an atmosphere regulated work station (SCI-tive, Ruskin Technology) at 1% O_2 /5% CO_2 for 48 hrs before being treated with BSO (10 or 100 µM) for 24 hrs or NAC (7.5 or 30 mM) for 2 hrs. Parallel plates were treated identically and incubated at 21% O_2/5% CO_2 for the same time periods. After treatment periods, BAEC viability was analysed via MTT assay as described earlier.

4.2.5 ^{64}Cu-ATSM hypoxia selectivity in BAEC

BAEC were incubated at 21% O_2/5% CO_2 or 1% O_2 /5% CO_2 and treated as in section 4.2.4. After treatment periods, the medium was aspirated and BAEC were washed twice with PBS (37^{o}C). 1 kBq ^{64}Cu-ATSM (for synthesis see chapter 2) diluted in FCS free DMEM (1kBq/ mL) was added to each well for 1 hr. Medium was then aspirated and GSH and protein was extracted as before. Half of the TCA and NaOH extracts were obtained for measurement of intracellular ^{64}Cu content using a gamma counter (1282 Compugamma, LKB Wallac, Australia). The medium and PBS aspirated from each well were also analysed for ^{64}Cu content.

4.2.6 Statistical analysis

All data are presented as means ± standard deviation. Statistical significance was evaluated using ANOVA followed by Bonferroni post hoc test.

4.3 Results

4.3.1 Preliminary dose response findings

4.3.1.1 Effect of modifying thiol concentration on BAEC viability

Preliminary MTT assays were performed on BAEC treated with DEM, BSO and NAC to assess cellular viability post-treatment (figure 4.1). BAEC treated with 100 µM DEM (0.66 ± 0.03 Abs 570 nm), 100 µM BSO (0.64 ± 0.04 Abs 570 nm), 100 µM DEM + 100 µM BSO (0.68 ± 0.11 Abs 570 nm) or 10mM NAC (0.73 ± 0.07 Abs 570 nm) for 24 hrs displayed similar viability to that of untreated BAEC (0.67 ± 0.05 Abs 570 nm). Treatment with 100 mM NAC, however, significantly decreased viability by 25% (0.50 ± 0.08 Abs 570 nm; $p<0.05$). H_2O_2 also decreased BAEC viability by 30% (0.46 ± Abs 570 nm; $p<0.05$).

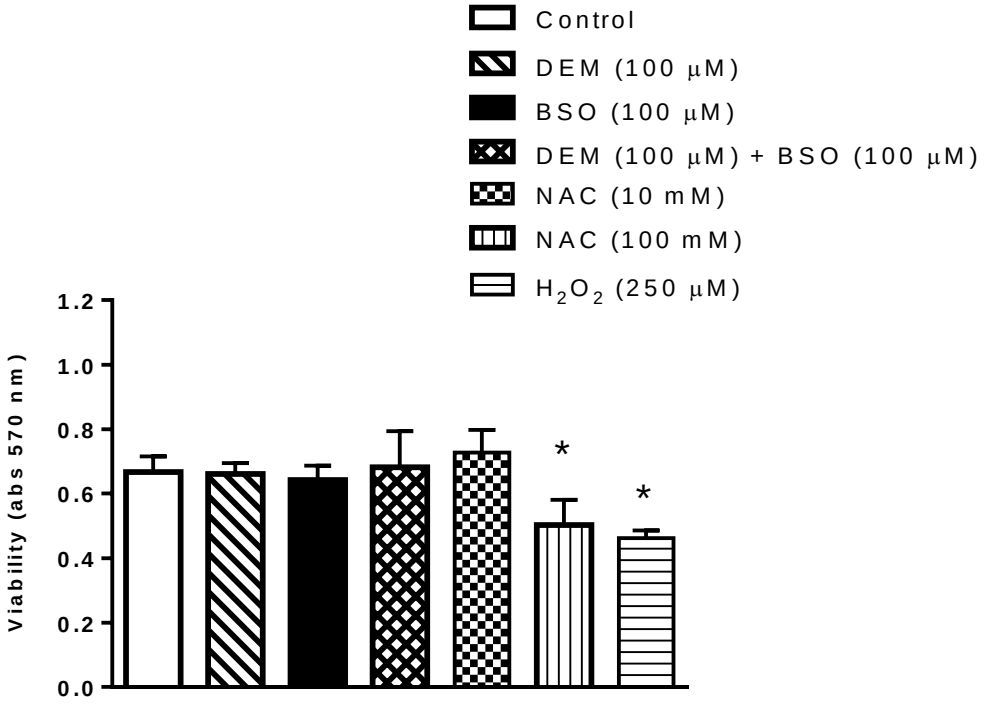

*Figure 4.1. BAEC viability. Data are expressed as means ± standard deviation, n=3 plates with five replicate wells per group. *p<0.05 vs. control.*

4.3.1.2 Effect of DEM, BSO and NAC on BAEC thiol concentration

In preliminary dose response studies BAEC were treated with DEM, BSO or a combination of both for 2, 4, 6, 8 and 24 hrs (figure 4.2). Thiol concentration in untreated control BAEC ranged between 26.4 ± 4.6 and 34.7 ± 4.3 nmol/ mg protein over 24 hrs. Incubation with 100 µM DEM for 2 hrs (27.3 ± 6.5 nmol/ mg protein) did not affect thiol concentration. Incubation with 100 µM DEM for 4, 6 and 8 hrs tended to increase thiol levels (42.2 ± 16.5, 45.1 ± 11.5 and 43.5 ± 9.0 nmol/ mg protein respectively); however, values were not significant compared with time-matched controls. Treatment with 100 µM DEM for 24 hrs, however, caused thiol concentration to significantly increase to above that of control BAEC (83.2 ± 16.0 nmol/ mg protein; $p<0.05$).

In the same study, incubation with 100 µM BSO for 2, 4, 6 or 8 hrs did not affect thiol concentration (26.6 ± 6.1, 37.5 ± 10.7, 38.2 ± 11.9 and 26.0 ± 4.4 nmol/ mg protein respectively). Incubation with 100 µM BSO for 24 hrs, however, significantly decreased thiol concentration to 50% of that in control BAEC (15.2 ± 1.3 nmol/ mg protein; $p<0.05$). Treatment with DEM + BSO combined had no effect on thiol concentration from 2-8 hrs. After 24 hrs treatment, however, DEM + BSO caused thiol concentration to decrease significantly (7.3 ± 2.2 nmol/ mg protein; $p<0.05$).

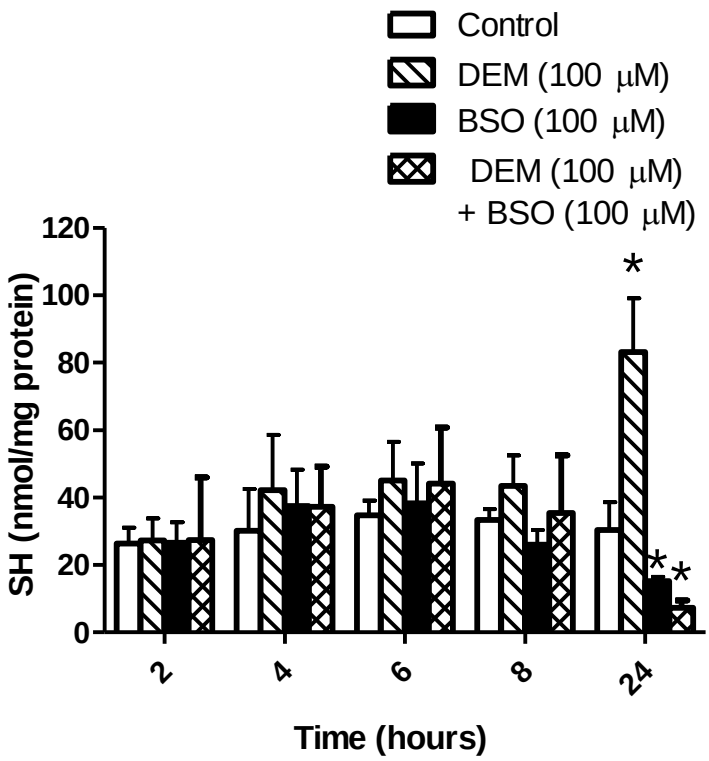

*Figure 4.2. Thiol concentrations of BAEC treated with thiol depletion agents. Data are expressed as means ± standard deviation, n= 3 plates with three replicate wells per group. *p<0.05 vs. untreated control.*

Following analysis of the results displayed in figure 4.2, a second study was executed to further confirm the effect of DEM and BSO on BAEC thiol concentration. The design of this study was altered to investigate the effects of a range of DEM and BSO doses on BAEC thiol concentration. In addition, thiol augmenting agent, NAC, was added to the protocol.

In this study thiol concentrations of untreated control BAEC remained similar to those displayed in figure 4.2, ranging between 29.1 ± 9.6 and 31.8 ± 11.0 nmol/ mg protein over the time course of 24 hrs. Contrary to preliminary results, incubation with 100μM DEM tended to decrease thiol content from 2-8 hrs,

however, after 24 hrs thiol concentration increased as before (figure 4.3; table 4.1). Incubation with lower concentrations of DEM (25 and 50 μM) from 2-8 hrs did not affect thiol concentration. Incubation with 25, 50 and 100 μM DEM for 24 hrs increased thiol concentration, however, was not significant compared to control BAEC.

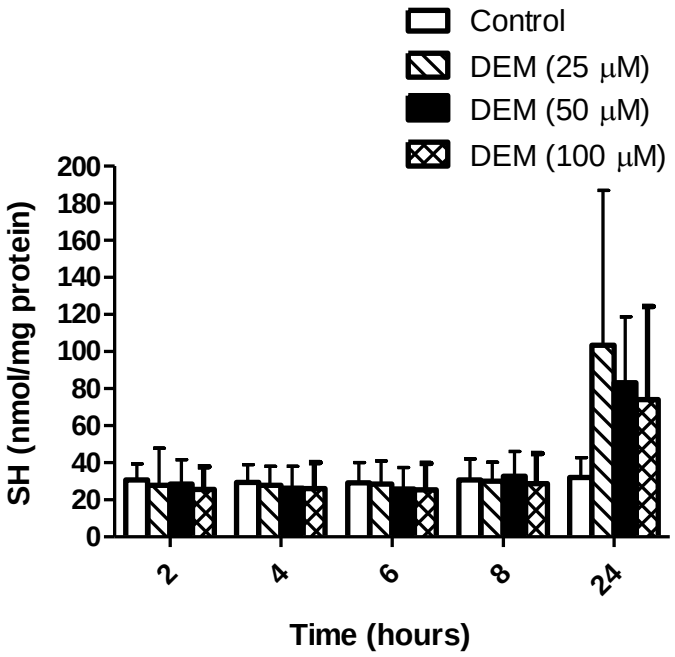

*Figure 4.3. Thiol concentrations of BAEC treated with DEM. Data are expressed as means ± standard deviation, n= 6 plates with three replicate wells per group. *p<0.05 vs. untreated control.*

Table 4.1. Thiol concentrations of BAEC incubated with DEM (as seen in figure 4.3).

	BAEC thiol concentration (nmol/ mg protein)			
Time (hrs)	Control	DEM (25 µM)	DEM (50 µM)	DEM (100 µM)
2	30.7 ± 8.5	27.8 ± 20.0	28.5 ± 13.2	25.5 ± 12.2
4	29.3 ± 9.6	27.8 ± 10.3	26.5 ± 11.5	25.9 ± 14.1
6	29.1 ± 10.7	28.5 ± 12.5	25.7 ± 11.5	25.4 ± 14.2
8	30.8 ± 11.4	30.0 ± 10.3	32.6 ± 13.4	28.6 ± 16.4
24	31.8 ± 11.0	103.4 ± 83.5	83.1 ± 35.7	74.1 ± 50.1

**p< 0.05 vs. control*

Similar to the preliminary results displayed in figure 4.2, treatment with 100µM BSO did not affect thiol levels from 2-8 hrs; however, after 24 hrs thiol concentration significantly decreased to 50% of control values (figure 4.4; table 4.2). Similarly, incubating BAEC with lower BSO concentrations (25 and 50 µM) resulted in a significant decrease ($p<0.05$) in thiol concentration after 24 hrs.

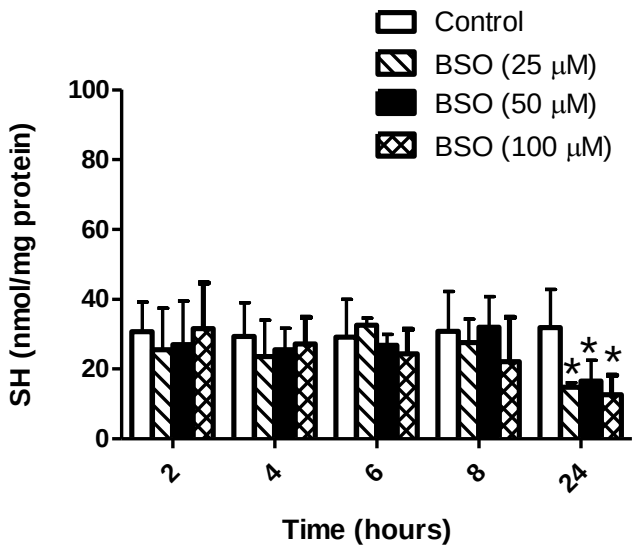

*Figure 4.4. Thiol concentrations in BAEC treated with BSO. Data are expressed as means ± standard deviation, n= 6 plates with three replicate wells per group. *p<0.05 vs. untreated control.*

Table 4.2. Thiol concentrations of BAEC incubated with BSO (as seen in figure 4.4).

	BAEC thiol concentration (nmol/ mg protein)			
Time (hrs)	Control	BSO (25 µM)	BSO (50 µM)	BSO (100 µM)
2	30.7 ± 8.5	25.4 ± 11.9	27.0 ± 12.4	27.2 ± 8.4
4	29.3 ± 9.6	23.5 ± 1.5	25.4 ± 6.2	25.0 ± 6.9
6	29.1 ± 10.7	32.5 ± 2.1	26.7 ± 3.1	30.1± 10.6
8	30.8 ± 11.4	27.6 ± 6.7	31.9 ± 8.8	24.0 ± 7.2
24	31.8 ± 11.0	* 14.8 ± 1.32	* 16.6 ± 5.9	* 14.3 ± 4.0

**p< 0.05 vs. control*

Initially, BAEC were incubated with 7.5 mM, 15 mM or 30 mM NAC for the same time periods as DEM and BSO. All NAC concentrations caused a significant increase ($p<0.05$) in thiol concentrations after 2 hrs (figure 4.5 A; table 4.3 A). Over time thiol concentration returned towards control levels in BAEC treated with 7.5 mM and 15 mM NAC, however, remained significantly higher ($p<0.05$) in the 30mM treatment group throughout the experiment. This discovery led to a second, smaller study which explored the effect of a larger range of NAC concentrations on BAEC thiol concentration at the shorter time points of 0.5 and 1 hr (figure 4.5 B; table 4.3 B). Incubation with concentrations less than10 mM for 0.5 hr or less than 20 mM for 1 hr did not increase BAEC thiol concentration.

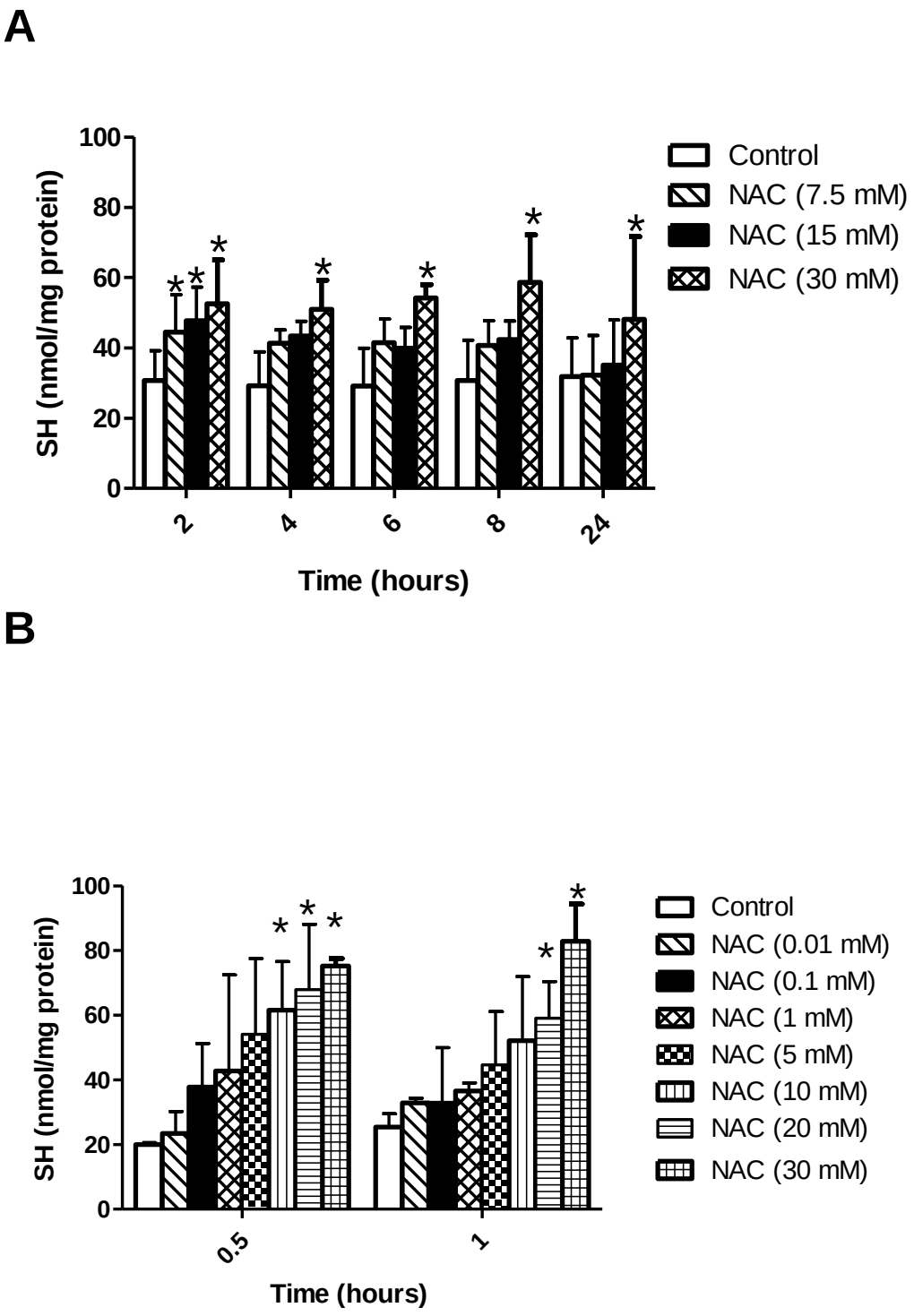

*Figure 4.5. Thiol concentrations of BAEC treated with NAC. Data are expressed as means ± standard deviation, (A) n= 6 (B) n=3 plates, each with three replicate wells per group. *p<0.05 vs. untreated control.*

Table 4.3A. Thiol concentrations of BAEC incubated with NAC (as displayed in figure 4.5A).

	BAEC thiol concentration (nmol/ mg protein)			
Time (hrs)	Control	NAC (7.5 mM)	NAC (15 mM)	NAC (30 mM)
2	30.7 ± 8.5	* 44.5 ± 10.7	* 47.8 ± 9.5	* 52.5 ± 12.5
4	29.3 ± 9.6	41.3 ± 3.8	43.4 ± 4.2	* 50.9 ± 8.3
6	29.1 ± 10.7	41.5 ± 6.7	39.9 ± 5.9	* 54.2 ± 3.8
8	30.8 ± 11.4	40.7 ± 7.0	40.4 ± 5.3	* 58.6 ± 13.6
24	31.8 ± 11.0	32.2 ± 11.3	35.1 ± 12.9	* 48.1 ± 23.5

*P < 0.05 vs. time-matched control

Table 4.3B. Thiol concentrations of BAEC incubated with NAC (as displayed in figure 4.5B).

	BAEC thiol concentration (nmol/ mg protein)	
	0.5 hrs	1 hrs
Control	20.0 ± 0.6	25.4 ± 4.1
NAC (0.01 mM)	23.5 ± 6.7	32.9 ± 1.5
NAC (0.1 mM)	37.8 ± 13.5	32.8 ± 17.1
NAC (1mM)	42.8 ± 29.7	36.6 ± 2.4
NAC (5mM)	54.1 ± 23.4	44.7 ± 16.4
NAC (10mM)	* 62.6 ± 15	52.1 ± 19.8
NAC (20 mM)	* 68.0 ± 20.1	* 59.1 ± 11.3
NAC (30 mM)	* 75.2 ± 2.4	* 82.9 ± 11.5

**p<0.05 vs. control*

The protocol was then further refined prior to experiments with ^{64}Cu-ATSM. From the results displayed in figures 4.2 and 4.3 it was clear that thiol concentrations of BAEC treated with DEM were much more variable compared to treatment with BSO and NAC. It was therefore decided that DEM was no longer suitable in the final protocol. In the final dose response study the highest and lowest doses of BSO and NAC at appropriate time points were used (100

and 25 µM BSO at 24 hrs, 30 and 7.5 mM NAC at 2 hrs). In addition, a concentration 10 fold lower than the highest concentration of each compound was added to the protocol.

In this study, thiol concentrations in untreated control BAEC averaged 21.6 ± 2.6 nmol/ mg protein (figure 4.6). Incubation with 10, 25 and 100 µM BSO for 24 hrs significantly decreased ($p<0.05$) thiol concentration to 15.3 ± 0.4, 8.0 ± 1.0 and 6.6 ± 0.2 nmol/ mg protein respectively. Incubation with 3 mM NAC for 2 hrs increased thiol concentration to 34.2 ± 3.3 nmol/ mg protein, however, this was not significant compared to control values. Incubation with 7.5 and 30 mM NAC significantly increased ($p<0.05$) BAEC thiol concentrations to 46.3 ± 5.3 and 106.3 ± 9.0 nmol/ mg protein respectively.

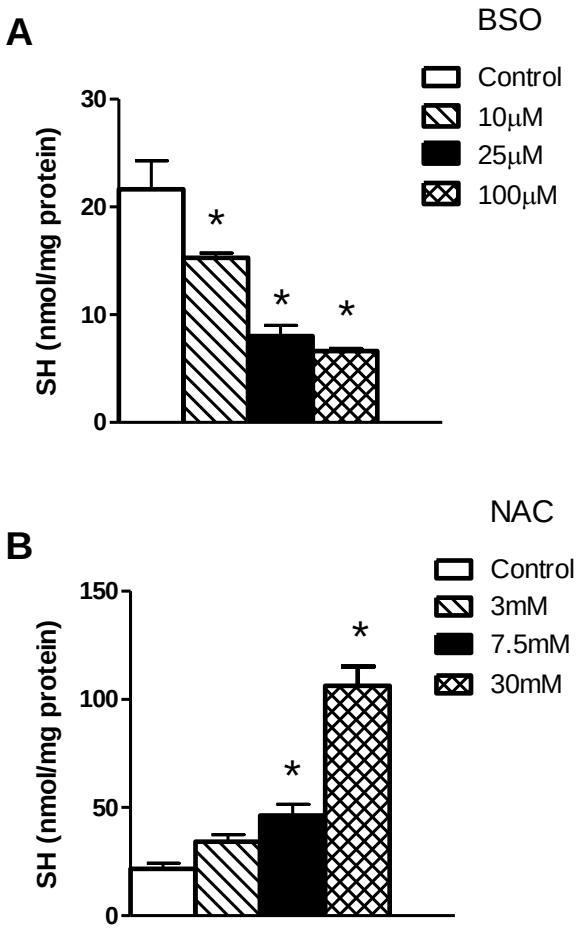

*Figure 4.6. Effect of tailored treatment protocols on BAEC thiol concentration. Cells were incubated with (A) BSO for 24 hrs and (B) NAC for 2 hrs. Data are expressed as means ± standard deviation, n= 3 plates with three replicate wells per group. *p<0.05 vs. control.*

4.3.1.3 Effect of low oxygen and thiol concentration on BAEC viability

In the next stage of designing a protocol, two doses of BSO (10 and 100μM) and two doses of NAC (7.5 and 30 mM) were utilised. BAEC were incubated in either 21% or 1% O_2 for 24 hrs before treatment (either with BSO for 24 hrs or NAC for 2 hrs) to assess the combined effect of low oxygen and thiol concentration modification on BAEC viability (figure 4.7). In 21% O_2, BSO or

NAC treatment did not compromise BAEC viability (table 4.4). Incubation with H_2O_2 decreased BAEC to approximately 50% control levels ($p<0.05$). Similarly, in 1% O_2 BSO or NAC did not compromise BAEC viability compared with BAEC incubated in the absence either of drug; however, there was a significant decrease ($p<0.05$) in cell viability across all treatment groups incubated in 1% O_2 compared with the 21% O_2 group. Furthermore, BAEC incubated in 1% O_2 contained significantly less protein in all treatment groups compared with their normoxic equivalent (figure 4.8, table 4.4).

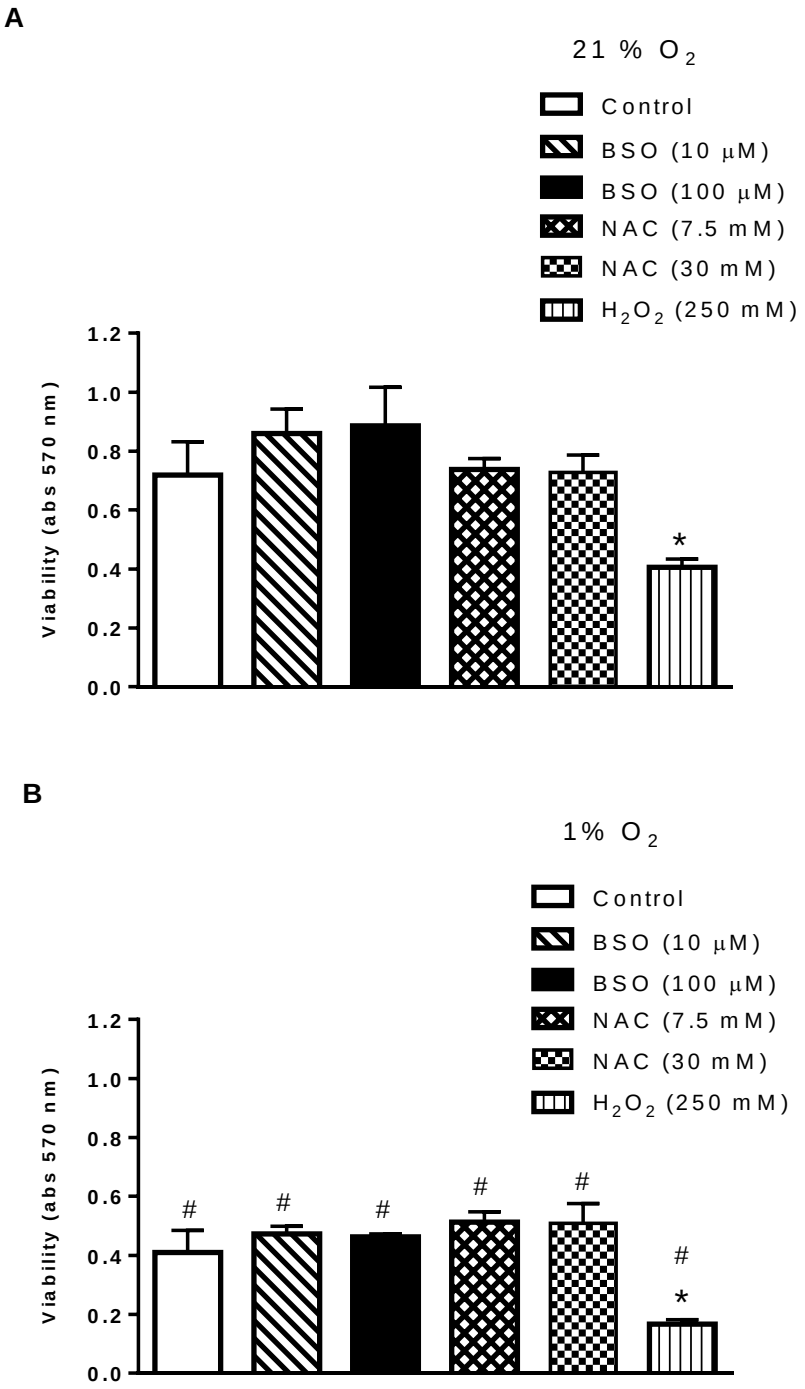

*Figure 4.7. Effect of low oxygen on BAEC viability, determined by the MTT assay. Data are expressed as means ± standard deviation, n=3 plates with four replicate wells per group. *p<0.05 vs. untreated control, #p<0.05 vs. 21% O_2 equivalent.*

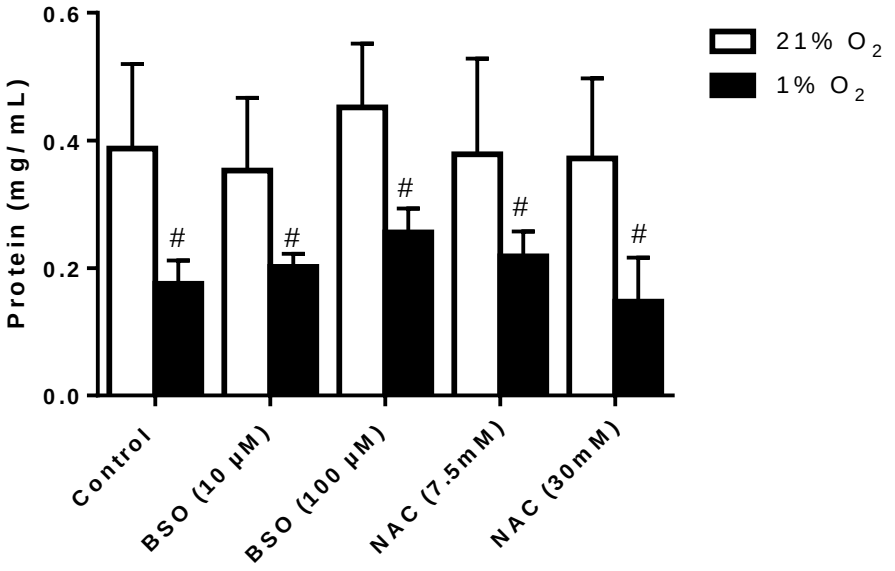

Figure 4.8. BAEC protein concentration in BAEC subject to treatment protocols in 4.7. Data are expressed as means ± standard deviation, n=3 plates with four replicate wells per group, #p<0.05 vs. 21% O_2 equivalent.

Table 4.4. BAEC viability and protein levels (as displayed in figures 4.7-4.8)

	BAEC viability (abs 570 nm)		Protein (mg/ mL)	
Time (hours)	20% O2	1% O2	20% O2	1% O2
Control	0.72 ± 0.11	0.41 ± 0.08	0.3 ± 0.13	# 0.18 ± 0.04
BSO (10 µM)	0.86 ± 0.08	0.47 ± 0.03	0.35 ± 0.11	# 0.2 ± 0.2
BSO (25 µM)	0.81 ± 0.17	0.41 ± 0.03	0.40 ± 0.14	# 0.18 ± 0.05
BSO (100 µM)	0.89 ± 0.13	0.46 ± 0.01	0.45 ± 0.10	# 0.26 ± 0.04
NAC (3 mM)	0.75 ± 0.08	0.42 ± 0.04	0.37 ± 0.09	# 0.16 ± 0.01
NAC (7.5 mM)	0.74 ± 0.04	0.5 ± 0.04	0.38 ± 0.15	# 0.22 ± 0.04
NAC (30 mM)	0.73 ± 0.06	0.5 ± 0.07	0.37 ± 0.13	# 0.15 ± 0.07
H_2O_2	* 0.41 ± 0.03	* 17 ± 0.01	-	-

*P < 0.05 vs. time-matched control

4.3.2 Effect of BAEC thiol concentration on ^{64}Cu retention from ^{64}Cu-ATSM

After establishing a protocol which depleted and augmented thiol concentration, the effects of thiol concentration on the hypoxia selectivity of ^{64}Cu-ATSM in BAEC were investigated. In this protocol BAEC were incubated with ^{64}Cu-ATSM in the absence BSO or NAC after thiol concentration had been modified. An extra group of NAC treated BAEC in which NAC was included in the medium during the ^{64}Cu-ATSM incubation period was therefore included in the study. Seeding BAEC was also staggered so that cells incubated in 21% O_2 contained a similar amount of protein as 1% O_2 group by the time of experiment.

4.3.2.1 BAEC thiol concentration

Thiol concentrations of BAEC incubated with ^{64}Cu-ATSM are displayed in figure 4.9. Incubation in 1% O_2 alone caused a significant decrease ($p<0.05$) in thiol concentration (14.6 ± 1.6 nmol/ mg protein) compared with 21% O_2 (21.8 ± 2.1 nmol/ mg protein). Incubation with 10 and 100 µM BSO significantly decreased ($p<0.05$) thiol concentration compared to control cells in 21% O_2 (9.8 ± 3.9 and 4.7 ± 1.2 nmol/ mg protein respectively). Similarly, BAEC incubated in 1% O_2 contained significantly lower ($p<0.05$) thiol concentrations after treatment with 10 µM (8.5 ± 2.3 nmol/ mg protein) and 100 µM (6.4 ± 2.3 nmol/ mg protein) BSO.

Treatment with NAC for 2 hrs prior to ^{64}Cu-ATSM incubation failed to increase thiol levels in BAEC incubated at 21% O_2 with either 7.5 or 30mM (20.6 ± 6.7 and 23.7 ± 2.2 nmol/ mg protein respectively). In 1% O_2, 7.5 and 30 mM NAC increased BAEC thiol concentration to (21.8 ± 16.8 nmol/ mg protein and 27.3 ± 153 nmol/ mg protein respectively, however, these increases were not

statistically significant when compared to BAEC incubated with 1% O_2 alone. Incubating BAEC with NAC for an additional hour during ^{64}Cu-ATSM incubation significantly increased ($p<0.05$) thiol concentrations with both 7.5 and 30 mM 21% O_2 (32.5 ± 3.4 and 67.0 ± 10.5 nmol/ mg protein respectively) and in 1% O_2 conditions (52.0 ± 12.3 and 208.3 ± 31.7 nmol/ mg protein respectively).

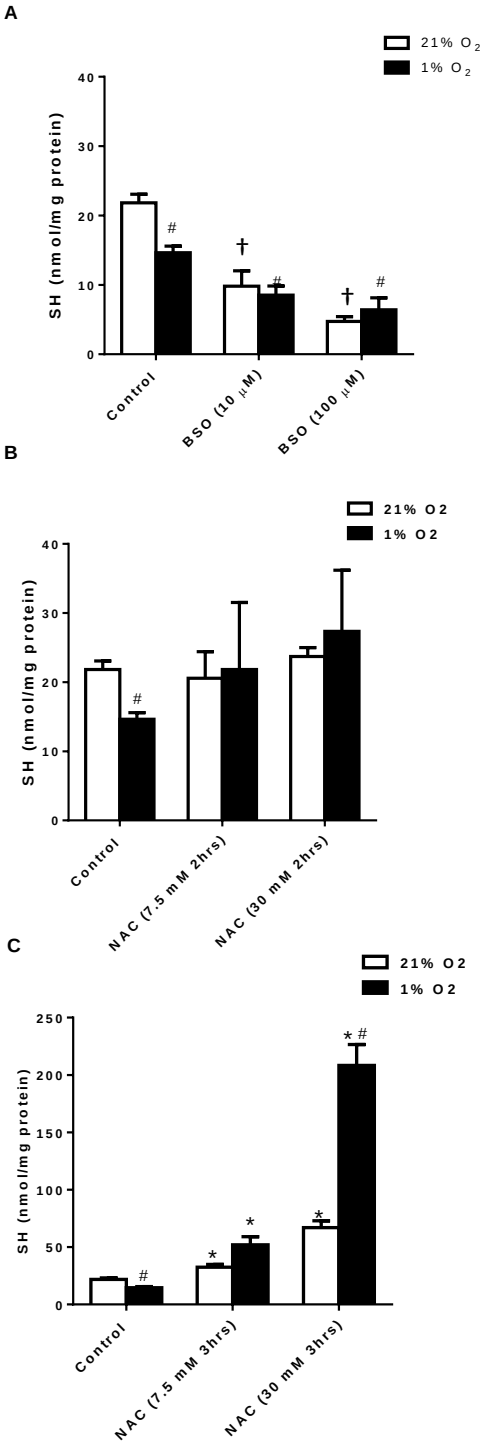

*Figure 4.9. Thiol concentrations in BAEC incubated with (A) BSO for 24hrs and (B) NAC for 2 hrs prior to 1 hour incubation with ^{64}Cu-ATSM in the absence of NAC or (C) NAC for 2 hrs prior to 1 hour incubation with ^{64}Cu-ATSM and NAC. Data are expressed as means ± standard deviation, n=3 plates with four replicate wells per group. *p<0.05 vs. control, #p<0.05 vs. normoxic equivalent.*

4.3.2.2 BAEC ^{64}Cu retention from ^{64}Cu-ATSM

Following incubation with ^{64}Cu-ATSM, the media was extracted and BAEC were washed with ice-cold PBS. The media and PBS were then analysed for extracellular ^{64}Cu activity (figure 4.10). Extracellular activity was similar in the media and PBS samples collected from control BAEC incubated in 21% and 1% O_2 (48.7 ± 1.3 and 47.8 ± 1.9 kBq/ mL respectively). Furthermore, 10 and 100 µM BSO did not affect extracellular activity from BAEC at 21% (48.7 ± 2.6 and 48.7 ± 2.5 kBq/ mL respectively) or 1% O_2 (48.0 ± 3.1 and 47.6 ± 2.6 kBq/ mL respectively). Similarly, incubation with 7.5 and 30 mM NAC for 2 hrs did not affect extracellular activity from BAEC incubated at 21% (49.7 ± 1.3 and 48.6 ± 2.3 kBq/ mL respectively) or 1% O_2 (47.0 ± 0.6 and 46.9 ± 1.7 kBq/ mL respectively). Extracellular activity was similar from BAEC treated with 7.5 mM and 30 mM NAC for 3 hrs in 21% O_2. In 1% O_2, incubation with 7.5 mM NAC did not significantly affect extracellular activity (45.9 ± 1.1 kBq/ mL) however, 30 mM NAC significantly decreased ($p<0.05$) extracellular activity (42.1 ± 0.8 kBq/ mL).

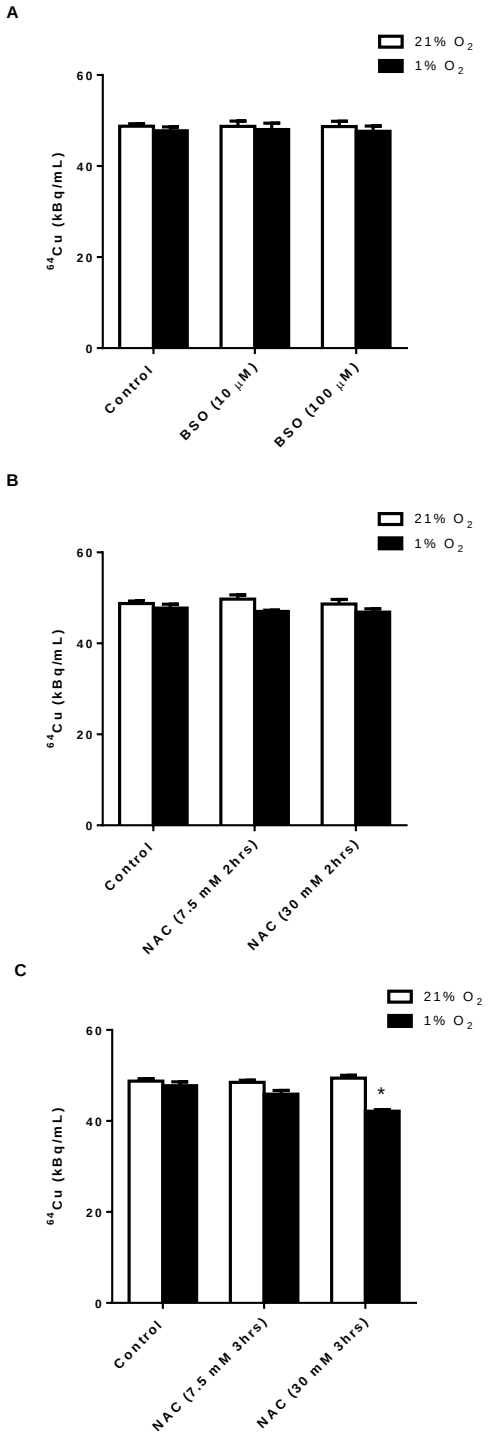

*Figure 4.10. ^{64}Cu in medium and PBS wash (combined) from BAEC incubated with (A) BSO for 24hrs and (B) NAC for 2 hrs prior to 1 hour incubation with ^{64}Cu-ATSM in the absence of NAC or (C) NAC for 2 hrs prior to 1 hour incubation with ^{64}Cu-ATSM and NAC. Data are expressed as means ± standard deviation, n=3 plates with four replicate wells per group. *p<0.05 vs. control, #p<0.05 vs. normoxic equivalent.*

Figure 4.11 displays the effect of thiol concentration modification on BAEC ^{64}Cu retention after incubation with ^{64}Cu-ATSM. Control BAEC retained 1.7 ± 0.1 kBq/ mg protein in 21% O_2 conditions. 1% O_2 caused a significant increase ($p<0.05$) in ^{64}Cu retention compared to 21% O_2 (3.0 ± 0.5 kBq/ mg protein). All treatment groups of BAEC in 1% O_2 retained significantly more ($p<0.05$) ^{64}Cu than 21% equivalents. In 21% O_2, ^{64}Cu retention remained similar to control levels in BAEC incubated with 10 µM BSO (1.9 ± 0.1 kBq/ mg protein), however, 100 µM BSO significantly increased ($p<0.05$) ^{64}Cu compared to controls (2.6 ± 1.0 kBq/ mg protein). 10 and 100 µM BSO did not alter ^{64}Cu retention in BAEC incubated at 1% O_2 (3.1 ± 0.6 and 3.9 ± 0.5 kBq/ mg protein respectively).

Incubation with 7.5 and 30 mM NAC for 2 hrs did not affect ^{64}Cu retention in BAEC incubated at 21% O_2 (2.0 ± 0.5 and 2.0 ± 0.01 kBq/ mg protein respectively). At 1% O_2, however, 7.5 and 30 Mm NAC significantly increased ($p<0.05$) ^{64}Cu retention to 5.4 ± 0.4 and 4.7 ± 1.0 kBq/ mL respectively. Under 21% O_2 treatment with 7.5 and 30 mM NAC for 3 hrs did affect ^{64}Cu retention compared to control BAEC (1.8 ± 0.03 and 2.7 ± 0.3 kBq/ mg protein respectively). At 1% O_2, however, 7.5 and 30 mM NAC caused significant increase ($p<0.05$) ^{64}Cu retention (5.2 ± 0.7 and 8.6 ± 1.5 kBq/ mg protein respectively).

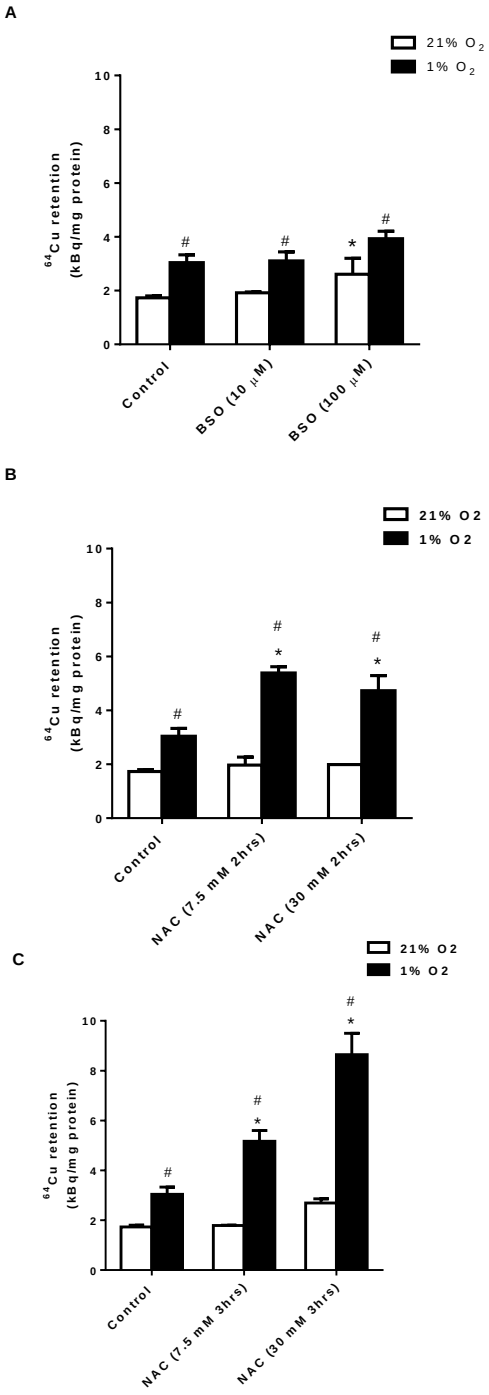

*Figure 4.11. ^{64}Cu retention in BAEC incubated with (A) BSO for 24hrs and (B) NAC for 2 hrs prior to 1 hour incubation with ^{64}Cu-ATSM in the absence of NAC or (C) NAC for 2 hrs prior to 1 hour incubation with ^{64}Cu-ATSM and NAC. Data are expressed as means ± standard deviation, n=3 plates with four replicate wells per group. *p<0.05 vs. control, #p<0.05 vs. normoxic equivalent.*

Figure 4.12 displays the correlation between BAEC thiol concentration and ^{64}Cu retention from ^{64}Cu-ATSM. Under 21% conditions there is no linearity observed in this relationship (r^2=0.1183). Under 1% conditions, however, there is a significant linear correlation between ^{64}Cu retention and thiol concentration (r^2=0.8107).

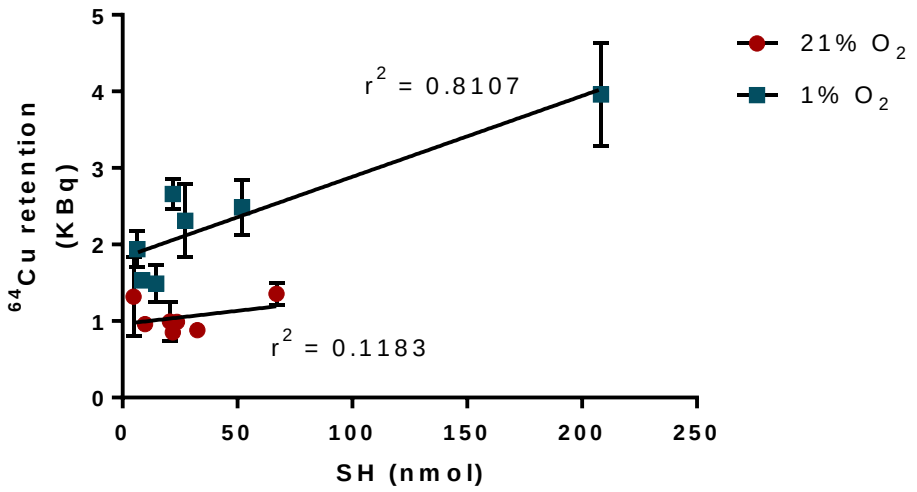

*Figure 4.12. Correlation between BAEC thiol concentration and ^{64}Cu retention from ^{64}Cu-ATSM incubated in 21% and 1% O_2. Data are expressed as means ± standard deviation, n=3 plates with 3 replicate wells per group.*p<0.05.*

4.4 Discussion and conclusions

4.4.1 Effect of thiol concentration and low oxygen on BAEC ^{64}Cu retention from ^{64}Cu-ATSM

As expected, there was significantly more retention of ^{64}Cu from ^{64}Cu-ATSM in low oxygen BAEC compared with BAEC incubated in 21 % O_2. Thiol augmentation did not affect ^{64}Cu retention from ^{64}Cu-ATSM in normoxic BAEC, however, thiol depleted cells treated with 100 µM BSO caused a significant increase in ^{64}Cu retention compared to normoxic controls. A possible explanation for this result is an increase in reducing ROS available in response to GSH depletion. It has been demonstrated that incubation with BSO for 24 hrs increases endothelial ROS generation in a dose dependent manner[189]. An increase in ROS generation could increase the rate at which ^{64}Cu-ATSM is reduced, therefore increasing ^{64}Cu retention.

Thiol depletion did not affect hypoxia selective retention of ^{64}Cu from ^{64}Cu-ATSM. Thiol augmentation by incubation with NAC, however, significantly increased ^{64}Cu retention from ^{64}Cu-ATSM under hypoxic conditions with all doses and time points. It is surprising that incubating BAEC with NAC for 2 hrs followed by a washout period for 1hr would increase ^{64}Cu retention as thiol concentrations were not significantly augmented in this group. It is possible, however, that excess intracellular NAC reduced ^{64}Cu-ATSM before sufficient amounts of NAC were washed from the cell. As BAEC were incubated in low oxygen conditions, the ^{64}Cu may have become trapped before NAC was washed out. Incubation with NAC and ^{64}Cu-ASTM together without NAC washout caused a further increase in hypoxic dependent ^{64}Cu trapping and was

dose dependent. This implies that high concentrations of cysteine substrates increase ^{64}Cu-ATSM reduction if incubated for a sufficient amount of time.

4.4.2 Modification of BAEC thiol concentration

In preliminary dose-response studies, DEM treatment for 2 - 8hrs did not affect BAEC thiol concentrations. As a GSH conjugating agent it was expected that DEM would decrease thiol concentration at these earlier time points. Previous studies investigating the effect of DEM on endothelial thiol concentration have reported mixed results. Incubation with a high concentration of DEM (0.5 mM) for 1 hr decreased thiol concentration by 60% in human umbilical vein endothelial cells (HUVEC)[190]. Kokura *et al.* observed a decrease in HUVEC thiol concentration after 15 mins incubation with 0.5 mM DEM followed by a gradual increase over 4 hours[191]. Lower concentrations of DEM (25 and 50 µM) had no effect on PAEC thiol concentration from 0.5 – 1 hr[192], however, 100 µM DEM decreased PAEC thiol concentration by 40% after 0.5 hr in a different study[193]. It has been suggested that at earlier time points, DEM is only effective at conjugating GSH to the point of depletion at a dose of 100 – 500 µM in most cell types[192]. As the lower end dose of 100 µM was used in these studies, it may be possible that DEM concentration was insufficient to significantly deplete thiols in BAEC.

In the initial, thiol depletion study, an increase in BAEC thiol concentration after 24 hrs incubation with DEM was observed, consistent with previous studies[192,194]. Conjugation of GSH by DEM increases *de novo* GSH synthesis over longer periods of time and GSH concentration often exceeds control values. When this study was repeated with a wider range of DEM

concentrations, thiol concentration still did not decrease over time and the rebound effect was highly variable between wells. It was therefore decided that DEM was not an appropriate thiol depletion agent for these studies. Treatment with BSO for 24 hrs, however, significantly decreased thiol concentration in all studies. The preliminary dose response results demonstrated that 100 and 50 µM BSO depleted GSH to a similar concentration; it was therefore decided that100, 25 and 10 µM were to be used in the next study. A short term decrease in GSH concentration in BSO treated BAEC (2-8 hrs) with any concentration was not observed in these studies. This was expected as BSO prevents GSH synthesis by inhibition of γ-glutamylcysteine synthetase, therefore without additional oxidative stress the depletion of existing GSH pools requires time. These findings were consistent with other endothelial GSH depletion studies utilising BSO over 16-24 hrs[192-194].

It is well established that NAC increases endothelial thiol levels by increasing GSH synthesis[195,196]. In these studies, incubation with a high concentration (30 mM) of NAC significantly increased BAEC thiol concentration at all time points; however, thiol concentrations were optimal after 2 hours of incubation with 7.5 – 30 mM NAC. Following this discovery, the effects of NAC incubation with a range of doses (0.01mM – 30 mM) for 05 - 1 hr were investigated. At these shorter incubation times thiol concentration was only increased with higher NAC concentrations (10-30mM). NAC traverses cell membranes through passive diffusion; it is therefore possible that incubation decreases over time due to equilibrium with the media, therefore a high concentration of NAC is required to significantly increase intracellular thiol concentration.

The protocol was further refined for experiments in low oxygen and with ^{64}Cu-ATSM. In the following study, BAEC were incubated with 10, 25 and 100 µM BSO for 24 hrs and 3, 7.5 and 30 mM NAC for 2 hrs. Thiol concentration was significantly decreased in response to all BSO doses, however, 10 and 25 µM BSO decreased thiol concentrations to the same extent. There was also no significant thiol increase observed with 3 mM NAC incubation. It was therefore decided that 10 and 100 µM BSO and 7.5 and 30 mM NAC were used in the final protocol.

Contrary to the results in chapter 3, incubation in low oxygen conditions significantly decreased thiol concentrations in untreated BAEC (figure 4.9). In this study, BAEC were subjected to low oxygen for a much longer period of time (48 hrs), therefore ROS generation (through mitochondrial ETC dysfunction) and consequent GSH depletion was likely. In thiol depleted BAEC, thiol levels were depleted to a similar level at 1% and 21 % O_2.

In the radiotracer retention study, it was noted that thiol concentration was not significantly affected by NAC incubation 1 hr incubation period with ^{64}Cu-ATSM post-treatment in the absence of NAC. As mentioned earlier, NAC passively diffuses from cells and it is probable that intracellular NAC equilibrates with the media after its removal; therefore augmentation of intracellular thiol concentration was less marked. It was therefore decided to add a further group to the study in which BAEC were incubated with NAC during the ^{64}Cu-ATSM treatment period. BAEC thiol concentration was significantly increased when NAC was left in the media during ^{64}Cu-ATSM incubation. In particular, at 1% O_2, incubation with 7.5 and 30 mM NAC increased thiol concentrations over 2 and 3 fold higher compared to 21% O_2 equivalents respectively. This may be a

cellular defence mechanism; increased ROS generation in response to hypoxia may increase cellular uptake of NAC for GSH synthesis.

4.4.3 Effect of thiol concentration and low oxygen on BAEC viability

To assess the effects of DEM, BSO and NAC on BAEC viability, different concentrations of each were incubated with BAEC for 24 hrs. Results from MTT assays confirmed that these drugs had no effect on BAEC viability, with the exception of 100 mM NAC, which caused a decrease in BAEC viability by 25%. This was comparable to the effect of 250 μM H_2O_2, a positive marker of cell death, therefore 100 mM NAC was not used in this study.

Before the final experiments with ^{64}Cu-ATSM, the effect of a combination of low oxygen and modified thiol concentration on BAEC viability were investigated. A significant decrease in cell viability was observed in all treatment groups incubated at 1% O_2 compared to 21% O_2. As the MTT assay is an assessment of mitochondrial activity, cell number could possibly affect the outcome. This led to a further study which mimicked the same conditions to assess the effects of low oxygen and thiol concentration modification on cell protein as a measure of cell population. BAEC incubated in 1% O_2 contained significantly less protein in all treatment groups compared with their normoxic equivalent. This data suggests that differences in cell density, as seen in this low oxygen model, will affect viability results measured by the MTT assay and should be accounted for in experimental protocol design.

The results obtained from NAC treated BAEC are contrary to those in chapter 3, where there was no observable increase in myocardial ^{64}Cu retention from ^{64}Cu-ATSM in NAC supplemented hearts. Our thiol augmented isolated

perfused heart model underwent constant perfusion, hence myocardial NAC supplementation and wash out was simultaneous. The concentrations of NAC in the BAEC study are far higher than physiological conditions *in vivo,* even with NAC supplementation. This study does, however, support that thiols can reduce Cu-ATSM under hypoxic conditions, supporting the theory that thiols are essential in Cu-ATSM reduction.

Chapter 5

Effect of acidosis on ^{64}Cu-ATSM hypoxia selectivity

5.1 Introduction

The myocardium must produce sufficient ATP to maintain contractility and cell viability. In the normoxic myocardium, oxygen is required for the efficient generation of ATP via fatty acid β-oxidation and the mitochondrial ETC. During hypoxia the heart switches from fatty acid β-oxidation to glycolysis to generate ATP anaerobically. Anaerobic glycolysis is not as efficient at generating ATP and the net hydrolysis of ATP leads to an increase in intracellular H^+ which decreases pH.

Myocardial hypoxia and ischaemia are therefore both potentially associated with acidosis, although the severity of that acidosis may vary between ischaemic and hypoxic pathologies. Acidosis activates sarcolemmal NHE which extrudes H^+ in exchange for Na^+ to help maintain a physiological pH at the expense of increasing intracellular Na+ concentrations. During ischaemia, however, lack of residual blood flow leads to an accumulation of H^+ and acidosis becomes more severe. Bak and Ingwall used ^{31}P NMR spectroscopy to demonstrate that acidosis as a result of ischaemia is more severe than that caused by hypoxia alone[197]. The severity of acidosis is dependent upon both the extent of tissue hypoxia and ischaemia; therefore intracellular pH may vary between different cardiac pathophysiologies.

As was discussed in chapter 1, it is possible that the hypoxia-selective retention of Cu from Cu-ATSM is dependent upon ligand protonation, and that acidosis may promote this. Changes in intracellular pH may therefore modify the rate of dissociation of the complex, and decrease the specificity and reliability of these complexes as hypoxia-specific tracers. To date, there have been no reports on the investigation of the effects of acidosis on cardiac Cu-ATSM hypoxia

selectivity. As acidosis is a common (and potentially variable) feature of cardiac ischaemia and hypoxia, the effect of acidosis on Cu-ATSM hypoxia selectivity and pharmacokinetics was investigated.

In this study, the ammonium prepulse technique was employed to induce acidosis in isolated perfused rat hearts. In solution, NH_4Cl dissociates to NH^{3+}, Cl^- and H^+. During the washout period, NH^{3+} is washed from the cell, leaving behind H^+ and therefore decreasing pH[198]. To further exacerbate acidosis, the NHE was inhibited with zoniporide. Zoniporide specifically inhibits NHE-1 which is the major isoform of NHE expressed in the myocardium[199]. Intracellular buffering capacity with HCO_3^- was also decreased by perfusing with HCO_3^- free buffer. The progression of myocardial acidosis was measured using ^{31}P NMR spectroscopy (described in chapter 2). The effect of acidosis on ^{64}Cu-ATSM hypoxia selectivity and pharmacokinetics was then determined in parallel hearts.

5.2 Materials and methods

5.2.1 Chemicals and reagents

NH_4Cl and the bicinchoninic acid (BCA) assay kit were obtained from Fischer Scientific, UK. Zoniporide was obtained from Tocris Bioscience, UK. ^{64}Cu-ATSM was synthesised as described in chapter 2.

5.2.2 Animals

Male Wistar rats (275-350g) were used throughout. Rats were given *ad libitum* access to food and water. All experimental procedures were carried out in accordance with Home Office regulations as detailed in the Home Office Guidance on the Operation of Animals (Scientific Procedures) Act 1986.

5.2.3 Perfusion protocols

Hearts were excised, cannulated, and perfused with KHB as described in chapter 2, and electrically paced at 320 b.p.m. All hearts were perfused with normoxic KHB for a stabilisation period of 10 min to ensure cardiac contractile function criteria were met before continuing the experiment. Hearts were perfused according to the protocols described in figure 5.1. To induce acidosis, hearts were infused with NH_4Cl and zoniporide solution (20 mmol/ L and 1 mmol/ L respectively) for 5 mins at 2 mL/ min followed by perfusion with zoniporide only for 20 mins. Perfusion buffer was also switched to $NaHCO_3$ free KHB supplemented with 20mM HEPES and 25 mM NaCl to prevent buffering. Three boluses of ^{64}Cu-ATSM (2MBq) were injected into the perfusion line at t=10 mins, t=42 mins and t=66 mins. Samples of perfusate (approximately 1.5

mL) were collected directly from the heart at appropriate time points and assessed for lactate, glucose and protein release (described in chapter 2).

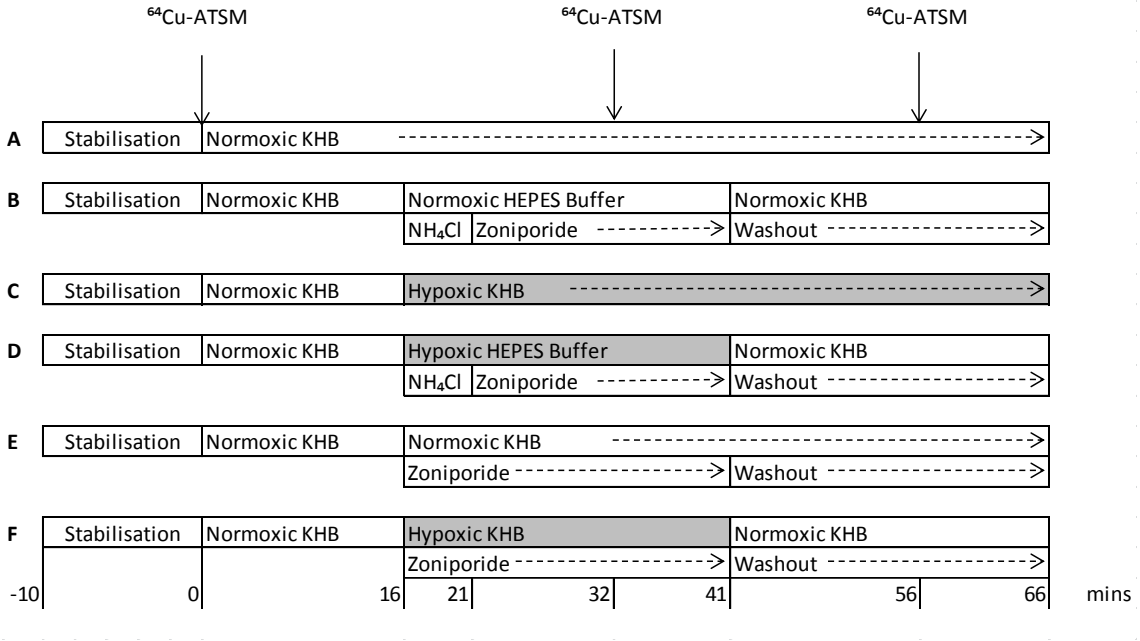

Figure 5.1. Perfusion protocols for hearts from all treatment groups. There were six perfusion protocols for (A) normoxic control, (B) normoxic acidosis, (C) 0% O_2, (D) 0% O_2 acidosis, (E) 20% O_2 and (F) 20% O_2 acidosis groups.

5.2.4 Measurement of cardiac acidosis via ^{31}P NMR spectroscopy

Parallel groups of hearts were subjected to the protocols outlined in figure 5.1 (omitting the ^{64}Cu-ATSM injections) and ^{31}P NMR spectra were obtained to measure intracellular pH (pH_i), as described in chapter 3.

5.2.5 ^{64}Cu-ATSM pharmacokinetic analysis

Cardiac ^{64}Cu-ATSM pharmacokinetics were characterised utilising a custom built triple detector system. Time activity curve data were analysed with Microsoft Excel and MATLAB® to provide radiocopper retention and pharmacokinetic measurements, as described in chapter 2.

5.2.5 Statistical analysis

All data are presented as the mean ± standard deviation. Statistical significance was evaluated using ANOVA followed by Bonferroni post hoc test.

5.3 Results

5.3.1 Effect of hypoxia and NH_4Cl prepulse protocols on cardiac pH_i

5.3.1.1 Myocardial pH_i during hypoxia

Figures 5.2-5.5 display representative spectra and average pH_i of the hearts from all 6 protocols. During normoxia, cardiac pH_i remained stable between 7.13 ± 0.03 and 7.18 ± 0.03 throughout the experimental perfusion (figure 5.2).

Hypoxia was induced by perfusing hearts with KHB gassed with 0% O_2 which caused a decrease in pH_i from 7.12 ± 0.07 to 7.03 ± 0.08 after 8 mins, however, this was not significant when compared to time-matched normoxic pH_i and returned to 7.1 ±0.09 after 28 mins (figure 5.3).

5.3.1.2 Effect of NH_4Cl prepulse and NHE inhibition on myocardial pH_i

Inducing acidosis in these experiments was a two-step procedure: infusing NH_4Cl in combination with zoniporide for 5 mins, and then washing NH_4Cl out in the presence of zoniporide for 20 mins. During normoxia, NH_4Cl and zoniporide caused pH_i to decrease from 7.1 ± 0.06 to 6.3 ± 0.12 ($p<0.05$) within 20 mins (figure 5.4). When zoniporide was washed out, pH_i returned to 7.1 ± 0.1 after 15 mins. Similarly, perfusion with 0% O_2 KHB plus NH_4Cl and zoniporide caused pH_i to decrease from 7.1 ± 0.07 to 6.3 ± 0.10 ($p<0.05$) within 15 mins, which returned to 7.1 ± 0.1 after reoxygenation and zoniporide wash out for 15 mins (figure 5.5).

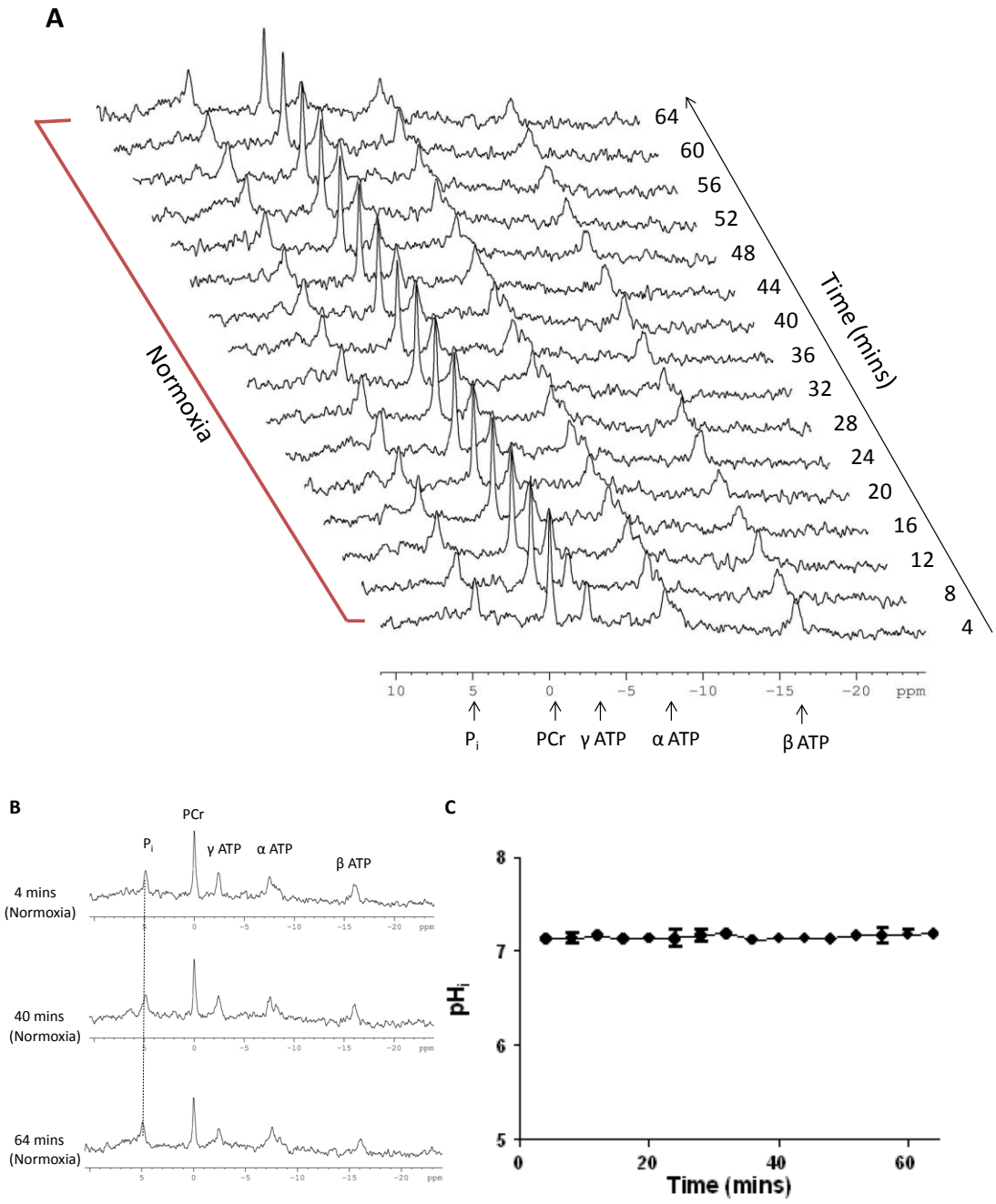

Figure 5.2. (A) Representative stacked plot of ^{31}P NMR spectra acquired from a normoxic control heart. (B) Single spectra from stacked plot. (C) Myocardial pH_i (data are expressed as means ± standard deviation, n = 5).

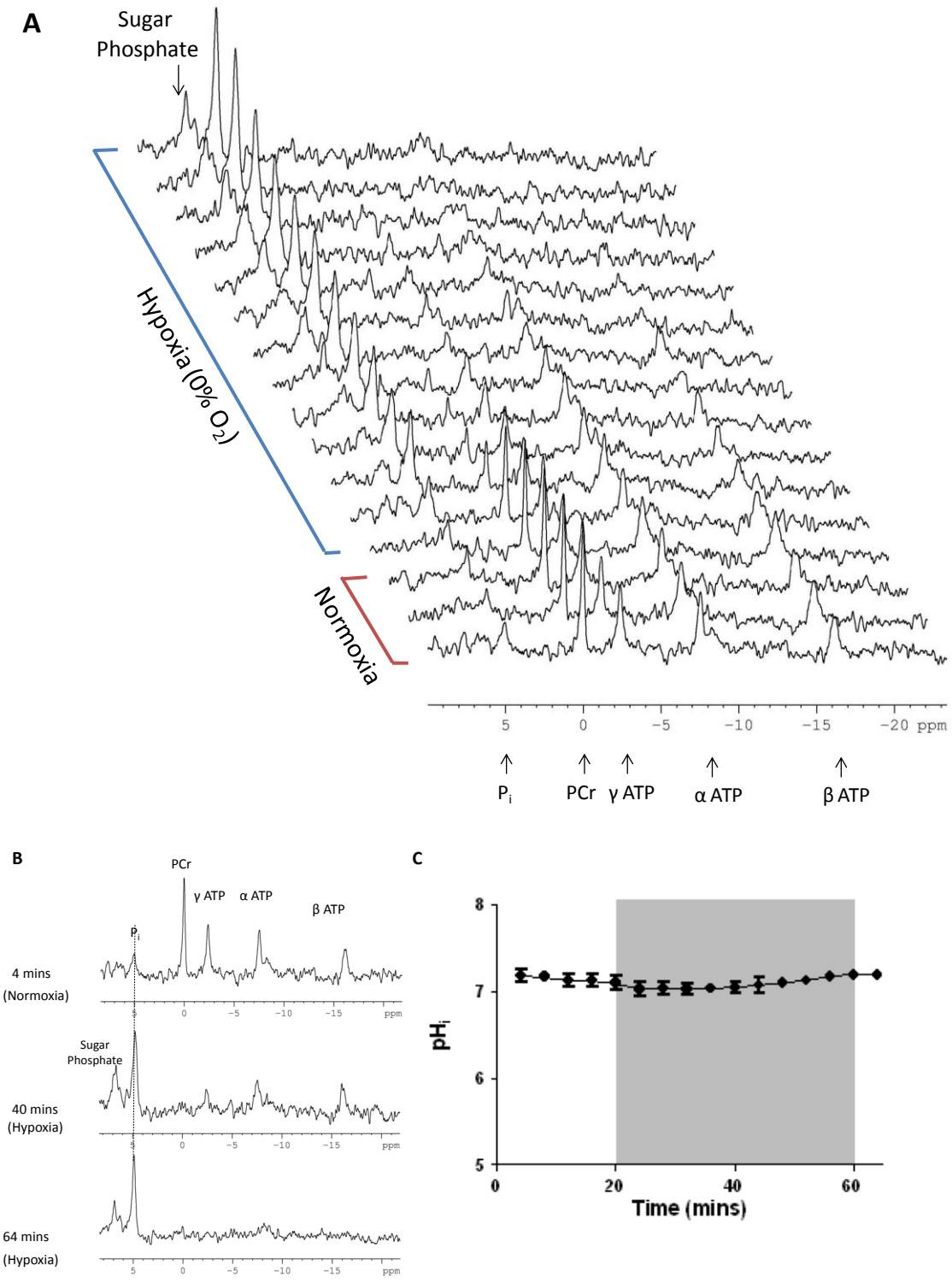

Figure 5.3. (A) Representative stacked plot of ^{31}P NMR spectra acquired from a hypoxic control (0% O_2) heart. (B) Single spectra from stacked plot. (C) Myocardial pH_i (data are expressed as means ± standard deviation, n = 5).

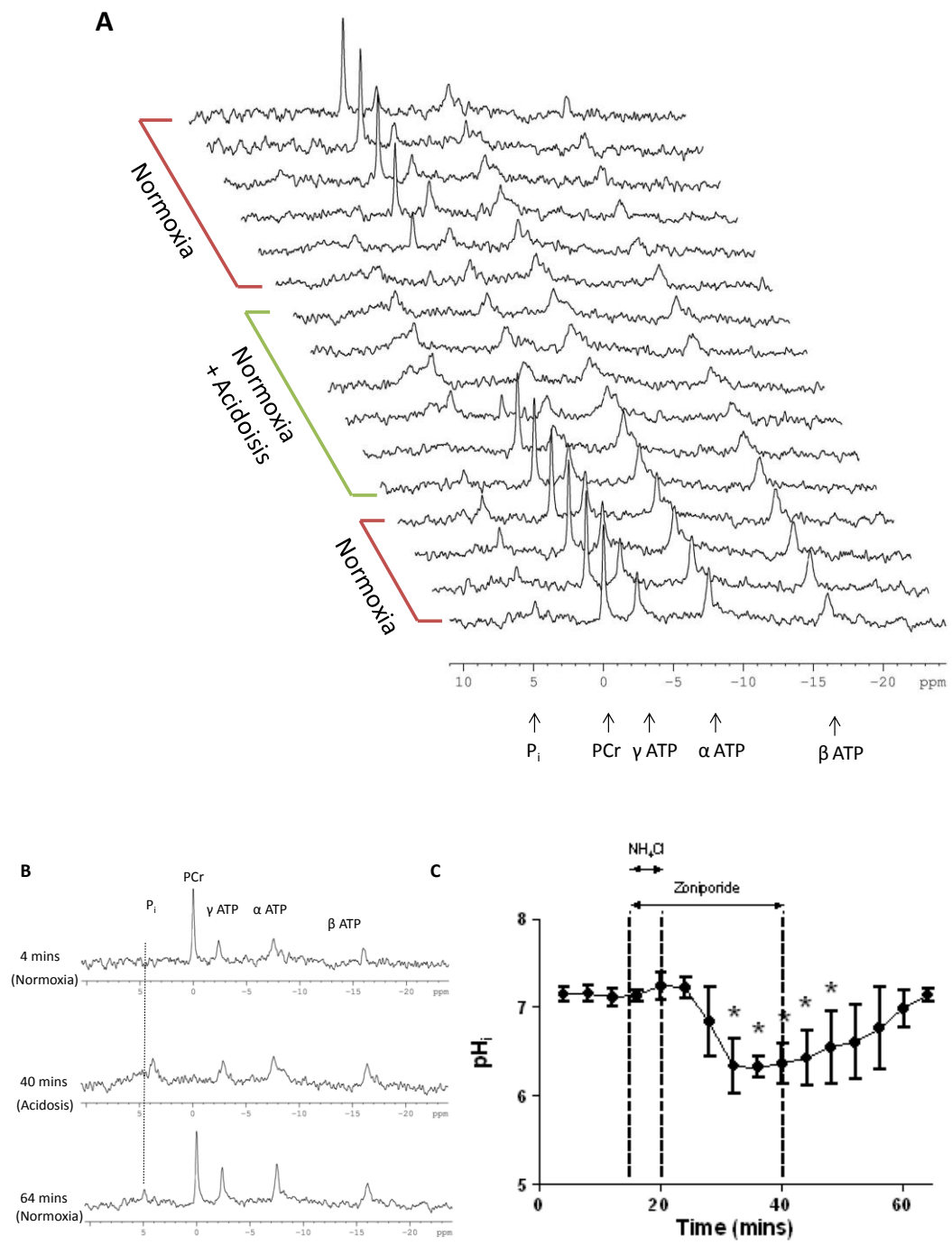

*Figure 5.4. (A) Representative stacked plot of ^{31}P NMR spectra acquired from a normoxic acidotic heart. (B) Single spectra from stacked plot. (C) Myocardial pH_i (data are expressed as means ± standard deviation, n = 5).*p<0.05 vs. time-matched normoxic control pH_i.*

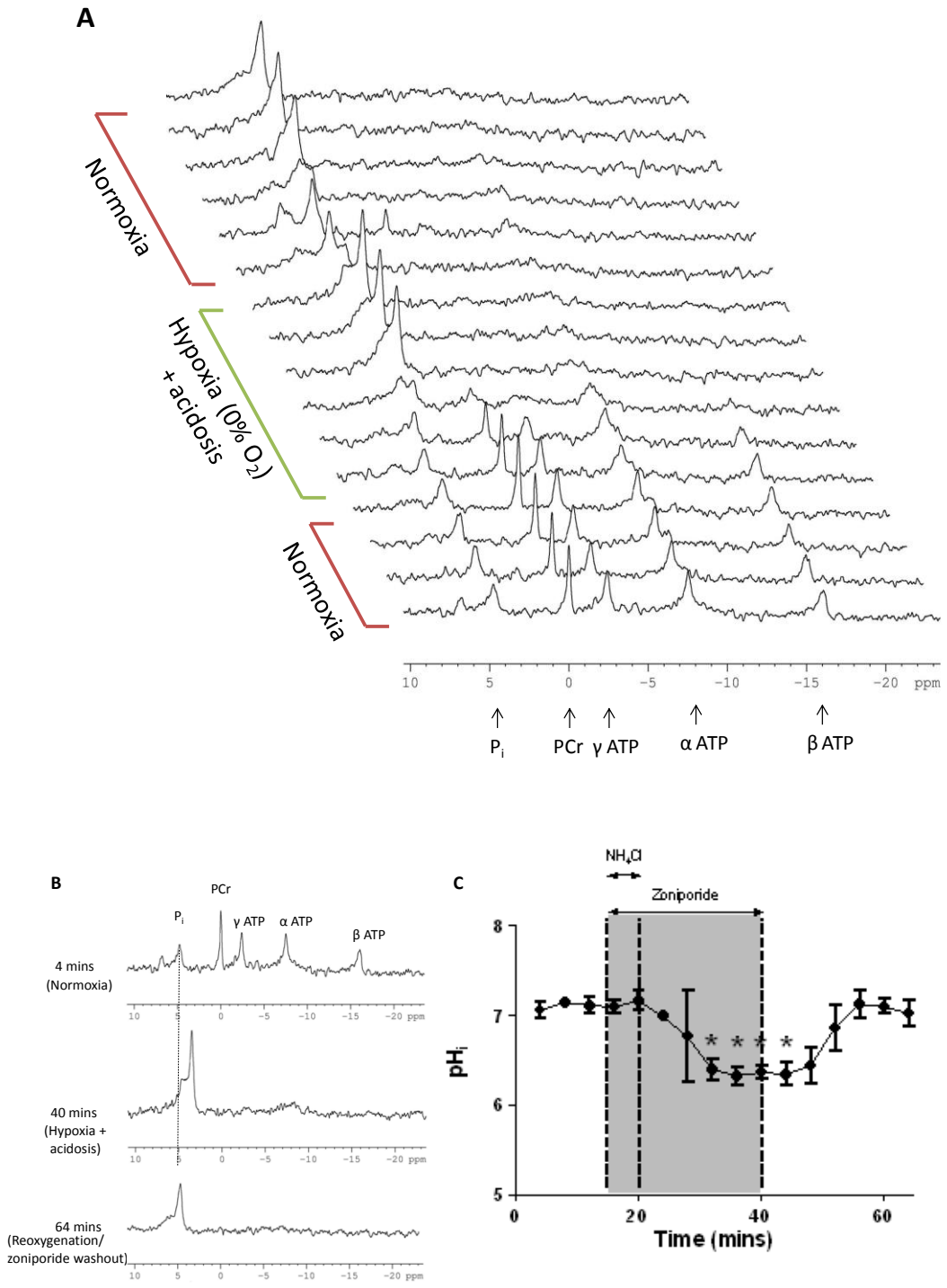

*Figure 5.5. (A) Representative stacked plot of ^{31}P NMR spectra acquired from a hypoxic (0% O_2) acidotic heart. (B) Single spectra from stacked plot. (C) Myocardial pH_i (data are expressed as means ± standard deviation, n = 5).*p<0.05 vs. time-matched normoxic control pH_i.*

5.3.1.3 Myocardial metabolite concentration

5.3.1.3.1 Phosphorous metabolite concentration during normoxia and hypoxia

To measure phosphorous metabolite concentration the area under each peak was compared to that of the initial PCr peak in the first spectrum of each heart; therefore all metabolite concentrations are expressed as arbitrary units (figures 5.6-5.9). Metabolite concentrations remained stable in normoxic untreated control hearts. PCr peak areas averaged between 0.75 ± 0.4 and 1.3 ± 0.3, P_i between 0.58 ± 0.09 and 1.01 ± 0.21 and ATP between 0.77 ± 0.08 and 1.27 ± 0.25. Hypoxia with 0% O_2 caused PCr levels to fall from 0.91 ± 0.10 to 0.15 ± 0.15 within 16 mins, while P_i peak area increased from 0.74 ± 0.29 to 1.33 ± 0.43 and ATP decreased from 0.56 ± 0.18 to 0.46 ± 0.24.

There was no measurable sugar phosphate peak in the spectra acquired from normoxic control hearts. Hypoxia with 0% O_2 caused a gradual increase in sugar phosphate concentration which peaked at 1.02 ± 0.30 after 28 mins.

5.3.1.3.2 Metabolite concentration during acidosis

In normoxic hearts, acidosis caused a decrease in PCr concentration from 0.85 ± 0.19 to 0.02 ± 0.02 within 20 mins, an increase in P_i concentration from 0.69 ± 0.29 to 1.76 ± 0.67 and a decrease in ATP concentration from 0.77 ± 0.13 to 0.55 ± 0.08. By the end of the experimental protocol when zoniporide had been washed out for 23 mins and metabolite concentration returned towards basal values, PCr increased to 0.78 ± 0.40, P_i decreased to 0.20 ± 0.17 and ATP increased to 0.67 ± 0.42. Similarly to normoxic control hearts, there were no measurable sugar phosphate peaks in spectra from normoxic acidotic hearts.

A combination of acidosis and hypoxia with 0% O_2 caused a decrease in PCr levels from 1.05 ± 0.15 to 0.17 ± 0.24, an increase in P_i from 0.78 ± 0.29 to 2.5 ± 0.29 and a decrease in ATP from 0.87 ± 0.18 to 0.46 ± 0.38 after NH_4Cl had been washed out for 15 mins. PCr and P_i values began to recover after NH_4Cl and zoniporide was washed out, but failed to return to basal values by the end of the experimental protocol (PCr 0.39 ± 0.22 and P_i 1.16 ± 0.60). ATP levels completely failed to recover by the end of the hypoxia/acidosis washout period (0.27 ± 0.12 at 64 mins). Sugar phosphate levels were undetectable from these spectra due to the high intensity of the P_i peak obscuring the sugar phosphate peak.

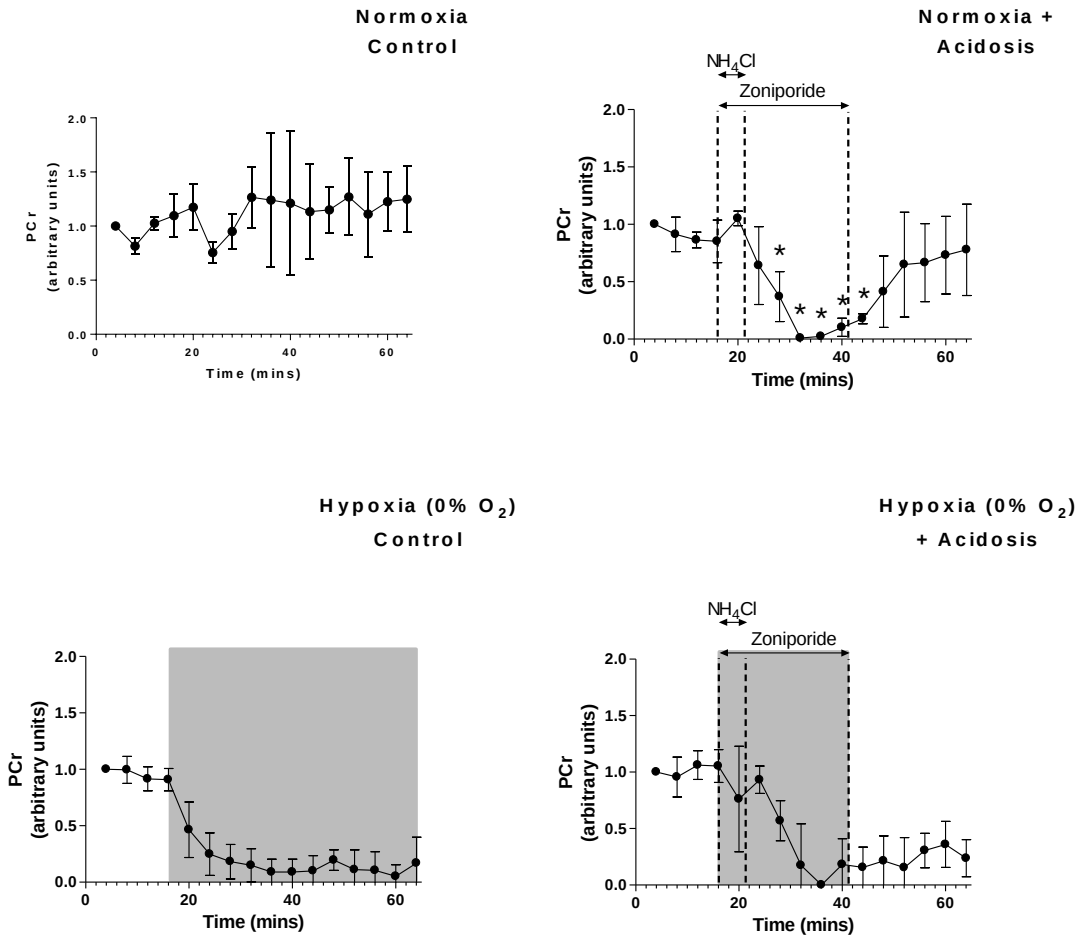

Figure 5.6. PCr levels of hearts undergoing normoxic, hypoxic (0% O_2) or acidotic perfusion protocols. Grey shaded areas represent perfusion with hypoxic buffer. PCr peak areas from the first spectra in each heart were normalised to 1. Data are expressed as means ± standard deviation (n = 5).

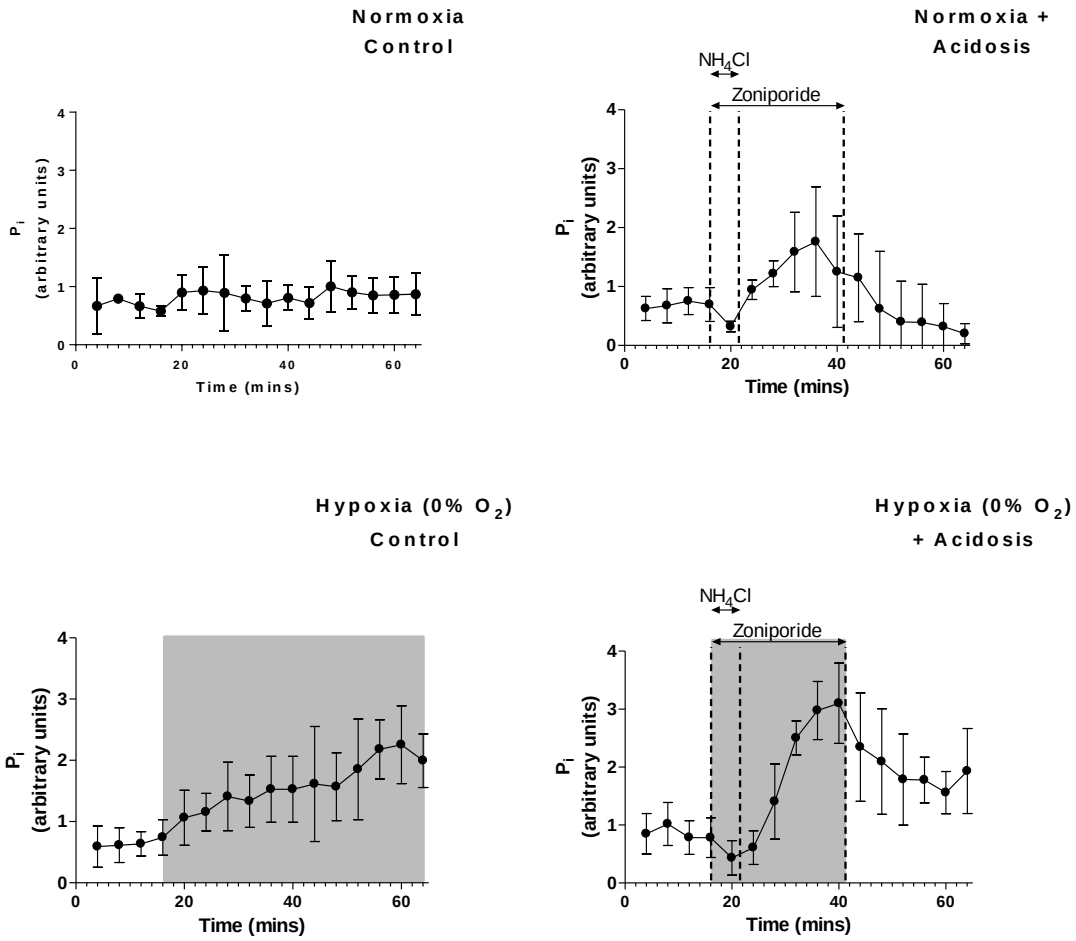

Figure 5.7. P_i levels of hearts undergoing normoxic, hypoxic (0% O_2) or acidotic perfusion protocols. Grey shaded areas represent perfusion with hypoxic buffer. P_i peak areas are with respect to PCr peaks. Data are expressed as means ± standard deviation (n = 5).

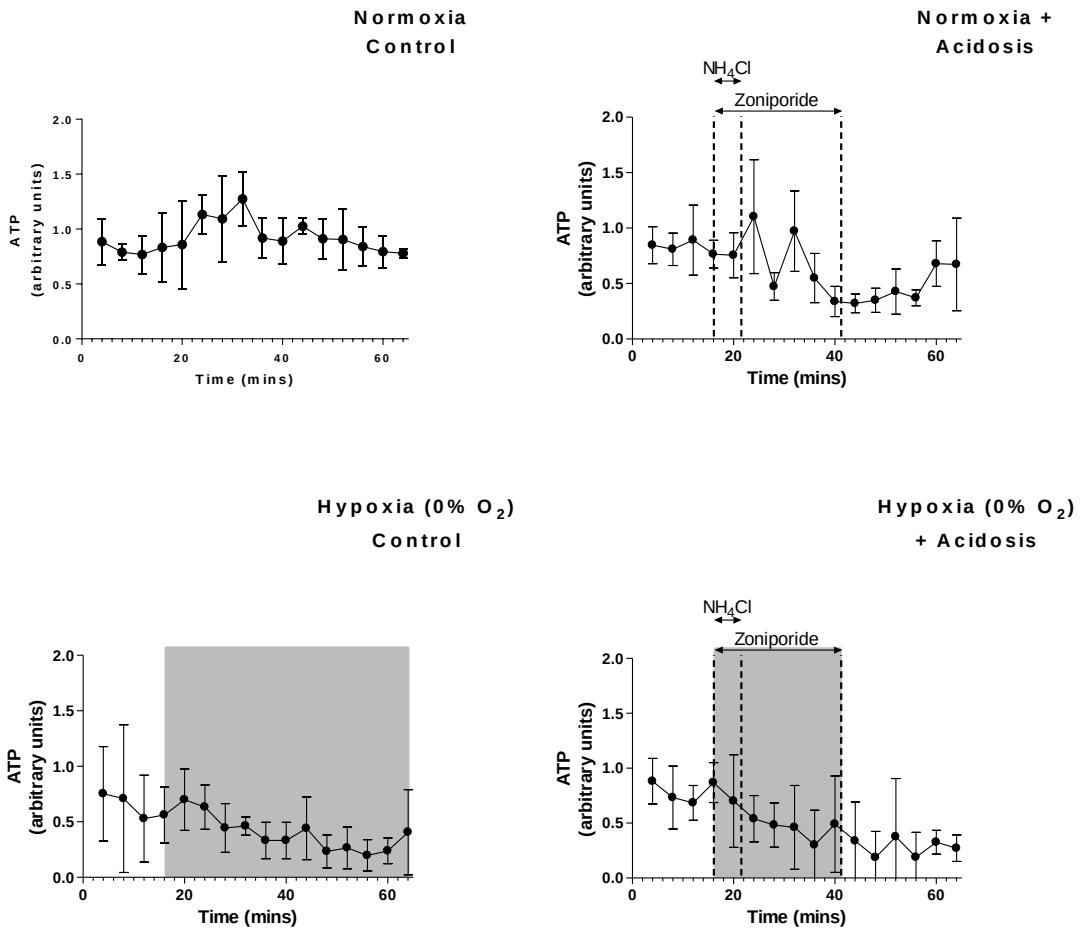

Figure 5.8. *ATP levels of hearts undergoing normoxic, hypoxic (0% O_2) or acidotic perfusion protocols. Grey shaded areas represent perfusion with hypoxic buffer. ATP peak areas are with respect to PCr peaks. Data are expressed as means ± standard deviation (n = 5).*

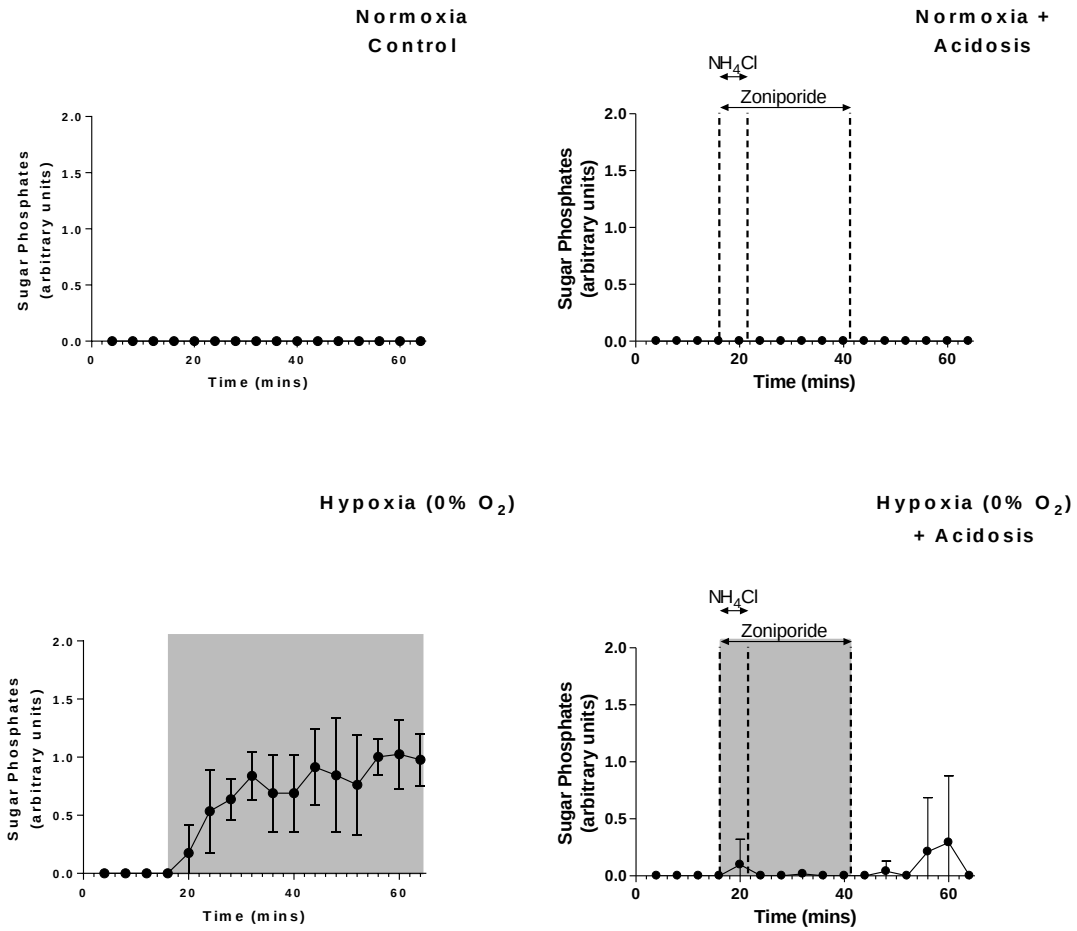

Figure 5.9. *Sugar phosphate levels of hearts undergoing normoxic, hypoxic (0% O_2) or acidotic perfusion protocols. Grey shaded areas represent perfusion with hypoxic buffer. Peak areas are with respect to PCr peaks. Data are expressed as means ± standard deviation (n = 5).*

5.3.1.4 Cardiac Function

5.3.1.4.1 Heart Rate

Heart rates from all protocols are displayed in figure 5.10. As hearts were paced at around 315 b.p.m., there was little variation in heart rate during normoxic control perfusion (314.3 ± 1.7 – 316.8 ± 3.9 b.p.m.). Hypoxia with 0% O_2 for 15 mins caused heart rate to fluctuate between 252 ± 127.4 and 360.3 ± 71.88 b.p.m, indicating spontaneous infrequent arrhythmias. After 35 mins, however, heart rates decreased to between 255 ± 37.9 and 282 ± 7.7 b.p.m. for the remainder of the experimental protocol.

Acidosis caused a decrease in heart rate from 319.2 ± 5.9 to 246.1 ± 151.3 b.p.m. within 5 mins of NH_4Cl infusion. Once acidosis was induced by washing out NH_4Cl, heart rates were not measurable as hearts lost all sinus rhythm. For this reason these values have not been included in figure 5.12. In normoxic hearts, washout of zoniporide for 15 mins caused a recovery in sinus rhythm and heart rate (319.3 ± 6.2 b.p.m.). Hypoxia with 0% O_2 plus acidosis induced a loss in sinus rhythm (from 317.9 ± 4.8 b.p.m.) within 1 min; however, reoxygenation and zoniporide washout did not lead to a recovery of sinus rhythm in these hearts.

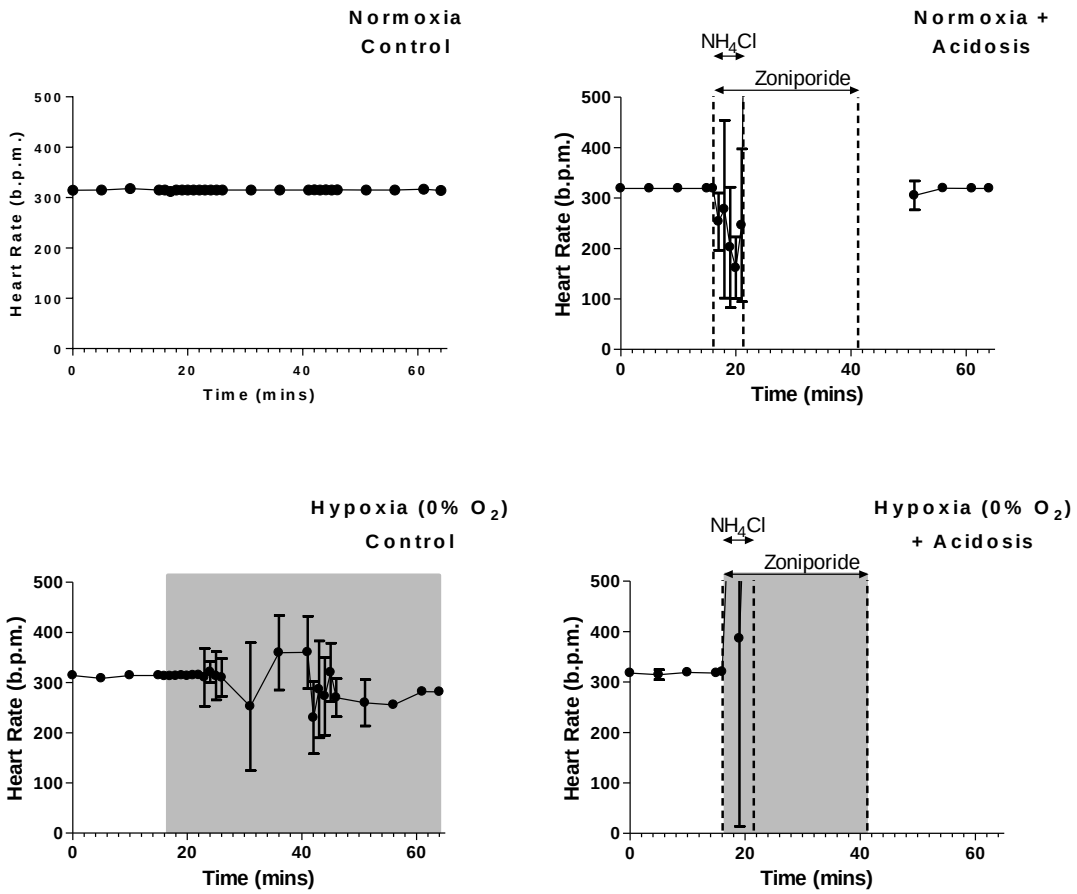

Figure 5.10. Heart rates (b.p.m) of hearts undergoing normoxic, hypoxic (0% O_2) or acidotic perfusion protocols). Grey shaded areas represent perfusion with hypoxic buffer. Data are expressed as means ± standard deviation (n = 5).

5.3.1.4.2 Coronary Perfusion Pressure

Coronary perfusion pressures of hearts from each protocol are displayed in figure 5.11. In normoxic control hearts, perfusion pressure increased slightly from 94.6 ± 4.7 to 107.2 ± 3.9 mmHg over the course of perfusion. Hypoxia with 0% O_2 caused an increase in perfusion pressure from 106.4 ± 16.6 mmHg to 131.2 ± 22.4 by the end of perfusion.

Infusion of NH_4Cl in normoxic hearts did not affect initial perfusion pressure (90.5 ± 10.0 mmHg); however, washout of NH_4Cl with zoniporide infusion caused an increase in perfusion pressure which reached a plateau after 10 mins at 131.1 ± 25.2 mmHg. This decreased slightly after zoniporide washout; however, final perfusion pressure remained at 121.5 ± 27.9 mmHg. Hypoxia with 0% O_2 plus acidosis appeared to cause an initial rapid decrease in perfusion pressure to 73.2 ± 71.5 mmHg; however, this gradually began to increase reaching 131.1 ± 38.7 mmHg by the end of the acidosis protocol and reoxygenation did not cause it to recover by the end of the experimental protocol (132.7 ± 37.3 mmHg).

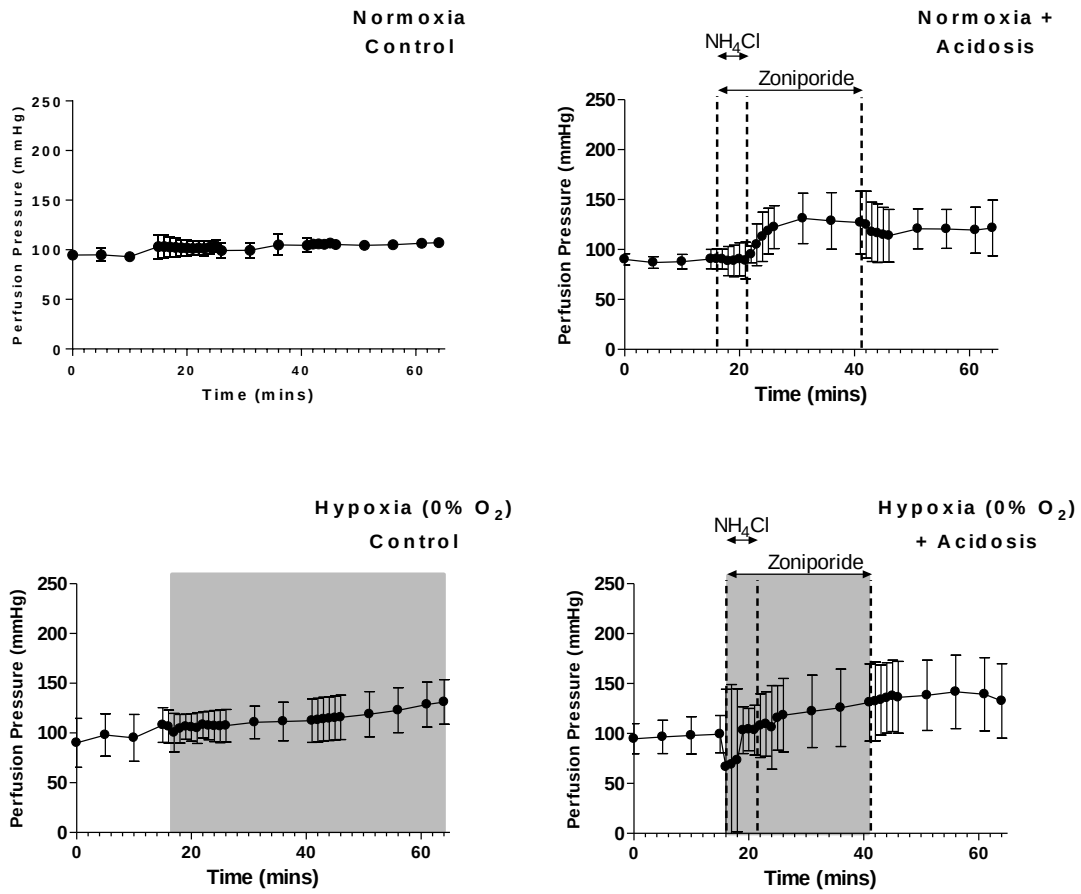

Figure 5.11. Coronary perfusion pressure (mmHg) of hearts undergoing normoxic, hypoxic (0% O_2) or acidotic perfusion protocols. Grey shaded areas represent perfusion with hypoxic buffer. Data are expressed as means ± standard deviation (n = 5).

5.3.1.4.3 Left ventricular developed pressure (LVDP)

During normoxic control protocols LVDP remained stable between 97.3 ± 19.2 and 121.3 ± 27.2 mmHg (figure 5.12). Hypoxia with 0% O_2 resulted in a gradual decrease in LVDP from 87.5 ± 32.9 to 5.1 ± 2.0 mmHg by the end of the experimental protocol.

In hearts from normoxic acidosis protocols, infusion with NH_4Cl caused a rapid reduction in LVDP from 90.7 ± 21.9 to 22.5 ± 11.1 mmHg within 5 mins. Washout of NH_4Cl caused a further decrease to 5.5 ± 4.7 mmHg within 1 minute. After zoniporide was washed out, LVDP returned to 67.2 ± 15.2 mmHg by the end of experimental protocols. Hypoxia with 0% O_2 plus acidosis also caused a decrease in LVDP from 97.1 ± 32.1 to 4.5 ± 3.7 mmHg after 25 mins. Reoxygenation did not cause the LDVP to recover which remained at 10.8 ± 10.2 mmHg by the end of the experimental protocol, suggesting the hearts were non-functional.

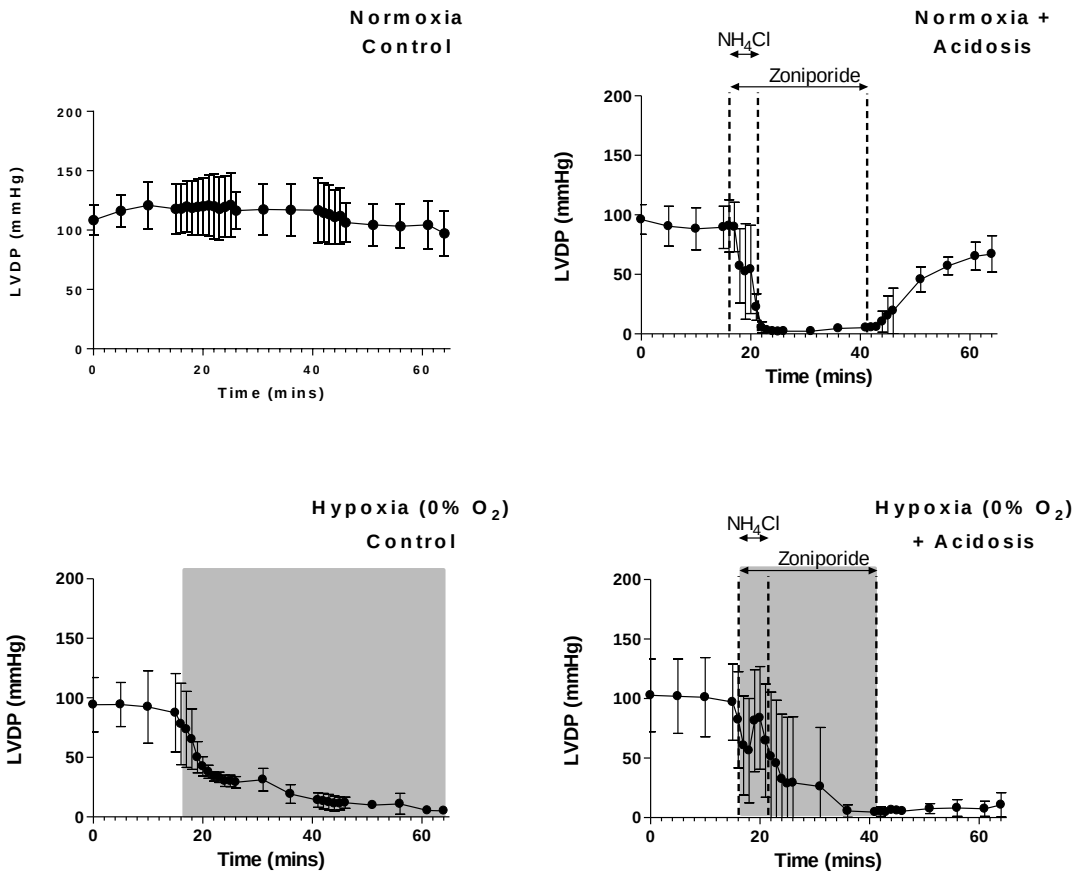

Figure 5.12. LVDP (mmHg) of hearts undergoing normoxic, hypoxic (0% O_2) or acidotic perfusion protocols. Grey shaded areas represent perfusion with hypoxic buffer. Data are expressed as means ± standard deviation (n = 5).

5.3.1.4.4 Left ventricular end diastolic pressure (LVEDP)

During normoxic control protocols, LVEDP remained stable throughout and ranged between 19.5 ± 4.79 and 24.6 ± 5.8 mmHg (figure 5.13). Hypoxia with 0% O_2 led to a rise in LVEDP from 28.3 ± 11.3 to 88.4 ± 25.9 mmHg by the end of the hypoxic period.

In normoxic hearts, acidosis caused a decrease in LVEDP from 16.4 ± 5.3 to 38.2 ± 24.8 mmHg after 25 mins, however, washout of zoniporide resulted in a fall in LVEDP to 29.1 ± 22.4 mmHg after 23 mins. Hypoxia with 0% O_2 KHB + acidosis caused an increase in LVEDP from 15.4 ± 18.9 to 48.6 ± 21.5 mmHg after 25 mins, however, continued to increase after reoxygenation and zoniporide washout reaching a final pressure of 88.4 ± 25.9 mmHg at the end of experiments.

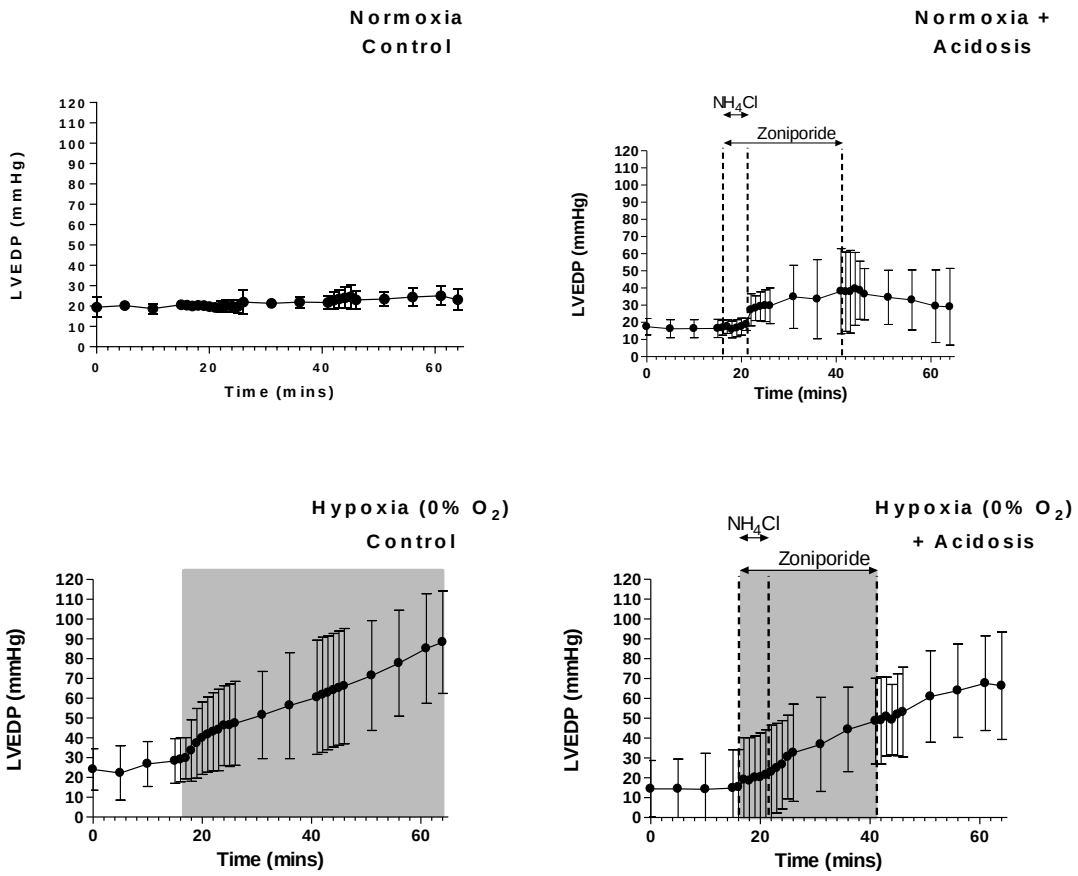

Figure 5.13. LVEDP (mmHg) of hearts undergoing normoxic, hypoxic (0% O_2) or acidotic perfusion protocols. Grey shaded areas represent perfusion with hypoxic buffer. Data are expressed as means ± standard deviation (n = 5).

5.3.1.4.5 Lactate release

Figure 5.14 displays the lactate concentration of perfusate samples collected from all hearts. Lactate release from normoxic control hearts was minimal during normoxic perfusion (0.85 ± 0.01 to 0.11 ± 0.03 nmol /mL /g dry wt). Hypoxia with 0% O_2 caused a rapid increase in lactate release within 5 mins (0.38 ± 0.03 nmol /mL /g dry wt). In normoxic hearts, perfusion with NH_4Cl caused a small increase in lactate release from 0.10 ± 0.03 to 0.15 ± 0.11 nmol /mL /g dry wt within 2 minutes which decreased again upon NH_4Cl washout. Lactate release from acidotic hearts perfused with 0% O_2 KHB was similar to that of normoxic acidotic hearts (lactate release peaking after 3 mins at 0.14 ± 0.01 nmol /mL /g dry wt).

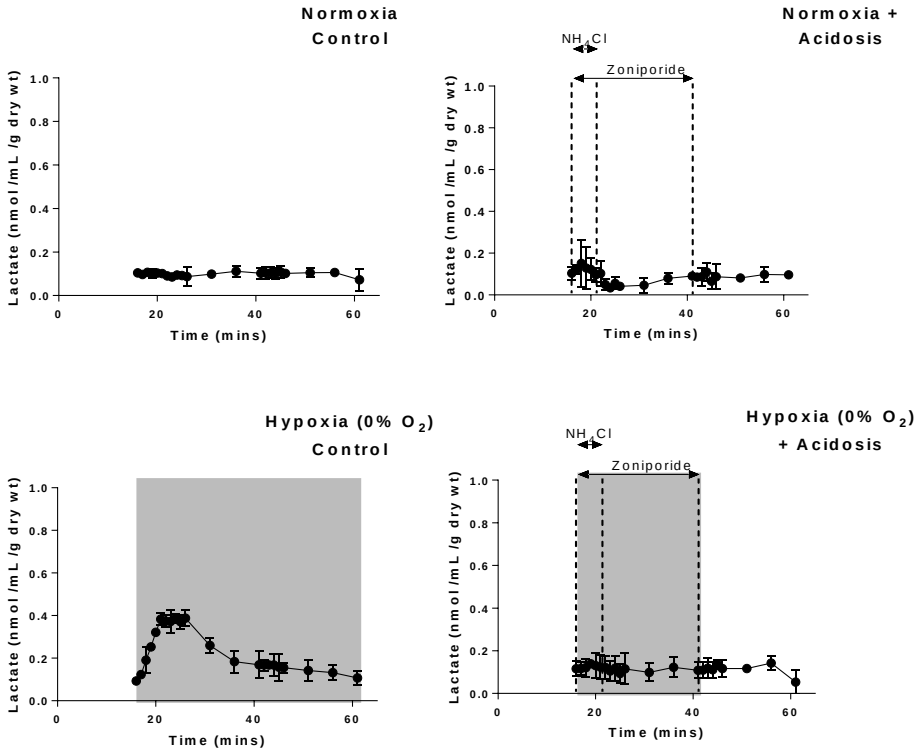

Figure 5.14. Lactate concentration of perfusate samples collected from hearts undergoing normoxic, hypoxic (0% O_2) or acidotic perfusion protocols. Data are expressed as means ± standard deviation (n = 5).

5.3.1.4.6 Glucose consumption

Perfusate glucose concentrations from all hearts are displayed in figure 5.15. During normoxic protocols, perfusate glucose ranged between 10.6 ± 1.1 and 11.4 ± 0.4 mmol/L. Glucose concentration also remained stable in hearts perfused with 0% O_2 KHB, ranging between 10.8 O_2 ± 1.7 and 11.5 ± 0.2 mmol/L). Induction of acidosis also had no effect on perfusate glucose concentration from hearts perfused with normoxic or 0% O_2 KHB (ranging from 10.7 ± 1.0 to 11.8 ± 1.7 mmol/L and 10.7 ± 1.2 to 11.8 ± 1.3 mmol/L).

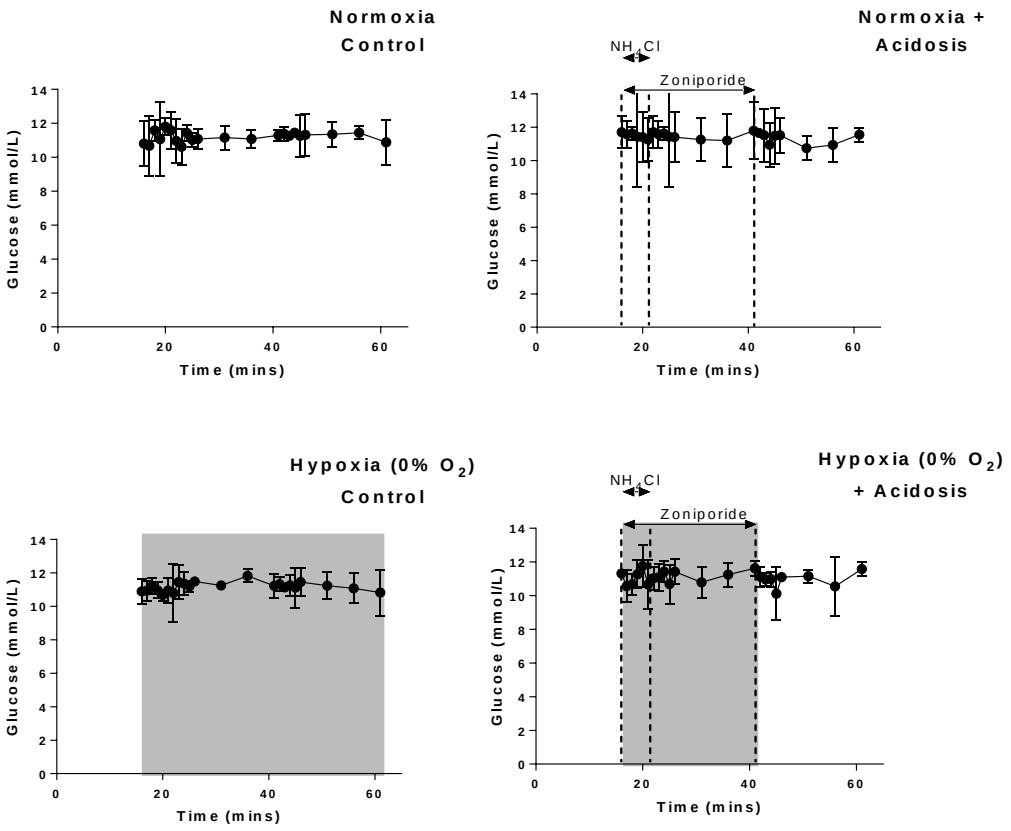

Figure 5.15. Glucose concentration of perfusate samples collected from hearts undergoing normoxic, hypoxic (0% O_2) or acidotic perfusion protocols. Data are expressed as means ± standard deviation (n = 5).

5.3.1.4.7 Protein release

Figure 5.17 displays the protein concentrations of perfusates from all hearts. There was no release of protein from untreated hearts perfused with normoxic or 0% O_2 KHB (ranging from 0.005 ± 0.008 to 0.02 ± 0.02 mg /mL /g dry wt and 0.004 ± 0.007 to 0.01 ± 0.01 mg /mL /g dry wt respectively). Induction of acidosis also did not induce protein release in normoxic perfused hearts. Hypoxia with 0% O_2 plus acidosis, however, caused an increase in cardiac protein release from 0.01 ± 0.008 to 0.04 ± 0.001 mg /mL /g dry wt after 26 mins, returning to 0.015 ± 0.016 mg /mL /g dry wt by the end of the experiments.

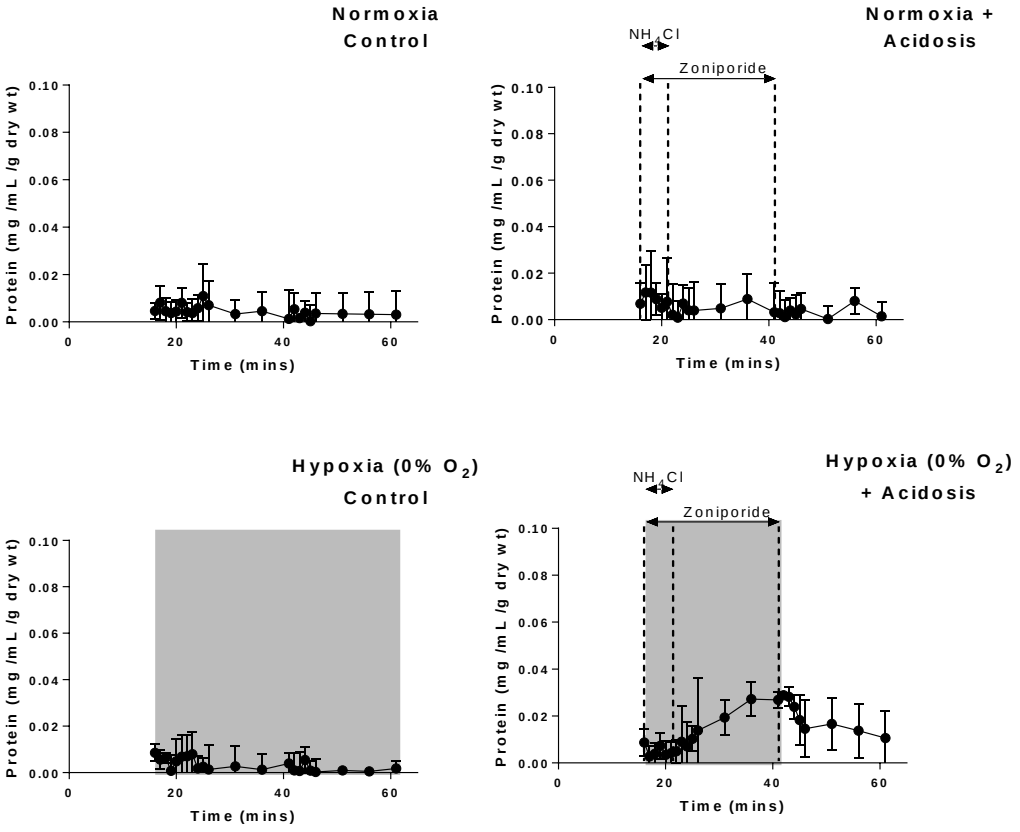

Figure 5.16. Protein concentration of perfusate samples collected from hearts undergoing normoxic, hypoxic (0% O_2) or acidotic perfusion protocols. Data are expressed as means ± standard deviation (n = 5).

5.3.2 Effect of hypoxia with 20% O_2 saturated buffers and ammonium prepulse protocols on cardiac pH_i

In the preliminary studies, it was found that hearts subjected to 0% O_2 hypoxia and acidosis combined did not recover contractile function upon reoxygenation (figure 5.10 and 5.12). As these tracers are intended to delineate hypoxically compromised, but viable tissue, it was apparent that this protocol was too extreme, and perhaps of limited relevance. A further less extreme protocol utilising hypoxia induced by perfusion with KHB gassed with 20% O_2 was therefore included in the study.

5.3.2.1 Myocardial pH_i during hypoxia with 20% O_2

Hypoxia with 20% O_2 did not affect pH_i which averaged between 7.13 ± 0.11 and 7.22 ± 0.1, and was the same when compared to time-matched normoxic control pH_i (figure 5.17).

5.3.2.2 Effect of hypoxia with 20% O_2, NH_4Cl prepulse and NHE inhibition on myocardial pH_i

Perfusion with 20% O_2 KHB plus NH_4Cl and zoniporide infusion caused pH_i to decrease from 7.1 ± 0.07 to 6.4 ± 0.06 ($p<0.05$) which returned to 7.1 ± 0.10 after zoniporide was washed out for 15 mins (figure 5.) and was the same when compared to time-matched normoxic controls (figure 5.18).

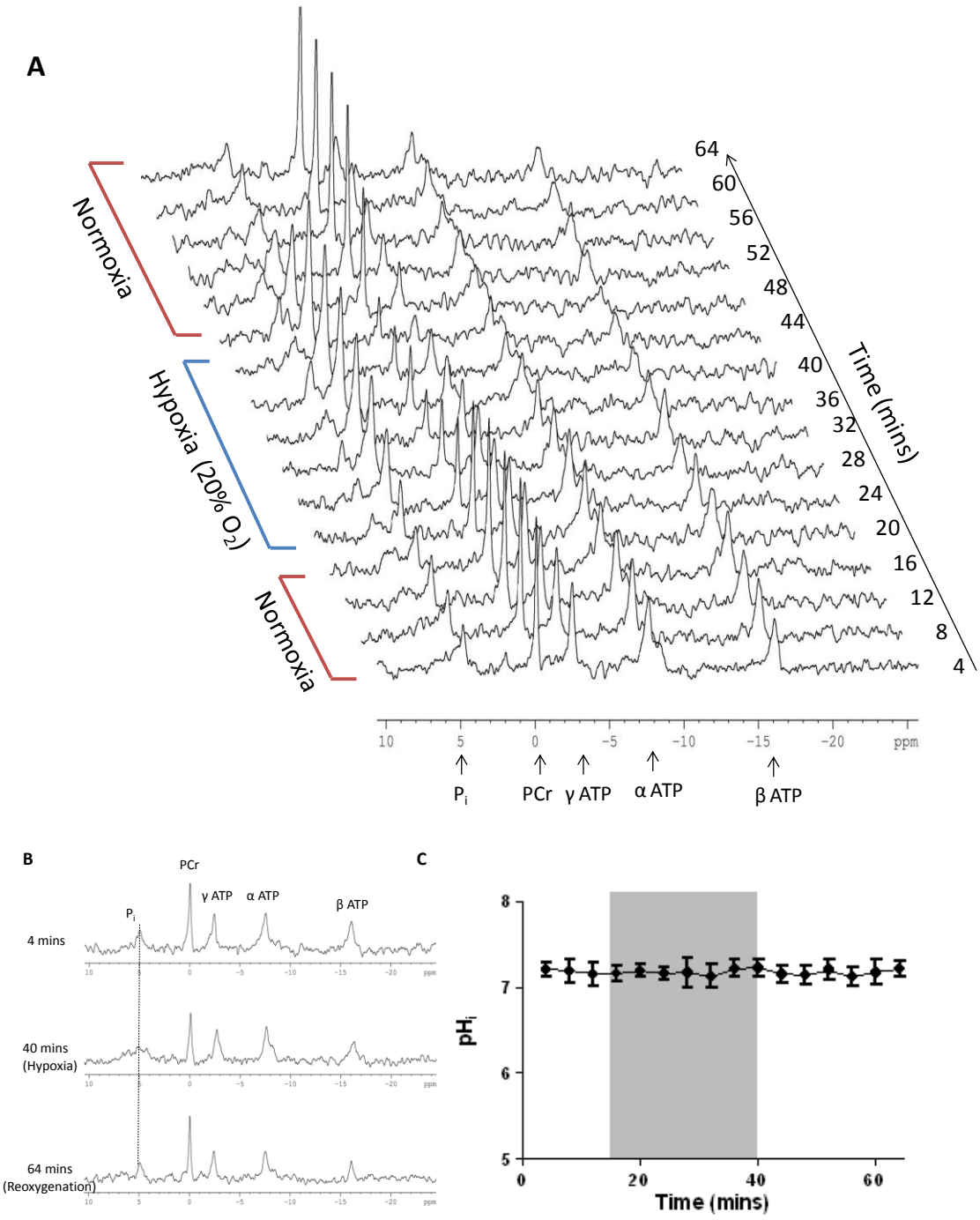

Figure 5.17. (A) Representative stacked plot of ^{31}P NMR spectra acquired from a hypoxic control (20% O_2) heart. (B) Single spectra from stacked plot. (C) Myocardial pH_i (data are expressed as means ± standard deviation, n = 5).

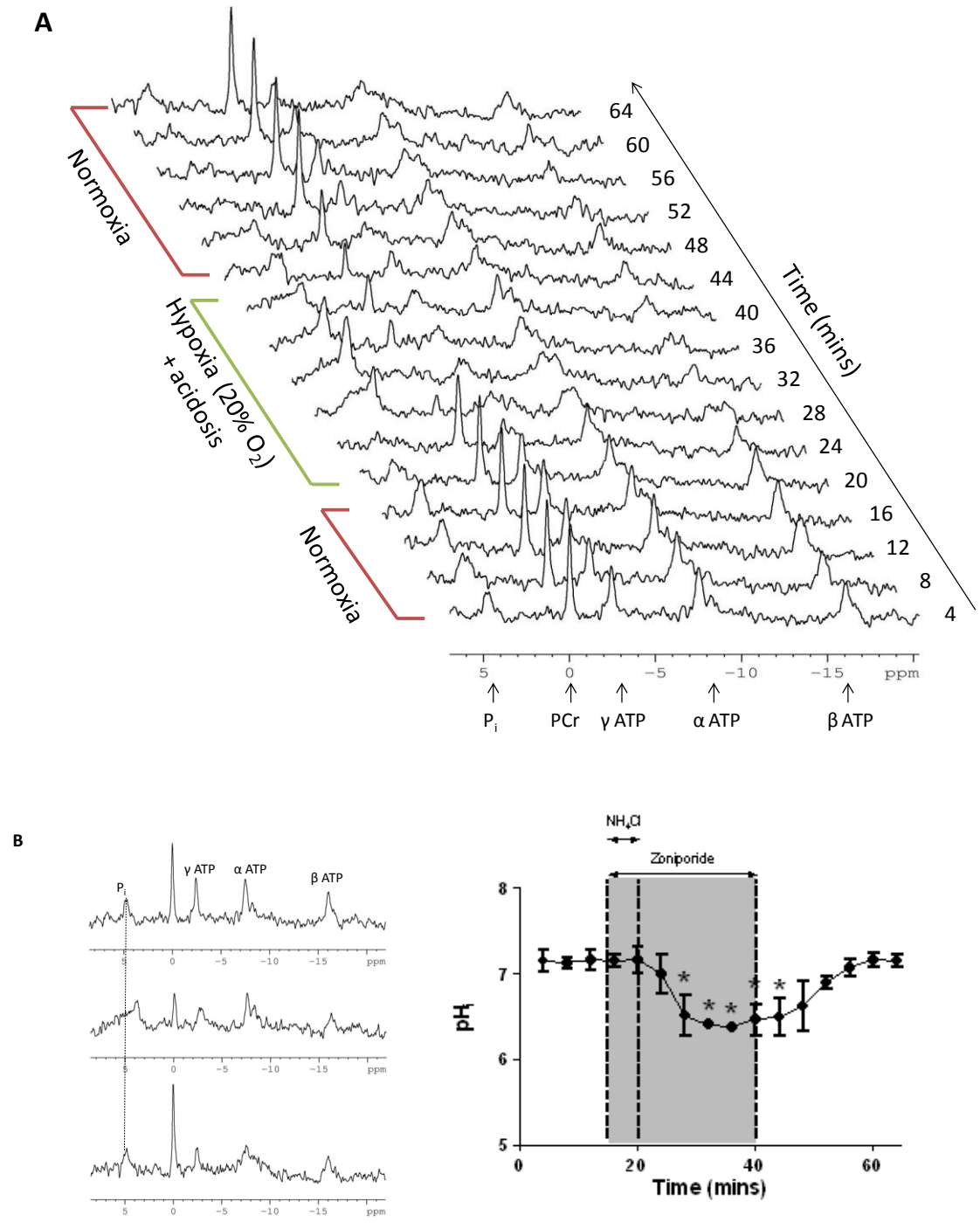

*Figure 5.18. (A) Representative stacked plot of ^{31}P NMR spectra acquired from a hypoxic (20% O_2) acidotic heart. (B) Single spectra from stacked plot. (C) Myocardial pH_i (data are expressed as means ± standard deviation, n = 5).*p<0.05 vs. time-matched normoxic control pH_i.*

5.3.2.3 Myocardial metabolite concentration

5.3.2.3.1 Phosphorous metabolite concentration during normoxia and hypoxia with 20% O_2

Phosphorous metabolite concentrations for hearts perfused with 20% O_2 KHB are displayed in figures 5.19-5.22. Compared to perfusion with 0% O_2 KHB, 20% O_2 had less of an effect on metabolite concentration with the same time period; PCr decreased from 1.04 ± 0.09 to 0.36 ± 0.18, while P_i peak area increased from 0.68 ± 0.07 to 1.11 ± 0.20 and ATP decreased from 0.59 ± 0.08 to 0.29 ± 0.22. Reoxygenation for 15 mins restored metabolite concentration in hypoxic (20% O_2) hearts; PCr values returned to 1.12 ± 0.21, P_i to 0.46 ± 0.21 and ATP to 0.40 ± 0.24. As with 0% O_2, perfusing hearts with 20% O_2 KHB also caused an increase in sugar phosphate concentration which peaked at 0.82 ± 0.10 after 28 mins, however, returned towards 0 after reoxygenation for 19 mins.

5.3.2.3.2 Metabolite concentration during acidosis

Similar to normoxic acidotic hearts, hypoxia with 20% O_2 plus acidosis caused a decrease in PCr from 0.88 ± 0.15 to 0.16 ± 0.31, an increase in P_i from 0.50 ± 0.21 to 1.61 ± 0.34 and a decrease in ATP from 0.70 ± 0.31 to 0.37 ± 0.18 within 15 mins. Phosphorus metabolite levels also returned towards basal values after NH_4Cl and zoniporide had been washed out; however, PCr and ATP were still depressed compared to normoxic control values by the end of the experiment (PCr 0.68 ± 0.25, P_i 0.55 ± 0.45 and ATP 0.43 ± 0.25). As in acidotic hearts perfused with 0% O_2 KHB, sugar phosphate levels were also undetectable in spectra from 20% O_2 acidotic hearts.

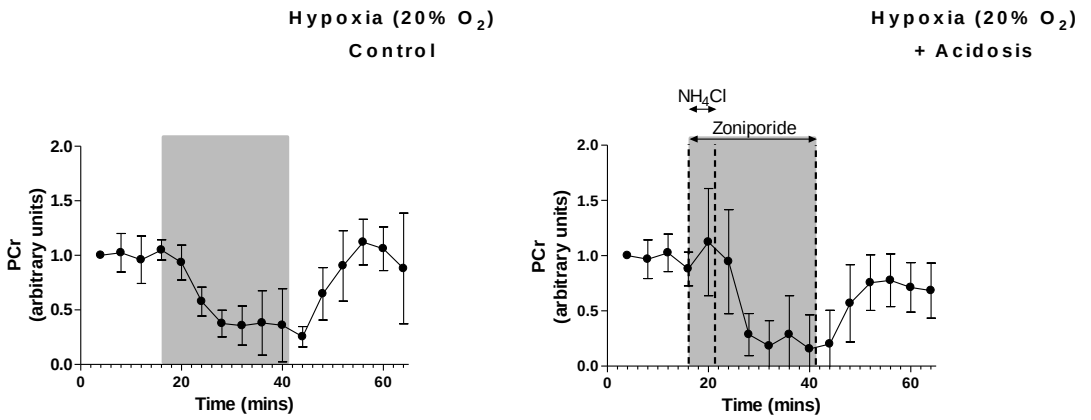

Figure 5.19. PCr levels of hearts of hearts undergoing hypoxic (20% O_2) or hypoxia (20% O_2) + acidosis protocols. Grey shaded areas represent perfusion with hypoxic buffer. PCr peak areas from the first spectrum in each heart were normalised to 1. Data are expressed as means ± standard deviation (n = 5).

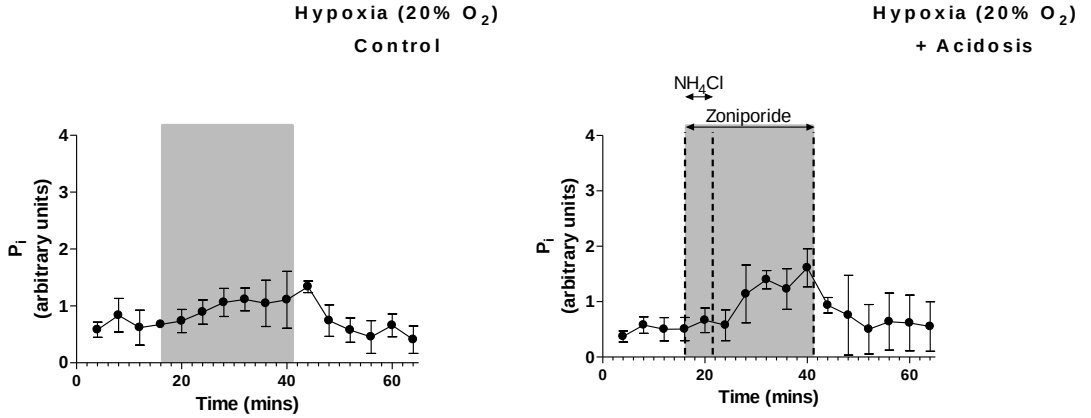

Figure 5.20. P_i levels of hearts undergoing hypoxic (20% O_2) or hypoxia (20% O_2) + acidosis protocols. Grey shaded areas represent perfusion with hypoxic buffer. P_i peak areas are with respect to PCr peaks. Data are expressed as means ± standard deviation (n = 5).

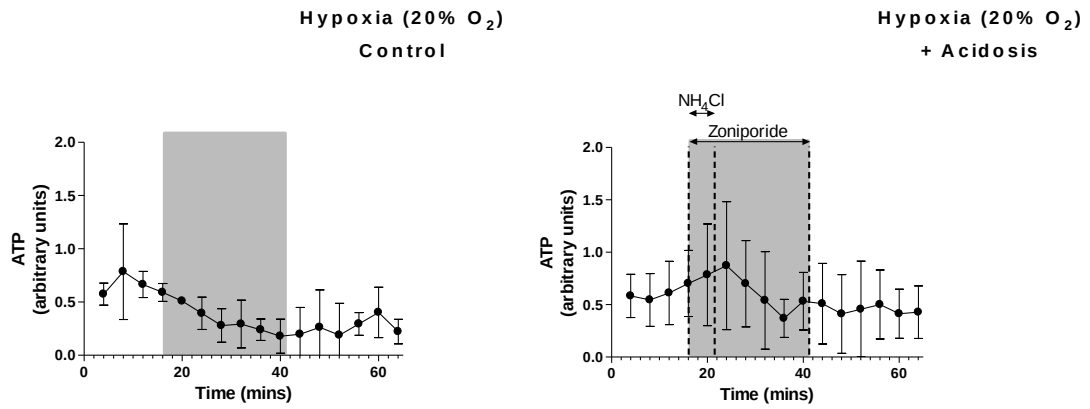

Figure 5.21. ATP levels of hearts undergoing hypoxic (20% O_2) or hypoxia (20% O_2) + acidosis protocols. Grey shaded areas represent perfusion with hypoxic buffer. ATP peak areas are with respect to PCr peaks. Data are expressed as means ± standard deviation (n = 5).

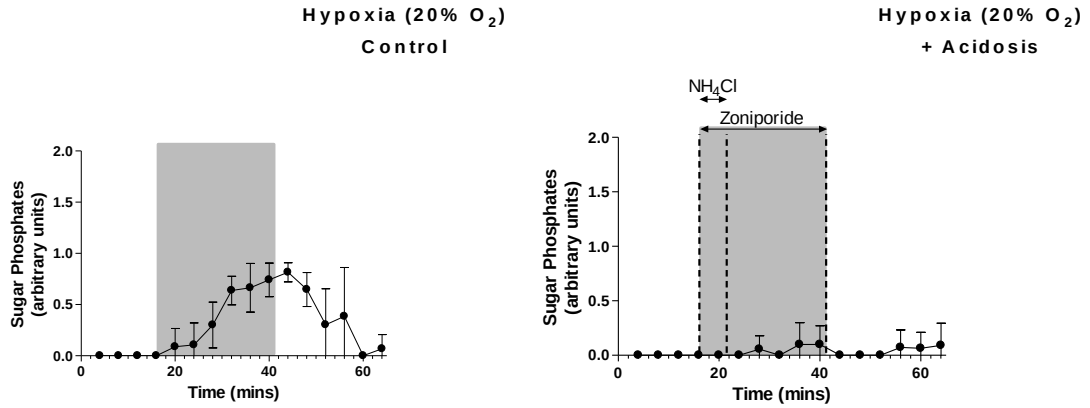

Figure 5.22. Sugar phosphate levels of hearts undergoing hypoxic (20% O_2) or hypoxia (20% O_2) + acidosis protocols. Grey shaded areas represent perfusion with hypoxic buffer. Peak areas are with respect to PCr peaks. Data are expressed as means ± standard deviation (n = 5).

5.3.2.4 Cardiac Function

5.3.2.4.1 Heart Rate

Hypoxia with 20% O_2 caused a gradual decrease in heart rate from 312.9 ± 9.0 b.p.m. to 287.83 ± 57.8 b.p.m. after 6 mins and decreased further to 211.7 ± 96.5 b.p.m. after 28 mins (figure 5.23). Reoxygenation led to the recovery of a regular sinus rhythm 311.9 ± 8.5 b.p.m. within 12 mins. Similar to normoxia plus acidosis, hypoxia with 20% O_2 KHB plus acidosis caused a gradual decrease in heart rate, falling from 311.0 ± 3.7 to 269.6 ± 66.1 over 5 mins. Shortly after NH_4Cl was washed from the hearts sinus rhythm was lost, however, reoxygenation and washout of zoniporide for 15 mins induced an increase in heart rate to 310.1 ± 5.1.

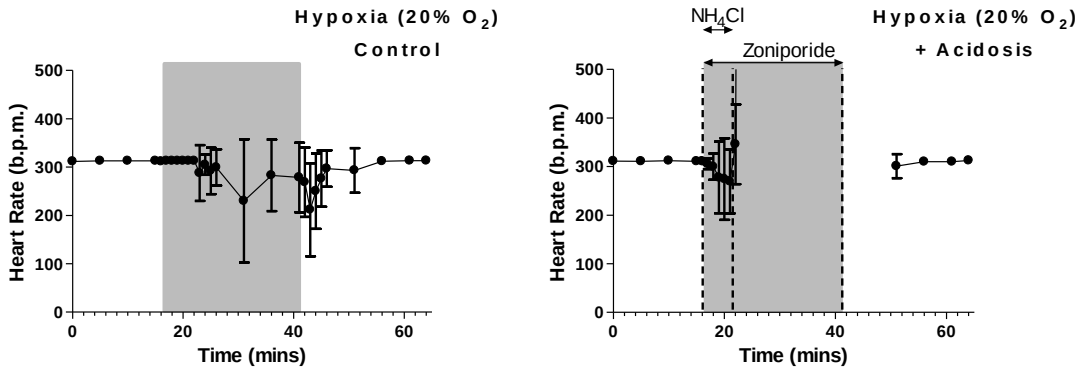

Figure 5.23. *Heart rates (b.p.m.) of hearts undergoing hypoxic (20% O_2) or hypoxia (20% O_2) + acidosis protocols. Grey shaded areas represent perfusion with hypoxic buffer. Data are expressed as means ± standard deviation (n = 5).*

5.3.2.4.2 Coronary Perfusion Pressure

Hypoxia with 20% O_2 caused a slight increase in perfusion pressure from 93.4 ± 9.2 to 101.7 ± 15.6 mmHg by the end of the perfusion protocol and was similar to that in hearts perfused with 0% O_2 KHB (figure 5.24). Hypoxia with 20% O_2 KHB plus acidosis also caused perfusion pressure to decrease from 115.0 ± 17.1 to 105.6 ± 9.4 mmHg within 5 mins which then increased to 188.56 ± 44.17 mmHg by the end of the acidosis period. Reoxygenation and zoniporide washout, however, caused a decrease to an end perfusion pressure of 152.3 ± 26.0 mmHg in hypoxic (20% O_2) hearts.

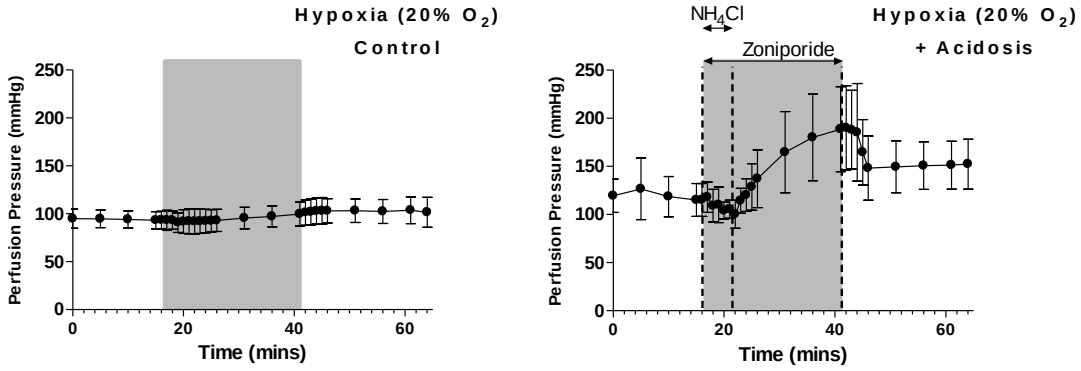

Figure 5.24. Perfusion pressure (mmHg) of hearts undergoing hypoxic (20% O_2) or hypoxia (20% O_2) + acidosis protocols. Grey shaded areas represent perfusion with hypoxic buffer. Data are expressed as means ± standard deviation (n = 5).

5.3.2.4.3 Left ventricular developed pressure (LVDP)

Hypoxia with 20% O_2 resulted in a decrease in LVDP from 115.4 ± 13.4 to 35.5 ± 12.5 mmHg after 25 mins which was similar to 0% O_2; however, reoxygenation caused the LVDP to return to 103.3 ± 13.1 mmHg by the end of experiments (figure 5.25). Hypoxia with 20% O_2 plus acidosis caused a rapid decrease in LVDP from 126.6 ± 10.4 to 15.8 ± 11.6 mmHg within 5 mins and was similar to normoxic acidosis hearts. Washout of NH_4Cl further decreased LVDP to 1.2 ± 0.8 mmHg within 3 mins, however, reoxygenation led to its recovery to 90.2 ± 26.5 mmHg after by the end of experiments.

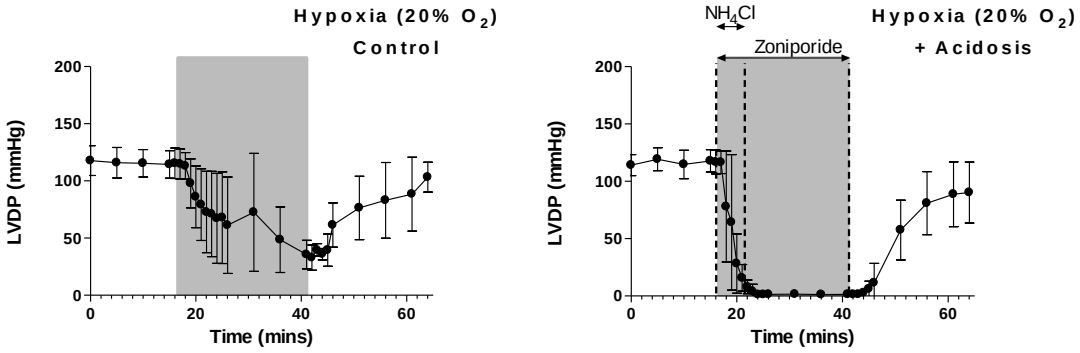

Figure 5.25. LVDP (mmHg) of hearts undergoing hypoxic (20% O_2) or hypoxia (20% O_2) + acidosis protocols. Grey shaded areas represent perfusion with hypoxic buffer. Data are expressed as means ± standard deviation (n = 5).

5.3.2.4.4 Left ventricular end diastolic pressure (LVEDP)

Perfusing hearts with 20% O_2 KHB also led to an increase in LVEDP from 7.5 ± 3.4 to 35.2 ± 12.9 mmHg which was similar to that in hearts perfused with 0% O_2 KHB (figure 5.26). Reoxygenation, however, caused LVEDP to return to 11.5 ± 9.3 mmHg by the end of experiments. Hypoxia with 20% O_2 plus acidosis caused an increase in LVEDP from 7.1 ± 2.6 to 44.1 ± 7.7 mmHg after 25 mins, again, similar to perfusion with 0% O_2 KHB. Reoxygenation and washout of zoniporide initially caused a transient rise in LVEDP to 59.4 ± 17.8 mmHg, however, decreased to 47.3 ± 27.7 mmHg by the end of experiments.

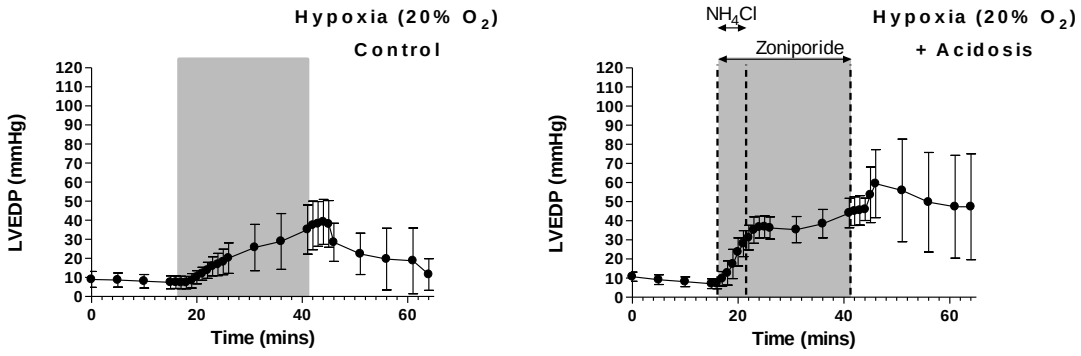

Figure 5.26. LVEDP (mmHg) of hearts undergoing hypoxic (20% O_2) or hypoxia (20% O_2) + acidosis protocols. Grey shaded areas represent perfusion with hypoxic buffer. Data are expressed as means ± standard deviation (n = 5).

5.3.2.4.5 Lactate release

Hypoxia with 20% O_2 KHB caused an increase in lactate release (figure 5.27), which was more gradual than occurred with perfusion with 0% O_2 equilibrated buffer, reaching a maximum of 0.35 ± 0.03 nmol /mL /g dry wt after 20 mins of hypoxia. Lactate release from acidotic hearts perfused with 20% O_2 KHB was similar to that of normoxic acidotic hearts (lactate release peaking after 3 mins at 0.12 ± 0.06 nmol /mL /g dry wt).

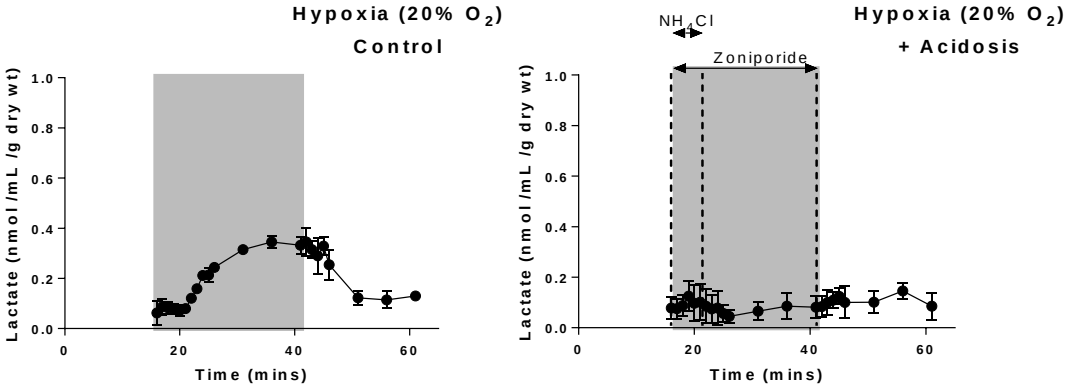

Figure 5.27. Lactate concentration of perfusate samples from hearts undergoing hypoxic (20% O_2) or hypoxia (20% O_2) + acidosis protocols. Data are expressed as means ± standard deviation (n = 5).

5.3.2.4.6 Glucose Consumption

As in normoxic control hearts, perfusate glucose concentration remained stable from hearts perfused with 20% O_2 KHB, ranging between 10.7 ± 1.3 and 11.6 ± 0.7 mmol/L (figure 5.28). Induction of acidosis also had no effect on perfusate glucose concentration from hearts perfused with 20% O_2 KHB, ranging from 10.7 ± 1.1 to 11.8 ± 0.4 mmol/L respectively and was similar to that of normoxic hearts.

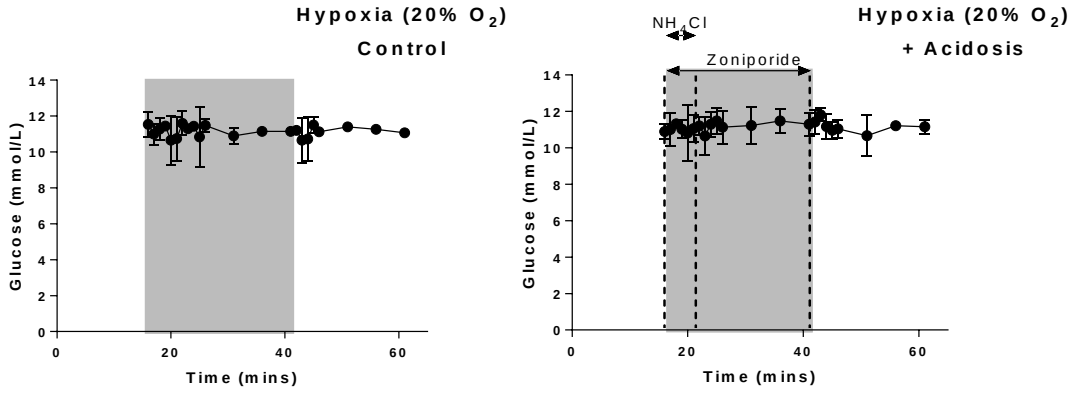

Figure 5.28. Glucose concentration of perfusate samples from hearts undergoing hypoxic (20% O_2) or hypoxia (20% O_2) + acidosis protocols. Data are expressed as means ± standard deviation (n = 5).

5.3.2.4.7 Protein release

Perfusion with 20% O_2 did not induce cardiac protein release into the perfusate (ranging from 0.004 ± 0.009 to 0.008 ± 0.07 mg /mL /g dry wt) and was similar to that of normoxic hearts (figure 5.29). Unlike 0% O_2, hypoxia with 20% O_2 plus acidosis did not cause an increase in cardiac protein release (ranging from 0.005 ± 0.01 to 02 ± 0.01 mg /mL /g dry wt).

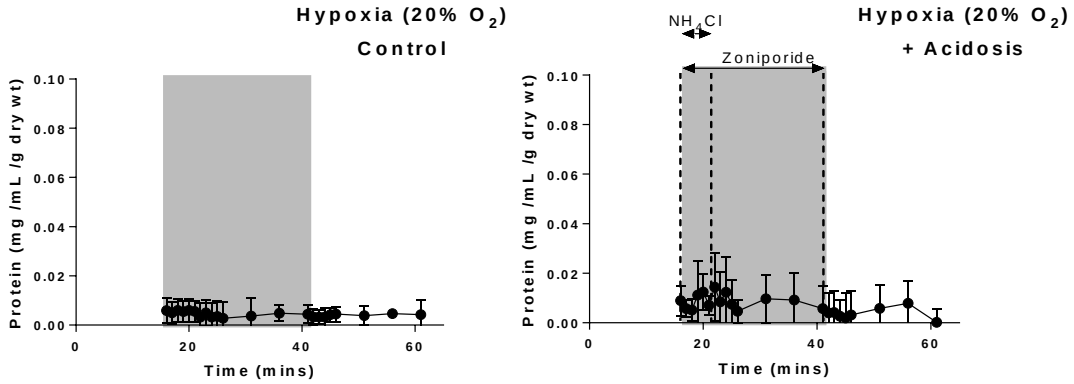

Figure 5.29. Protein concentration of perfusate samples from hearts undergoing hypoxic (20% O_2) or hypoxia (20% O_2) + acidosis protocols. Data are expressed as means ± standard deviation (n = 5).

5.3.3 Effect of acidosis on ^{64}Cu-ATSM hypoxia selectivity and pharmacokinetics

In section 5.3.2.4 the effect of inducing less severe hypoxia (20% O_2 compared to 0% which was used previously) in combination with acidosis on cardiac contractile function was described. As heart rate and LVDP began to recover once zoniporide/acid was washed from these hearts, it was determined that these groups would be added to ^{64}Cu retention studies in place of 0% O_2 groups.

5.3.3.1 ^{64}Cu retention from ^{64}Cu-ATSM in acidic hearts

Representative time-activity curves of ^{64}Cu-ATSM injections and ^{64}Cu retention with and without intracellular acidosis are shown in figure 5.30. During normoxic buffer perfusion, there was relatively little tissue retention of ^{64}Cu from ^{64}Cu-ATSM at any point during the perfusion protocol. This was unaffected by induction of acidosis (figure 5.30A). Hypoxia caused a notable increase in ^{64}Cu retention from ^{64}Cu-ATSM; however, acidosis suppressed hypoxia dependent ^{64}Cu retention (5.30 B).

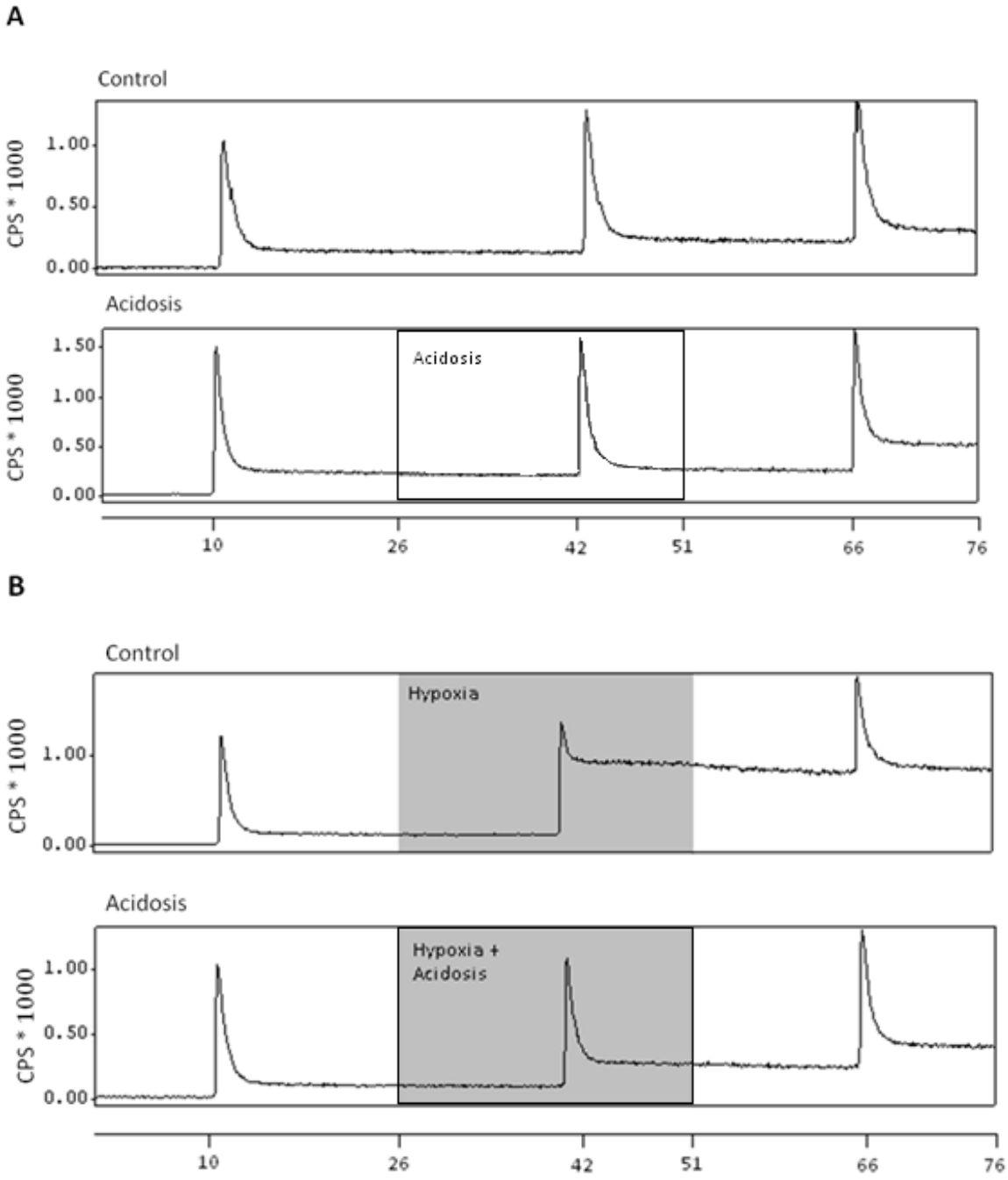

Figure 5.30. Representative time-activity curves from the triple detector system demonstrating ^{64}Cu uptake from ^{64}Cu-ATSM in (A) normoxic hearts and (B) hypoxic hearts. Each trace represents control hearts (no treatment; top) and heart undergoing acidosis (bottom). Black outlined boxes represent period of acidosis and grey shaded areas represent perfusion with hypoxic buffer.

The data from 5 replicate experiments are summarised in figure. 5.31. There was no significant difference in ^{64}Cu retention between all three injections of ^{64}Cu-ATSM in normoxic control hearts (10.0 ± 2.5, 9.5 ± 2.1 and 8.9 ± 1.8 %), but during normoxic acidosis ^{64}Cu retention significantly decreased from 9.3 ± 2.7 % during the control period to 2.4 ± 1.6 % (figure 5.31 A; $p<0.05$), and returned to pre-acidotic values (12.7 ± 3.0 %) 15 mins after zoniporide/acid washout.

Hypoxia significantly increased ^{64}Cu retention from 11.0 ± 2.2 to 46.5 ± 12.0 % ($p<0.05$), which returned to 3.9 ± 4.6 % upon reoxygenation (Figure 5.31 B). Inducing acidosis, however, abolished ^{64}Cu retention from ^{64}Cu-ATSM during hypoxia such that it was not significantly different from pre-hypoxic values.

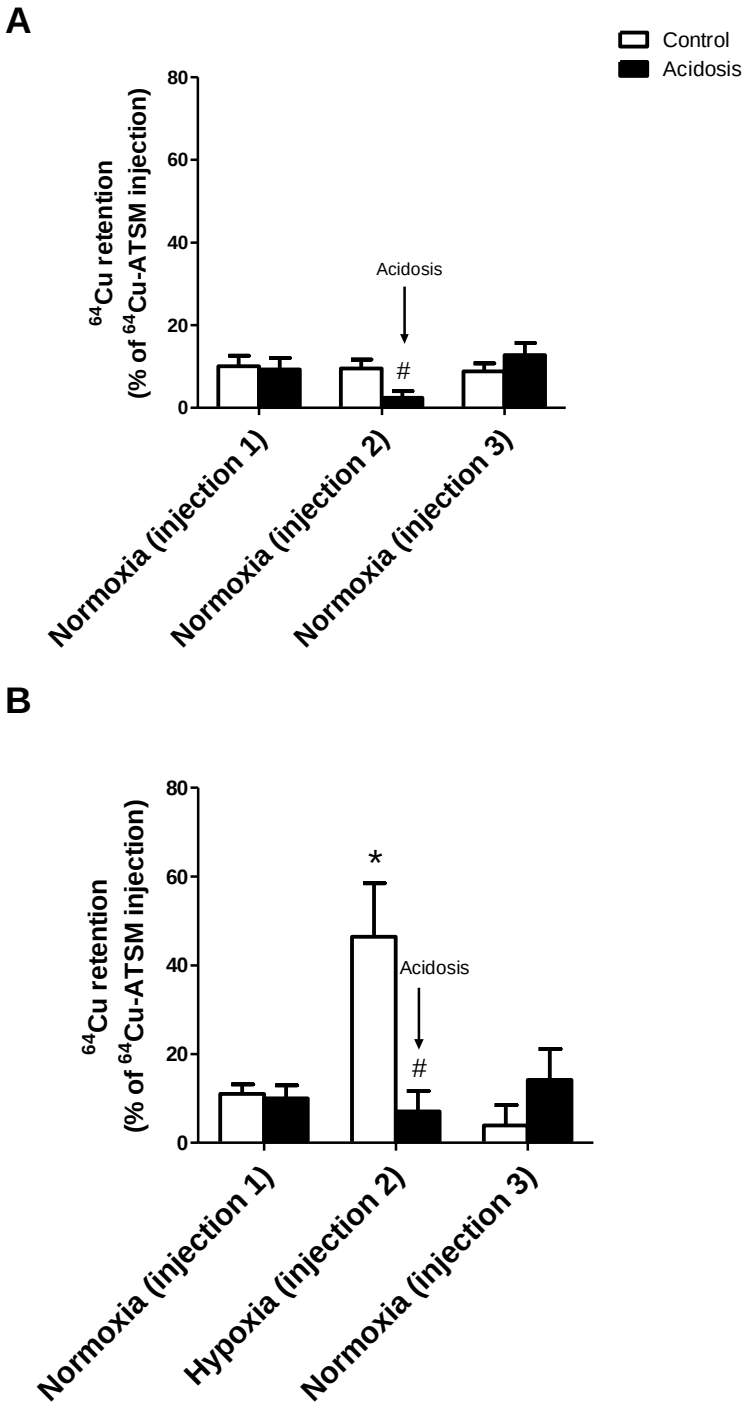

*Figure 5.31. Effect of acidosis on ^{64}Cu retention in normoxic and hypoxic isolated perfused rat hearts. Hearts were administered three bolus injections of ^{64}Cu-ATSM. Data are expressed as the % of total activity injected (means ± standard deviation, n=5 per group). *p<0.05 vs. control and #p<0.05 vs. normoxic equivalent.*

5.3.3.2 Pharmacokinetic analysis of time-activity curve data

To determine whether acidosis changed the pharmacokinetics of ^{64}Cu-ATSM washout time-activity curves of tracer washout were fitted with a bi-exponential function to obtain a fast clearance rate (FCR), a slow clearance rate (SCR), and their respective importance in governing overall washout (their amplitudes). Data is summarised in tables 5.1-5.2. The FCR, SCR or their amplitudes did not change during the normoxic perfusion protocol (figures 5.32-5.34). Acidosis had no effect on FCR, SCR or their amplitudes during normoxia. The FCR was always significantly higher than that of the SCR ($p<0.05$) during normoxia and this was unaffected by acidosis.

During hypoxia, the FCR increased significantly over control values however, SCR remained the same in the non-acidosis group. Reoxygenation caused a decrease in FCR and a significant increase in SCR ($p<0.05$) compared to that of normoxic control values. Hypoxia in combination with acidosis, did not affect FCR or SCR or respective amplitudes. Reoxygenation and zoniporide washout also did not affect FCR, SCR or their respective amplitudes compared to reoxygenation alone.

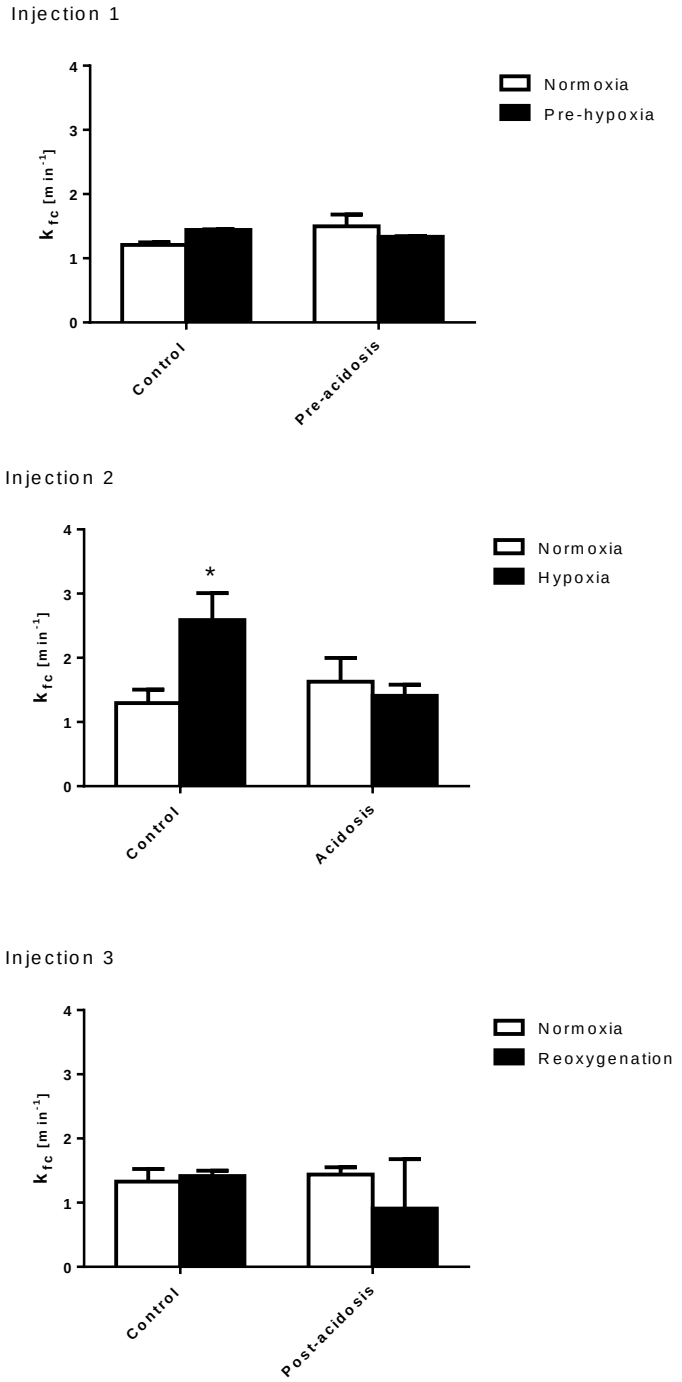

*Figure 5.32. FCR for each Cu –ATSM injection as determined by the bi-exponential analysis of ^{64}Cu clearance from heart tissue based on time-activity curve data. Data are expressed as means ± standard deviation, n=5 per group, *p<0.05 vs. normoxic equivalent.*

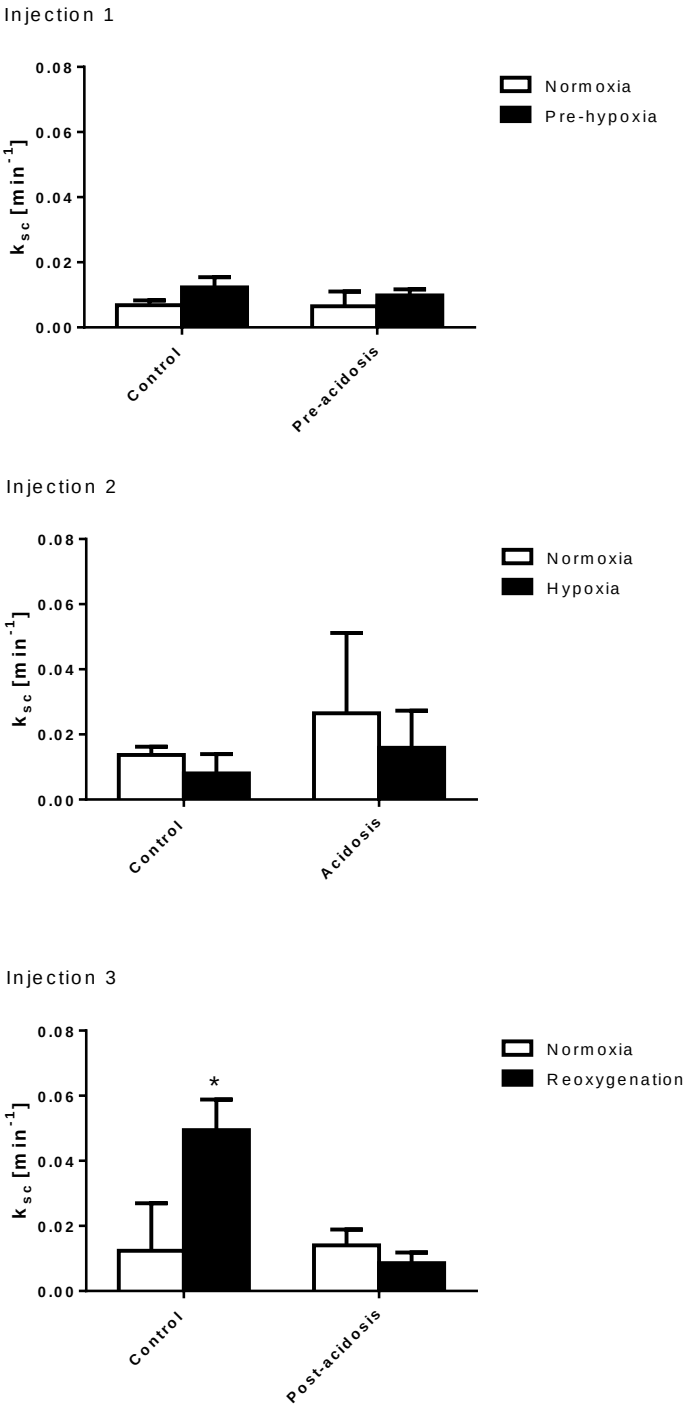

*Figure 5.33. SCR for each Cu –ATSM injection as determined by the bi-exponential analysis of ^{64}Cu clearance from heart tissue based on time-activity curve data. Data are expressed as means ± standard deviation, n=5 per group, *p<0.05 vs. normoxic equivalent.*

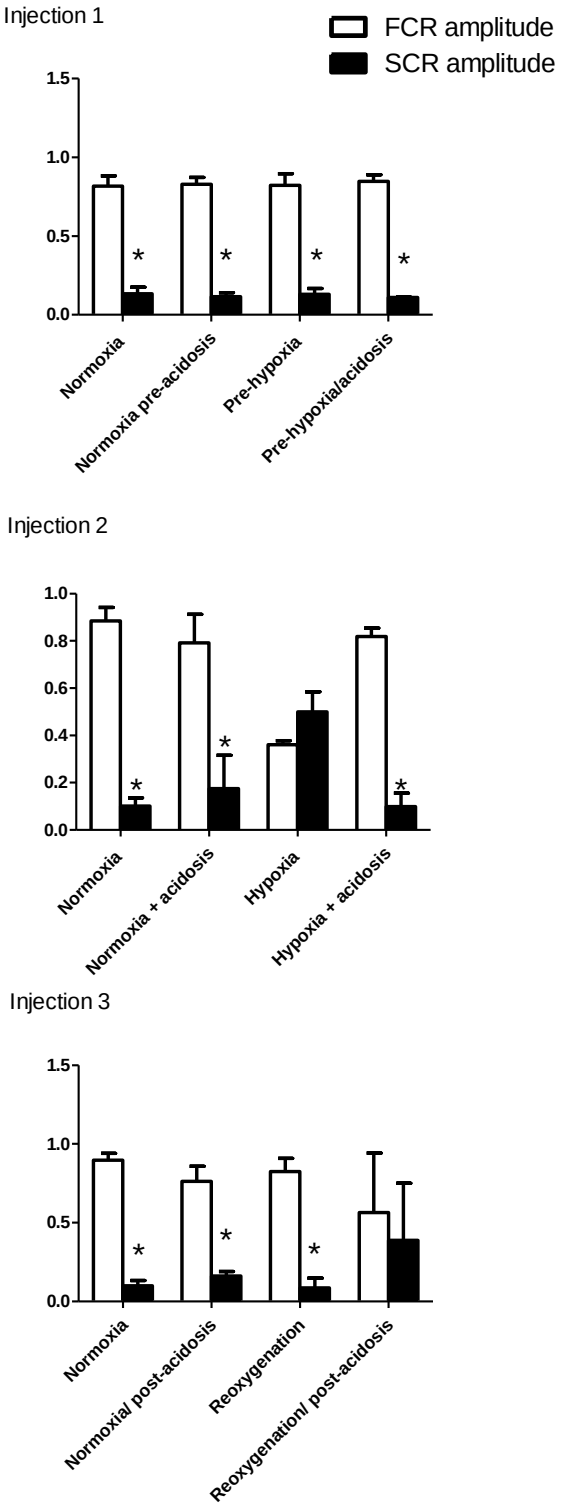

*Figure 5.34 Amplitudes of the FCR and SCR for all injections of ^{64}Cu-ATSM. Data are expressed as means ± standard deviation, n=5 per group, *p<0.05 vs. normoxic equivalent.*

Table 5.1. FCR and SCR values from figures 5.33 and 5.34. Data are expressed as rates of ^{64}Cu clearance from the heart (k_{fc}[min-^{1}] or k_{sc}[min^{-1}]; means ± standard deviation, n=5 per group).

		Non-acidotic	Acidotic	
	Injection	FCR (kfc [min-1])		
Normoxic hearts	1: Normoxia	1.21 ± 0.04	1.50 ± 0.18	(pre-acidosis)
	2: Normoxia	1.29 ± 0.21	1.63 ± 0.37	(acidosis)
	3: Normoxia	1.32 ± 0.20	1.43 ± 0.11	(post-acidosis)
Hypoxic hearts	1: Normoxia	1.44 ± 0.01	1.34 ± 0.01	(pre-acidosis)
	2: Hypoxia	* 2.59 ± 0.42	1.41 ± 0.17	(acidosis)
	3: Reoxygenation	1.42 ± 0.08	0.91 ± 0.77	(post-acidosis)
		SCR (kfc [min-1])		
Normoxic hearts	1: Normoxia	* 0.007 ± 0.001	0.006 ± 0.004	(pre-acidosis)
	2: Normoxia	* 0.013 ± 0.003	0.027 ± 0.024	(acidosis)
	3: Normoxia	* 0.012 ± 0.015	0.14 ± 0.005	(post-acidosis)
Hypoxic hearts	1: Normoxia	* 0.012 ± 0.003	0.010 ± 0.002	(pre-acidosis)
	2: Hypoxia	0.008 ± 0.005	0.016 ± 0.011	(acidosis)
	3: Reoxygenation	* 0.049 ± 0.009	* 0.009 ± 0.003	(post-acidosis)

**p < 0.05 vs. normoxic equivalent*

Table 5.2. Amplitudes of FCR and SCR from figure 5.34. Data are expressed as amplitudes corresponding to the ^{64}Cu FCR or SCR of each ^{64}Cu-ATSM injection (means ± standard deviation, n=5 per group).

		Non-acidotic	Acidotic	
	Injection	FCR amplitude (arbitrary units)		
Normoxic hearts	1: Normoxia	0.81 ± 0.07	0.82 ± 0.04	(pre-acidosis)
	2: Normoxia	0.88 ± 0.06	0.79 ± 0.12	(acidosis)
	3: Normoxia	0.89 ± 0.04	0.76 ± 0.10	(post-acidosis)
Hypoxic hearts	1: Normoxia	0.82 ± 0.07	0.84 ± 0.04	(pre-acidosis)
	2: Hypoxia	0.36 ± 0.02	0.81 ± 0.04	(acidosis)
	3: Reoxygenation	0.82 ± 0.08	0.79 ± 0.18	(post-acidosis)
		SCR amplitude (arbitrary units)		
Normoxic hearts	1: Normoxia	* 0.13 ± 0.04	* 0.12 ± 0.02	(pre-acidosis)
	2: Normoxia	* 0.10 ± 0.03	* 0.17 ± 0.14	(acidosis)
	3: Normoxia	* 0.10 ± 0.03	* 0.16 ± 0.03	(post-acidosis)
Hypoxic hearts	1: Normoxia	* 0.13 ± 0.04	* 0.11 ± 0.003	(pre-acidosis)
	2: Hypoxia	0.49 ± 0.09	* 0.98 ± 0.06	(acidosis)
	3: Reoxygenation	* 0.09 ± 0.06	* 0.29 ± 0.10	(post-acidosis)

**p < 0.05 vs. FCR amplitude*

5.3.4 Effect of perfusion with zoniporide in the absence of NH_4Cl

As it was observed that found that hearts subjected to a combination of hypoxia and acidosis completely abolished the hypoxic dependent retention of ^{64}Cu from ^{64}Cu-ATSM (figure 5.31), next the effect of zoniporide infusion in the absence of NH_4Cl was investigated to determine if this effect was caused by acidosis or interaction between zoniporide and ^{64}Cu-ATSM.

5.3.4.1 Cardiac contractile function

Infusion of zoniporide did not affect heart rate in normoxic hearts, which remained stable between 302 ± 4.7 and 313 ± 12.3 b.p.m. (figure 5.35). Similar to hypoxic control hearts, hypoxia + zoniporide caused a decrease in heart rate, although its onset was more rapid and more severe (decreasing from 303 ± 17.9 to 209 ± 69.9 b.p.m. within 7 mins).

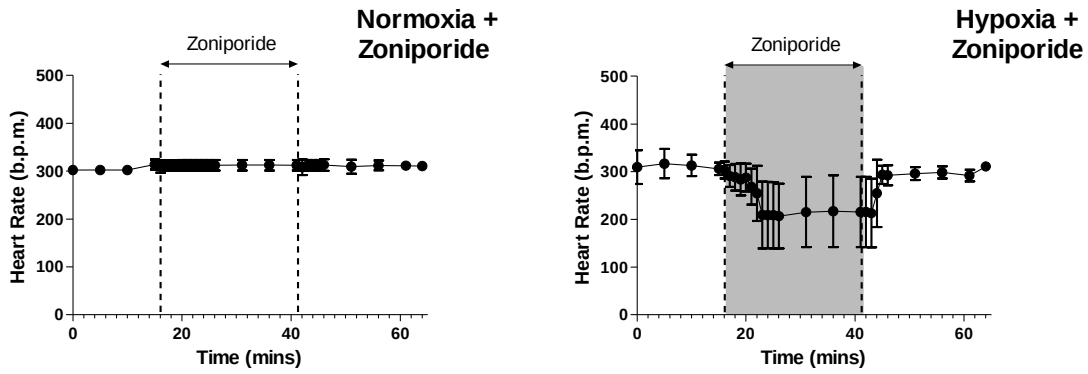

Figure 5.35. Heart rates (b.p.m) of normoxic and hypoxic hearts infused with zoniporide only. Grey shaded areas represent perfusion with hypoxic buffer. Data are expressed as means ± standard deviation (n = 5).

Infusion with zoniporide caused an increase in coronary perfusion pressure in normoxic hearts from 71.3 ± 21.3 to 101.2 ± 24.1 mmHg after 25 mins. As soon as zoniporide was washed out this decreased immediately, reaching 76.5 ± 9.1 mmHg by the end of the experimental protocol (figure 5.36). Similar to hypoxic hearts, hypoxia and zoniporide combined caused an increase in perfusion pressure from 88.7 ± 39.2 to 102.4 ± 48.8 mmHg , which did not recover upon reoxygenation.

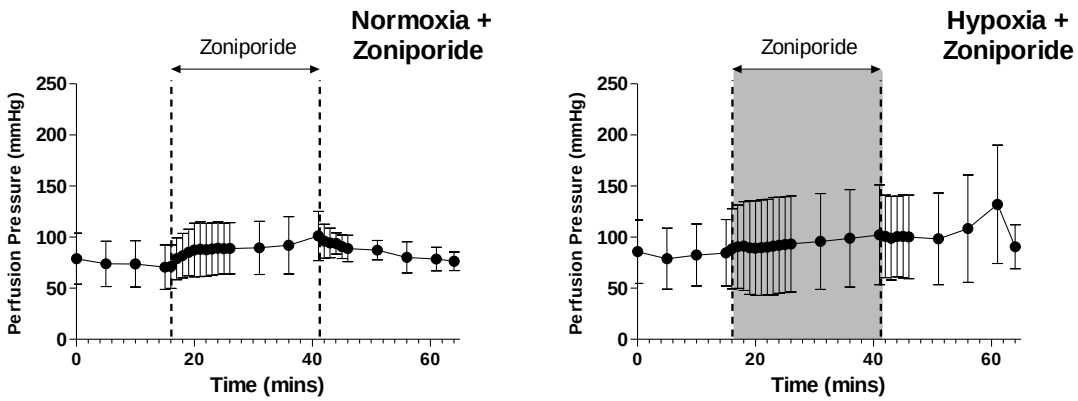

Figure 5.36. Coronary perfusion pressures (mmHg) of normoxic and hypoxic hearts infused with zoniporide only. Grey shaded areas represent perfusion with hypoxic buffer. Data are expressed as means ± standard deviation (n = 5).

Zoniporide infusion had little effect on LVDP in normoxic hearts (98.8 ± 6.6 to 109.8 ± 10.7 mmHg (figure 5.37). A combination of zoniporide and hypoxia induced a decrease in LVDP from 93.9 ± 31.0 to 65.9 ± 39.5 mmHg after 25 mins which was similar to hypoxia alone. Reoxygenation and zoniporide washout caused this to recover to 113.7 ± 5.4 mmHg by the end of the experimental protocol.

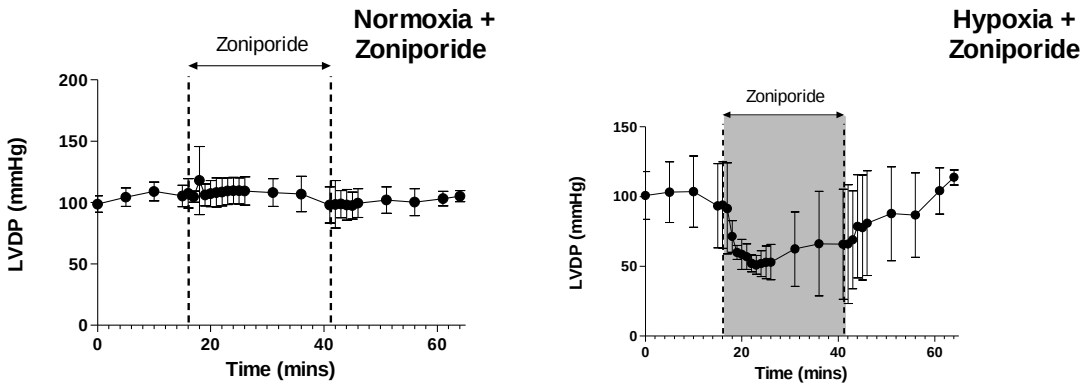

Figure 5.37. LVDP (mmHg) of normoxic and hypoxic hearts infused with zoniporide only. Grey shaded areas represent perfusion with hypoxic buffer. Data are expressed as means ± standard deviation (n = 5).

Zoniporide did not affect LVEDP in normoxic hearts which (4.9 ± 3.3 and 7.1 ± 4.0 mmHg; figure 5.38). Hypoxia combined with zoniporide infusion caused a gradual increase in LVEDP from 8.41 ± 1.7 to 23.4 ± 21.7 mmHg after 25 mins which is similar to the effects of hypoxia alone.

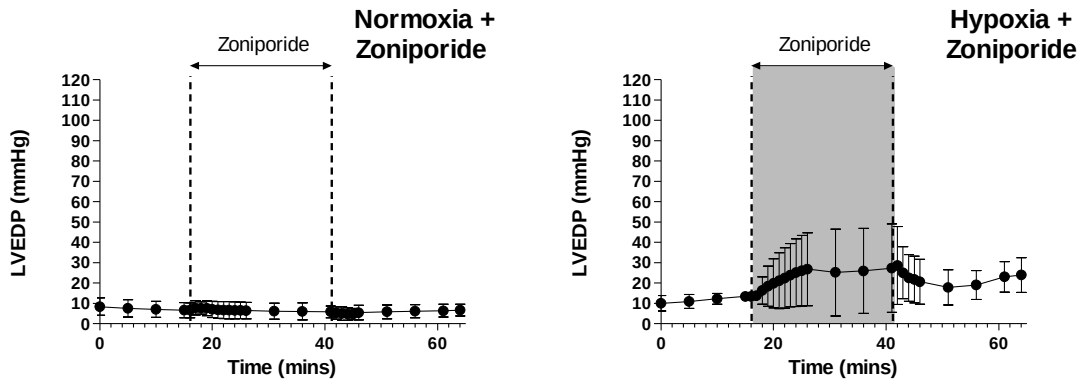

Figure 5.38. LVEDP (mmHg) of normoxic and hypoxic hearts infused with zoniporide only. Grey shaded areas represent perfusion with hypoxic buffer. Data are expressed as means ± standard deviation (n = 5).

5.3.4.2 ^{64}Cu retention from ^{64}Cu-ATSM during zoniporide infusion alone

Figure 5.39 displays the ^{64}Cu retention from ^{64}Cu-ATSM injections in hearts infused with zoniporide alone. In normoxic hearts, zoniporide had no effect upon ^{64}Cu retention (9.5 ± 2.1 % normoxia control *vs.* 14.42 ± 2.05 normoxia plus zoniporide). Furthermore, zoniporide alone had no effect on the hypoxia dependent retention of ^{64}Cu from ^{64}Cu-ATSM, which was significantly higher than normoxic control values (46.5 ± 12.0 % hypoxia *vs.* 50.7 ± 5.7 % hypoxia plus zoniporide; $p<0.05$).

5.3.4.3 Pharmacokinetic analysis of time-activity curve data

Pharmacokinetic data for normoxic and hypoxic hearts infused with zoniporide alone are summarised in tables 5.3 and 5.4. In normoxic hearts, zoniporide did not affect ^{64}Cu FCR, SCR or their respective amplitudes across all three ^{64}Cu-ATSM injections and were similar to that of normoxic control hearts (figures 5.40-5.42). Zoniporide also did not affect ^{64}Cu FCR or SCR in hypoxic hearts, as ^{64}Cu FCR significantly increased and SCR significantly decreased ($p<0.05$) compared to that of normoxic controls; similar to that of hearts perfused with hypoxic buffer alone. FCR and SCR amplitudes were also similar to that of hypoxic hearts in the absence of zoniporide across all three ^{64}Cu-ATSM injections.

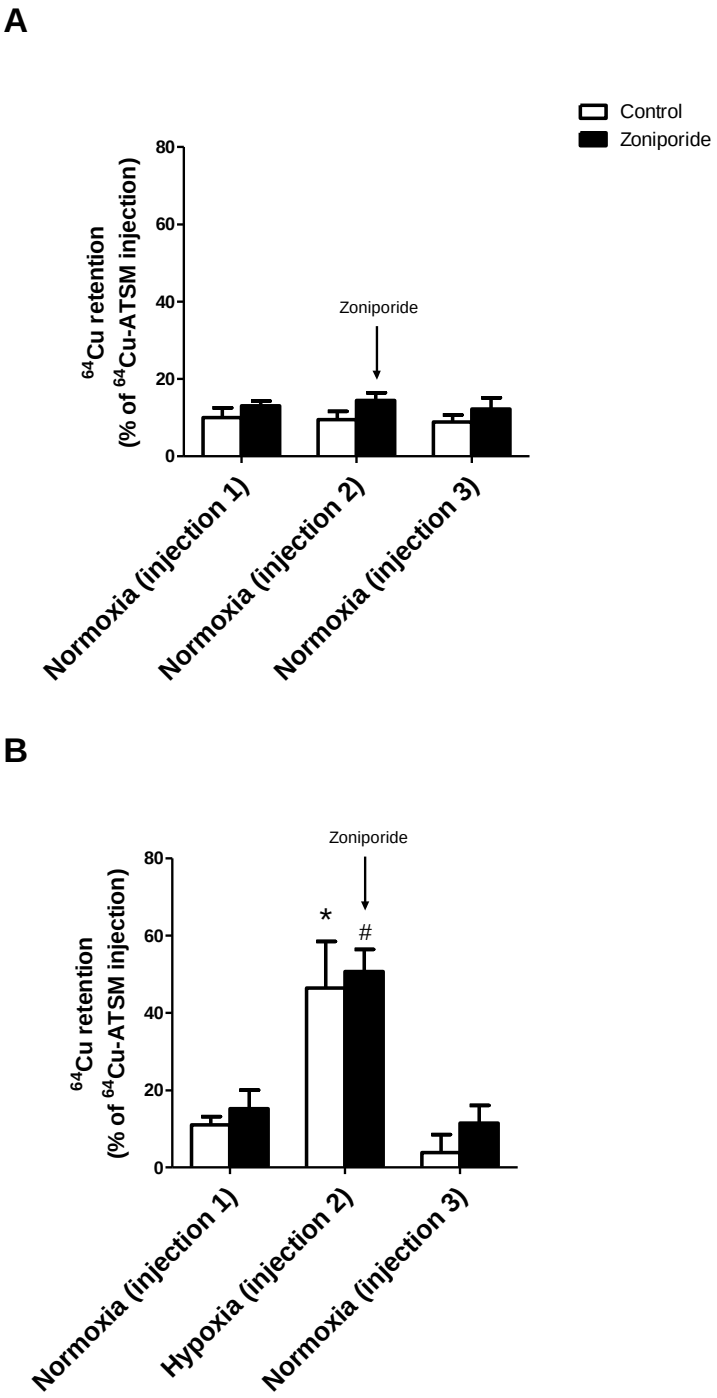

*Figure 5.39 Effect of zoniporide alone on ^{64}Cu retention in normoxic and hypoxic isolated perfused rat hearts. Hearts were administered three bolus injections of ^{64}Cu-ATSM. Data are expressed as the % of total activity injected (means ± standard deviation, n=5 per group). *p<0.05 vs. control and #p<0.05 vs. normoxic equivalent (A).*

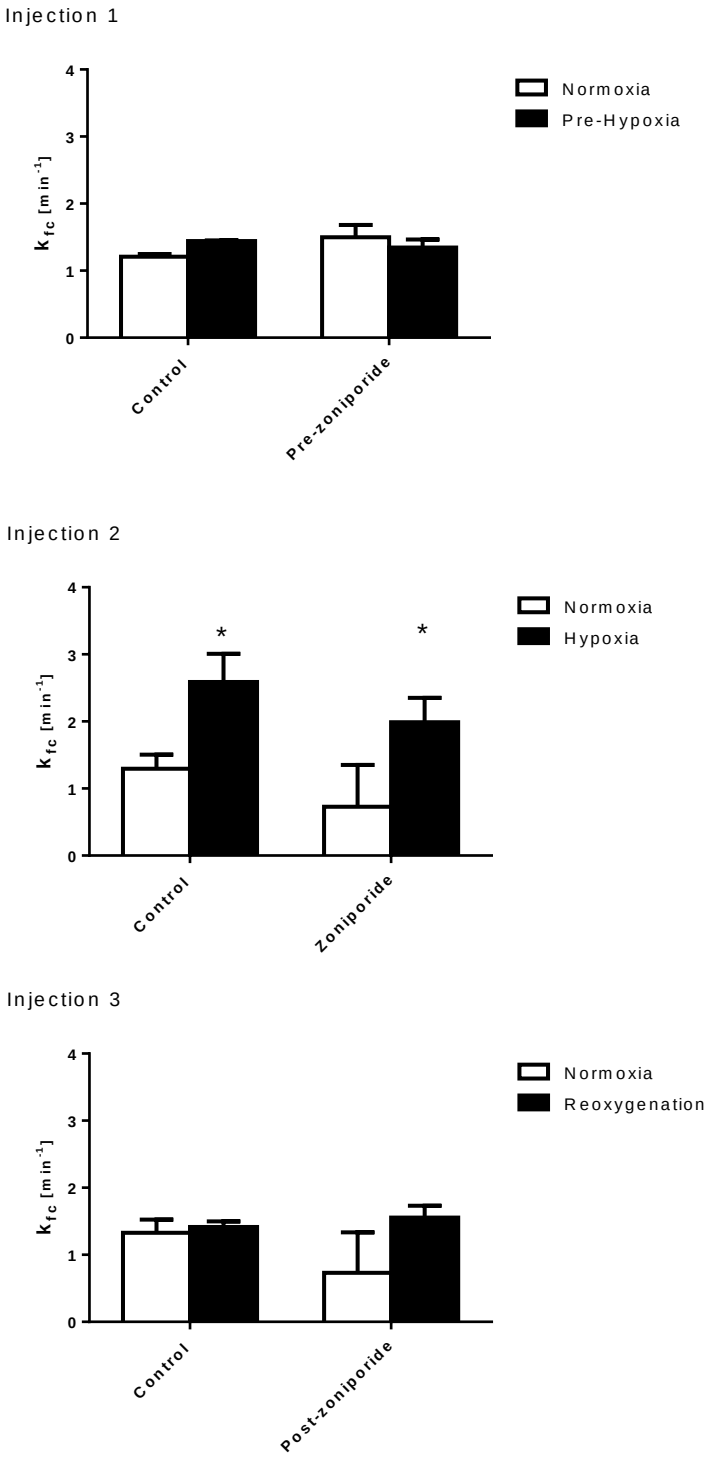

*Figure 5.40 FCR for each Cu–ATSM injection as determined by the bi-exponential analysis of ^{64}Cu clearance from heart tissue based on time-activity curve data. Data are expressed as means ± standard deviation, n=5 per group, *p<0.05 vs. normoxic equivalent.*

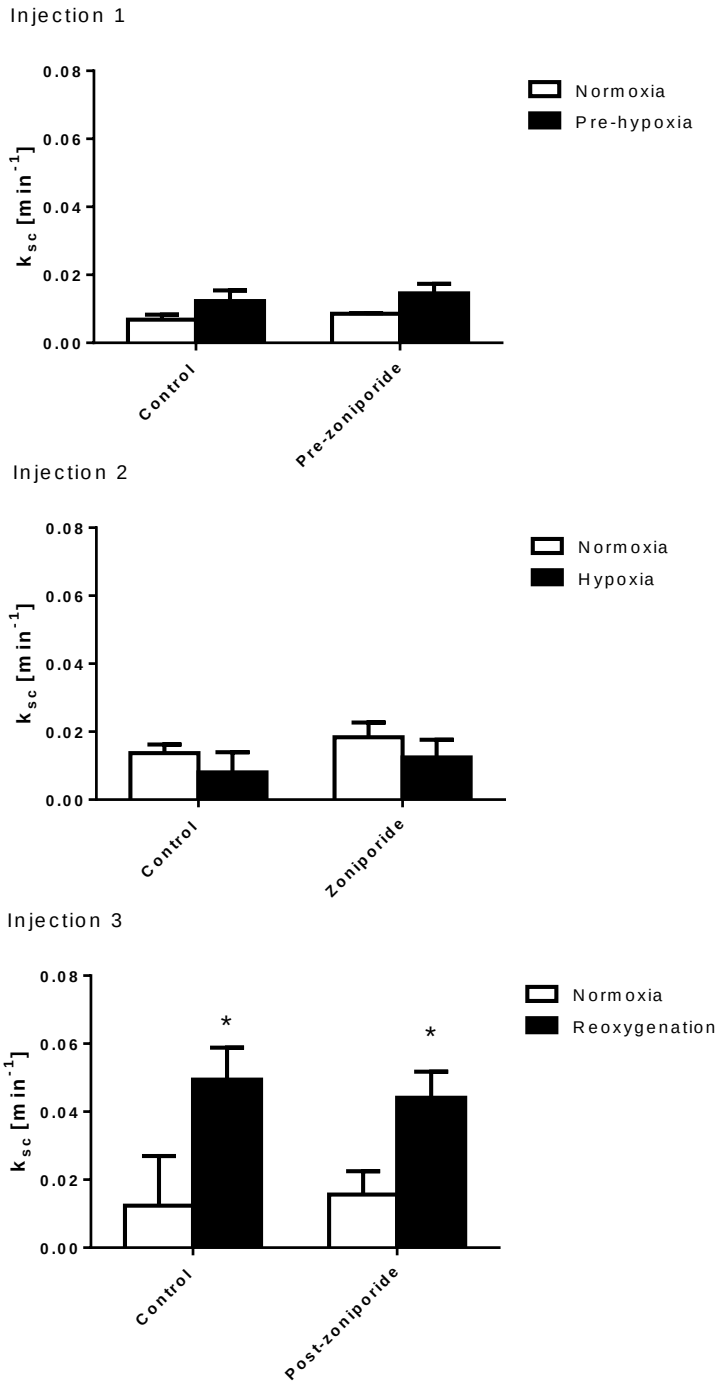

*Figure 5.41. FCR for each Cu–ATSM injection as determined by the bi-exponential analysis of ^{64}Cu clearance from heart tissue based on time-activity curve data. Data are expressed as means ± standard deviation, n=5 per group, *p<0.05 vs. normoxic equivalent.*

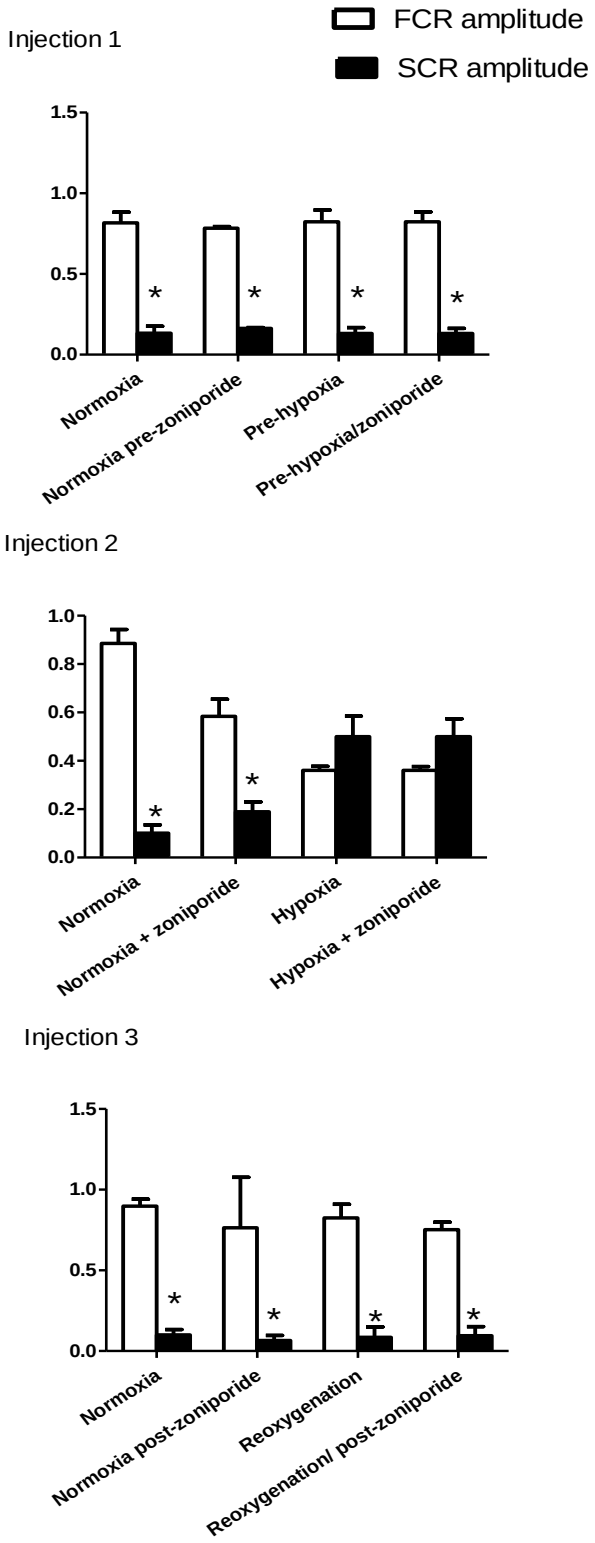

*Figure 5.42. Amplitudes of the FCR and SCR for injections of ^{64}Cu-ATSM in hearts infused with zoniporide. Data are expressed as means ± standard deviation, n=5 per group, *p<0.05 vs. normoxic equivalent.*

Table 5.3. FCR and SCR values from figures 5.40-5.41. Data are expressed as rates of ^{64}Cu clearance from the heart (k_{fc}[min^{-1}] or k_{sc}[min^{-1}]; means ± standard deviation, n=5 per group).

		Control	Zoniporide	
	Injection	FCR (kfc [min-1])		
Normoxic	1: Normoxia	1.21 ± 0.04	1.50 ± 0.18	(pre-zoniporide)
hearts	2: Normoxia	1.29 ± 0.21	0.73 ± 0.62	(zoniporide)
	3: Normoxia	1.32 ± 0.20	0.73 ± 0.60	(post-zoniporide)
Hypoxic	1: Normoxia	1.44 ± 0.01	1.35 ± 0.12	(pre-zoniporide)
hearts	2: Hypoxia	* 2.59 ± 0.42	* 1.99 ± 0.36	(zoniporide)
	3: Reoxygenation	1.42 ± 0.08	1.55 ± 0.18	(post-zoniporide)
		SCR (kfc [min-1])		
Normoxic	1: Normoxia	0.007 ± 0.001	0.009 ± 0.001	(pre-zoniporide)
hearts	2: Normoxia	0.014 ± 0.003	0.018 ± 0.004	(zoniporide)
	3: Normoxia	0.012 ± 0.015	0.016 ± 0.007	(post-zoniporide)
Hypoxic	1: Normoxia	0.012 ± 0.003	0.014 ± 0.003	(pre-zoniporide)
hearts	2: Hypoxia	0.008 ± 0.005	0.012 ± 0.005	(zoniporide)
	3: Reoxygenation	* 0.049 ± 0.009	* 0.044 ± 0.008	(post-zoniporide)

**p < 0.05 vs. normoxic equivalent*

Table 5.4. Amplitudes of FCR and SCR from figure 5.42. Data are expressed as amplitudes corresponding to the ^{64}Cu FCR or SCR of each ^{64}Cu-ATSM injection (means ± standard deviation, n=5 per group).

		Control	Zoniporide	
	Injection	FCR amplitude (arbitrary units)		
Normoxic hearts	1: Normoxia	0.81 ± 0.07	0.78 ± 0.008	(pre-zoniporide)
	2: Normoxia	0.88 ± 0.06	0.58 ± 0.07	(zoniporide)
	3: Normoxia	0.89 ± 0.04	0.76 ± 0.31	(post-zoniporide)
Hypoxic hearts	1: Normoxia	0.82 ± 0.07	0.79 ± 0.06	(pre-zoniporide)
	2: Hypoxia	0.36 ± 0.02	0.34 ± 0.01	(zoniporide)
	3: Reoxygenation	0.82 ± 0.08	0.75 ± 0.05	(post-zoniporide)
		SCR amplitude (arbitrary units)		
Normoxic hearts	1: Normoxia	* 0.13 ± 0.04	* 0.12 ± 0.03	(pre-zoniporide)
	2: Normoxia	* 0.10 ± 0.03	* 0.19 ± 0.04	(zoniporide)
	3: Normoxia	* 0.10 ± 0.03	* 0.06 ± 0.03	(post-zoniporide)
Hypoxic hearts	1: Normoxia	* 0.13 ± 0.04	* 0.13 ± 0.03	(pre-zoniporide)
	2: Hypoxia	0.49 ± 0.09	* 0.50 ± 0.07	(zoniporide)
	3: Reoxygenation	* 0.09 ± 0.06	* 0.10 ± 0.06	(post-zoniporide)

**p < 0.05 vs. FCR amplitude*

5.4 Discussion and conclusions

5.4.1 Effect of hypoxia on myocardial pH_i and ^{64}Cu retention from ^{64}Cu-ATSM

In chapter 3, the hypoxia-dependent retention of ^{64}Cu from ^{64}Cu-ATSM in isolated perfused rat hearts was demonstrated. Using ^{31}P NMR spectroscopy, it was estabilished that induction of this degree of hypoxia, in a system where there is normal coronary flow, causes no significant change in intracellular pH. A transient but insignificant decrease in pH_i from 7.12 to pH 7.03 was observed, which recovered to 7.1 by the end of the experiment. This is consistent with a previous study which demonstrated that perfusion with normoxic buffer only decreased rat heart pH_i to pH 7.01[197]. Inducing hypoxia with a less severe model by perfusion with buffers equilibrated with 20% O_2 did not affect cardiac pH_i at all. Cave et al. used ^{31}P NMR spectroscopy to demonstrate that ischaemia caused pH_i to decrease from 7.05 to 6.2-6.3 which was sustained while coronary flow was limited[200]. In contrast, the current study demonstrates that the myocardium is hypoxic, but as coronary flow is maintained, the heart is still efficient at extruding H^+ via NHE exchange and extruding lactate via MCT to prevent acidosis. In both this chapter and chapter 3, an increase in ^{64}Cu retention from ^{64}Cu-ATSM was observed during early hypoxia and a further increase during late hypoxia. As shown here, under these conditions the hearts were not acidotic, and it can be confirmed that acidosis is not a key determinant in the hypoxia selectivity of Cu-ATSM.

5.4.2 Effect of acidosis on ^{64}Cu retention from ^{64}Cu-ATSM

The reverse situation was also investigated in these studies; whether acidosis itself increased ^{64}Cu-ATSM dissociation and ^{64}Cu trapping under either normoxic or hypoxic conditions. To induce acidosis hearts were infused with NH_4Cl, during which pH_i remained stable, but fell to 6.3-6.4 ($p<0.05$) when NH_4Cl was washed from the heart in the presence of NHE inhibitor, zoniporide. The extent of this acidosis was not exacerbated by additional hypoxia. Similar, but less severe intracellular acidosis of pH 6.7 has previously been demonstrated with a similar protocol in isolated perfused ferret hearts using the NHE inhibitor 5-(N-ethyl-N-isopropyl)amiloride (EIPA) [201].

It has previously been suggested that protonation of the Cu-ATSM complex would decrease its stability and increase copper dissociation[119]. An acidic environment should therefore increase ^{64}Cu-ATSM dissociation and the retention of ^{64}Cu. The observations of a decrease in ^{64}Cu retention from ^{64}Cu-ATSM in acidotic hearts during normoxia, and that acidosis appeared to abolish hypoxia dependent ^{64}Cu retention, were therefore very surprising. To ensure the decrease in ^{64}Cu retention from ^{64}Cu-ATSM was not due to interaction with zoniporide, these experiments were repeated in the absence of NH_4Cl. Zoniporide alone had no effect on ^{64}Cu retention during normoxia or hypoxia, confirming there was no interaction between zoniporide and ^{64}Cu-ATSM which may have affected myocardial uptake or dissociation. The decrease in ^{64}Cu retention observed was therefore due to acidosis itself.

Using spectrophotometry, Petering demonstrated that the stability of Cu-KTS decreased with decreasing pH[126]. He later demonstrated that decreasing the pH also decreased the reaction rate between various Cu-BTSC complexes and

GSH[134]. This implied that the initial reduction of Cu-BTSC complexes by thiols is hindered by decreasing pH; and that intracellular acidosis may decrease Cu-ATSM dissociation.

5.4.3 Effect of hypoxia and acidosis on contractile function

Contractile function of normoxic control hearts remained stable throughout the perfusion protocol. Switching to hypoxic 0% O_2 KHB caused a decrease in heart rate and LVDP and an increase in perfusion pressure and LVEDP within 5 mins. This is consistent with previous reports[174,175]. During hypoxia, the heart generates ATP via anaerobic glycolysis which is not as efficient at generating ATP as aerobic metabolism; therefore less ATP is available to sustain cardiac contractility which results in a fall in heart rate and LVDP. Increased intracellular Ca^{2+} during hypoxia prevents complete ventricular relaxation and consequently increases LVEDP and perfusion pressure[176].

Acidosis also adversely affected contractile function; decreases in LVDP and increases in LVEDP and coronary perfusion pressure were observed in these hearts. Heart rate declined as a result of acidosis and was not measureable for part of the protocol due to ventricular fibrillation. A similar study investigating the effects of NH_4Cl infusion and NHE-1 inhibitor cariporide reported similar changes to contractile function in isolated perfused rat hearts[202]. In particular, LVDP depression coincided with the onset of acidosis. While NHE inhibition is associated with a loss of Ca^{2+} uptake via NCX, acidosis-mediated loss of contractile function is not due to the decrease in Ca^{2+} concentration, but a decrease in contractile protein responsiveness to Ca^{2+} [40]. High concentrations of H^+ are known to compete with Ca^{2+} for the binding site of troponin C[27,41].

It was also observed that contractile function failed to recover after zoniporide (and therefore acid) was washed from the heart in the 0% O_2 group. It was therefore apparent that hearts treated with this extreme degree of hypoxia were not viable with the combined insult of acidosis and that this protocol was not suitable for the ^{64}Cu-ATSM experiments, where the aim was to generate hypoxically compromised but viable myocardium. A revised less extreme hypoxic injury was therefore devised in which hearts were perfused with KHB gassed with 20% O_2. This degree of hypoxia caused less of a deficit in contractile function which recovered upon reoxygenation and acid washout, which was a more suitable model upon which to examine the effect of acidosis on ^{64}Cu-ATSM pharmacokinetics.

5.4.4 Effect of hypoxia and acidosis on lactate release, glucose consumption and viability

Consistent with the results in chapter 3, lactate was only released into the perfusate in hearts perfused with hypoxic (0% or 20% O_2) buffer in the absence of acidosis. There was no lactate release from hypoxic hearts during acidosis, implying that these hearts were not hypoxic. As it was also observed that acidosis decreases myocardial contractility the energy demand of these hearts would have been lower; therefore decreasing oxygen consumption and becoming less hypoxic.

The amount of glucose extracted by the heart during hypoxia is negligible compared to the high concentration in KHB (11mM), therefore changes in first pass glucose extraction were unfortunately not measurable by this insensitive approach.

There was no myocardial protein released from normoxic, hypoxic (0% or 20%) or normoxic acidotic hearts, confirming that these protocols did not compromise myocardial viability, as opposed to hearts exposed to the acidosis protocol and 0% O_2 buffer perfusion, which did. This supports the contractile data which demonstrated that hypoxia with 0% O_2 plus acidosis caused an irreversible loss of contractility.

5.4.5 Effect of hypoxia on myocardial metabolism

Decreases in both PCr and ATP concentrations and increases in P_i concentrations during hypoxia and acidosis protocols were observed. During hypoxia and ischaemia, ATP hydrolysis is not matched by ATP production, leading to increases in net ATP consumption and increases in intracellular P_i and H^+ release[27]. PCr is consumed in the regeneration of ATP until it is also depleted. The regeneration of ATP by PCr also utilises H^+ such that PCr and creatine kinase (CK) play a role in maintaining ATP concentration[95].

Hypoxia also induced an increase in sugar phosphate concentration in hypoxia protocols. As described in chapter 1, glycolysis converts glucose to ATP through a number of enzymatic processes, some of which produce sugar phosphate compounds such as glucose-6-phosphate. As glucose is delivered to the cell it is phosphorylated to glucose-6-phosphate, fructose-6-phosphate and fructose-1,6-diphosphate. As the oxygen reserve is used up, substrates such as NADH accumulate as they can no longer be utilised by the ETC and inhibit further glycolysis[95]. In addition, fructose-1,6-diphosphate accumulates and inhibits phosphofructokinase; the main rate limiting enzyme in glycolysis, resulting in an accumulation of glucose-6-phosphate and fructose-6-phosphate

as glucose is still delivered and entering the glycolytic pathway[27]. The frequency of the sugar phosphate peak is in close range of the P_i peak and was obscured by the larger increase of P_i observed during the hypoxia and acidosis protocols, hence the sugar phosphate peak was only measureable in hypoxic hearts in the absence of acidosis where the concentration of P_i was lower.

While it may be possible that acidosis decreases tracer retention by inhibiting thiol induced Cu-BTSC reduction, it is more likely that tracer retention decreased in these acidotic hearts because they were no longer hypoxic. It was demonstrated that acidosis had a profound inhibitory effect on cardiac contractility. As myocardial contractility decreases, less energy is required and oxygen consumption decreases, such that the residual aerobic glycolysis that the heart is capable of can support myocardial metabolism. A lack of lactate released from the hearts during hypoxia as a result of acidosis was also observed, which supports this hypothesis. It is likely that acidosis has an O_2 sparing effect in both the normoxic and hypoxic heart which decreases ^{64}Cu retention from ^{64}Cu-ATSM. A decrease in background ^{64}Cu retention in normoxic hearts during acidosis was also observed. KHB is well known to have a lower oxygen-carrying capacity than blood, even under normoxic conditions where the buffer is gassed with 95% O_2/ 5% CO_2, isolated hearts perfused with KHB are almost maximally vasodilated, and is possible that they may be slightly hypoxic, particularly in the endocardium, where energy (and oxygen) demands are highest[140]. This would explain the small background uptake of ^{64}Cu-ATSM, which reduces with acidosis (and therefore decreased hypoxia severity). Although the data collected thus far can therefore not absolutely confirm the

effect of acidosis on ^{64}Cu retention from ^{64}Cu-ATSM, it does support the specificity of ^{64}Cu-ATSM as a hypoxia selective agent.

Chapter 6

Summary and further work

6.1 Summary of main conclusions

The proposed mechanism governing Cu-ATSM hypoxia selectivity involves the reduction of Cu(II)-ATSM to a less stable Cu(I)-ATSM^{-} species, which dissociates in the absence of oxygen to release its copper core. It is therefore possible that Cu-ATSM hypoxia selectivity would be altered in environments which encourage reduction and/ or dissociation. The aim of this thesis was to identify the importance of two key parameters known to change during ischaemia on the hypoxia selectivity of Cu-ATSM; thiol concentration and acidosis.

Petering originally suggested that Cu-BTSC complexes were reduced by intracellular thiols such as GSH, and that changes in GSH concentration would impact reduction, subsequent dissociation and the hypoxia selectivity of these complexes[134]. Ischaemia can cause decreases in myocardial GSH; since GSH concentration may affect the rate of Cu-ATSM reduction, this would complicate the interpretation of Cu-ATSM images of the ischaemic myocardium. Through depletion and augmentation of GSH in isolated perfused rat hearts, it was demonstrated that large changes in thiol concentration do not affect background ^{64}Cu retention from ^{64}Cu-ATSM injections, nor do they impact upon the degree of hypoxia selective ^{64}Cu retention in the heart, demonstrating that thiol concentration is not a rate limiting step for Cu-ATSM reduction. It cannot confirmed, however, that thiols such as GSH are not essential for Cu-ATSM reduction. Even in the thiol depleted hearts, where concentrations (3-4 nmol/mg protein) were far lower than that observed in ischaemic myocardial tissue (6-7 nmol/mg protein)[157,203], thiol concentrations were still in the mM range, whilst ^{64}Cu-ATSM was present in fM concentrations. The amount of intracellular thiol

present will always be in vast excess of the radiotracer concentration, and it appears that changes in thiol concentration within the physiological or even pathophysiological range do not impact upon the activity of Cu-ATSM as a hypoxia selective PET tracer in the heart.

Interestingly, supraphysiological thiol augmentation with NAC decreased hypoxia dependent retention of ^{64}Cu from ^{64}Cu-ATSM during late hypoxia in the current isolated perfused heart model. As a precursor for GSH synthesis, NAC is known to increase intracellular ROS scavenging capacity[149]. It is therefore possible that in these hearts, prolonged perfusion with NAC scavenged some portion of intracellularly generated ROS, resulting in a loss of maximal tracer trapping capacity. Hypoxia is often associated with ROS generation as a result of the accumulation and leakage of electrons from the mitochondrial electron transport chain. ROS have also been suggested to play a role in the reduction of Cu-ATSM[132,133,204], although it has not yet been explored empirically. Further studies need to be carried out in order to clarify if Cu-ATSM and other Cu-BTSC complexes are sensitive to increased ROS generation before they can be used to image increased ROS generation and oxidative stress.

It was also demonstrated the retention of ^{64}Cu from ^{64}Cu-ATSM in hypoxic BAEC. This is the first time that the hypoxia selectivity of Cu-ATSM has been investigated in vascular endothelial cells and supports its use as a hypoxia avid probe. Thiol depletion did not affect hypoxia dependent retention in BAEC which supports the data obtained from thiol depleted hearts; however, NAC supplementation further increased ^{64}Cu retention in hypoxic cells. This conflicts with the isolated perfused heart model, where NAC supplementation decreased ^{64}Cu retention from ^{64}Cu-ATSM during hypoxia. In other BAEC model, however,

^{64}Cu-ATSM was incubated with the cells for 1 hr. This does not represent the 1st pass extraction of tracer which occurs in isolated perfused hearts. As BAEC had a longer radiotracer incubation time, reaction between excess intracellular thiol and ^{64}Cu-ATSM was potentially more likely, which may explain the increased ^{64}Cu-ATSM reduction and ^{64}Cu retention observed. The thiol concentration of hypoxic BAEC supplemented with NAC for three hours were also 3 fold higher than that of hypoxic, thiol augmented hearts. Hypoxic BAEC supplemented with NAC for 2 hours only contained a thiol concentration of 22-27 nmol/ mg protein, which although was more than BAEC subject to hypoxia alone, was less than half that of NAC supplemented hypoxic hearts. Both these groups of BAEC still retained significantly more ^{64}Cu from ^{64}Cu-ATSM than hypoxic BAEC alone, confirming that thiols promote Cu retention from Cu-ATSM and therefore their presence may be essential in Cu-ATSM reduction.

It has previously been suggested that the dissociation of the Cu(I)-ATSM^{-} species is dependent on protonation, and may therefore be accelerated by acidosis[119,120]. Again, since the ischaemic heart is known to be acidotic, it was possible that this would impact upon the hypoxia selectivity of Cu-ATSM[5,118]. Although the retention of ^{64}Cu from ^{64}Cu-ATSM in hypoxic isolated perfused hearts was demonstrated, it was also shown by ^{31}P NMR spectroscopy that these hearts were not acidotic. Since these hearts were perfused at a constant flow rate, any protons generated during hypoxia were washed out, and a physiological pH was maintained. This confirms that the hypoxia selectivity of ^{64}Cu-ATSM is not dependant on acidosis. It was, however, surprising to see that pharmacologically induced acidosis decreased ^{64}Cu retention in both normoxic and hypoxic hearts. It is apparent that acidosis causes a decline in contractile

function, which had an oxygen sparing effect, which decreased the degree of hypoxia, such that ^{64}Cu from ^{64}Cu-ATSM was no longer retained. The lack of lactate released into the perfusate in these hearts when they were made hypoxic supports this suggestion. The protons in an acidotic myocyte compete with Ca^{2+} for the binding site of troponin c in contractile proteins, which results in decreased contractility, even in a normoxic heart[41]. In EMT6 tumour cells equilibrated with different pO_2, it has been demonstrated that ^{64}Cu retention from ^{64}Cu-ATSM falls rapidly between 0 and 0.1% O_2, therefore Cu-ATSM may only be useful in detecting extremely low levels of hypoxia[110]. In isolated perfused hearts, perfusion with 20% O_2 alone increased ^{64}Cu-retention from ^{64}Cu-ATSM, therefore these hearts were sufficiently hypoxic for radiotracer retention. When acidosis was induced and myocardial contractility and oxygen demand decreased, it is proposed that myocardial oxygen concentrations increased above the hypoxia-selective threshold of ^{64}Cu-ATSM.

6.2 Recommendations for future work

Following the results described in this thesis, further investigation is required to understand the mechanisms of Cu-ATSM hypoxia selectivity and its use as a cardiovascular hypoxia imaging agent. To achieve this it is recommend that the following are investigated:

- The effect of decreased contractility on Cu retention from Cu-ATSM
- The effect of zoniporide alone on pH_i
- The effect of acidosis on thiol mediated Cu-ATSM reduction
- The role of ROS in Cu-ATSM hypoxia selectivity
- The hypoxia selectivities of other Cu-BTSC complexes

To fully understand the effect of acidosis on ^{64}Cu-ATSM hypoxia selectivity the current results should be compared to those obtained from non-acidotic hearts with similar deficits in contractile function. An arrested heart model is therefore required. This can be achieved by perfusing the heart with a hyperkalaemic perfusion buffer, which reduces the transmembrane potential and maintains the heart in a non-contracting, depolarised state[205]. As such, cardiac contractility (and therefore oxygen consumption) could be normalised between all groups, to allow the investigation of the effect of tissue acidosis alone on Cu-ATSM pharmacokinetics and hypoxia selectivity. A suggestion would be to confirm and evaluate acidosis in each experimental model using ^{31}P NMR spectroscopy as has been done here. As zoniporide inhibits the NHE, it is possible that perfusion with zoniporide alone also decreases pH_i. In this model it was unlikely as hearts were perfused with a bicarbonate buffer during NHE inhibition, which buffered pH_i. Again, ^{31}P NMR spectroscopy should be used to confirm zoniporide does not affect pH_i.

Alternatively it is possible that the decrease in ^{64}Cu retention from ^{64}Cu-ATSM observed during acidosis may result from decreased reduction rates of Cu-ATSM by thiols. It has previously been reported that thiol mediated Cu-KTS reduction progressively slows with decreasing pH, although Cu-ATSM was not included in that study[134]. As thiols may be an essential reductant, acidosis may decrease Cu-ATSM reduction and subsequent dissociation of the complex and radiocopper release. Although thiol concentration did not affect ^{64}Cu retention in isolated perfused hearts, increases in ^{64}Cu retention as a result of thiol augmentation were not observed in isolated BAEC. A combination of thiol augmentation and acidosis in BAEC could therefore provide a model in which the effect of acidosis on thiol mediated ^{64}Cu-ATSM reduction could be investigated.

As the hypoxia selectivities of Cu-BTSC are governed by redox potential, it is possible that Cu-ATSM or its analogs could be utilised as markers of oxidative stress. Although some studies have used ^{62}Cu-ATSM as a marker of oxidative stress[133,204], to date no studies have been carried out to investigate the direct effect of ROS generation on Cu-ATSM reduction or Cu retention. It would therefore be interesting to determine the importance of ROS in Cu-ATSM reduction.

Finally, the hypoxia selectivities of other Cu-BTSC complexes must be determined. Cu-ATSM only detects extremely low levels of hypoxia which may not be relevant in a pathophysiological setting for cardiology[5]. The main purpose of developing a radiotracer to image the hypoxic myocardium is to diagnose ischaemia earlier on to allow for the earliest possible intervention. As the myocardium becomes acidotic soon after the onset of ischaemia and

possibly decreases myocardial oxygen demand, other Cu-BTSC complexes which detect less severe levels of hypoxia may be better suited in imaging the ischaemic myocardium[5]. A range of other ^{64}Cu-BTSC complexes with different redox potentials are currently being evaluated for their sensitivity at less extreme levels of cardiac hypoxia. This is being performed using a gas mixer to titrate buffer pO_2 to more pathophysiologically relevant levels before the ^{64}Cu-BTSC complexes are administered. It is hoped that this approach may identify other Cu-BTSC complexes in this family which may be better suited to delineating hypoxic myocardium in the setting of chronic ischaemic heart disease.

References

1. Finegold, J.A., Asaria, P. & Francis, D.P. Mortality from ischaemic heart disease by country, region, and age: Statistics from World Health Organisation and United Nations. *Int J Cardiol* **168**, 934-945 (2012).
2. Mathers, C.D., Lopez, A.D. & Murray, C.J.L. The Burden of Disease and Mortality by Condition: Data, Methods, and Results for 2001. in *Global Burden of Disease and Risk Factors* (eds. Lopez, A.D., Mathers, C.D., Ezzati, M., Jamison, D.T. & Murray, C.J.L.) (Washington (DC), 2006).
3. Hearse, D.J. Myocardial ischaemia: can we agree on a definition for the 21st century? *Cardiovasc Res* **28**, 1737-1744 (1994).
4. Buja, L.M. Myocardial ischemia and reperfusion injury. *Cardiovasc Pathol* **14**, 170-175 (2005).
5. Handley, M.G., Medina, R.A., Nagel, E., Blower, P.J. & Southworth, R. PET imaging of cardiac hypoxia: opportunities and challenges. *J Mol Cell Cardiol* **51**, 640-650 (2011).
6. Hansson, G.K. Inflammation, atherosclerosis, and coronary artery disease. *N Engl J Med* **352**, 1685-1695 (2005).
7. Vogiatzi, G., Tousoulis, D. & Stefanadis, C. The role of oxidative stress in atherosclerosis. *Hellenic J Cardiol* **50**, 402-409 (2009).
8. Giordano, F.J. Oxygen, oxidative stress, hypoxia, and heart failure. *J Clin Invest* **115**, 500-508 (2005).
9. Weber, C. & Noels, H. Atherosclerosis: current pathogenesis and therapeutic options. *Nat Med* **17**, 1410-1422 (2011).
10. Marzilli, M.*, et al.* Obstructive coronary atherosclerosis and ischemic heart disease: an elusive link! *J Am Coll Cardiol* **60**, 951-956 (2012).
11. Sluimer, J.C. & Daemen, M.J. Novel concepts in atherogenesis: angiogenesis and hypoxia in atherosclerosis. *J Pathol* **218**, 7-29 (2009).
12. Hinkel, R., Trenkwalder, T. & Kupatt, C. Gene therapy for ischemic heart disease. *Expert Opin Biol Ther* **11**, 723-737 (2011).
13. Lanza, G.A., Careri, G. & Crea, F. Mechanisms of coronary artery spasm. *Circulation* **124**, 1774-1782 (2011).
14. Pries, A.R.*, et al.* A review of methods for assessment of coronary microvascular disease in both clinical and experimental settings. *Cardiovasc Res* **80**, 165-174 (2008).
15. Camici, P.G. & Crea, F. Coronary microvascular dysfunction. *N Engl J Med* **356**, 830-840 (2007).
16. Underwood, S.R. Imaging techniques in the assessment of myocardial hibernation. *Eur J Nucl Med Mol Imaging* **31**, 1209; author reply 1210-1201 (2004).
17. Heusch, G., Schulz, R. & Rahimtoola, S.H. Myocardial hibernation: a delicate balance. *Am J Physiol Heart Circ Physiol* **288**, H984-999 (2005).
18. Slezak, J.*, et al.* Hibernating myocardium: pathophysiology, diagnosis, and treatment. *Can J Physiol Pharmacol* **87**, 252-265 (2009).
19. Depre, C. & Vatner, S.F. Mechanisms of cell survival in myocardial hibernation. *Trends Cardiovasc Med* **15**, 101-110 (2005).

20. El Jamali, A.*, et al.* Reoxygenation after severe hypoxia induces cardiomyocyte hypertrophy in vitro: activation of CREB downstream of GSK3beta. *FASEB J* **18**, 1096-1098 (2004).
21. Tan, T., Scholz, P.M. & Weiss, H.R. Hypoxia inducible factor-1 improves the negative functional effects of natriuretic peptide and nitric oxide signaling in hypertrophic cardiac myocytes. *Life Sci* **87**, 9-16 (2010).
22. Weber, K.T., Sun, Y., Tyagi, S.C. & Cleutjens, J.P. Collagen network of the myocardium: function, structural remodeling and regulatory mechanisms. *J Mol Cell Cardiol* **26**, 279-292 (1994).
23. Conrad, C.H.*, et al.* Myocardial fibrosis and stiffness with hypertrophy and heart failure in the spontaneously hypertensive rat. *Circulation* **91**, 161-170 (1995).
24. Nakamura, K.*, et al.* Inhibitory effects of antioxidants on neonatal rat cardiac myocyte hypertrophy induced by tumor necrosis factor-alpha and angiotensin II. *Circulation* **98**, 794-799 (1998).
25. Lopaschuk, G.D., Ussher, J.R., Folmes, C.D., Jaswal, J.S. & Stanley, W.C. Myocardial fatty acid metabolism in health and disease. *Physiol Rev* **90**, 207-258 (2010).
26. Kolwicz, S.C., Jr. & Tian, R. Glucose metabolism and cardiac hypertrophy. *Cardiovasc Res* **90**, 194-201 (2011).
27. Katz, A.M. (ed.) *Physiology of the heart*, (Raven Press, New York, 1977).
28. Lopaschuk, G.D., Belke, D.D., Gamble, J., Itoi, T. & Schonekess, B.O. Regulation of fatty acid oxidation in the mammalian heart in health and disease. *Biochim Biophys Acta* **1213**, 263-276 (1994).
29. Jafri, M.S., Dudycha, S.J. & O'Rourke, B. Cardiac energy metabolism: models of cellular respiration. *Annu Rev Biomed Eng* **3**, 57-81 (2001).
30. Depre, C., Vanoverschelde, J.L. & Taegtmeyer, H. Glucose for the heart. *Circulation* **99**, 578-588 (1999).
31. Fillmore, N. & Lopaschuk, G.D. Targeting mitochondrial oxidative metabolism as an approach to treat heart failure. *Biochim Biophys Acta* **1833**, 857-865 (2013).
32. Papa, S.*, et al.* The oxidative phosphorylation system in mammalian mitochondria. *Adv Exp Med Biol* **942**, 3-37 (2012).
33. DiMauro, S. & Schon, E.A. Mitochondrial respiratory-chain diseases. *N Engl J Med* **348**, 2656-2668 (2003).
34. Venditti, P., Di Stefano, L. & Di Meo, S. Mitochondrial metabolism of reactive oxygen species. *Mitochondrion* **13**, 71-82 (2013).
35. Whitmer, J.T., Idell-Wenger, J.A., Rovetto, M.J. & Neely, J.R. Control of fatty acid metabolism in ischemic and hypoxic hearts. *J Biol Chem* **253**, 4305-4309 (1978).
36. Wheaton, W.W. & Chandel, N.S. Hypoxia. 2. Hypoxia regulates cellular metabolism. *Am J Physiol Cell Physiol* **300**, C385-393 (2010).
37. Klimova, T. & Chandel, N.S. Mitochondrial complex III regulates hypoxic activation of HIF. *Cell Death Differ* **15**, 660-666 (2008).
38. Cassavaugh, J. & Lounsbury, K.M. Hypoxia-mediated biological control. *J Cell Biochem* **112**, 735-744 (2011).
39. Lodish, H.*, et al. Molecular Cell Biology*, (W. H. Freeman, New York, 2000).

40. Crampin, E.J., Smith, N.P., Langham, A.E., Clayton, R.H. & Orchard, C.H. Acidosis in models of cardiac ventricular myocytes. *Philos Trans A Math Phys Eng Sci* **364**, 1171-1186 (2006).
41. Steenbergen, C., Deleeuw, G., Rich, T. & Williamson, J.R. Effects of acidosis and ischemia on contractility and intracellular pH of rat heart. *Circ Res* **41**, 849-858 (1977).
42. Barth, A.S. & Tomaselli, G.F. Cardiac metabolism and arrhythmias. *Circ Arrhythm Electrophysiol* **2**, 327-335 (2009).
43. Heather, L.C. & Clarke, K. Metabolism, hypoxia and the diabetic heart. *J Mol Cell Cardiol* **50**, 598-605 (2011).
44. Kulisz, A., Chen, N., Chandel, N.S., Shao, Z. & Schumacker, P.T. Mitochondrial ROS initiate phosphorylation of p38 MAP kinase during hypoxia in cardiomyocytes. *Am J Physiol Lung Cell Mol Physiol* **282**, L1324-1329 (2002).
45. Duranteau, J., Chandel, N.S., Kulisz, A., Shao, Z. & Schumacker, P.T. Intracellular signaling by reactive oxygen species during hypoxia in cardiomyocytes. *J Biol Chem* **273**, 11619-11624 (1998).
46. Hamanaka, R.B. & Chandel, N.S. Mitochondrial reactive oxygen species regulate cellular signaling and dictate biological outcomes. *Trends Biochem Sci* **35**, 505-513 (2010).
47. Hoffman, D.L., Salter, J.D. & Brookes, P.S. Response of mitochondrial reactive oxygen species generation to steady-state oxygen tension: implications for hypoxic cell signaling. *Am J Physiol Heart Circ Physiol* **292**, H101-108 (2007).
48. Guzy, R.D. & Schumacker, P.T. Oxygen sensing by mitochondria at complex III: the paradox of increased reactive oxygen species during hypoxia. *Exp Physiol* **91**, 807-819 (2006).
49. Spahr, R., Krutzfeldt, A., Mertens, S., Siegmund, B. & Piper, H.M. Fatty acids are not an important fuel for coronary microvascular endothelial cells. *Mol Cell Biochem* **88**, 59-64 (1989).
50. Mertens, S., Noll, T., Spahr, R., Krutzfeldt, A. & Piper, H.M. Energetic response of coronary endothelial cells to hypoxia. *Am J Physiol* **258**, H689-694 (1990).
51. Helies-Toussaint, C*., et al.* Lipid metabolism in human endothelial cells. *Biochim Biophys Acta* **1761**, 765-774 (2006).
52. Davidson, S.M. & Duchen, M.R. Endothelial mitochondria: contributing to vascular function and disease. *Circ Res* **100**, 1128-1141 (2007).
53. Peters, K*., et al.* Changes in human endothelial cell energy metabolic capacities during in vitro cultivation. The role of "aerobic glycolysis" and proliferation. *Cell Physiol Biochem* **24**, 483-492 (2009).
54. Shah, A.M. & Channon, K.M. Free radicals and redox signalling in cardiovascular disease. *Heart* **90**, 486-487 (2004).
55. Lopez Farre, A. & Casado, S. Heart failure, redox alterations, and endothelial dysfunction. *Hypertension* **38**, 1400-1405 (2001).
56. Belch, J.J., Bridges, A.B., Scott, N. & Chopra, M. Oxygen free radicals and congestive heart failure. *Br Heart J* **65**, 245-248 (1991).
57. Kukreja, R.C.a.H., M.L. *Free radicals, cardiovascular dysfunction and protection strategies.*, (R.G. Landes Company, Austin, Texas, 1994).
58. Kontos, H.A. Oxygen radicals in cerebral ischemia: the 2001 Willis lecture. *Stroke* **32**, 2712-2716 (2001).

59. Halliwell, B. & Gutteridge, J.M.C. *Free radicals in biology and medicine*, (Clarendon Press ; Oxford University Press, New York, 1985).
60. Jordan, J.E., Zhao, Z.Q. & Vinten-Johansen, J. The role of neutrophils in myocardial ischemia-reperfusion injury. *Cardiovasc Res* **43**, 860-878 (1999).
61. Ellis, G.R.*, et al.* Neutrophil superoxide anion--generating capacity, endothelial function and oxidative stress in chronic heart failure: effects of short- and long-term vitamin C therapy. *J Am Coll Cardiol* **36**, 1474-1482 (2000).
62. Romson, J.L.*, et al.* Reduction of the extent of ischemic myocardial injury by neutrophil depletion in the dog. *Circulation* **67**, 1016-1023 (1983).
63. Becker, L.B. New concepts in reactive oxygen species and cardiovascular reperfusion physiology. *Cardiovasc Res* **61**, 461-470 (2004).
64. Lemasters, J.J.*, et al.* The mitochondrial permeability transition in cell death: a common mechanism in necrosis, apoptosis and autophagy. *Biochim Biophys Acta* **1366**, 177-196 (1998).
65. Bernardi, P. & Forte, M. The mitochondrial permeability transition pore. *Novartis Found Symp* **287**, 157-164; discussion 164-169 (2007).
66. Misra, M.K., Sarwat, M., Bhakuni, P., Tuteja, R. & Tuteja, N. Oxidative stress and ischemic myocardial syndromes. *Med Sci Monit* **15**, RA209-219 (2009).
67. Chambers, D.E.*, et al.* Xanthine oxidase as a source of free radical damage in myocardial ischemia. *J Mol Cell Cardiol* **17**, 145-152 (1985).
68. McNally, J.S., Saxena, A., Cai, H., Dikalov, S. & Harrison, D.G. Regulation of xanthine oxidoreductase protein expression by hydrogen peroxide and calcium. *Arterioscler Thromb Vasc Biol* **25**, 1623-1628 (2005).
69. Werns, S.W.*, et al.* Reduction of the size of infarction by allopurinol in the ischemic-reperfused canine heart. *Circulation* **73**, 518-524 (1986).
70. Stadtman, E.R. Protein oxidation and aging. *Free Radic Res* **40**, 1250-1258 (2006).
71. Piper, H.M., Garcia-Dorado, D. & Ovize, M. A fresh look at reperfusion injury. *Cardiovasc Res* **38**, 291-300 (1998).
72. Deanfield, J.E., Halcox, J.P. & Rabelink, T.J. Endothelial function and dysfunction: testing and clinical relevance. *Circulation* **115**, 1285-1295 (2007).
73. Sies, H. Oxidative stress: oxidants and antioxidants. *Exp Physiol* **82**, 291-295 (1997).
74. Chen, Z.*, et al.* Overexpression of MnSOD protects against myocardial ischemia/reperfusion injury in transgenic mice. *J Mol Cell Cardiol* **30**, 2281-2289 (1998).
75. van Deel, E.D.*, et al.* Extracellular superoxide dismutase protects the heart against oxidative stress and hypertrophy after myocardial infarction. *Free Radic Biol Med* **44**, 1305-1313 (2008).
76. Ambrosio, G., Weisfeldt, M.L., Jacobus, W.E. & Flaherty, J.T. Evidence for a reversible oxygen radical-mediated component of reperfusion injury: reduction by recombinant human superoxide dismutase administered at the time of reflow. *Circulation* **75**, 282-291 (1987).
77. Blaustein, A.*, et al.* Myocardial glutathione depletion impairs recovery after short periods of ischemia. *Circulation* **80**, 1449-1457 (1989).
78. Saleh, N.K. & Saleh, H.A. Protective effects of vitamin E against myocardial ischemia/reperfusion injury in rats. *Saudi Med J* **31**, 142-147 (2010).

79. Chakrabarty, S., Nandi, A., Mukhopadhyay, C.K. & Chatterjee, I.B. Protective role of ascorbic acid against lipid peroxidation and myocardial injury. *Mol Cell Biochem* **111**, 41-47 (1992).
80. Garlick, P.B., Davies, M.J., Hearse, D.J. & Slater, T.F. Direct detection of free radicals in the reperfused rat heart using electron spin resonance spectroscopy. *Circ Res* **61**, 757-760 (1987).
81. Angelos, M.G*., et al.* Hypoxic reperfusion of the ischemic heart and oxygen radical generation. *Am J Physiol Heart Circ Physiol* **290**, H341-347 (2006).
82. Zweier, J.L. Measurement of superoxide-derived free radicals in the reperfused heart. Evidence for a free radical mechanism of reperfusion injury. *J Biol Chem* **263**, 1353-1357 (1988).
83. Bartosz, G. Use of spectroscopic probes for detection of reactive oxygen species. *Clin Chim Acta* **368**, 53-76 (2006).
84. Dikalov, S., Griendling, K.K. & Harrison, D.G. Measurement of reactive oxygen species in cardiovascular studies. *Hypertension* **49**, 717-727 (2007).
85. Gomes, A., Fernandes, E. & Lima, J.L. Fluorescence probes used for detection of reactive oxygen species. *J Biochem Biophys Methods* **65**, 45-80 (2005).
86. Kevin, L.G., Camara, A.K., Riess, M.L., Novalija, E. & Stowe, D.F. Ischemic preconditioning alters real-time measure of O2 radicals in intact hearts with ischemia and reperfusion. *Am J Physiol Heart Circ Physiol* **284**, H566-574 (2003).
87. Prutz, W.A. Inhibition of DNA-ethidium bromide intercalation due to free radical attack upon DNA. II. Copper(II)-catalysed DNA damage by O.2. *Radiat Environ Biophys* **23**, 7-18 (1984).
88. Toufektsian, M.C., Boucher, F.R., Tanguy, S., Morel, S. & de Leiris, J.G. Cardiac toxicity of singlet oxygen: implication in reperfusion injury. *Antioxid Redox Signal* **3**, 63-69 (2001).
89. Keshari, K.R*., et al.* Hyperpolarized 13C dehydroascorbate as an endogenous redox sensor for in vivo metabolic imaging. *Proc Natl Acad Sci U S A* **108**, 18606-18611.
90. Keshari, K.R*., et al.* Hyperpolarized [1-13C]dehydroascorbate MR spectroscopy in a murine model of prostate cancer: comparison with 18F-FDG PET. *J Nucl Med* **54**, 922-928.
91. Bohndiek, S.E*., et al.* Hyperpolarized [1-13C]-ascorbic and dehydroascorbic acid: vitamin C as a probe for imaging redox status in vivo. *J Am Chem Soc* **133**, 11795-11801.
92. Chitneni, S.K., Palmer, G.M., Zalutsky, M.R. & Dewhirst, M.W. Molecular imaging of hypoxia. *J Nucl Med* **52**, 165-168 (2011).
93. Griffiths, J.R. & Robinson, S.P. The OxyLite: a fibre-optic oxygen sensor. *Br J Radiol* **72**, 627-630 (1999).
94. Krohn, K.A., Link, J.M. & Mason, R.P. Molecular imaging of hypoxia. *J Nucl Med* **49 Suppl 2**, 129S-148S (2008).
95. Gadian, D.G. *NMR and its applications to living systems*, (Oxford University Press, New York, 1995).
96. Egred, M*., et al.* Blood oxygen level-dependent (BOLD) MRI: A novel technique for the assessment of myocardial ischemia as identified by nuclear imaging SPECT. *Eur J Intern Med* **18**, 581-586 (2007).

97. Carlier, P.G., Bertoldi, D., Baligand, C., Wary, C. & Fromes, Y. Muscle blood flow and oxygenation measured by NMR imaging and spectroscopy. *NMR Biomed* **19**, 954-967 (2006).
98. Wernick, M.N. & Aarsvold, J. *Emission Tomography: The fundamentals of PET and SPECT*, (Elsevier Academic Press, Oxford, 2004).
99. Anagnostopoulos, C., Georgakopoulos, A., Pianou, N. & Nekolla, S.G. Assessment of myocardial perfusion and viability by Positron Emission Tomography. *Int J Cardiol* **167**, 1737-1749 (2013).
100. Beller, G.A. & Bergmann, S.R. Myocardial perfusion imaging agents: SPECT and PET. *J Nucl Cardiol* **11**, 71-86 (2004).
101. Mochizuki, T.*, et al.* FDG uptake and glucose transporter subtype expressions in experimental tumor and inflammation models. *J Nucl Med* **42**, 1551-1555 (2001).
102. Southworth, R., Parry, C.R., Parkes, H.G., Medina, R.A. & Garlick, P.B. Tissue-specific differences in 2-fluoro-2-deoxyglucose metabolism beyond FDG-6-P: a 19F NMR spectroscopy study in the rat. *NMR Biomed* **16**, 494-502 (2003).
103. Sinusas, A.J. The potential for myocardial imaging with hypoxia markers. *Semin Nucl Med* **29**, 330-338 (1999).
104. Martin, G.V.*, et al.* Fluoromisonidazole. A metabolic marker of myocyte hypoxia. *Circ Res* **67**, 240-244 (1990).
105. Martin, G.V.*, et al.* Enhanced binding of the hypoxic cell marker [3H]fluoromisonidazole in ischemic myocardium. *J Nucl Med* **30**, 194-201 (1989).
106. Shelton, M.E.*, et al.* In vivo delineation of myocardial hypoxia during coronary occlusion using fluorine-18 fluoromisonidazole and positron emission tomography: a potential approach for identification of jeopardized myocardium. *J Am Coll Cardiol* **16**, 477-485 (1990).
107. Martin, G.V.*, et al.* Noninvasive detection of hypoxic myocardium using fluorine-18-fluoromisonidazole and positron emission tomography. *J Nucl Med* **33**, 2202-2208 (1992).
108. Lee, S.T. & Scott, A.M. Hypoxia positron emission tomography imaging with 18f-fluoromisonidazole. *Semin Nucl Med* **37**, 451-461 (2007).
109. Dearling, J.L.*, et al.* Design of hypoxia-targeting radiopharmaceuticals: selective uptake of copper-64 complexes in hypoxic cells in vitro. *Eur J Nucl Med* **25**, 788-792 (1998).
110. Dearling, J.L., Lewis, J.S., Mullen, G.E., Welch, M.J. & Blower, P.J. Copper bis(thiosemicarbazone) complexes as hypoxia imaging agents: structure-activity relationships. *J Biol Inorg Chem* **7**, 249-259 (2002).
111. Holland, J.P., Giansiracusa, J.H., Bell, S.G., Wong, L.L. & Dilworth, J.R. In vitro kinetic studies on the mechanism of oxygen-dependent cellular uptake of copper radiopharmaceuticals. *Phys Med Biol* **54**, 2103-2119 (2009).
112. Lewis, J.S., McCarthy, D.W., McCarthy, T.J., Fujibayashi, Y. & Welch, M.J. Evaluation of 64Cu-ATSM in vitro and in vivo in a hypoxic tumor model. *J Nucl Med* **40**, 177-183 (1999).
113. Lewis, J.S., Sharp, T.L., Laforest, R., Fujibayashi, Y. & Welch, M.J. Tumor uptake of copper-diacetyl-bis(N(4)-methylthiosemicarbazone): effect of changes in tissue oxygenation. *J Nucl Med* **42**, 655-661 (2001).

114. Handley, M.G., Medina, R.A., Paul, R.L., Blower, P.J. & Southworth, R. Demonstration of the retention of 64Cu-ATSM in cardiac myocytes using a novel incubation chamber for screening hypoxia-dependent radiotracers. *Nucl Med Commun*, 1015-1022 (2013).
115. Fujibayashi, Y.*, et al.* Copper-62-ATSM: a new hypoxia imaging agent with high membrane permeability and low redox potential. *J Nucl Med* **38**, 1155-1160 (1997).
116. Lewis, J.S.*, et al.* Delineation of hypoxia in canine myocardium using PET and copper(II)-diacetyl-bis(N(4)-methylthiosemicarbazone). *J Nucl Med* **43**, 1557-1569 (2002).
117. Takahashi, N.*, et al.* Copper-62 ATSM as a hypoxic tissue tracer in myocardial ischemia. *Ann Nucl Med* **15**, 293-296 (2001).
118. Dearling, J.L. & Packard, A.B. Some thoughts on the mechanism of cellular trapping of Cu(II)-ATSM. *Nucl Med Biol* **37**, 237-243 (2010).
119. Maurer, R.I.*, et al.* Studies on the mechanism of hypoxic selectivity in copper bis(thiosemicarbazone) radiopharmaceuticals. *J Med Chem* **45**, 1420-1431 (2002).
120. Holland, J.P., Green, J.C. & Dilworth, J.R. Probing the mechanism of hypoxia selectivity of copper bis(thiosemicarbazonato) complexes: DFT calculation of redox potentials and absolute acidities in solution. *Dalton Trans*, 783-794 (2006).
121. Baerga, I.D., Maickel, R.P. & Green, M.A. Subcellular distribution of tissue radiocopper following intravenous administration of 67Cu-labeled Cu-PTSM. *Int J Rad Appl Instrum B* **19**, 697-701 (1992).
122. Dearling, J.L. & Blower, P.J. Redox-active metal complexes for imaging hypoxic tissues: structure-activity relationships in copper(II) bis(thiosemicarbazone) complexes. *Chemical Communications* **0**, 2531-2532 (1998).
123. Handley, M.G.*, et al.* Cardiac Hypoxia Imaging: Second-Generation Analogues of 64Cu-ATSM. *J Nucl Med* **3**, 488-494 (2014).
124. Shelton, M.E., Green, M.A., Mathias, C.J., Welch, M.J. & Bergmann, S.R. Kinetics of copper-PTSM in isolated hearts: a novel tracer for measuring blood flow with positron emission tomography. *J Nucl Med* **30**, 1843-1847 (1989).
125. Ballard, F.J. Regulation of gluconeogenesis during exposure of young rats to hypoxic conditions. *Biochem J* **121**, 169-178 (1971).
126. Petering, D.H. Physico-chemical properties of the antitumor agent, 3-Ethoxy-2-Oxobutyraldehyde bis (Thiosemicarbazonato) Copper(II). *Bioinorg Chem* **1**, 255-271 (1972).
127. Taniuchi, H.*, et al.* Cu-pyruvaldehyde-bis(N4-methylthiosemicarbazone) (Cu-PTSM), a metal complex with selective NADH-dependent reduction by complex I in brain mitochondria: a potential radiopharmaceutical for mitochondria-functional imaging with positron emission tomography (PET). *Biol Pharm Bull* **18**, 1126-1129 (1995).
128. Obata, A.*, et al.* Retention mechanism of hypoxia selective nuclear imaging/radiotherapeutic agent cu-diacetyl-bis(N4-methylthiosemicarbazone) (Cu-ATSM) in tumor cells. *Ann Nucl Med* **15**, 499-504 (2001).

129. Minkel, D.T. & Petering, D.H. Initial reaction of 3-ethyoxy-2-oxobutyraldehyde bis(thiosemicarbazonato) copper(II) with Ehrlich ascites tumor cells. *Cancer Res* **38**, 117-123 (1978).
130. Barnhart-Bott, A. & Green, M.A. The effects of glutathione depletion on the biodistribution of Cu(PTSM) in rats. *Int J Rad Appl Instrum B* **18**, 865-869 (1991).
131. Xiao, Z., Donnelly, P.S., Zimmermann, M. & Wedd, A.G. Transfer of copper between bis(thiosemicarbazone) ligands and intracellular copper-binding proteins. insights into mechanisms of copper uptake and hypoxia selectivity. *Inorg Chem* **47**, 4338-4347 (2008).
132. Donnelly, P.S*., et al.* An impaired mitochondrial electron transport chain increases retention of the hypoxia imaging agent diacetylbis(4-methylthiosemicarbazonato)copperII. *Proc Natl Acad Sci U S A* **109**, 47-52 (2011).
133. Ikawa, M*., et al.* PET imaging of redox and energy states in stroke-like episodes of MELAS. *Mitochondrion* **9**, 144-148 (2009).
134. Petering, D.H. The reaction of 3-ethoxy-2-oxobutyraldehyde bis (thiosemicarbazonato) copper(II) with thiols. *Bioinorg Chem* **1**, 273-288 (1972).
135. Holland, J.P*., et al.* Spectroelectrochemical and computational studies on the mechanism of hypoxia selectivity of copper radiopharmaceuticals. *Chemistry* **14**, 5890-5907 (2008).
136. Klabunde, R.E. *Cardiovascular physiology concepts*, (Lippincott Williams & Wilkins/Wolters Kluwer, Philadelphia, PA).
137. Langendorff, O. Untersuchungen am überlebenden Säugetierherzen. *Pflügers Arch* **61**, 291-332 (1895).
138. Skrzypiec-Spring, M., Grotthus, B., Szelag, A. & Schulz, R. Isolated heart perfusion according to Langendorff---still viable in the new millennium. *J Pharmacol Toxicol Methods* **55**, 113-126 (2007).
139. Sutherland, F.J. & Hearse, D.J. The isolated blood and perfusion fluid perfused heart. *Pharmacol Res* **41**, 613-627 (2000).
140. Southworth, R., Blackburn, S.C., Davey, K.A., Sharland, G.K. & Garlick, P.B. The low oxygen-carrying capacity of Krebs buffer causes a doubling in ventricular wall thickness in the isolated heart. *Can J Physiol Pharmacol* **83**, 174-182 (2005).
141. Dhein, S., Mohr, F.W. & Delmar, M. *Practical methods in cardiovascular research*, (Springer, Berlin ; New York, 2005).
142. Life Sciences, Y. How does the YSI sensor technology work? , Vol. 2013.
143. Florini, J.R. Assay of creatine kinase in microtiter plates using thio-NAD to allow monitoring at 405 nM. *Anal Biochem* **182**, 399-404 (1989).
144. Smith, P.K*., et al.* Measurement of protein using bicinchoninic acid. *Anal Biochem* **150**, 76-85 (1985).
145. Schwartz, S.M. Selection and characterization of bovine aortic endothelial cells. *In Vitro* **14**, 966-980 (1978).
146. Petty, R.D., Sutherland, L.A., Hunter, E.M. & Cree, I.A. Comparison of MTT and ATP-based assays for the measurement of viable cell number. *J Biolumin Chemilumin* **10**, 29-34 (1995).
147. Boyland, E. & Chasseaud, L.F. Enzyme-catalysed conjugations of glutathione with unsaturated compounds. *Biochem J* **104**, 95-102 (1967).

148. Griffith, O.W. Mechanism of action, metabolism, and toxicity of buthionine sulfoximine and its higher homologs, potent inhibitors of glutathione synthesis. *J Biol Chem* **257**, 13704-13712 (1982).
149. Ceconi, C.*, et al.* The role of glutathione status in the protection against ischaemic and reperfusion damage: effects of N-acetyl cysteine. *J Mol Cell Cardiol* **20**, 5-13 (1988).
150. Ellman, G.L. Tissue sulfhydryl groups. *Arch Biochem Biophys* **82**, 70-77 (1959).
151. Murray, G.I., Burke, M.D. & Ewen, S.W. Glutathione localization by a novel o-phthalaldehyde histofluorescence method. *Histochem J* **18**, 434-440 (1986).
152. Murray, A.J.*, et al.* Insulin resistance, abnormal energy metabolism and increased ischemic damage in the chronically infarcted rat heart. *Cardiovasc Res* **71**, 149-157 (2006).
153. McCarthy, D.W.*, et al.* Efficient production of high specific activity 64Cu using a biomedical cyclotron. *Nucl Med Biol* **24**, 35-43 (1997).
154. Wu, G., Fang, Y.Z., Yang, S., Lupton, J.R. & Turner, N.D. Glutathione metabolism and its implications for health. *J Nutr* **134**, 489-492 (2004).
155. Shan, X.Q., Aw, T.Y. & Jones, D.P. Glutathione-dependent protection against oxidative injury. *Pharmacol Ther* **47**, 61-71 (1990).
156. Jain, M.*, et al.* Increased myocardial dysfunction after ischemia-reperfusion in mice lacking glucose-6-phosphate dehydrogenase. *Circulation* **109**, 898-903 (2004).
157. Rigobello, M.P. & Bindoli, A. Effect of pyruvate on rat heart thiol status during ischemia and hypoxia followed by reperfusion. *Mol Cell Biochem* **122**, 93-100 (1993).
158. Ferrari, R.*, et al.* Oxygen free radicals and myocardial damage: protective role of thiol-containing agents. *Am J Med* **91**, 95S-105S (1991).
159. Gu, W.J., Wu, Z.J., Wang, P.F., Aung, L.H. & Yin, R.X. N-Acetylcysteine supplementation for the prevention of atrial fibrillation after cardiac surgery: a meta-analysis of eight randomized controlled trials. *BMC Cardiovasc Disord* **12**, 1-10 (2012).
160. Komniski, M.S., Yakushev, S., Bogdanov, N., Gassmann, M. & Bogdanova, A. Interventricular heterogeneity in rat heart responses to hypoxia: the tuning of glucose metabolism, ion gradients, and function. *Am J Physiol Heart Circ Physiol* **300**, H1645-1652.
161. Guarnieri, C., Flamigni, F. & Rossoni-Caldarera, C. Glutathione peroxidase activity and release of glutathione from oxygen-deficient perfused rat heart. *Biochem Biophys Res Commun* **89**, 678-684 (1979).
162. Seiler, K.S. & Starnes, J.W. Exogenous GSH protection during hypoxia-reoxygenation of the isolated rat heart: impact of hypoxia duration. *Free Radic Res* **32**, 41-55 (2000).
163. Handley, M.G.*, et al.* PET imaging of hypoxia: second genertion analogues of ^{64}Cu-ATSM. *J Nucl Med* (Accepted, in press 2014).
164. Ng, C.K., Sinusas, A.J., Zaret, B.L. & Soufer, R. Kinetic analysis of technetium-99m-labeled nitroimidazole (BMS-181321) as a tracer of myocardial hypoxia. *Circulation* **92**, 1261-1268 (1995).

165. Wischmeyer, P.E.*, et al.* Single dose of glutamine enhances myocardial tissue metabolism, glutathione content, and improves myocardial function after ischemia-reperfusion injury. *JPEN J Parenter Enteral Nutr* **27**, 396-403 (2003).
166. Connaughton, M., Kelly, F.J., Haddock, P.S., Hearse, D.J. & Shattock, M.J. Ventricular arrhythmias induced by ischaemia-reperfusion are unaffected by myocardial glutathione depletion. *J Mol Cell Cardiol* **28**, 679-688 (1996).
167. Bernier, M. & Hearse, D.J. Reperfusion-induced arrhythmias: mechanisms of protection by glucose and mannitol. *Am J Physiol* **254**, H862-870 (1988).
168. Suzuki, M. & Kurata, M. Effects of ATP level on glutathione regeneration in rabbit and guinea-pig erythrocytes. *Comp Biochem Physiol B* **103**, 859-862 (1992).
169. Papadopoulos, M.C., Koumenis, I.L., Dugan, L.L. & Giffard, R.G. Vulnerability to glucose deprivation injury correlates with glutathione levels in astrocytes. *Brain Res* **748**, 151-156 (1997).
170. Brennan, J.P.*, et al.* Mitochondrial uncoupling, with low concentration FCCP, induces ROS-dependent cardioprotection independent of KATP channel activation. *Cardiovasc Res* **72**, 313-321 (2006).
171. Favaloro, J.L. & Kemp-Harper, B.K. The nitroxyl anion (HNO) is a potent dilator of rat coronary vasculature. *Cardiovasc Res* **73**, 587-596 (2007).
172. Klawitter, P.F., Murray, H.N., Clanton, T.L. & Angelos, M.G. Reactive oxygen species generated during myocardial ischemia enable energetic recovery during reperfusion. *Am J Physiol Heart Circ Physiol* **283**, H1656-1661 (2002).
173. Chen, W., Gabel, S., Steenbergen, C. & Murphy, E. A redox-based mechanism for cardioprotection induced by ischemic preconditioning in perfused rat heart. *Circ Res* **77**, 424-429 (1995).
174. Suner, S. & Jay, G. Carbon monoxide has direct toxicity on the myocardium distinct from effects of hypoxia in an ex vivo rat heart model. *Acad Emerg Med* **15**, 59-65 (2008).
175. Endoh, H., Kaneko, T., Nakamura, H., Doi, K. & Takahashi, E. Improved cardiac contractile functions in hypoxia-reoxygenation in rats treated with low concentration Co(2+). *Am J Physiol Heart Circ Physiol* **279**, H2713-2719 (2000).
176. Serizawa, T., Vogel, W.M., Apstein, C.S. & Grossman, W. Comparison of acute alterations in left ventricular relaxation and diastolic chamber stiffness induced by hypoxia and ischemia. Role of myocardial oxygen supply-demand imbalance. *J Clin Invest* **68**, 91-102 (1981).
177. Werns, S.W., Fantone, J.C., Ventura, A. & Lucchesi, B.R. Myocardial glutathione depletion impairs recovery of isolated blood-perfused hearts after global ischaemia. *J Mol Cell Cardiol* **24**, 1215-1220 (1992).
178. Chatham, J.C., Seymour, A.L., Harmsen, E. & Radda, G.K. Depletion of myocardial glutathione: its effects on heart function and metabolism during ischaemia and reperfusion. *Cardiovasc Res* **22**, 833-839 (1988).
179. Barbosa, V.A.*, et al.* Acute exercise induce endothelial nitric oxide synthase phosphorylation via Akt and AMP-activated protein kinase in aorta of rats: Role of reactive oxygen species. *Int J Cardiol* **167**, 2983-2988 (2012).
180. Mohanraj, P., Merola, A.J., Wright, V.P. & Clanton, T.L. Antioxidants protect rat diaphragmatic muscle function under hypoxic conditions. *J Appl Physiol (1985)* **84**, 1960-1966 (1998).

181. Williamson, J.R. Glycolytic control mechanisms. II. Kinetics of intermediate changes during the aerobic-anoxic transition in perfused rat heart. *J Biol Chem* **241**, 5026-5036 (1966).
182. Ishibashi, T., Hara, A. & Abiko, Y. Relationship between coronary flow and adenosine release during severe and mild hypoxia in the isolated perfused rat heart with special reference to time-course change. *Heart Vessels* **3**, 113-121 (1987).
183. Zhang, D.X. & Gutterman, D.D. Mitochondrial reactive oxygen species-mediated signaling in endothelial cells. *Am J Physiol Heart Circ Physiol* **292**, H2023-2031 (2007).
184. Li, J.M. & Shah, A.M. Endothelial cell superoxide generation: regulation and relevance for cardiovascular pathophysiology. *Am J Physiol Regul Integr Comp Physiol* **287**, R1014-1030 (2004).
185. Prasad, A., Andrews, N.P., Padder, F.A., Husain, M. & Quyyumi, A.A. Glutathione reverses endothelial dysfunction and improves nitric oxide bioavailability. *J Am Coll Cardiol* **34**, 507-514 (1999).
186. Motterlini, R*., et al.* Endothelial heme oxygenase-1 induction by hypoxia. Modulation by inducible nitric-oxide synthase and S-nitrosothiols. *J Biol Chem* **275**, 13613-13620 (2000).
187. Singh, R.J., Hogg, N., Joseph, J. & Kalyanaraman, B. Mechanism of nitric oxide release from S-nitrosothiols. *J Biol Chem* **271**, 18596-18603 (1996).
188. Bhat, G.B., Tinsley, S.B., Tolson, J.K., Patel, J.M. & Block, E.R. Hypoxia increases the susceptibility of pulmonary artery endothelial cells to hydrogen peroxide injury. *J Cell Physiol* **151**, 228-238 (1992).
189. Hong, H., Lu, Y., Ji, Z.N. & Liu, G.Q. Up-regulation of P-glycoprotein expression by glutathione depletion-induced oxidative stress in rat brain microvessel endothelial cells. *J Neurochem* **98**, 1465-1473 (2006).
190. Harlan, J.M., Levine, J.D., Callahan, K.S., Schwartz, B.R. & Harker, L.A. Glutathione redox cycle protects cultured endothelial cells against lysis by extracellularly generated hydrogen peroxide. *J Clin Invest* **73**, 706-713 (1984).
191. Kokura, S., Wolf, R.E., Yoshikawa, T., Granger, D.N. & Aw, T.Y. Molecular mechanisms of neutrophil-endothelial cell adhesion induced by redox imbalance. *Circ Res* **84**, 516-524 (1999).
192. Deneke, S.M., Baxter, D.F., Phelps, D.T. & Fanburg, B.L. Increase in endothelial cell glutathione and precursor amino acid uptake by diethyl maleate and hyperoxia. *Am J Physiol* **257**, L265-271 (1989).
193. Suttorp, N., Toepfer, W. & Roka, L. Antioxidant defense mechanisms of endothelial cells: glutathione redox cycle versus catalase. *Am J Physiol* **251**, C671-680 (1986).
194. Jornot, L. & Junod, A.F. Variable glutathione levels and expression of antioxidant enzymes in human endothelial cells. *Am J Physiol* **264**, L482-489 (1993).
195. Phelps, D.T., Deneke, S.M., Daley, D.L. & Fanburg, B.L. Elevation of glutathione levels in bovine pulmonary artery endothelial cells by N-acetylcysteine. *Am J Respir Cell Mol Biol* **7**, 293-299 (1992).
196. Mukherjee, T.K., Mishra, A.K., Mukhopadhyay, S. & Hoidal, J.R. High concentration of antioxidants N-acetylcysteine and mitoquinone-Q induces

intercellular adhesion molecule 1 and oxidative stress by increasing intracellular glutathione. *J Immunol* **178**, 1835-1844 (2007).
197. Bak, M.I. & Ingwall, J.S. Acidosis during ischemia promotes adenosine triphosphate resynthesis in postischemic rat heart. In vivo regulation of 5'-nucleotidase. *J Clin Invest* **93**, 40-49 (1994).
198. Boron, W.F. & De Weer, P. Intracellular pH transients in squid giant axons caused by CO2, NH3, and metabolic inhibitors. *J Gen Physiol* **67**, 91-112 (1976).
199. Marala, R.B.*, et al.* Zoniporide: a potent and highly selective inhibitor of human Na(+)/H(+) exchanger-1. *Eur J Pharmacol* **451**, 37-41 (2002).
200. Cave, A.C. & Garlick, P.B. Ischemic preconditioning and intracellular pH: a 31P NMR study in the isolated rat heart. *Am J Physiol* **272**, H544-552 (1997).
201. Grace, A.A.*, et al.* Regulation of intracellular pH in the perfused heart by external HCO3- and Na(+)-H+ exchange. *Am J Physiol* **265**, H289-298 (1993).
202. Shipolini, A.R.*, et al.* Na+/H+ exchanger activity does not contribute to protection by ischemic preconditioning in the isolated rat heart. *Circulation* **96**, 3617-3625 (1997).
203. Curello, S.*, et al.* Changes in the cardiac glutathione status after ischemia and reperfusion. *Experientia* **41**, 42-43 (1985).
204. Ikawa, M.*, et al.* Evaluation of striatal oxidative stress in patients with Parkinson's disease using [62Cu]ATSM PET. *Nucl Med Biol* **38**, 945-951 (2011).
205. Sternbergh, W.C., Brunsting, L.A., Abd-Elfattah, A.S. & Wechsler, A.S. Basal metabolic energy requirements of polarized and depolarized arrest in rat heart. *Am J Physiol* **256**, H846-851 (1989).